THE BIG SQUEEZE: INVESTIGATING NOVEL MECHANISMS OF PROSTATE SMOOTH MUSCLE FUNCTION IN MALE LOWER URINARY TRACT DYSFUNCTION

By

Anne Elise Turco

A dissertation submitted in partial fulfillment of the requirements for the degree of

Doctor of Philosophy

(Molecular and Environmental Toxicology)

At the

UNIVERSITY OF WISCONSIN-MADISON

2021

Date of final oral examination: April 13th, 2021

The dissertation is approved by the following members of the Final Oral Committee:

Lisa Arendt, Associate Professor, Comparative Biosciences

Robert J. Lipinski, Assistant Professor, Comparative Biosciences

William Ricke, Professor, Department of Urology

Jyoti J Watters, Professor, Comparative Biosciences

Chad M. Vezina, Professor, Molecular and Environmental Toxicology

Dedicated to:

My parents, family, friends for all their love and support

Acknowledgements

As former Vezina lab member Kyle Wegner said, “if a PhD was easy everyone would do it.” It is true the pursuit of a PhD was certainty not easy, but it was never done alone. Thank you to everyone who has supported me on my scientific journey. It has not always been easy, but I grew exponentially as a person and scientist every step of the way. I would like to acknowledge my lab members (past and present) Kyle Wegner, Royal Oakes, Lisa Abler, Hannah Ruetten, Diya Joseph, Brandon Scharpf, Thomas Peterson, Jonathan Zhu, and Mark Cadena for being great company and challenging me scientifically. Your helpful guidance on research direction and our discussions about social norms bolstered my thesis quality and challenged my thoughts about everyday life. As I learned during the quarantine of spring of 2020, your company and advice made getting a doctorate tolerable.

Thank you to my collaborators Dr. Nathan Tykocki, Dr. Kim Keil, and Dr. Janet Keast, for always saying what I needed to hear (even if I didn’t know it immediately) and offering limitless advice. I would not have been able to establish our methods for GCaMP analysis or nerve quantification without your expertise. Thank you to Dr. Zunyi Wang and Dr. Dale Bjorling for aiding in the rodent urinary analysis and spending countless hours quantifying rodent urination events and always answering my panicked emails and sharing equipment. I would also like to acknowledge the developmental endocrinology research group who provided great support, research direction, and food throughout the years. You have been a great audience and I grew as a presenter as a result of having such a comfortable group to which to practice presenting.

A huge thank you to my committee members Dr. William Ricke, Dr. Robert Lipinski, Dr. Jyoti Watters, and Dr. Lisa Arendt. You were a great help on research direction and a good motivation to complete experiments. Thanks for being supportive and believing in my ability as a scientist and being just the right amount of scary. Further, I’d like to thank the Molecular and Environmental Toxicology program for providing valuable foundational courses, teaching experience, valuable seminars, and useful professional development activities. I acknowledge the

MET course administrator Mark Marohl for always being supportive and always listening to my problems and offering the best advice. Without your assistance and support, my mental health would definitely have taken a beating.

I would like to also acknowledge my parents Glenn and Kathy Turco, family, and my graduate school, undergraduate, and high school friends who have supported me through this journey. Thank you to my bio baes, Morgan Walcheck, Lily Gonzalez, and Maisie Dantuma. Morgan, we will take over the world someday, thanks for always being the President to my vice president. Lily, thanks for going on lunch time walks and always being there when I needed you. You always know the right things to say. You all have been my rocks and I couldn't have made it through without necessary ice cream breaks, craft time, and your friendship. I would also like to thank my wonderful boyfriend, Adam Luthin, for being a tireless cheerleader and always being there to talk me through anything. Through endless phone calls, text messages, video calls, and ranting dinner dates, I could not have made it through without you. Thank you for always supporting me and putting me in check when I start to catastrophize things.

Lastly, I would like to thank Dr. Chad Vezina, my exceptional PhD mentor. Graduate school would have been an entirely different experience without your positive outlook, mentorship, and sense of humor. I would not be the scientist I have become without your insights, knowledge, patience, and advice. I have learned so much from you not only about science, but how to mediate conflict effectively, and how to be a good person. I always said if I could leave my PhD being 1/4th as good of a person as you are, I would be doing very well. I don't know if I've accomplished that, but thanks for setting the best example. I've accomplished so much from winning awards, publishing papers, and getting a grant funded, finding a job, and I could have done none of it without you, Chad. I hope every future graduate student has a mentor that invests so much time and energy into creating successful scientists. I will forever benefit from your guidance as I take it with me in the next step of my career. Thank you infinitely for everything and I appreciate everything you do.

Abstract

Lower urinary tract dysfunction (LUTD) is characterized by symptoms including weak stream and increased urinary frequency. LUTD affects most aging men, commanding billions in annual health care expenses. Although benign prostatic hyperplasia was originally thought to be the only risk factor, new evidence suggests additional mechanisms contribute to LUTD. Exposure to the persistent environmental contaminant 2,3,7,8 tetrachlorobenzo-*p*-dioxin (TCDD), during development and via lactation, thickens prostatic smooth muscle in non-human primates and worsens LUTD in adult mice. TCDD-mediated prostatic smooth muscle thickening is likely important because smooth muscle dysfunction is proposed as a cause of LUTD and is a target for current therapeutics. Here, we identified two mechanisms by which aggregate prostate smooth muscle tone may be increased in men: (1) by changes in circulating testosterone and estradiol concentrations, such as those that occur during aging, and which impair muscle relaxation, and (2) by chemical exposure during *in utero* development, which increases the density of axons that drive prostatic smooth muscle contraction. These studies establish several novel methods including an unbiased method for axon quantification tissue sections, a genetic method in which fluorescent encoded calcium sensors are deployed in prostate smooth muscle to quantify muscle dynamics, and a real-time imaging method that uses contrast-enhanced ultrasound to measure fluid dynamics in the urethra of anesthetized mice. The new assays developed in this dissertation build a solid foundation for the future assessment of interactions between the autonomic nervous system, prostatic smooth muscle, and urethral fluid dynamics. The new assays were also instrumental in shifting the paradigm for how LUTD emerges and progresses. A male's environment is generally accepted as a modifiable LUTD risk factor, but the focus has been inappropriately limited to the 5^{th}+ decade of life when male LUTD becomes clinically evident and worsens with age. This dissertation offers evidence that a male's environment can influence LUTD beginning in the womb.

Table of Contents

List of abbreviations (listed alphabetically)

ACTA2	Smooth muscle alpha actin- 2
ADRA1a	Alpha-1 adrrenoceptors
ANOVA	analysis of variance analysis
AUA	American Urological Association
ARTN	Artemin
AR	Androgen receptor
ASIC	Acid sensing ion channels
BPA	Bisphenol-A
BPH	Benign prostatic hyperplasia
BMI	Body mass index
CGRP	Calcitonin- gene related peptide
CDH1	E-Cadherin
DPC	Days post conception
E2	17B- estradiol
E	Embryonic Day
ER	Estrogen receptor
GCaMP	Genetically encoded calcium sensors
GPER	G protein coupled estrogen receptor
IPSS	International prostate symptom score
IUL	*In utero* and lactational
KRT5	Keratin 5
LUTD	Lower urinary tract dysfunction
OVX	Ovariectomy
P	Postnatal Day
PDE-5	Phosphodiesterase type 5

Ppp1r12a	protein phosphatase 1 regulator subunit 12a
Ppp1r12b	protein phosphatase 1 regulator subunit 12B
Ppp1r12c	protein phosphatase 1 regulator subunit 12c
Ppp1r16a	protein phosphatase 1 regulator subunit 16a
Ppp1r16b	protein phosphatase 1 regulator subunit 16b
SYP	Synaptophysin
SE	Standard Error
SERM	Selective estrogen receptor modulators
TCDD	2,3,7,8- tetrachlorodibenzo- p -dioxin
TUBB3	Class III B- tubulin
T	Testosterone
TH	Tyrosine- hydroxylase
TRP	Transient receptor potential
UGS	Urogenital Sinus
UPK3	Uroplakin III
UV	Ultraviolet
VaCHT	Vesicular acetylcholine transporter
VSA	Void Spot Assay

Chapter 1: Introduction- Developmental Origins of Health and Disease- Perinatal Environmental Toxicants and Visceral Organ Function.

Adapted from Turco AE and Vezina CM. *Impact of androgens and estrogens on bladder and lower urinary tract function*. Neurourology of the Bladder. Elsevier. Under review. March 2021.

Introduction

Perceived contributions of thesis

My dissertation research focuses on elucidating novel mechanisms of prostate smooth muscle dysfunction as a cause of lower urinary tract dysfunction (LUTD). LUTD occurs in most aging men and includes straining to urinate, increased urinary frequency, and weak stream. Prostate smooth muscle has been hypothesized to cause lower urinary tract dysfunction because alpha-1 adrenergic antagonists, drugs prescribed to relax prostate smooth muscle, alleviate LUTD in some men.

The prostate is comprised of numerous cell types including epithelial cells, fibromuscular cells, perivascular cells, and axons (1). Smooth muscle myocytes reside in prostatic stroma and contract to expel prostatic fluid during ejaculation. Noradrenergic axons regulate prostate smooth muscle contraction. Men with LUTD often have increased autonomic activity but the organization, development, and distribution of axon subtypes in the prostate is not fully understood. A neuroanatomical map of normal healthy prostate in mice, which are commonly used to model LUTD, was needed to begin to understand whether changes in the patterns or abundance of axons contribute to LUTD. In chapter 2, I present a neuroanatomical map of axons in developing and adult mouse prostate. We mapped the normal innervation patterns of noradrenergic, cholinergic, and sensory axons. We determined that axons begin to innervate the prostate at embryonic (E)13.5 and their density increases until at least early adulthood. Autonomic axon (noradrenergic and cholinergic) density is homogeneous across the proximodistal axis of adult mouse dorsal and ventral prostate lobes. Sensory axons are most dense in the proximal region and less dense in the distal regions of dorsal and ventral prostate. Our mapping study was foundational to future studies in this dissertation. Determining when axons develop, how their density changes during development, and how they are distributed across prostate ducts enabled us to test whether environmental chemical exposures drive abnormal neuroanatomical development in the prostate. We also made the surprising and important finding that prostatic

axon density does not decrease during the postnatal period. Axons in most tissues undergo postnatal pruning, but in prostate their density either continues to increase or plateaus. Thus, factors that influence prostatic axon density in the perinatal period have the potential to cause durable changes, perhaps even lifelong changes to prostatic muscle and urinary voiding function.

New studies by our group and others support the hypothesis that perinatal exposure to environmental chemicals is a risk factor for male urinary voiding dysfunction in advancing age. One study found that exposure to 2,3,7,8-tetrachlorodibenzo-p-dioxin (TCDD) (a ubiquitous environmental contaminant) *in utero* and during lactation (IUL) exacerbated urinary voiding dysfunction in a susceptible mouse model (2). The same group showed that TCDD exposure thickens mouse prostate smooth muscle, a potential sign of activity induced hypertrophy. In chapter 3, I explored the innovative idea that TCDD exposure increases the prostatic density of noradrenergic axons during perinatal development and persisting into adulthood. TCDD-induced changes to prostatic neuroanatomy appear to be functionally significant because prostatic smooth muscle from TCDD exposed mice is more sensitive to axon-evoked contraction. The prenatal period between E13.5- E17.5 is the critical period for this TCDD action, and it appears that TCDD mediates its actions on prostate neuroanatomical development by altering the abundance of a neurotrophin, artemin. Our studies focused on one environmental chemical, but they raise questions about whether other chemicals and dietary factors could also influence neuroanatomical development of the prostate and other urinary tract organs.

Plasma concentrations of testosterone (T) decrease while estrogen (E2) concentrations increase as men age. These aging-related endocrine changes can be recapitulated in young male mice by delivering subcutaneous slow-release hormone implants, which increase bladder volume, urinary frequency, and hydronephrosis incidence (3). It was shown previously that IUL TCDD exposure, followed by exposure to exogenous T+E2 in adulthood, causes male mice to experience exacerbated urinary dysfunction (2). The previous study was conducted in mice that were genetically predisposed to prostate neoplasia and cancer. Because prostate hypertrophy is

by itself a mechanism of urinary voiding dysfunction; the previous study did not address whether TCDD exacerbates urinary dysfunction through a malignant or non-malignant mechanism. In chapter 4, I show TCDD acts through a non-malignant mechanism to cause voiding dysfunction in T+E2 treated mice and can change urinary voiding patterns even in the absence of exogenous T+E2 treatment. We identified proteins in prostate that were uniquely up- or down-regulated by TCDD/T+E2 and T+E2 alone. The significance of our work is it reveals interactions between environmental and endocrine factors, potentially mediated by independent mechanisms, to impair male urinary voiding function.

Sustained release subcutaneous implants of T and E2 increase urinary frequency, bladder volume, and hydronephrosis incidence in male mice but mechanisms were not known. In chapter 5, I test the hypothesis that T+E2 interferes with prostatic smooth muscle relaxation, driving a state of tonic muscle contraction that interferes with urine outflow through the prostatic urethra. Using two novel methods, contrast enhanced ultrasound and genetically encoded calcium sensors bred into prostate smooth muscle, I established that T+E2 interferes with prostate smooth muscle relaxation. I showed that T+E2 exposure downregulates, one subunit of the myosin phosphatase responsible for prostate smooth muscle relaxation, *Ppp1r12b,* which impairs prostate smooth muscle relaxation. *Ppp1r12b* null male mice partially phenocopy T+E2 exposed mice by also exhibiting impaired prostate smooth muscle relaxation. The historical paradigm is T and E2 obstruct voiding by sensitizing to adrenoreceptor-mediated muscle contraction. Our findings are important because they draw new focus on impaired smooth muscle relaxation as a clinically relevant and hormone sensitive mechanism of bladder outflow obstruction. PPP1R12B may be an important druggable target, due to its specificity in prostate. PPP1R12B inactivation could potentially prolong muscle contraction and increase urethral tone in individuals with stress urinary incontinence. PPP1R12B activation may be an effective strategy to drive prostatic muscle relaxation and alleviate urinary obstruction.

The following sections provide a survey of current state of knowledge on mechanisms of prostate smooth muscle dysfunction.

Overview

Almost all men will develop lower urinary tract dysfunction (LUTD) by the age of 80 (4). In fact, one out of every four men in the United states is currently being treated for LUTD (5). Urinary symptoms associated with LUTD are classified as obstructive voiding symptoms (including hesitancy, poor or intermittent stream, straining, and incomplete bladder emptying, or dribbling) and irritative symptoms (increased frequency, urgency, and nighttime urination) (6). Symptom severity is graded using the International Prostate Symptom Score (IPSS) or the American Urological Association (AUA) symptom index. Symptom severity and rate of symptomatic progression differs among men. Some risk factors for LUTD include increased age, sedentary lifestyle, stress, and smoking (7). Further, ethnicity can be a risk factor with Hispanic and black men at an increased risk for moderate LUTD while Asian men are at a lower risk for developing LUTD compared to white men (8). Causes of LUTD are unknown but are considered multi-factorial. The prostate is hypothesized to contribute to LUTD because, if removed, symptoms are eliminated (9). Below, I describe the prostate and the mechanisms proposed to contribute to LUTD.

Prostate development

The prostate is among relatively few anatomic organs that continue development throughout life. The processes of forming prostatic neostructures in fetuses and in males of advancing age are so similar that some have suggested benign prostatic hyperplasia arises from a reawakening of prostate development signaling pathways (10–12). Prostate development has been studied in the greatest detail in mouse and rat and closely parallels human prostate

development. A parallel chronology of human and mouse prostate development can be found in a review by Cunha G *et al* (12).

Testicular androgen production, beginning at 13.5 days post conception (dpc) in mice and 10 weeks of gestation in humans (13–15) initiates prostate development from a swelling of the urinary tract known as the urogenital sinus (UGS). Androgens activate androgen receptors to confer inductive activity to UGS mesenchyme. Inductive UGS mesenchyme is marked by wnt inhibitory factor 1, steroid 5 alpha reductase type 2, and androgen receptor (16, 17).

Studies of prostatic bud patterning have been important in elucidating factors that support expansion of fetal prostatic progenitors. The initial formation of prostatic buds is stochastic. It occurs in wildtype male and female mouse fetuses and *Ar* mutant male mouse fetuses, suggesting that androgens are not required for this initial phase of prostate development (18–20). Certain prostatic buds are stabilized (21) in a specified pattern for continued outgrowth (22), in part through activation of beta-catenin signaling in prostatic bud epithelium (23). Testicular androgens, acting on androgen receptors in UGS mesenchyme (24), are essential for stabilization and continued outgrowth of prostatic buds. Even small stochastic buds in the female UGS can be driven by androgens to form prostate (19, 25). There is some evidence the fetal prostate epithelial cell DNA methylation landscape determines when it becomes competent to respond to signals from inductive UGS mesenchyme, as removal of DNA methyl marks can drive precocious prostate development (26).

The UGS begins as a pseudostratified epithelial tube consisting of what appears to be a homogenous population of e-cadherin+ epithelial cells and mesenchyme (23). Neuroendocrine cells migrate into the prostate from ectoderm-derived neural crest and may also differentiate from endoderm-derived UGS epithelium as early as E13.5 in mice and gestation week 9 in humans (27, 28)(29). CGRP, VaCHT, and TH+ axons first develop in prostate between E13.5 and E14.5 (30). See chapter 2 for more details on this study.

Prostatic cell types: A new interest in axons

The prostate gland is heterogeneous and comprised of axons, fibromuscular cells, vascular-associated cells, and epithelial cells (1). LUTD can be caused by benign prostatic hyperplasia (BPH) which is characterized by a nodular pattern of epithelial and fibromuscular cell proliferation (31). BPH is a multifactorial process involving several cell types including basal epithelial cells, luminal epithelial cells, stromal cells, inflammatory cells, and extracellular matrix (32). Though epithelial and stromal cells are the historical focus of BPH and LUTD research, neurons that innervate the prostate have arisen as an additional cell type of interest. Axons have been linked to the growth and dissemination of prostatic tumors (33) and may also drive benign prostatic growth to cause BPH, though this possibility has not been investigated.

Axons are distributed throughout prostatic stroma and epithelium and can secrete growth factors that contribute to prostate growth and function (34). In fact, men with spinal cord injuries have significantly smaller prostates than able bodied men and almost never have LUTD (34). Numerous axon subtypes innervate the prostate including autonomic (noradrenergic, cholinergic, ekephalinergic, nitrigenic) and sensory (peptidergic, purinergic). Autonomic axons regulate prostate epithelial cell secretory function while sensory axons relay environmental information (presence of noxious stimuli, for example) to the brain.

There is some evidence linking prostatic neuroanatomy to histological and physiological features of LUTD. Enkephalinergic and nitrigenic axons, which relax prostate smooth muscle, are less abundant in some men with BPH (35–37). Neural nitric oxide synthase, localized to prostate smooth muscle nerve fibers, is less abundant in BPH lesions than in histologically normal prostate tissue from the same men (37). Autonomic nervous system hyperactivity is significantly associated with LUTD severity (38) and there is evidence supporting the possibility that a systemic imbalance of autonomic activity underlies LUTD in some men (39). Clearly, prostate axon function is needed for prostate health and changes in axon density can contribute to disease. As a result, many studies have mapped prostatic neuroanatomy in healthy animals and humans to

understand normal innervation and determine whether changes in prostatic neuroanatomy can drive LUTD.

Most studies of prostate neuroanatomy were conducted exclusively in adults because LUTD is a disease of aging. However, several classical diseases of aging (cancer, heart disease, diabetes) have been linked to maternal diet and environment during the gestational and early postnatal periods (40). Prostatic axon patterns during pre- and early postnatal development are therefore of interest. We found that noradrenergic, cholinergic, and sensory axons first enter the mouse prostate at E13.5 (before prostate ductal budding) and their density continues to increase during the early postnatal period and into adulthood (30). The density of autonomic (noradrenergic and cholinergic) axons is homogenous along the proximodistal axis of adult mouse dorsal and ventral prostate whereas sensory axons are denser in the proximal region of dorsal and ventral prostate (30). Spinal connections of pelvic autonomic nerves innervating the prostate were mapped in rats (41). Most sympathetic noradrenergic prostate projecting neurons were noradrenergic, but some were non-noradrenergic vasoactive intestinal peptide neurons. A study of cat prostate showed that most sensory axons derive from sacral dorsal root ganglia and consist of nociceptive and non-nociceptive axons, and that there are three sources of autonomic efferent axons (42). Another study showed that noradrenaline and other neurotransmitters regulate prostatic smooth muscle tone, which is a therapeutic target for LUTD (43).

Human prostate mapping studies have been used to determine axon density, location, and functional significance and to understand how to certain axons maintain erectile function (44). A nerve map from cadaver specimens showed that periprostatic nerve fibers were evenly distributed in lateral and dorsal prostatic regions but were thinner in ventral region (45). Another study found somatic nerves account for almost 5% of all periprostatic nerve fibers and due to their location are at increased risk for injury during radical prostatectomy (46). A map of trizonal neural architecture was developed from cadavers and from patients undergoing radical proctectomy. Three neurovascular plates were identified, the proximal, predominant, and anterior plates and

these studies helped to standardize nerve-sparing robotic prostatectomies (47). One study used polarization-sensitive optical coherence tomography to image prostatic nerves non-invasively and confirmed structures by histology. They found that prostatic fibrous nerve anatomy differs among men and if imaged prior to surgery, could guide axon sparing and improve surgical outcomes (44). Additional studies visualized neurovascular bundles using photoacoustic and thermal imaging or interoperative nerve stimulation (48–50). Though the studies discussed here have been paramount to improving surgical outcomes for radical prostatectomy, they have focused on peripheral nerve bundles that control erectile function. A more comprehensive analysis, which includes nerve fibers that regulate prostate function, is needed to understand variability across the human population and to test whether neuroanatomical features associate with a male's risk of developing LUTD or developing severe LUTD. In addition, there is growing interest in understanding the entire peripheral nervous system for the potential of neurostimulation or brain stem medicine. Understanding spinal connections to the prostate and which axons are required for bladder or prostate contraction are critical to generate stimulators that could be placed at various spinal cord levels and used to treat diseases including LUTD. Specifically, one goal is to develop stimulators for urination in patients with spinal cord injuries.

Novel causes of LUTD: Size does not always matter

Does size matter?

Most men will experience LUTD during their lifetime. Despite the prevalence, LUTD causes are unknown. Historically, prostate enlargement was considered the main cause of bladder outlet obstruction (4). As a result, drugs to reduce prostate size were designed to treat LUTD. Five-alpha reductase inhibitors reduce prostate volume by blocking production of dihydrotestosterone, which provides trophic support to the prostate (51). One study measured prostate size via MRI and correlated it with age, voiding symptoms, and sexual health and

determined prostate volume correlates with LUTD in most individuals (52). The study also showed some outliers indicating prostate volume that did not always correlate with LUTD severity (52, 53). Resultantly, there must be additional causes of LUTD.

Do men with LUTD have increased smooth muscle tone?

Approximately 20-80% of hyperplastic prostate tissue is comprised of stromal and epithelial elements (54). Half of the stromal hyperplastic tissue is comprised of smooth muscle (54). Recognizing the potential importance of prostate smooth muscle in LUTD, researchers began studying it. Human prostate smooth muscle was first recognized to be innervated by noradrenergic axons in 1968 by HG Baumgarten et al at the University of Lund in Sweden (55). In this study, sections of human LUT tissue were stained and fluorescently imaged to identify the density of noradrenergic axons in prostate (55). This was the first study to report axon subtypes in human prostate tissue. To further that study, in 1973 Shlomo Raz et al were the first group to show noradrenaline activates rat ventral prostate contraction (56). They used muscle bath studies to determine that rat ventral prostatic smooth muscle was rich in alpha-adrenergic receptors, cholinergic receptors were moderately present, but beta-adrenergic receptors were absent (56). Next, in 1975, Marco Caine extended this finding and identified that noradrenaline, the neurotransmitter released from noradrenergic axons and that activates alpha-adrenergic receptors, activates human prostate gland and capsular tissue contraction (57). Transverse sections of the glandular component of human prostate were isolated during surgery for BPH and evaluated for isometric contractions using tissue bath (57). Noradrenaline stimulated human prostatic tissue contraction and an alpha-adrenergic antagonist prevented contraction (57). Interestingly, epithelial nodules from BPH patients were also tested for neurotransmitter contraction and were resistant to noradrenergic, cholinergic, and beta-adrenergic stimulation (57). Caine is the first to propose that elevated prostatic smooth muscle tone may be responsible for acute urinary retention in BPH (57).

In 1976, Caine took his studies one step further to design the first case study to test if treatment with alpha-adrenergic antagonists improved acute urinary retention in men (58). In this study, several patients presenting with urinary frequency and almost complete urinary retention due to enlarged prostates and were used to test whether alpha-adrenergic antagonists improved bladder emptying (58). Phentolamine IV and subsequently phenoxybenzamine (nonspecific alpha-adrenergic antagonist) was administered orally and all subjects examined had a significant improvement of urinary symptoms with increased flow rate, shortening of bladder emptying time, and complete bladder emptying measured via uroflowmetry and cystograms (58). Lastly, Lepor and Shapiro used radioligand binding studies on epithelial BPH nodules to demonstrate the presence of alpha 1 and 2 adrenoceptors in human prostate (59). This was the last study to further to push for the production of alpha-1 adrenergic receptor antagonists in the treatment of LUTD.

Interestingly, pressure flow urodynamic studies have been performed in men by filling the bladder with saline and measuring the pressure along sections of urethra. These studies show that the prostatic urethra has the highest pressure along the male lower urinary tract. Interestingly, alpha-1 adrenergic antagonists, that reduce prostate smooth muscle contraction, decrease pressure in the prostatic urethra without changing prostatic volume. Therefore, increased smooth muscle tension can be pharmacologically treated with alpha-1 adrenergic antagonists.

Terazosin, doxazosin, and tamsulosin are the most commonly prescribed alpha-1 adrenergic receptor antagonists (alpha blockers). When given at the correct dosage, alpha blockers improve IPSS by 30-45% and improve urinary flow by 15-30% (60) and their side effect profile is relatively narrow (61). Side effects of alpha blockers including hypotension, constipation, impotence, and headaches (62, 63). Alpha-1-adrenergic receptor antagonists are the first drug prescribed after watchful waiting in the clinic (64). If BPH is suspected, a patient will receive a 5-alpha reductase inhibitor because alpha-1-adrenergic receptor antagonists do not reduce prostatic volume (65). Combining an alpha blocker with a 5 alpha-reductase inhibitor reduces overall clinical progression of LUTD compared to monotherapy (66).

Many mechanisms have been proposed for prostatic smooth muscle hyperactivity. Prostate smooth muscle develops spontaneous myogenic tone which is controlled by autonomic innervation (67). It has been reported an age- related increase in prostatic ATP cleavage drives purinergic nerve activation and prostate smooth muscle contraction (67). Excessive autonomic activity, resulting in increased smooth muscle tone in the prostatic transition zone, is another potential mechanism of prostatic muscle contraction (68, 69). Interstitial cells of Cajal, which harbor smooth muscle pacemaker activity, may also drive prostatic smooth muscle hyperactivity (70). LIM kinases have also been linked to prostatic smooth muscle activity (71). The studies described above, and many others focus on mechanisms of prostate smooth muscle contraction. There has been limited focus on the alternate process of smooth muscle relaxation and its role in male LUTD. In this dissertation, we discuss an endocrine-mediated downregulation of a myosin phosphatase subunit. Myosin phosphatase participates in smooth muscle relaxation by dephosphorylating myosin light chain kinase. Our results raise new questions about whether prostatic smooth muscle is maintained in a state of tonic contraction in some men because it cannot relax, and this paradigm opens a new direction of investigation in LUTD research.

Does increased smooth muscle thickness increase activity?

Autonomic activity is associated with muscle thickness in many organs including the rat caudal artery (72). Smooth muscle comprises an estimated 24% of human prostate stroma (73). While aging increases the abundance of prostatic stroma relative to prostatic epithelium (74), relatively few studies have examined whether autonomic activity is associated with prostatic smooth muscle thickness. One study found ventral prostate size was increased and the stroma was thickened in hypertensive rats, which have excessive sympathetic activity (75). Another study identified an inverse relationship between prostatic smooth muscle thickness and urine flow through the prostatic urethra (76).

How does exposure to environmental chemicals impact prostate smooth muscle abundance or activity?

An environmental influence over prostatic smooth muscle tone may contribute to the onset, severity, or progression of LUTD. It has been shown that exposure to environmental chemicals during development can predispose to development of adult diseases. In LUTD, exposure to TCDD can exacerbate voiding dysfunction and thicken prostate smooth muscle (2). Noradrenergic axons regulate prostate smooth muscle contraction. In this dissertation, we hypothesize TCDD increases the density of noradrenergic axons which increases stimulation and prostate smooth muscle thickness.

TCDD is a polychlorinated dibenzo-*p*-dioxin that is colorless and odorless solid at room temperature. It is produced as the unwanted byproduct of burning organic materials or during bleaching processes. Phenoxyherbicides, chlorophenols, hexachlorophene and other related compounds have all been found to be contaminated with TCDD (77). Humans are exposed to TCDD through inhaling dust, drinking ground water, or touching pesticides or herbicides that are contaminated with TCDD (78). Most commonly, exposure occurs through eating meat, dairy products and fish containing TCDD. Further, TCDD is lipophilic so can be found in the greatest concentration in body fat and the liver. The half-life of TCDD in adults is about 9.6 years and is strongly associated with age (79). In the environment TCDD is often found in soil surface. The half-life of TCDD in surface soil is estimated to be 9-15 years while subsurface soil is estimated to be 25-100 year (78). It has diverse health effects, especially to developing organisms (77). Acute exposure to TCDD in humans can use nausea, vomiting, headache, and irritation. Chronic exposure can lead to chloracne, weight loss, and altered liver, kidney, immune, and neurotransmitter function. It is teratogenic in rats and mice and can cause birth defects in human populations and is a human carcinogen (80).

TCDD is toxic to the vertebrate nervous system (81–83). For example, TCDD disrupts neural control of temperature regulation in golden hamsters and increases activity of axons

controlling rat aortic smooth muscle tone (81, 84). TCDD causes neuropathy of peripheral nerves in red sea bream embryos. Suspected TCDD exposure in humans has been associated with abnormal electrophysiological parameters including reduced sensory action potential, reduced motor conduction velocity, and reduced compound muscle action potential (the result of damage to nerves outside the brain and spinal cord) (85–87). TCDD exposure in rats sensitizes to the satiating effects of glucose and fructose, indicating that TCDD may make the gut hypersensitive to stimuli (88). The impact of TCDD exposure on noradrenergic innervation of visceral organs has not been thoroughly examined.

Alterations in the density of autonomic axons in visceral organs has been proposed as a mechanism of several diseases. Increased density of adrenergic nerve networks is found in patients suffering from ulcerative colitis (89). Sympathetic fiber density is a suspected risk factor for lung cancer (90). Autonomic nerve density is reduced in the bladder in response to bladder outlet obstruction (91). We show that TCDD exposure increases noradrenergic axon density in mouse prostate smooth muscle and sensitizes prostatic smooth muscle to axon-evoked contraction (92). The impact of perinatal TCDD exposure on noradrenergic axon density in human prostate has not been examined.

Effect of androgens and estrogens on bladder and lower urinary tract function

Aging is inextricably linked to benign urinary voiding dysfunction, including stress incontinence, overactive bladder, and prostate-related disease. Aging-related changes in sex hormone concentrations are clear contributors to urinary disease processes. In men, testosterone plasma concentrations decrease while estradiol concentrations increase with age. In women, estradiol concentrations decrease while testosterone concentrations increase with age (93). Here, we outline known impacts of testosterone and estradiol on female and male bladder anatomy, physiology, and benign bladder-related disease. We also summarize emerging evidence that

environmental chemical exposures modulate sex hormones to influence bladder structure and function.

Sex differences in bladder histology

Sex differences in male and female lower urinary tracts are typically classified as anatomical or physiological, but differences also exist at the cellular level. Understanding these differences is critical because sex and gender can impact diagnosis and treatment of urinary dysfunction (94). Many bladder diseases are rooted in cellular irregularities. We begin by describing bladder histology and influence of genetic sex and sex hormones on bladder cell behavior and function.

Sex differences in anatomy and physiology

The bladder is divided into multiple anatomical regions that differ with respect to innervation, muscle thickness, and muscle expression of neurotransmitter receptors. The trigone is a triangular region near the junction of the bladder and urethra that contributes to urine storage. Left and right lateral walls straddle the trigone, the dome constitutes the roof (dorsal aspect) of the bladder, and the posterior wall (bladder apex) is joined by the umbilical ligament to the umbilicus (95). A cross section of the bladder reveals a multilayered bladder wall comprised of a specialized epithelium that forms a barrier between urine and underlying tissue, lamina propria, which is enriched in blood vessels and sensory axons, and smooth muscle (also known as detrusor) (96).

Sex differences in histology

The mature detrusor contains three layers. Longitudinal and circular cells make up the layers and collagen fibers are distributed throughout (97). Sex differences exist in adult detrusor. The muscle is thicker in men and the pressure required for bladder emptying is also greater in adult men than in adult women (98). Even though sex hormones are present at the onset of gonadal steroidogenesis in the fetus (99), and in sufficient concentrations to masculinize or

feminize internal and external genitalia, bladder muscle sexual dimorphism does not become grossly apparent until later in life. Questions remain about when bladder sex differences emerge. One possibility is hormones gradually impact the bladder and when directly exposed to high concentration of sex hormones; divergence occurs. Another possibility is bladder sexual dimorphism may be driven by secondary processes. The factors that support sex differences in adult bladder muscle function have not been fully identified, and further studies are needed to identify if direct or indirect exposure is required.

Muscle and collagen

Exogenous estrogens and androgens influence additional aspects of bladder histology beyond the detrusor. Here, we discuss the impact of estrogens and androgens, individually and in combination, on bladder muscle and collagen. **Table 1** summarizes the impact of sub and supraphysiological estrogens and testosterone described in this section. Estrogens are clearly important for the maintained bladder muscle and wall homeostasis. Ovariectomy (OVX) in mice and rats degenerates the female rat detrusor: gaps appear between muscle fascicles and bladder weight decreases (100, 101) (**Table 1**). OVX also predisposes to bladder to inflammation, characterized by infiltrating leukocytes, and collagen accumulation. OVX furthermore causes detrusor atrophy and decreases bladder wall thickness (100–102)(**Table 1**). Supplementary estrogens increase rat bladder collagen fiber density and bladder cell proliferation and reduce bladder cell apoptosis (103, 104)(**Table 1**). The bladder response to estrogens is non-monotonic and a single 1 mg/kg dose of estradiol benzoate (a relatively high dose for rats) reduces detrusor thickness in OVX rats, suggesting very high concentrations of supplementary estrogens may be deleterious to bladder function in aging women (100). These studies are important because they support the idea that estrogens are required for bladder homeostasis and supplementation can protect from physiological decline due to an aging-related loss in circulating estrogens in post-menopausal women (102, 103). Importantly, the relationship between estrogen dose and bladder

response appears to be non-monotonic, suggesting the need to achieve an optimal estrogen concentration for homeostatic bladder maintenance.

An aging-related decline in circulating testosterone concentrations in men is linked to a decline in bladder muscle function, a reduction in bladder muscle abundance and an increase in bladder collagen content (105)(**Table 1**). The concentration of circulating testosterone in men declines by 1% a year after 40 years of age (106). There is experimental evidence that testosterone supplementation may be beneficial to bladder health in aging men. Castration of young mice, to simulate aging-related hypogonadism, causes significant bladder atrophy, decreases smooth muscle thickness, and increases bladder collagen content (**Table 1**). Testosterone treatment of castrated young adult rats increases bladder capacity, increases bladder smooth muscle content and reduces bladder collagen abundance (107)(**Table 1**). One study examined bladder histology and mechanical properties in aged (18-20) month old control rats and in rats treated with testosterone undeconoate (androgen and anabolic steroid medication) (50 mg/kg) (108). The outcome of this study supports the idea that testosterone replacement may afford therapeutic benefit in men with voiding dysfunction by increasing bladder smooth muscle (107, 108). However, another study reported a lower testosterone dose (10 mg/kg) contributed to bladder fibrosis after bladder outlet obstruction in castrated mice, indicating the bladder responds to testosterone at the cellular level (109)(**Table 1**). The relationship between testosterone concentration and male bladder response is likely to be non-monotonic, such that high doses may be therapeutic whereas low doses are deleterious.

Changes in basal plasma concentrations of testosterone and estradiol cause the bladder to remodel. Male rabbits were castrated or sham operated and administered daily injections of testosterone, polyestradiol, or progesterone (110). Polyestradiol increases bladder capacity and compliance while testosterone and progesterone reduce both parameters in male rabbits (110). Another study assessed the impact of testosterone on voiding in female and male mice. Females

typically void in a stream-like pattern while males exhibit more droplet-like voids. Mice were castrated and treated with exogenous testosterone or estradiol to determine the influence on voiding function. Castration feminized male urinary physiology while exogenous testosterone masculinized female urinary voiding physiology (111). The urethral histology of these mice were analyzed in a follow-up study. Exogenous testosterone increased urethral epithelial cell count in female mice but did not masculinize female urethral histology (112). None of the treatments feminized male urethral histology or increased urethral epithelial area. Another study found the combination of androgen and estrogen increased bladder blood vessel density, urothelial thickness, and number of muscle fibers (104). Estrogen and testosterone and the concentration ratio of both hormones in circulation influence bladder muscle health.

Urothelium

The urothelium is a specialized epithelium of the bladder and consists of at least three cell types: superficial cells (also called umbrella cells), intermediate cells and basal cells. Bladder superficial epithelial cells synthesize proteins called uroplakins, which assemble to form hexagonal structures contributing to the bladder permeability barrier (113). A role for urothelial cells and their uroplakin products in conferring sexually dimorphic bladder function was revealed by depleting Uroplakin III (*Upk3*) in mice (114). Male *Upk3* null mice are prone to urinary retention, increased bladder pressure and are susceptible to bladder decompensation (114)(Table 1). Yet, bladder function in female *Upk3* null mice is remarkably normal (114)(Table 1). It is unclear how sex differences in *Upk3* null mice derive and whether they are driven by differential responses to a loss of barrier function or by a cell specific signaling mechanism.

Male and female bladders differ in responsiveness to changes in urinary pH. Acid sensing ion channels (ASIC) and H+ gated ion channels maintain pH within the urothelium (115). ASIC1 is more abundant in male mouse urothelium while ASIC2 is more abundant in female mouse urothelium. Although the functional significance of sex differences in bladder ASIC expression are

not fully known, it has been hypothesized that ASICs control sensitivity to pathogens. The acidity of urine and the presence of some small molecules may facilitate the growth of bacteria in the urinary tract to cause urinary tract infections. Recent studies using female dogs found the more acidic the urine, the greater *E. coli* growth, and the more alkaline the urine, the lower *E. coli* bacterial growth (116). Clinically significant urinary tract infections are more common in women than men and sex hormones are at least partially responsible. Supplementary estrogen mediates a urothelial defense against uropathogenic *E. coli* (117, 118). Conversely, depletion of gonadal estrogens by OVX sensitizes the bladder to endotoxin and increases urinary frequency (119).

Hormone Receptors

Male canine estrogen receptor (ER) immunostaining intensity within the lower urinary tract is most abundant in the prostatic urethra (120). The ER staining pattern in males is comparable to females (120). However, males have a higher concentration of ER staining in the urethra than the prostate (120). The ER staining pattern in male and female dogs is consistent with the location of histological changes caused by estrogen administration (120). Androgen receptor (AR) expression is primarily located in urothelial cells of human tissue (121). AR expression has been widely characterized in bladder cancer, but few studies have examined sex specific expression in benign or normal tissue. Further studies are necessary to fill this gap and build the foundation for understanding sex differences in AR receptor density.

Single Cell RNA sequencing of bladder has helped identify transcriptionally unique cell types in human and animal models. Using this technique, it will be possible to define bladder cell populations that define normal and abnormal. It will also be possible to test whether testosterone and estradiol change bladder resident and inflammatory cell populations, as these changes may underlie hormone-mediated changes in bladder function.

Impact of testosterone and estradiol on smooth muscle physiology

Smooth muscle

There is evidence for a role of testosterone and estradiol in smooth muscle physiology. Muscle cells in bladder are long spindle-shaped cells with a central nucleus, similar to those in other muscular organs. During bladder filling, smooth muscle cells relax, elongate, and rearrange to accommodate volumetric expansion (122). The micturition reflex generates a force and synchronously shortens muscle fibers quickly over a large area. The bladder contains both single and multiunit muscle units. Single units have sheets or bundles and cell membranes that have many gap junctions. Gap junctions are formed by connexin subunits and are low resistance pathways through which ions flow between cells to spread electrical signal rapidly through the tissue (123). Single unit muscle cells can sometimes exhibit spontaneous pace maker activation. Multiunit smooth muscle cells are comprised of muscle fibers or fiber bundles that operate independently. They are innervated by autonomic fibers and controlled through direct nerve stimulation. Multiunit smooth muscle cells exhibit no spontaneous activity (97).

During force generation and shortening of muscle, myosin cross-bridges with actin and hydrolyzes MgATP to produce MgADP and inorganic phosphate (Pi). Smooth muscle contraction is initiated by an increase in intracellular Ca2+ concentration. Ca2+ enters the cytoplasm through the cell membrane via Ca2+ channels or can be released from the sarcoplasmic reticulum (124). Calcium release is triggered by inositol trisphosphate via IP3 receptors and ryanodine receptors (125). Interestingly, stretch in rabbit urinary bladder smooth muscle cells can also activate Ca2+ release (126). In addition to Ca2+ storage and release, the sarcoplasmic reticulum has another important function which involves modulation of K+ channel activity to induce relaxation. Calcium activates contractile proteins via a phosphorylation pathway where Ca2+ binds to calmodulin and the Ca2+/calmodulin complex activates the myosin light chain kinase to phosphorylate the myosin regulator light chains (127). Relaxation is caused by dephosphorylation of the regulatory light chain via the myosin light chain phosphatase (97).

Testosterone and estradiol inhibit voltage operated Ca2+ channels essential for detrusor function (128). Estradiol decreases spontaneous phasic contractions from single unit smooth muscle cells and reduces nerve-evoked contractions in human detrusor strips. These activities are linked to a rise in depolarization-induced whole-cell K+ currents (129) and because they are rapid and abolished by paxilline, suggest a non-genomic mechanism on conductance voltage and Ca2+ activated K+ (BK) channels. However, estradiol and testosterone can act alone to influence bladder physiology as described in the sections below. Figure 1 summarizes the impacts of testosterone and estradiol on smooth muscle contraction and relaxation.

Estradiol influences the bladder's response to cholinergic stimulation. OVX significantly diminishes atropine-resistant stimulation in rats (101). OVX also increased the contractile response to carbachol, a response that is reversed by estradiol (102). OVX increases the bladder relaxation response to isoproterenol in female rats, but it is unknown whether testosterone or estradiol are driving these changes (102). OVX + testosterone increases the maximal contractile response of isolated bladder preparations to carbachol and electrical field stimulation. OVX + estrogen decreases urothelial damage, inflammatory cell infiltration, and decreases collagen accumulation caused by OVX (102). The smooth muscle contraction inhibitory effects of sex steroids may prove therapeutic in treating overactive bladder from elevated muscarinic or purinergic receptor activity (128). These phenotypes suggest menopause may cause significant structural and functional bladder problems that can be treated by combined estrogen and testosterone supplementation (101).

Testosterone concentrations are also critical to bladder muscle health, but testosterone may impact bladder function more than it influences structure (106, 130). A study delivered letrozole, a potent aromatase inhibitor, to adult female rabbits (131). Aromatase metabolizes testosterone into estradiol and aromatase inhibition increases the plasma concentration of testosterone. A week of letrozole treatment is sufficient to reduce female bladder smooth muscle contractile responses to ATP, carbachol, and electrical stimuli, increase bladder collagen density

and reduce bladder smooth muscle and bladder compliance (131). Bladder contractile responses returned to baseline 2-3 week after letrozole treatment. Overall, this study shows that testosterone may be just as important to the contractility of female bladder as estrogens and its actions are reversible. Testosterone appears to influence male and female bladder differently. In females, it reduces bladder contractility and response to stimuli and increases bladder collagen content. In males, testosterone relaxes bladder muscle, specifically the trigone, and reduces collagen content. The sexually dimorphic influence of testosterone on male and female bladders may help explain gendered bladder disease progression and indicate an interaction with other endogenous hormones or a concentration dependent impact on bladder function or histology.

Bladder outlet obstruction in aging males leads to bladder remodeling characterized by a loss of detrusor smooth muscle, an increase in bladder collagen content, and a decrease in voiding power (132–135). There is some evidence that testosterone replacement in aging males could protect against a decline in bladder function or even restore bladder function. Supraphysiological testosterone given in adulthood or during the pre-pubertal period reduces bladder collagen content and increases bladder capacity compared to castrated male rats (107, 136). Supplementary testosterone increases bladder capacity in aging men (137). The mechanism of testosterone activity is linked in part to its action on bladder tone, specifically in the bladder neck region where it serves to relax smooth muscle and promote bladder emptying. A study using isolated preparations of pig bladder neck showed that testosterone relaxes the bladder neck via mechanisms independent of the urothelium, AR, aromatase, 5α-reductase, NO synthase, COX and K (+) channels, and guanylyl cyclase but dependent on inhibition of extracellular Ca2+ L-type VOC channels (137).

Nerves

The bladder is innervated by many nerve subtypes and the composition and distribution of nerve fibers in the bladder differs between females and males. Innervation of the fetal urinary

bladder is established by 13 weeks post conception (138). In humans, the inferior hypogastric plexus contains sympathetic fibers originating from the hypogastric nerve and the sacral splanchnic nerve branching from the T11-L2 ganglia (139). The inferior hypogastric plexus also contains sympathetic fibers that derive from pelvic splanchnic nerves of the ventral rami of S2-4 (139). Nerve branches to the bladder in women originate from the inferior hypogastric plexus and distribute to the lateral surface of the bladder while independent branches follow the ureters from the hypogastric nerve to terminate in the trigone region (140). In males, the inferior hypogastric plexus is located on the dorsolateral side of the prostate and bladder, making the location of the hypogastric plexus lower in male than in female pelvises (140). Further, the independent branches running along the ureter are smaller and less present in males than females (140).

Pelvic ganglia provide motor nerve supply to reproductive organs and are sexually dimorphic. There are more pelvic neurons in males than females (141). In addition, males possess a higher proportion of noradrenergic neurons in the pelvic ganglia than females (142). Males also have a larger number of preganglionic neurons that exist in the lumbar spinal cord. Lastly, lumbar dorsal root ganglia are larger in males than females as a result of greater neuronal death in females (143). Rat dorsal root ganglia neurons express estrogen receptors and estrogens have been shown to up and downregulate one sensory axon subtype, calcitonin gene related peptide (CGRP) (144). Bladder projecting afferent neurons in lumbosacral dorsal root ganglia of female rats express estrogen receptor (145). Estrogen receptor (ERα and ERβ colocalization) is expressed in many sensory neurons in the upper lumbar or sacral ganglia (145). ER positive bladder projecting neurons that innervate the lower urinary tract are likely targets for circulating estrogens (145).

There are sex differences in the type and pattern of axons innervating the bladder. Although the bladder receives sparse noradrenergic innervation, the terminal ureter and its junction with the bladder (vesicoureteral junction) is richly innervated by noradrenergic axons. A study of male and female canine bladder revealed that noradrenaline is more abundant in the

proximal urethra and bladder dome than other bladder regions (146). Noradrenaline is more abundant in proximal urethra of males than females, but in the bladder base and distal urethra, noradrenaline is more abundant in females than in males (146). These data suggest that bladder sympathetic innervation is greatest in the proximal urethra and there is a sex difference in innervation (146). The male rabbit bladder is more sensitive to high frequency electrical stimulation than female bladder (147). Even though there are no sex differences in rabbit bladder sensitivity to phenylephrine (alpha-1 adrenoreceptor agonist) or bethanechol (cholinergic receptor agonist) stimulation (147), phentolamine (alpha adrenoreceptor antagonist) stimulates female rabbit bladder neck more than male bladder neck (147). Female rabbit bladders are more sensitive to isoproterenol-mediated relaxation than male rabbit bladders (148, 149). Overall, the differential responses to neuromodulatory drugs suggest sex differences in alpha adrenoceptors and beta- adrenoceptors but not alpha-1 adrenoceptors or cholinergic receptors.

Micturition reflexes can be influenced by circulating testosterone and estradiol concentrations. Noradrenergic pelvic neurons are dramatically impacted by castration. Androgens do not appear to affect bladder cholinergic axon activity, even though androgens do affect cholinergic axon activity in reproductive tissues such as penis and glandular tissues (150). A more recent study contradicts this and found testosterone reduces male rat bladder responsiveness to carbachol (cholinergic agonist) in a dose dependent manner (100-300 microM) and has a greater inhibitory response in older males than younger males, indicating receptor densities may change with age (151). This recent study also reported sex differences in testosterone's impact on cholinergic stimuli. Testosterone more potently (1000X) inhibits bladder responsiveness to carbachol (cholinergic agonist) in females than in males (151). Taken together, these studies reveal clear sex differences in cholinergic receptors (muscarinic and nicotinic) in rat bladder that may be driven by testosterone.

The human bladder exhibits sex differences in abundance of alpha1 adrenergic receptors (Adra1) (152). Alpha adrenergic receptors are the receptors for noradrenaline released by

noradrenergic axons. The abundance of Adra1 in the bladder neck and detrusor is similar between males and females, but in the trigone, women have significantly more Adra1 than men. The expression of Adra subtypes also differs between men and women. Men express more Adra1a1 and Adra1d than women (152). Castration changes Adra1, Adra2, Adrab and muscarinic cholinergic receptor densities in the bladder and proximal urethra (153). Castration decreases Adra1 abundance in the proximal urethra and muscarinic cholinergic receptor abundance in the bladder dome (153). The response of bladder muscle strips to autonomic drugs parallels the densities of the receptors they target, indicating the changes in receptor densities are functionally relevant (153).

Pelvic neurons are also impacted by changes in circulating testosterone and estradiol concentrations. The autonomic nervous system contributes to male reproductive organ smooth muscle contraction, exocrine secretion, and blood flow. Castration of pre-pubescent male rats affects the structure, chemistry, and function of pelvic autonomic neurons. Noradrenergic pelvic neurons supplying the prostate and urinary bladder are reduced in size compared to controls and cholinergic pelvic neurons are unchanged (150). Castration of male rats also reduces the size of pre- and paravertebral sympathetic neurons that supply the pelvic viscera (150). Overall, circulating androgens are essential for maturation and maintenance of autonomic neurons and pelvic ganglia supplying the prostate and bladder and testosterone may have direct effects on neuronal gene expression (150).

Testosterone and estradiol in benign bladder diseases

Lower urinary tract dysfunction

Urinary disorders are classified as problems with storage, voiding, or postmicturition diagnosed according to criteria established by the International Continence Society (154). Lower urinary tract dysfunction (LUTD) are a manifestation of urinary dysfunction and occur in men and women (4). LUTD are characterized by increased urinary frequency, dribbling, and incomplete

bladder emptying, among others, but causes thought to be multifactorial (155). Some hypothesized causes may be increased prostate size, smooth muscle dysfunction, or increased prostate fibrosis. Testosterone and estradiol have been long thought to contribute to disease progression. Here, the potential causative roles of testosterone and estradiol in LUTD is examined. Table 2 summarizes the impacts of testosterone and estradiol together and independently on LUTD susceptibility.

Aging and Testosterone and Estradiol

Men and women experience changes in plasma testosterone and estradiol concentrations as they age. In men, the plasma concentration of testosterone decreases and estradiol concentration increases. In women, the concentration of estradiol decreases and that of testosterone increase (93, 156). LUTD occur in 60% of men and 57.7% of women over the age of 60 (155). LUTD in men and women appear to be driven by testosterone and estradiol therefore many researchers are examining how changes in ratio of these sex hormones impacts disease.

Body mass index (BMI) influences the ratio of testosterone to estradiol and predisposes men and women to LUTD. Circulating testosterone concentrations in aging men with benign prostatic hyperplasia are inversely associated with BMI (157). In addition, estradiol concentrations correlate with BMI in men (158). This observation is not surprising since aromatase activity in adipose tissue converts testosterone to estradiol. Interestingly, when compressed pellets of testosterone and estradiol are delivered to mice to mimic the hormone environment of aging men, these mice develop severe urinary dysfunction characterized by increased prostate size, bladder volume, urinary retention, eventual decompensation, and risk of hydronephrosis (3).

An aging related decline in plasma testosterone concentrations can drive LUTD in elderly men. Exposure of human bladders to a castration-relevant concentration of testosterone negatively influences active and passive properties of human bladders by decreasing volume threshold for micturition and mean flow rate, both of which contribute to LUTD (159)(Table 2).

Subphysiological testosterone concentrations in men also correlate with risk of metabolic syndrome and erectile dysfunction (160). One study reported that administration of parenteral testosterone undecanoate decreased patient reported LUTD and post-void residual urine volumes (161). These studies suggests that an aging-related decrease in testosterone concentration has the capacity to influence LUTD severity in aging men, but because testosterone can be aromatized to estradiol, it is unclear which hormone is responsible.

Estrogens have a role in benign prostatic hyperplasia and LUTD in aging men and women, but no current therapies directly target estrogen action for these diseases. Estrogens act through two receptor subtypes ER alpha (ERα, also known as estrogen receptor 1, Esr1) and ER beta (Erβ, also known as estrogen receptor 2, Esr2). GPCR 30 (g protein coupled estrogen receptor, GPER) can also bind estrogens and mediate its response through non-genomic actions (162). Few studies are reported on GPCR 30 in bladder, but one study found while GPCR 30 is important to mediate estrogen's action in prostate, ERα mainly acts in bladder (162). Estrogens are hypothesized to be important in LUTD because lower baseline serum estradiol levels are associated with improved international prostate symptom score (IPSS) following pharmaceutical treatment (163)(**Table 2**). Some clinical trials have investigated the impact of selective estrogen receptor modulators (SERMs) in treating LUTD, but results have been mixed. For example, one study administered Tamoxifen to patients with benign prostatic hyperplasia and found Tamoxifen was not effective enough to increase max flow or decrease symptoms in men (164)(**Table 2**). Further, an ERβ agonist LY500307 was not effective in treating LUTD in patients with enlarged prostates and benign prostatic hyperplasia (165)(**Table 2**). The benefits of estradiol treatment for LUTD is not fully understood and may still present a benefit clinically if varied estrogen doses or routes of treatment are studied.

Both testosterone and estradiol seem to contribute to LUTD, indicating it is likely the interaction of both that contributes to severity. The administration of sustained release implants of testosterone and estradiol to mice, to mimic the hormonal environment of aging men, causes

progressive bladder outlet obstruction, characterized by prostate hypertrophy, detrusor compensation and decompensation and bladder fibrosis (3)(**Table 2**). Rats and dogs generally respond to exogenous testosterone and estradiol the same as mice (3, 166–171)(Table 2). The progressive voiding dysfunction mediated by exogenous testosterone and estradiol require ERα but not ERβ (172). This finding led to an examination of selective estrogen receptor modulators (SERM) to prevent bladder complications in T+E2 treated mice (172)(**Table 2**). Clomiphene is a SERM approved for treatment of ovulatory dysfunction in women and has also been used to increase serum T and E2 concentrations in men suffering from LUTD with successful alleviation of some symptoms (173).

Women experiencing menopause experience a reduction in plasma estradiol concentrations and are at a greater risk of experiencing LUTD (174). Supplementary estrogens are effective for the treatment of urge urinary incontinence, overactive bladder, stress urinary incontinence, and reduces the risk of urinary tract infections in post-menopausal women (175).

LUTD, testosterone and estradiol, and innervation

An aging-related change in circulating concentrations of testosterone and estradiol in part causes benign prostatic hyperplasia and detrusor overactivity in mice. Alpha(1)-adrenoceptor antagonists relax prostatic and bladder neck smooth muscle to suppress irritative symptoms in humans. The alpha(1)-adrenoceptor antagonist silodosin reduces T+E2-mediated detrusor overactivity indicating that excessive response to sympathetic nerve stimulation mediated via alpha(1A)-adrenoceptor in prostate gives rise to detrusor overactivity (176). Autonomic nervous system overactivity has also been associated with subphysiological testosterone concentrations and aging (160). This overactivity may contribute to the severity of LUTD, but further studies are needed.

Muscle sensitivity

A role for smooth muscle in the onset or progression of LUTD is supported by the fact that smooth muscle relaxing agents provide benefit to some men with LUTD. Interestingly, the concentration of circulating sex hormones influences detrusor sensitivity to contraction. Estradiol reduces spasmogenity, antagonizes bladder muscle contractions, and reduces the amplitude and frequency of spontaneous Ca2+ flashes of isolated preparations of male rat bladder (177). Testosterone can decrease bladder smooth muscle excitability via activation of Ca2+ activated (BK) channels (178). Working together, estradiol and testosterone concentration modulation can influence bladder smooth muscle contractility to contribute to bladder muscle contraction.

Phosphodiesterase type 5 (PDE-5) inhibitors are prescribed for erectile dysfunction and LUTD (179). Their exact mechanism is unclear, but they inhibit PDE-5, increase cyclic guanosine monophosphate and mediate smooth muscle relaxation. PDE-5 inhibitors function as vasodilators by impeding break down of cyclic guanosine monophosphate, a second messenger involved in smooth muscle relaxation. PDE5 is highly expressed in the bladder (180). PDE5 activity is more pronounced in males versus female rabbit bladders, testosterone increases PDE5 abundance in male but not female rat bladder, and the testosterone to estradiol ratio regulates the bladder responsiveness to PDE5 inhibitors (181).

Testosterone as a therapy for LUTD

The role of testosterone as a therapy for LUTD is controversial. Some studies report testosterone as a therapeutic. Testosterone replacement therapy has been used clinically to treat male lower urinary tract dysfunction (LUTD). Although many studies failed to observe significant improvement in symptoms among healthy aging men, men with metabolic syndrome may be specifically responsive (182–184). One study found that one year of transdermal testosterone improved sexual function and bladder function characterized by increased bladder capacity and compliance and reduced voiding pressure (185). Long-term testosterone therapy reduces IPSS scores and post void bladder residual in hypogonadal men (186). Further, aromatase inhibitors

are an effective treatment of BPH-related voiding symptoms in some men and reduce prostatic and bladder volumes and increase in the testosterone/ estradiol ratio (187). In addition testosterone, has been considered a therapy in females with overactive bladder which is often associated with LUTD (178).

Some studies report that testosterone is harmful to bladder structure and function. As mentioned above, castration causes significant bladder atrophy and detrusor remodeling. Treatment with a 100 mg/kg testosterone significantly increases urothelial thickness and smooth muscle to collagen ratio (188). Increased collagen content stiffens the bladder and reduces its compliance. One study found that testosterone did not improve urodynamics or reduce bladder obstruction in patients with irritable or obstructive bladder symptoms due to BPH (189). Patients treated with the luteinizing hormone-releasing hormone (LHRH) analogue, buserelin, for six months exhibited castration-like testosterone levels but had no significant effect on bladder outflow obstruction (190).

Stress Incontinence

Stress incontinence is defined as “involuntary leakage on effort or exertion or on sneezing or coughing” by the International Continence Society (154). Incontinence results from a variety of causes including bladder dysfunction, urethral dysfunction, pelvic floor dysfunction, sphincter dysfunction, or a combination (191). The prevalence of urinary incontinence is lower in men than in women (191). The prevalence of stress and mixed (stress and urge) incontinence is higher than urge incontinence alone (191). The following section will describe the impacts of testosterone and estradiol on bladder cells in men and women with stress incontinence.

Aging and T and E2

Severe incontinence is not prevalent in young women but increases with age and the incidence typically peaks around menopause (191). Stress urinary incontinence affects

approximately 15-30% of women (192, 193). The impact of declining estrogen concentrations on bladder function was examined in young (2 month) and mature (10 month) rats. Estrogen deprivation reduces young rat bladder responsiveness to cholinergic stimuli (194). Estrogen supplementation in mature rats increases bladder contractile force relative to that of sham operated rats (194). Mature OVX rats exhibited the most significant decrease in response to cholinergic stimulation (194). Overall, these findings suggest that supplementary estradiol partially restores bladder function in young adult OVX rats and fully restores bladder function in aged OVX rats (194).

Estrogen and innervation

Estrogens have pronounced trophic effects on neurons throughout the peripheral and central nervous system. Most studies support a therapeutic role for supplementary estrogens after neurological injury. The pudendal nerve innervates the pelvic floor and the external urethral sphincter. This nerve is often injured during childbirth. Pudendal nerve injury reduces external urethral sphincter activity, causing atrophy and leading to stress urinary incontinence. The impact of estradiol treatment on pudendal nerve damage was examined in a rat model of stress incontinence. OVX rats received a bilateral pudendal nerve crush and a subcutaneous slow-release estradiol capsule. Tissues were examined two weeks later. Estradiol supplementation after pudendal nerve crush causes unmyelinated axons to be spared and regenerated (195). This indicates a therapeutic role of estrogen supplementation in women with stress urinary incontinence. Clearly, estrogen plays an important role in modifying nerves in stress incontinence and future studies should identify whether nerves are remodeled as estrogen concentrations change.

Estradiol as a therapy for stress incontinence

There is a wealth of experimental evidence supporting the benefits of supplementary estrogens on stress urinary incontinence. Estrogen treatment is effective in treating spay

incontinence in dogs and is used clinically to treat stress incontinence in women (196–198). Though there are some reported differences in clinical outcome based on the type of estrogen and route of administration, clinical studies historically supports a beneficial effect of supplementary estrogen with respect to patient reported symptoms, urine leakage, and urodynamic parameters including maximum urethral pressure, urethral closure pressure and volume to sense bladder fullness (199, 200). Recent studies indicate a disputed role of estrogens in treating urinary incontinence and do not recommend its prescription (201, 202). Route of administration may contribute to disputes in estrogens efficacy.

Overactive Bladder

Overactive bladder can be defined as “urgency with or without urgency incontinence usually with increased daytime frequency and nocturia” (154). Overactive bladder is common in both women and men (16% in men and 16.9% in women) (203). With advancing age, overactive bladder becomes much more prevalent in women than men (203). Despite the sex differences in prevalence, there are no clinically relevant differences in circulating hormone concentrations relative to improvement in overactive bladder, indicating sex hormones may not play as important of a role in this bladder disease (204).

TRPs in overactive bladder

Transient receptor potential (TRP) subfamily is comprised of cation channels involved in various cellular functions. They are encoded by 27 genes and grouped into six subfamilies based on amino acid sequence and homology (205). TRP receptors are thermosensors with most responding to heat, but some responding to cold. TRP receptors are expressed in the lower urinary tract in neuronal fibers and urothelial and muscle layers of bladder and urethra including TRPV1, TRPV2, TRPV4, TRM4, TRPM8, and TRPA1 (206). TRP receptors are expressed by bladder urothelial cells and by demyelinated C fibers that project onto the urothelium (207). The

urinary bladder contains a high density of TRPV1 receptors that regulate pain perception and bladder contraction. TRPV4 receptors are mechanoreceptors that regulate bladder excitability and contractability. TRPV4 is expressed in rat and mouse urothelial and detrusor muscle cells (208). Genetic depletion of TRPV4 in mice significantly increases urinary spotting, reduces intervoid intervals and increases non-voiding contractions (209). These findings suggest TRPV4 plays a unique role in maintaining normal urination and may be involved in regulating the mechanical pressure of bladder filling (209).

Our understanding of hormonal regulation of TRP receptor expression in the bladder is incomplete, but possible lines of new research are guided by knowledge of how gonadal hormones influence TRP abundance. Estrogens, progesterone, and androgens change TRP channel expression in the brain, lung, and mammary gland (210). For example, progesterone decreases the expression of TRPV4 in human airway and mammary gland epithelia cells (211). In endometrium, estrogens increase TRPA1 and TRPV1 abundance in rat sensory neurons (212). The hormonal control of TRP abundance is physiologically relevant, as 17β estradiol interferes with TRPV1 activation by capsaicin in sensory neurons (207) and increases TRPV1 abundance in endometrium (212). Future research opportunities include assessment of how TRP receptor density and distribution in the bladder changes with age, in response to changes in circulating testosterone and estradiol concentrations, and with disease processes such as overactive bladder.

Environmental factors that mediate changes in testosterone and estradiol concentrations

Plasma concentrations of testosterone and estradiol can be modified by physiological factors such as age and pregnancy, but also by environmental factors such as diet or chemical exposure. This section describes how the environment modifies testosterone and estrogen concentrations or actions in bladder disease. **Table 3** summarizes specific environmental chemicals, how they modulate testosterone and estradiol, and their impact on bladder.

Diet

Diet can influence bladder function in many ways, some of which are related to fluid volume regulation, others to neurogenic mechanisms, and yet others to direct actions. One study showed that a folic-acid enriched diet protects against progression of urinary voiding dysfunction in mice exposed to testosterone and estradiol (213)(**Table 3**). A potential mechanism involves a folic acid diet dependent increase in dorsal root ganglia *Trpv1* abundance and increased bladder sensitivity to filling (213). Though the study described above was conducted in male mice, its results may be relevant in the context of pregnancy induced urinary incontinence, as folic acid supplements are recommended to pregnant women to support fetal development and may also support maternal bladder health.

Soy products such as tofu, edamame, miso, and soy milk are increasingly consumed by individuals worldwide for their health effects. Soy has estrogenic properties and can influence bladder function. The soy phytoestrogens genistein and daidzein protect against rat bladder hyperactivity from ischemia/reperfusion injury (214)(**Table 3**). Genistein and daidzein also decrease rat detrusor contractions from electrical field stimulation, indicating potential benefit for overactive or hyperactive bladder or nerve damage (214). One study compared the ability of endogenous, pharmacological, and dietary estrogens to antagonize purinergic- or muscarinic-mediated bladder contractions. 17β estradiol and progesterone inhibit purinergic contractions, estradiol and ethinyl estradiol inhibit muscarinic contractions, but dietary estrogens daidzein and genistein are minimally effective, reducing muscarinic contractions by a meager 7% (128). This study shows that dietary estrogens have weak estrogenic activity but may be minimally useful in treating overactive bladder, especially overactive bladder from elevated muscarinic or purinergic activity. Importantly, soy isoflavones do not significantly alter circulating testosterone or estradiol concentrations, so they are not likely to predispose to LUTD or other bladder diseases influenced by testosterone and estradiol (214).

The Korean plant panax ginseng (200 mg/kg) protects against the urinary symptoms of benign prostatic hyperplasia in rats through a neurogenic mechanism (215)(**Table 3**). Panax ginseng downregulates nerve growth factor in the rat pontine nucleus, the key regulatory region for micturition (215). Dietary supplements can clearly influence sex hormone concentrations or bladder function so further research on other estrogenic foods is needed to determine its role in bladder disease. Studying patient's diets may provide important insights into why variability in disease severity presents in bladder.

Environmental chemical exposure

Some environmental chemicals can modulate testosterone and estradiol concentrations to predispose to bladder disease. Here, we describe some examples of chemicals known to impact bladder and hormone concentrations. 2,3,7,8-tetrachlorodibenzo-*p*-dioxin (TCDD) is a ubiquitous environmental contaminant that persists in the environment. The primary mechanism of exposure for humans is through diet by eating contaminated dairy and meats (216). TCDD is released into today's environment primarily through waste incineration (216). Interestingly, TCDD has been found to have estrogenic properties. One study found maternal exposure to low concentrations of TCDD (10 ng/kg) increased the abundance of ERα and ERβ in male rat offspring (217). Environmental contaminant exposure during fetal, neonatal or pubertal development are risk modifiers of many diseases of advancing age, including urinary voiding dysfunction. For example, perinatal exposure to TCDD worsens T+E2 mediated urinary voiding dysfunction in adulthood (2, 218)(**Table 3**). The mechanism through which TCDD acts to worsen LUTD in mice is unknown. TCDD is an endocrine disruptor, so perhaps its modulation of estrogen concentrations can predispose to LUT development.

Bisphenol A (BPA), a plasticizer in polycarbonate plastics, has also been implicated in susceptibility to male voiding dysfunction. The primary mechanism for human exposure is through the diet, specifically leaching of BPA from resins in food and beverage container linings and dental

implants. BPA was shown to have estrogenic activity in 1936 (219). Testosterone + BPA treatment of adult male mice significantly change spontaneous voiding behaviors by inducing an intermittent voiding pattern and causing urinary retention and bladder dysfunction, reminiscent of the T + E2 phenotype (220)(**Table 3**). Exposure to BPA during the fetal and neonatal periods sensitizes to T+E2 mediated voiding dysfunction in adult mice (221).

The impact of environmental chemicals on urinary function is only beginning to be unraveled. There are a host of natural chemicals and pesticides that are known to influence reproductive hormone concentrations and thereby have the potential to influence urinary voiding function. Lead (100 or 1000 ppm in drinking water for 7 or 13 weeks) reduces the mass of rat seminal vesicles, epididymis, and reproductive capacity (222). Cadmium (0.5 mg/kg) impairs the regeneration of rat Leydig cells (223). DDT exposure in adulthood increases free and bioavailable testosterone and lowers FSH concentrations in human men (224). Deltamethrin, a pyrethroid insecticide, decreases sperm quality and impairs libido and decreases inhibin B abundance and reproductive performance (225).

Industries have recently developed an interest in ultraviolet (UV) filters present in sunscreens. Several reports of negative health effects have inspired further studies investigating which chemicals are toxic to humans. UV filter exposure during development can have a significant impact on prostate, bladder, and testosterone and estradiol concentrations. Exposure to UV filters in adulthood can have additionally concerning impacts. The urinary concentrations of BPA, parabens, and UV filters were observed after two weeks of exposure (226). The organic UV filter, octocrylene, level was found to be significantly more concentrated in the urine of women with polycystic ovarian syndrome in women with a BMI >24 (227). BPA has been previously shown to cause urinary dysfunction in mice, as mentioned above, so it is possible UV filter exposure may influence bladder similarly, but more studies are needed.

The UV filter 4-MBC (0.7, 7, 24, 47 mg/kg/day delays male rat puberty and decreases adult prostate weight and increases testis weight (228). 2-hydroxy-4-methoxybenzopheone is

also a UV filter used in sunscreens, cosmetics, and plastics. It has weak estrogenic activity and activates candidate biomarker genes for testicular and prostatic toxicity in rats (229). Benzophenone-3, 4-MBC, octocrylene, benzyl salicylate, and homosalate are all UV filters that may act similarly and cause similar phenotypes (230). They are present in 85% of Swiss breast milk samples which make them a risk to developing children (230). There are increasing numbers of studies that have reported the endocrine disrupting effects of UV filters so future research into these chemicals are necessary to determine safety (230).

Developing new technologies to understanding prostatic smooth muscle anatomy and function

New techniques are needed to address the role of prostate smooth muscle contraction in lower urinary tract dysfunction. Gaps in current techniques are discussed below. As mentioned above, in the past, pressure flow urodynamic studies have been performed in men and determined the prostatic urethra has the highest pressure along the male lower urinary tract. A variety of mechanisms are likely responsible, including BPH which could compress the urethra, prostate which could stiffen the urethra, and hyperactive smooth muscle which could impinge the urethra. Pressure flow studies cannot differentiate between these underlying mechanisms.

A variety of techniques are available to study prostate smooth muscle activity. *Ex vivo* analysis of prostate muscle activity in isolated tissue baths enables treatment with multiple drugs or electrical field stimulation (231, 232). Despite its diverse utility, organ baths require tension on the tissue which may cause damage and it does not represent a physiologically normal state. Further, measured contractions are unidirectional. To keep the tissue in its physiologically normal state and to measure multi-directional contractions, one group used light microscopy to image isolated prostate tissue *in vitro* and its response to pharmacological or electrical stimuli (233). The response was measured by the change in area before and after drug stimuli. In addition, fluorescent imaging dyes including FURA or Fluo4 can be used to investigate smooth muscle contraction *in vitro*, though these studies require dye perfusion and are often conducted with

cultured prostate smooth muscle myocytes. Imaging dyes provide information on directionality of contraction, calcium transience, duration of contraction and relaxation, and physiologically normal response to stimuli. Fluo4 in prostate was used to identify that prostate interstitial cells generate spontaneous Ca2+ through L-type channels (234). Penetration of the dye into tissues can be one issue with this method and signal to noise ratio can make data analysis difficult. Further, this imaging modality cannot be used *in vivo* to assess interactions of organs.

Genetically encoded calcium sensors (GCaMP) have been bred into a variety of calcium responsive cells. These sensors were first pioneered in Drosophila brain, but have since been used in heart, kidney, gut, and skin (235–241). GCaMP functions similarly to imaging dyes but have an enhanced signal to noise ratio and are increasingly cell specific. Further, these sensors can be imaged in vivo, allowing for investigation of organ interactions before and after stimuli. GCaMPs fluoresce when bound to calcium and fluorescent intensity over time can be determined by time-lapse imaging. It is also possible to measure muscle contraction by time-lapse imaging by measuring the interval between peak fluorescence and return to baseline. Sensitivity to stimuli can be measured by delivering low frequency or voltage electrical impulses and examining fluorescent responses. In order to answer questions about prostate smooth muscle sensitivity to contraction and relaxation time, we created a genetically modified mouse strain that express GCaMP in prostate smooth muscle. In this dissertation, we bred GCaMP5g mice with *Myh11*^{cre} mice to generate *Myh11*^{cre};GCaMP5g. We tested the impact of T+E2 on prostate smooth muscle relaxation time and the impact of IUL TCDD exposure on the sensitivity of smooth muscle to electrically induced contraction. We found T+E2 slows the prostate smooth muscle relaxation time and IUL TCDD exposure increases the sensitivity of prostate smooth muscle to electrical stimuli (92, 242).

Cardiologists use contrast enhanced ultrasound to measure the flow of blood through veins and arteries. They can use contrast enhanced ultrasound to determine if arteries are blocked by plaques and whether blood flow is impacted. A contrast agent is administered into the

cardiovascular system and its flow through the vessels can be recognized as a velocity. The contrast agent consists of gas filled microbubbles that resonate when exposed to an ultrasound beam and can be used to measure fluid speed and vascular lumen diameter (243). The relationship between fluid speed and diameter follows the Venturi effect, an incompressible fluid's velocity increases as it passes through a constriction (244). In this dissertation, we tested the hypothesis that contrast enhanced ultrasound could measure the speed of fluid flow through the mouse prostatic urethra (242). We found that phenylephrine administration increased the speed of urine through the mouse prostatic urethra, therefore indicating prostate smooth muscle can cause urethral obstruction in mice. Using contrast enhanced ultrasound, we have opened new lines of investigation into how prostatic fibrosis and inflammation impact urine flow through the prostatic urethra.

New techniques enable a new hypothesis

Prostate smooth muscle activity has been studied since the 1960's and has been a major target of pharmacological treatments. However, there are critical gaps in knowledge that if answered may enable more specific and personalized treatment. My dissertation presents two novel mechanisms of prostate smooth muscle dysfunction and establishes new techniques that can generate new hypothesis. It is my hope that the research presented here will help to address some of the gaps in knowledge and give others new techniques to address others.

References

1. K. A. Wegner, *et al.*, An immunohistochemical identification key for cell types in adult mouse prostatic and urethral tissue sections. *PLoS ONE* **12**, e0188413 (2017).

2. W. A. Ricke, *et al.*, In Utero and Lactational TCDD Exposure Increases Susceptibility to Lower Urinary Tract Dysfunction in Adulthood. *Toxicol Sci* **150**, 429–440 (2016).

3. T. M. Nicholson, *et al.*, Testosterone and 17β-estradiol induce glandular prostatic growth, bladder outlet obstruction, and voiding dysfunction in male mice. *Endocrinology* **153**, 5556–5565 (2012).

4. H. Lepor, Pathophysiology of Lower Urinary Tract Symptoms in the Aging Male Population. *Rev Urol* **7**, S3–S11 (2005).

5. O. M. Bautista, *et al.*, Study design of the Medical Therapy of Prostatic Symptoms (MTOPS) trial. *Controlled Clinical Trials* **24**, 224–243 (2003).

6. G. Haidinger, *et al.*, Risk factors for lower urinary tract symptoms in elderly men. For the Prostate Study Group of the Austrian Society of Urology. *Eur. Urol.* **37**, 413–420 (2000).

7. K. S. Kim, J. K. Jo, J. A. Lee, B. Y. Choi, H. S. Moon, Do Lifestyle Factors Affect Lower Urinary Tract Symptoms? Results from the Korean Community Health Survey. *Int Neurourol J* **23**, 125–135 (2019).

8. S. K. Van Den Eeden, *et al.*, Evaluating race/ethnic disparities in lower urinary tract symptoms (LUTD) in men. *J Urol* **187**, 185–189 (2012).

9. L. Dommer, *et al.*, Lower urinary tract symptoms (LUTD) before and after robotic-assisted laparoscopic prostatectomy: does improvement of LUTD mitigate worsened incontinence after robotic prostatectomy? *Transl Androl Urol* **8**, 320–328 (2019).

10. J. E. McNeal, Origin and evolution of benign prostatic enlargement. *Invest Urol* **15**, 340–345 (1978).

11. J. T. Isaacs, D. S. Coffey, Etiology and disease process of benign prostatic hyperplasia. *The Prostate* **15**, 33–50 (1989).

12. G. R. Cunha, *et al.*, Development of the human prostate. *Differentiation* **103**, 24–45 (2018).

13. E. Bloch, M. Lew, M. Klein, Studies on the inhibition of fetal androgen formation: testosterone synthesis by fetal and newborn mouse testes in vitro. *Endocrinology* **88**, 41–46 (1971).

14. L. J. Pelliniemi, M. Niemi, Fine structure of the human foetal testis. I. The interstitial tissue. *Z Zellforsch Mikrosk Anat* **99**, 507–522 (1969).

15. G. Pointis, M.-T. Latreille, T.-M. Mignot, Y. Janssens, L. Cedard, Regulation of testosterone synthesis in the fetal mouse testis. *Journal of Steroid Biochemistry* **11**, 1609–1612 (1979).

16. K. P. Keil, *et al.*, Wnt inhibitory factor 1 (Wif1) is regulated by androgens and enhances androgen-dependent prostate development. *Endocrinology* **153**, 6091–6103 (2012).

17. H. Takeda, I. Lasnitzki, T. Mizuno, Change of mosaic pattern by androgens during prostatic bud formation in XTfm/X+ heterozygous female mice. *J. Endocrinol.* **114**, 131–137 (1987).

18. J. Müntzing, The activity and distribution of some hydrolases in the prostate of various mammals. *International Journal of Biochemistry* **3**, 401–407 (1972).

19. D. Price, An Analysis of the Factors Influencing Growth and Development of the Mammalian Reproductive Tract. *Physiological Zoology* **20**, 213–247 (1947).

20. A. Raynaud, Experimental modification of sexual differentiation of mouse embryos by treatment with androgenic and oestrogenic hormones. (Parts 1 and 2). (Part 3). *Experimental modification of sexual differentiation of mouse embryos by treatment with androgenic and oestrogenic hormones. (Parts 1 and 2). (Part 3).* (1942) (August 26, 2020).

21. N. Hayashi, G. R. Cunha, M. Parker, Permissive and instructive induction of adult rodent prostatic epithelium by heterotypic urogenital sinus mesenchyme. *Epithelial Cell Biol* **2**, 66–78 (1993).

22. S. H. Allgeier, *et al.*, Androgenic regulation of ventral epithelial bud number and pattern in mouse urogenital sinus. *Dev. Dyn.* **239**, 373–385 (2010).

23. V. Mehta, *et al.*, Beta-catenin (CTNNB1) induces Bmp expression in urogenital sinus epithelium and participates in prostatic bud initiation and patterning. *Dev. Biol.* **376**, 125–135 (2013).

24. I. Lasnitzki, T. Mizuno, Prostatic induction: interaction of epithelium and mesenchyme from normal wild-type mice and androgen-insensitive mice with testicular feminization. *J. Endocrinol.* **85**, 423–428 (1980).

25. G. R. Cunha, *et al.*, The endocrinology and developmental biology of the prostate. *Endocr. Rev.* **8**, 338–362 (1987).

26. K. P. Keil, *et al.*, DNA methylation of E-cadherin is a priming mechanism for prostate development. *Dev Biol* **387**, 142–153 (2014).

27. J. Szczyrba, *et al.*, Neuroendocrine Cells of the Prostate Derive from the Neural Crest. *J. Biol. Chem.* **292**, 2021–2031 (2017).

28. S. C. Kirkland, Clonal origin of columnar, mucous, and endocrine cell lineages in human colorectal epithelium. *Cancer* **61**, 1359–1363 (1988).

29. G. Aumüller, *et al.*, Semiquantitative morphology of human prostatic development and regional distribution of prostatic neuroendocrine cells. *Prostate* **46**, 108–115 (2001).

30. A. E. Turco, *et al.*, A temporal and spatial map of axons in developing mouse prostate. *Histochem. Cell Biol.* (2019) https:/doi.org/10.1007/s00418-019-01784-6.

31. K. B. Egan, The Epidemiology of Benign Prostatic Hyperplasia Associated with Lower Urinary Tract Symptoms: Prevalence and Incident Rates. *Urologic Clinics of North America* **43**, 289–297 (2016).

32. D. G. Bostwick, *et al.*, The association of benign prostatic hyperplasia and cancer of the prostate. *Cancer* **70**, 291–301 (1992).

33. C. Magnon, *et al.*, Autonomic nerve development contributes to prostate cancer progression. *Science* **341**, 1236361 (2013).

34. J. Pannek, P. Bartel, K. Göcking, A. Frotzler, Prostate volume in male patients with spinal cord injury: a question of nerves? *BJU International* **112**, 495–500 (2013).

35. T. Jungblut, G. Aumüller, B. Malek, H. Melchior, Age-Dependency and Regional Distribution of Enkephalinergic Nerves in Human Prostate. *UIN* **44**, 352–356 (1989).

36. C. R. Chapple, R. Crowe, S. A. Gilpin, J. Gosling, G. Burnstock, The innervation of the human prostate gland--the changes associated with benign enlargement. *J. Urol.* **146**, 1637–1644 (1991).

37. A. L. Burnett, *et al.*, Characterization and localization of nitric oxide synthase in the human prostate. *Urology* **45**, 435–439 (1995).

38. K. T. McVary, A. Rademaker, G. L. Lloyd, P. Gann, Autonomic nervous system overactivity in men with lower urinary tract symptoms secondary to benign prostatic hyperplasia. *J. Urol.* **174**, 1327–1433 (2005).

39. J. B. Choi, J. G. Lee, Y. S. Kim, Characteristics of Autonomic Nervous System Activity in Men With Lower Urinary Tract Symptoms (LUTD): Analysis of Heart Rate Variability in Men With LUTD. *Urology* **75**, 138–142 (2010).

40. K. Calkins, S. U. Devaskar, Fetal Origins of Adult Disease. *Curr Probl Pediatr Adolesc Health Care* **41**, 158–176 (2011).

41. M. Kepper, J. Keast, Immunohistochemical properties and spinal connections of pelvic autonomic neurons that innervate the rat prostate gland. *Cell Tissue Res.* **281**, 533–542 (1995).

42. H. Danuser, J. P. Springer, M. A. Katofiasc, K. B. Thor, Extrinsic innervation of the cat prostate gland: a combined tracing and immunohistochemical study. *J. Urol.* **157**, 1018–1024 (1997).

43. J. N. Pennefather, W. A. Lau, F. Mitchelson, S. Ventura, The autonomic and sensory innervation of the smooth muscle of the prostate gland: a review of pharmacological and histological studies. *J Auton Pharmacol* **20**, 193–206 (2000).

44. Y. Yoon, *et al.*, Visualization of prostatic nerves by polarization-sensitive optical coherence tomography. *Biomed Opt Express* **7**, 3170–3183 (2016).

45. W. Sung, S. Lee, Y.-K. Park, S.-G. Chang, Neuroanatomical study of periprostatic nerve distributions using human cadaver prostate. *J. Korean Med. Sci.* **25**, 608–612 (2010).

46. F. Reeves, S. Battye, J. F. Borin, N. M. Corcoran, A. J. Costello, High-resolution Map of Somatic Periprostatic Nerves. *Urology* **97**, 160–165 (2016).

47. A. Tewari, *et al.*, The proximal neurovascular plate and the tri-zonal neural architecture around the prostate gland: importance in the athermal robotic technique of nerve-sparing prostatectomy. *BJU International* **98**, 314–323 (2006).

48. S. S. Chang, M. Peterson, J. A. Smith, Intraoperative nerve stimulation predicts postoperative potency. *Urology* **58**, 594–597 (2001).

49. A. Mandhani, *et al.*, Real time monitoring of temperature changes in neurovascular bundles during robotic radical prostatectomy: thermal map for nerve-sparing radical prostatectomy. *J. Endourol.* **22**, 2313–2317 (2008).

50. A. Horiguchi, *et al.*, A pilot study of photoacoustic imaging system for improved real-time visualization of neurovascular bundle during radical prostatectomy. *Prostate* **76**, 307–315 (2016).

51. E. D. Vaughan, Long-Term Experience with 5-α-Reductase Inhibitors. *Rev Urol* **5**, S28–S33 (2003).

52. B. Turkbey, *et al.*, Age related changes in prostate zonal volume as measured by high resolution prostate MRI: a cross sectional study in over 500 patients. *BJU Int* **110** (2012).

53. M. D. Eckhardt, G. E. van Venrooij, T. A. Boon, Symptoms and quality of life versus age, prostate volume, and urodynamic parameters in 565 strictly selected men with lower urinary tract symptoms suggestive of benign prostatic hyperplasia. *Urology* **57**, 695–700 (2001).

54. E. Shapiro, M. J. Becich, V. Hartanto, H. Lepor, The relative proportion of stromal and epithelial hyperplasia is related to the development of symptomatic benign prostate hyperplasia. *J. Urol.* **147**, 1293–1297 (1992).

55. H. G. Baumgarten, B. Falck, A. F. Holstein, C. Owman, T. Owman, Adrenergic innervation of the human testis, epididymis, ductus deferens and prostate: a fluorescence microscopic and fluorimetric study. *Z Zellforsch Mikrosk Anat* **90**, 81–95 (1968).

56. S. Raz, M. Zeigler, M. Caine, Pharmacological receptors in the prostate. *Br J Urol* **45**, 663–667 (1973).

57. M. Caine, S. Raz, M. Zeigler, Adrenergic and cholinergic receptors in the human prostate, prostatic capsule and bladder neck. *Br J Urol* **47**, 193–202 (1975).

58. M. Caine, A. Pfau, S. Perlberg, The use of alpha-adrenergic blockers in benign prostatic obstruction. *Br J Urol* **48**, 255–263 (1976).

59. H. Lepor, E. Shapiro, Characterization of alpha1 adrenergic receptors in human benign prostatic hyperplasia. *J. Urol.* **132**, 1226–1229 (1984).

60. C. F. Shum, W. Lau, C. P. C. Teo, Medical therapy for clinical benign prostatic hyperplasia: α1 Antagonists, 5α reductase inhibitors and their combination. *Asian J Urol* **4**, 185–190 (2017).

61. H. W. Moon, *et al.*, Prescription pattern of alpha-blockers for management of lower urinary tract symptoms/benign prostatic hyperplasia. *Sci Rep* **8** (2018).

62. C. G. Roehrborn, Efficacy of α-Adrenergic Receptor Blockers in the Treatment of Male Lower Urinary Tract Symptoms. *Rev Urol* **11**, S1–S8 (2009).

63. J.-Q. Yuan, *et al.*, Comparative Effectiveness and Safety of Monodrug Therapies for Lower Urinary Tract Symptoms Associated With Benign Prostatic Hyperplasia: A Network Meta-analysis. *Medicine* **94**, e974 (2015).

64. S. R. Fine, P. Ginsberg, Alpha-Adrenergic Receptor Antagonists in Older Patients With Benign Prostatic Hyperplasia: Issues and Potential Complications. *J Am Osteopath Assoc* **108**, 333–337 (2008).

65. E. J. Kruep, S. L. Hogue, M. T. Eaddy, M. D. Chandra, Clinical and Economic Impact of Early Versus Delayed 5-Alpha Reductase Inhibitor Therapy in Men Taking Alpha Blockers for Symptomatic Benign Prostatic Hyperplasia. *P T* **36**, 493–507 (2011).

66. J. D. McConnell, *et al.*, The long-term effect of doxazosin, finasteride, and combination therapy on the clinical progression of benign prostatic hyperplasia. *N. Engl. J. Med.* **349**, 2387–2398 (2003).

67. M. Lam, R. Mitsui, H. Hashitani, Electrical properties of purinergic transmission in smooth muscle of the guinea-pig prostate. *Auton Neurosci* **194**, 8–16 (2016).

68. S. N. Lee, *et al.*, Age Related Differences in Responsiveness to Sildenafil and Tamsulosin are due to Myogenic Smooth Muscle Tone in the Human Prostate. *Sci Rep* **7**, 10150 (2017).

69. B. Chakrabarty, S. Lee, B. Exintaris, “Generation and Regulation of Spontaneous Contractions in the Prostate” in *Smooth Muscle Spontaneous Activity: Physiological and Pathological Modulation*, Advances in Experimental Medicine and Biology., H. Hashitani, R. J. Lang, Eds. (Springer Singapore, 2019), pp. 195–215.

70. A. Dey, D.-T. T. Nguyen, R. J. Lang, B. Exintaris, Spontaneous electrical waveforms in aging guinea pig prostates. *J. Urol.* **181**, 2797–2805 (2009).

71. Q. Yu, *et al.*, Inhibition of human prostate smooth muscle contraction by the LIM kinase inhibitors, SR7826 and LIMKi3. *British Journal of Pharmacology* **175**, 2077–2096 (2018).

72. V. Albert, G. R. Campbell, Relationship between the sympathetic nervous system and vascular smooth muscle: A morphometric study of adult and juvenile spontaneously hypertensive rat/Wistar-Kyoto rat caudal artery. *Heart Vessels* **5**, 129–139 (1990).

73. M. a. Chagas, M. a. Babinski, W. s. Costa, F. j. b. Sampaio, Stromal and acinar components of the transition zone in normal and hyperplastic human prostate. *BJU International* **89**, 699–702 (2002).

74. D. Bianchi-Frias, *et al.*, The Effects of Aging on the Molecular and Cellular Composition of the Prostate Microenvironment. *PLoS One* **5** (2010).

75. E. Golomb, N. Rosenzweig, R. Eilam, A. Abramovici, Spontaneous hyperplasia of the ventral lobe of the prostate in aging genetically hypertensive rats. *J. Androl.* **21**, 58–64 (2000).

76. E. Shapiro, V. Hartanto, H. Lepor, The response to alpha blockade in benign prostatic hyperplasia is related to the percent area density of prostate smooth muscle. *Prostate* **21**, 297–307 (1992).

77. A. K. Giri, Mutagenic and genotoxic effects of 2,3,7,8-tetrachlorodibenzo-p-dioxin, a review. *Mutation Research/Reviews in Genetic Toxicology* **168**, 241–248 (1986).

78. I. W. G. on the E. of C. R. to Humans, *2,3,7,8-TETRACHLORODIBENZO-para-DIOXIN, 2,3,4,7,8-PENTACHLORODIBENZOFURAN, AND 3,3',4,4',5-PENTACHLOROBIPHENYL* (International Agency for Research on Cancer, 2012) (June 2, 2020).

79. J. E. Michalek, *et al.*, Pharmacokinetics of 2,3,7,8-tetrachlorodibenzo- p -dioxin in Seveso adults and veterans of operation Ranch Hand. *Journal of Exposure Science & Environmental Epidemiology* **12**, 44–53 (2002).

80. J. A. Hanify, P. Metcalf, C. L. Nobbs, K. J. Worsley, Aerial spraying of 2,4,5-T and human birth malformations: an epidemiological investigation. *Science* **212**, 349–351 (1981).

81. C. J. Gordon, Y. Yang, L. E. Gray, Autonomic and behavioral thermoregulation in golden hamsters exposed perinatally to dioxin. *Toxicol. Appl. Pharmacol.* **137**, 120–125 (1996).

82. M. Iida, E.-Y. Kim, Y. Murakami, Y. Shima, H. Iwata, Toxic effects of 2,3,7,8-tetrachlorodibenzo-p-dioxin on the peripheral nervous system of developing red seabream (Pagrus major). *Aquat. Toxicol.* **128–129**, 193–202 (2013).

83. C. Parng, N. M. Roy, C. Ton, Y. Lin, P. McGrath, Neurotoxicity assessment using zebrafish. *J Pharmacol Toxicol Methods* **55**, 103–112 (2007).

84. R. M. Bruno, *et al.*, Sympathetic regulation of vascular function in health and disease. *Front Physiol* **3**, 284 (2012).

85. S. Barbieri, *et al.*, Long-term effects of 2,3,7,8-tetrachlorodibenzo-p-dioxin on the peripheral nervous system. Clinical and neurophysiological controlled study on subjects with chloracne from the Seveso area. *Neuroepidemiology* **7**, 29–37 (1988).

86. M. H. Sweeney, M. A. Fingerhut, J. C. Arezzo, R. W. Hornung, L. B. Connally, Peripheral neuropathy after occupational exposure to 2,3,7,8-tetrachlorodibenzo-p-dioxin (TCDD). *Am. J. Ind. Med.* **23**, 845–858 (1993).

87. A. 't Mannetje, *et al.*, Morbidity in New Zealand pesticide producers exposed to 2,3,7,8-tetrachlorodibenzo-p-dioxin (TCDD). *Environ Int* **110**, 22–31 (2018).

88. R. Pohjanvirta, J. Tuomisto, Remarkable residual alterations in responses to feeding regulatory challenges in Han/Wistar rats after recovery from the acute toxicity of 2,3,7,8-tetrachlorodibenzo-p-dioxin (TCDD). *Food Chem. Toxicol.* **28**, 677–686 (1990).

89. K. Kyösola, O. Penttilä, M. Salaspuro, Rectal mucosal adrenergic innervation and enterochromaffin cells in ulcerative colitis and irritable colon. *Scand. J. Gastroenterol.* **12**, 363–367 (1977).

90. J. Shao, *et al.*, Autonomic nervous infiltration positively correlates with pathological risk grading and poor prognosis in patients with lung adenocarcinoma. *Thorac Cancer* **7**, 588–598 (2016).

91. F. M. Hughes, *et al.*, Bladder decompensation and reduction in nerve density in a rat model of chronic bladder outlet obstruction are attenuated with the NLRP3 inhibitor glyburide. *Am. J. Physiol. Renal Physiol.* **316**, F113–F120 (2019).

92. A. E. Turco, *et al.*, A developmental origin of lower urinary tract dysfunction. *JCI Insight* **Under Review** (2021).

93. A. Bélanger, *et al.*, Changes in serum concentrations of conjugated and unconjugated steroids in 40- to 80-year-old men. *J. Clin. Endocrinol. Metab.* **79**, 1086–1090 (1994).

94. I. of Medicine, B. on H. S. Policy, C. on U. the B. of S. and G. Differences, *Exploring the Biological Contributions to Human Health: Does Sex Matter?* (National Academies Press, 2001).

95. E. S. Shermadou, S. Rahman, S. W. Leslie, “Anatomy, Abdomen and Pelvis, Bladder” in *StatPearls*, (StatPearls Publishing, 2020) (October 30, 2020).

96. B. Abelson, *et al.*, Sex differences in lower urinary tract biology and physiology. *Biol Sex Differ* **9**, 45 (2018).

97. K.-E. Andersson, A. Arner, Urinary bladder contraction and relaxation: physiology and pathophysiology. *Physiol. Rev.* **84**, 935–986 (2004).

98. A. Mangera, N. I. Osman, C. R. Chapple, Anatomy of the lower urinary tract. *Surgery (Oxford)* **31**, 319–325 (2013).

99. J. P. Preslock, A review of in vitro testicular steroidogenesis in rodents, monkeys and humans. *Journal of Steroid Biochemistry* **13**, 965–975 (1980).

100. J. Chen, Y. Zhou, Y. Yu, Z. Shen, [Effects of sex hormones on bladder function and structure: experiment with ovariectomized female rats]. *Zhonghua Yi Xue Za Zhi* **88**, 1851–1854 (2008).

101. B. Eika, *et al.*, Long-term observation of the detrusor smooth muscle in rats. Its relationship to ovariectomy and estrogen treatment. *Urol. Res.* **18**, 439–442 (1990).

102. Y. Tanidir, F. Ercan, T. Tarcan, Exogenous testosterone and estrogen affect bladder tissue contractility and histomorphology differently in rat ovariectomy model. *J Sex Med* **8**, 1626–1637 (2011).

103. C.-C. Liang, T.-H. Lee, S.-D. Chang, Effects of sex hormones on cell proliferation and apoptosis in the urinary bladder muscle of ovariectomized rat. *Taiwan J Obstet Gynecol* **52**, 335–340 (2013).

104. A. Madeiro, *et al.*, Effects of the association of androgen/estrogen on the bladder and urethra of castrated rats. *Clin Exp Obstet Gynecol* **29**, 117–120 (2002).

105. R. de Fraga, M. Dambros, R. Miyaoka, C. L. Zanettini Riccetto, P. C. Rodrigues Palma, Role of 17 β-estradiol on type IV collagen fibers volumetric density in the basement membrane of bladder wall. *Int Urogynecol J* (2007) (October 21, 2020).

106. G. Bravo, *et al.*, Effect of short-term androgen deficiency on bladder contractility and urothelial mediator release. *Naunyn Schmiedebergs Arch Pharmacol* **390**, 547–556 (2017).

107. M. Tek, *et al.*, The effect of testosterone replacement therapy on bladder functions and histology in orchiectomized mature male rats. *Urology* **75**, 886–890 (2010).

108. C. A. V. de Barros, F. Lorenzetti, V. Ortiz, M. Dambros, Testosterone supplementation's effects on age-related bladder remodeling - experimental study in rats. *Aging Male* **16**, 102–107 (2013).

109. A. S. Flum, *et al.*, Testosterone Modifies Alterations to Detrusor Muscle after Partial Bladder Outlet Obstruction in Juvenile Mice. *Front Pediatr* **5** (2017).

110. S. Celayir, Effects of different sex hormones on male rabbit urodynamics: an experimental study. *Horm. Res.* **60**, 215–220 (2003).

111. H. Ruetten, *et al.*, Impact of sex, androgens, and prostate size on C57BL/6J mouse urinary physiology: functional assessment. *Am J of Physio-Ren- Physio* **317**, F996–F1009 (2019).

112. H. Ruetten, *et al.*, Impact of sex, androgens, and prostate size on C57BL/6J mouse urinary physiology: urethral histology. *Am J Physiol Renal Physiol* **318**, F617–F627 (2020).

113. T. Walz, *et al.*, Towards the molecular architecture of the asymmetric unit membrane of the mammalian urinary bladder epithelium: a closed "twisted ribbon" structure. *J. Mol. Biol.* **248**, 887–900 (1995).

114. T. Aboushwareb, *et al.*, Alterations in Bladder Function Associated With Urothelial Defects in Uroplakin II and IIIa Knockout Mice. *Neurourol Urodyn* **28**, 1028–1033 (2009).

115. H. Kobayashi, M. Yoshiyama, H. Zakoji, M. Takeda, I. Araki, Sex differences in the expression profile of acid-sensing ion channels in the mouse urinary bladder: a possible involvement in irritative bladder symptoms. *BJU Int.* **104**, 1746–1751 (2009).

116. L. A. Thornton, *et al.*, The Effect of Urine Concentration and pH on the Growth of Escherichia Coli in Canine Urine In Vitro. *J Vet Intern Med* **32**, 752–756 (2018).

117. P. Lüthje, *et al.*, Estrogen supports urothelial defense mechanisms. *Sci Transl Med* **5**, 190ra80 (2013).

118. C. Wang, J. W. Symington, E. Ma, B. Cao, I. U. Mysorekar, Estrogenic modulation of uropathogenic Escherichia coli infection pathogenesis in a murine menopause model. *Infect. Immun.* **81**, 733–739 (2013).

119. M. Acevedo-Alvarez, *et al.*, Mouse urothelial genes associated with voiding behavior changes after ovariectomy and bladder lipopolysaccharide exposure. *Neurourol. Urodyn.* **37**, 2398–2405 (2018).

120. H. Schulze, E. R. Barrack, Immunocytochemical localization of estrogen receptors in the normal male and female canine urinary tract and prostate. *Endocrinology* **121**, 1773–1783 (1987).

121. M. Yasui, *et al.*, Distribution of androgen receptor expression in the urinary bladder. *International Journal of Urology* **26**, 305–306 (2019).

122. J. S. Dixon, J. A. Gosling, “Ultrastructure of smooth muscle cells in the urinary system” in *Ultrastructure of Smooth Muscle*, Electron Microscopy in Biology and Medicine., P. M. Motta, Ed. (Springer US, 1990), pp. 153–169.

123. P. R. Brink, Gap junctions in vascular smooth muscle. *Acta Physiol Scand* **164**, 349–356 (1998).

124. J. C. Rüegg, *Calcium in Muscle Contraction: Cellular and Molecular Physiology* (Springer Science & Business Media, 2012).

125. A. F. Brading, The sarcoplasmic reticulum in disease and smooth muscle dysfunction: therapeutic potential. *Novartis Found Symp* **246**, 244–254; discussion 254-257, 272–276 (2002).

126. G. Ji, R. J. Barsotti, M. E. Feldman, M. I. Kotlikoff, Stretch-induced calcium release in smooth muscle. *J Gen Physiol* **119**, 533–544 (2002).

127. A. Arner, G. Pfitzer, Regulation of cross-bridge cycling by Ca2+ in smooth muscle. *Rev Physiol Biochem Pharmacol* **134**, 63–146 (1999).

128. P. H. Ratz, *et al.*, Differential effects of sex hormones and phytoestrogens on peak and steady state contractions in isolated rabbit detrusor. *J. Urol.* **162**, 1821–1828 (1999).

129. K. L. Hristov, S. P. Parajuli, A. Provence, E. S. Rovner, G. V. Petkov, Nongenomic modulation of the large conductance voltage- and Ca2+-activated K+ channels by estrogen: A novel regulatory mechanism in human detrusor smooth muscle. *Physiol Rep* **5** (2017).

130. V. A. Coit, I. F. Gibson, N. P. Evans, F. J. Dowell, Neutering affects urinary bladder function by different mechanisms in male and female dogs. *Eur J Pharmacol* **584**, 153–158 (2008).

131. W.-Y. Lin, *et al.*, Effect of letrozole on urinary bladder function in the female rabbit. *BJU Int.* **100**, 1391–1395 (2007).

132. N. Li, H. Ding, X. He, Z. Li, Y. Liu, Expression and function of the small-conductance Ca2+-activated K+ channel is decreased in urinary bladder smooth muscle cells from female guinea pig with partial bladder outlet obstruction. *Int Urol Nephrol* **49**, 1147–1155 (2017).

133. M. C. Stanton, *et al.*, Partial bladder outlet obstruction selectively abolishes protein kinase C induced contraction of rabbit detrusor smooth muscle. *J Urol* **176**, 2716–2721 (2006).

134. F. M. Hughes, S. J. Sexton, H. Jin, V. Govada, J. T. Purves, Bladder fibrosis during outlet obstruction is triggered through the NLRP3 inflammasome and the production of IL-1β. *Am J Physiol Renal Physiol* **313**, F603–F610 (2017).

135. R. Kranse, R. van Mastrigt, Weak correlation between bladder outlet obstruction and probability to void to completion. *Urology* **62**, 667–671 (2003).

136. L. M. D. Shortliffe, Y. Ye, B. Behr, B. Wang, Testosterone changes bladder and kidney structure in juvenile male rats. *J. Urol.* **191**, 1913–1919 (2014).

137. V. S. Fernandes, *et al.*, Mechanisms involved in testosterone-induced relaxation to the pig urinary bladder neck. *Steroids* **77**, 394–402 (2012).

138. J. A. Gosling, J. S. Dixon, P. Y. Jen, The distribution of noradrenergic nerves in the human lower urinary tract. A review. *Eur. Urol.* **36 Suppl 1**, 23–30 (1999).

139. B. Baader, M. Herrmann, Topography of the pelvic autonomic nervous system and its potential impact on surgical intervention in the pelvis. *Clinical Anatomy* **16**, 119–130 (2003).

140. K. Yamaguchi, M. Kobayashi, T. Kato, K. Akita, Origins and distribution of nerves to the female urinary bladder: New anatomical findings in the sex differences. *Clinical Anatomy* **24**, 880–885 (2011).

141. D. Greenwood, R. E. Coggeshall, C. E. Hulsebosch, Sexual dimorphism in the number of neurons in the pelvic ganglia of adult rats. *Brain Research* **340**, 160–162 (1985).

142. W. G. Dail, A. P. Evan, H. R. Eason, The major ganglion in the pelvic plexus of the male rat: a histochemical and ultrastructural study. *Cell Tissue Res.* **159**, 49–62 (1975).

143. A. C. Mills, D. R. Sengelaub, Sexually dimorphic neuron number in lumbosacral dorsal root ganglia of the rat: development and steroid regulation. *J. Neurobiol.* **24**, 1543–1553 (1993).

144. Y. Yang, *et al.*, Immunocytochemical analysis of sex differences in calcitonin gene-related peptide in the rat dorsal root ganglion, with special reference to estrogen and its receptor. *Brain Research* **791**, 35–42 (1998).

145. H. L. Bennett, J.-Å. Gustafsson, J. R. Keast, Estrogen receptor expression in lumbosacral dorsal root ganglion cells innervating the female rat urinary bladder. *Autonomic Neuroscience* **105**, 90–100 (2003).

146. S. Dohkita, T. Nishimoto, T. Morita, Noradrenaline content in canine lower urinary tract tissue. *Tohoku J. Exp. Med.* **151**, 117–119 (1987).

147. J. G. Lee, A. J. Wein, R. M. Levin, Comparative Pharmacology of the Male and Female Rabbit Bladder Neck and Urethra: Involvement of Nitric Oxide. *Pharmacology* **48**, 250–259 (1994).

148. T. Morita, *et al.*, Sex differences in function and distribution of beta-adrenoceptors in rabbit urinary bladder. *J. Urol.* **159**, 555–558 (1998).

149. D. Felsen, STUDIES ON GENDER DIFFERENCES IN beta-ADRENERGIC RECEPTORS IN RABBIT BLADDER. *The Journal of Urology* **159**, 346 (1998).

150. J. R. Keast, R. J. Saunders, Testosterone has potent, selective effects on the morphology of pelvic autonomic neurons which control the bladder, lower bowel and internal reproductive organs of the male rat. *Neuroscience* **85**, 543–556 (1998).

151. R. Hall, P. L. R. Andrews, C. H. V. Hoyle, Effects of testosterone on neuromuscular transmission in rat isolated urinary bladder. *European Journal of Pharmacology* **449**, 301–309 (2002).

152. S. Sigala, *et al.*, Alpha1 adrenoceptor subtypes in human urinary bladder: sex and regional comparison. *Life Sci.* **76**, 417–427 (2004).

153. S. Takyu, [Effects of testosterone on the autonomic receptor-mediated function in lower urinary tract from male rabbits]. *Nippon Hinyokika Gakkai Zasshi* **84**, 330–338 (1993).

154. P. Abrams, *et al.*, The standardisation of terminology of lower urinary tract function: Report from the standardisation sub-committee of the international continence society. *American Journal of Obstetrics and Gynecology* **187**, 116–126 (2002).

155. J.-Y. Wang, L. Liao, M. Liu, B. Sumarsono, M. Cong, Epidemiology of lower urinary tract symptoms in a cross-sectional, population-based study. *Medicine (Baltimore)* **97** (2018).

156. J. M. Kaufman, A. Vermeulen, The decline of androgen levels in elderly men and its clinical and therapeutic implications. *Endocr. Rev.* **26**, 833–876 (2005).

157. S. A. Kaplan, E. O'Neill, R. Lowe, M. Hanson, A. G. Meehan, Prevalence of low testosterone in aging men with benign prostatic hyperplasia: data from the Proscar Long-term Efficacy and Safety Study (PLESS). *Aging Male* **16**, 48–51 (2013).

158. I. Fejes, *et al.*, Effect of body weight on testosterone/estradiol ratio in oligozoospermic patients. *Arch Androl* **52**, 97–102 (2006).

159. C.-L. Cheng, W. C. de Groat, Effect of orchiectomy and testosterone replacement on lower urinary tract function in anesthetized rats. *American Journal of Physiology-Renal Physiology* **311**, F864–F870 (2016).

160. A. A. Yassin, A. I. El-Sakka, F. Saad, L. J. G. Gooren, Lower urinary-tract symptoms and testosterone in elderly men. *World J Urol* **26**, 359–364 (2008).

161. A. Haider, L. J. G. Gooren, P. Padungtod, F. Saad, A safety study of administration of parenteral testosterone undecanoate to elderly men over minimally 24 months. *Andrologia* **42**, 349–355 (2010).

162. P. Comeglio, *et al.*, Opposite effects of tamoxifen on metabolic syndrome-induced bladder and prostate alterations: a role for GPR30/GPER? *Prostate* **74**, 10–28 (2014).

163. K. B. Egan, *et al.*, Do baseline estrogen and testosterone affect lower urinary tract symptoms (LUTD) prior to or after pharmacologic treatment with tadalafil? *Andrology* **3**, 1165–1172 (2015).

164. M. Hanus, M. Matousková, [Antiestrogens (tamoxifen) in the alternative therapy of benign prostatic hyperplasia]. *Rozhl Chir* **72**, 316–318 (1993).

165. C. G. Roehrborn, *et al.*, Estrogen receptor beta agonist LY500307 fails to improve symptoms in men with enlarged prostate secondary to benign prostatic hypertrophy. *Prostate Cancer Prostatic Dis* **18**, 43–48 (2015).

166. W. Mahapokai, *et al.*, Cell kinetics and differentiation after hormonal-induced prostatic hyperplasia in the dog. *Prostate* **44**, 40–48 (2000).

167. P. C. Walsh, J. D. Wilson, The induction of prostatic hypertrophy in the dog with androstanediol. *J. Clin. Invest.* **57**, 1093–1097 (1976).

168. G. Aumüller, *et al.*, Phenotypic modulation of the canine prostate after long-term treatment with androgens and estrogens. *Prostate* **3**, 361–373 (1982).

169. M. L. Winter, *et al.*, Induction of benign prostatic hyperplasia in intact dogs by near-physiological levels of 5 alpha-dihydrotestosterone and 17 beta-estradiol. *Prostate* **26**, 325–333 (1995).

170. Y. Zhou, *et al.*, Proliferation and phenotypic changes of stromal cells in response to varying estrogen/androgen levels in castrated rats. *Asian J Androl* **11**, 451–459 (2009).

171. C. E. Constantinou, S. Omata, Analysis of the relative biomechanical effects of alpha 1 and alpha 2 antagonists in modifying the compliance of the prostate and micturition parameters of the hormonally manipulated male rat. *Neurourol Urodyn* **15**, 85–101 (1996).

172. T. M. Nicholson, *et al.*, Estrogen receptor-alpha is a key mediator and therapeutic target for bladder complications of benign prostatic hyperplasia. *J Urol* **193**, 722–729 (2015).

173. A. Shabsigh, *et al.*, Clomiphene citrate effects on testosterone/estrogen ratio in male hypogonadism. *J Sex Med* **2**, 716–721 (2005).

174. L. R. D. Varella, *et al.*, Assessment of lower urinary tract symptoms in different stages of menopause. *J Phys Ther Sci* **28**, 3116–3121 (2016).

175. R. E. Nappi, S. R. Davis, The use of hormone therapy for the maintenance of urogynecological and sexual health post WHI. *Climacteric* **15**, 267–274 (2012).

176. S. Tatemichi, *et al.*, A Selective α1A-Adrenoceptor Antagonist Inhibits Detrusor Overactivity in a Rat Model of Benign Prostatic Hyperplasia. *The Journal of Urology* (2006) (September 18, 2020).

177. A. Valeri, K. L. Brain, J. S. Young, G. Sgaragli, F. Pessina, Effects of 17β-oestradiol on rat detrusor smooth muscle contractility. *Exp Physiol* **94**, 834–846 (2009).

178. K. L. Hristov, S. P. Parajuli, A. Provence, G. V. Petkov, Testosterone decreases urinary bladder smooth muscle excitability via novel signaling mechanism involving direct activation of the BK channels. *American Journal of Physiology-Renal Physiology* **311**, F1253–F1259 (2016).

179. M. Brasure, *et al.*, Table 1, Medications used to treat LUTD attributed to BPH (2016) (October 22, 2020).

180. S. Filippi, *et al.*, Characterization and functional role of androgen-dependent PDE5 activity in the bladder. *Endocrinology* **148**, 1019–1029 (2007).

181. L. Vignozzi, *et al.*, Testosterone/Estradiol Ratio Regulates NO-Induced Bladder Relaxation and Responsiveness to PDE5 Inhibitors. *The Journal of Sexual Medicine* **9**, 3028–3040 (2012).

182. M. Kathrins, *et al.*, The Relationship Between Testosterone-Replacement Therapy and Lower Urinary Tract Symptoms: A Systematic Review. *Urology* **88**, 22–32 (2016).

183. F. Saad, L. Gooren, A. Haider, A. Yassin, An Exploratory Study of the Effects of 12 Month Administration of the Novel Long-Acting Testosterone Undecanoate on Measures of Sexual Function and the Metabolic Syndrome. *Archives of Andrology* **53**, 353–357 (2007).

184. D. Yassin, G. Doros, P. G. Hammerer, A. A. Yassin, Long-Term Testosterone Treatment in Elderly Men with Hypogonadism and Erectile Dysfunction Reduces Obesity Parameters and Improves Metabolic Syndrome and Health-Related Quality of Life. *The Journal of Sexual Medicine* **11**, 1567–1576 (2014).

185. S. Karazindiyanoğlu, S. Cayan, The effect of testosterone therapy on lower urinary tract symptoms/bladder and sexual functions in men with symptomatic late-onset hypogonadism. *Aging Male* **11**, 146–149 (2008).

186. K. S. Haider, A. Haider, G. Doros, A. Traish, Long-Term Testosterone Therapy Improves Urinary and Sexual Function, and Quality of Life in Men with Hypogonadism: Results from a Propensity Matched Subgroup of a Controlled Registry Study. *J. Urol.* **199**, 257–265 (2018).

187. H. U. Schweikert, U. W. Tunn, Effects of the aromatase inhibitor testolactone on human benign prostatic hyperplasia. *Steroids* **50**, 191–200 (1987).

188. A. A. M. Abdel-Hamid, E. M. T. Ali, Effect of testosterone therapy on the urinary bladder in experimental hypogonadism of rats. *J. Mol. Histol.* **46**, 263–272 (2015).

189. J. Flamm, H. Kiesswetter, M. Englisch, [An urodynamic study of patients with benign prostatic hypertrophy treated conservatively with phytotherapy or testosterone (author's transl)]. *Wien. Klin. Wochenschr.* **91**, 622–627 (1979).

190. P. F. Keane, A. G. Timoney, E. Kiely, G. Williams, G. Stamp, Response of the benign hypertrophied prostate to treatment with an LHRH analogue. *Br J Urol* **62**, 163–165 (1988).

191. V. W. Nitti, The Prevalence of Urinary Incontinence. *Rev Urol* **3**, S2–S6 (2001).

192. J. I. Mäkinen, *et al.*, Transdermal estrogen for female stress urinary incontinence in postmenopause. *Maturitas* **22**, 233–238 (1995).

193. G. Legendre, X. Fritel, V. Ringa, M. Lesavre, H. Fernandez, [Urinary incontinence and menopause]. *Prog. Urol.* **22**, 615–621 (2012).

194. N. Diep, C. E. Constantinou, Age dependent response to exogenous estrogen on micturition, contractility and cholinergic receptors of the rat bladder. *Life Sci.* **64**, PL 279-289 (1999).

195. D. D. Kane, J. M. Kerns, D. L. Lin, M. S. Damaser, Early structural effects of oestrogen on pudendal nerve regeneration in the rat. *BJU International* **93**, 870–878 (2004).

196. D. K. Kim, M. B. Chancellor, Is Estrogen for Urinary Incontinence Good or Bad? *Rev Urol* **8**, 91–92 (2006).

197. M. C. Veronesi, A. Rota, M. Battocchio, M. Faustini, A. Mollo, Spaying-related urinary incontinence and oestrogen therapy in the bitch. *Acta Vet Hung* **57**, 171–182 (2009).

198. K. Hirai, H. Tsuda, Estrogen and urinary incontinence. *International Journal of Urology* **16**, 45–48 (2009).

199. F. Sacco, G. Rigon, A. Carbone, D. Sacchini, [Transvaginal estrogen therapy in urinary stress incontinence]. *Minerva Ginecol* **42**, 539–544 (1990).

200. J. D. Cody, M. L. Jacobs, K. Richardson, B. Moehrer, A. Hextall, Oestrogen therapy for urinary incontinence in post-menopausal women. *Cochrane Database Syst Rev* **10**, CD001405 (2012).

201. S. L. Hendrix, Effects of Estrogen With and Without Progestin on Urinary Incontinence. *JAMA* **293**, 935 (2005).

202. M. K. TOWNSEND, G. C. CURHAN, N. M. RESNICK, F. GRODSTEIN, Postmenopausal hormone therapy and incident urinary incontinence in middle-aged women. *Am J Obstet Gynecol* **200**, 86.e1-86.e5 (2009).

203. W. F. Stewart, *et al.*, Prevalence and burden of overactive bladder in the United States. *World J Urol* **20**, 327–336 (2003).

204. H. K. Kallner, C. Elmér, K.-E. Andersson, D. Altman, Hormonal influence on the effect of mirabegron treatment for overactive bladder. *Menopause* **23**, 1303–1306 (2016).

205. Z. Pan, H. Yang, P. S. Reinach, Transient receptor potential (TRP) gene superfamily encoding cation channels. *Hum Genomics* **5**, 108–116 (2011).

206. K.-E. Andersson, TRP Channels as Lower Urinary Tract Sensory Targets. *Med Sci (Basel)* **7** (2019).

207. S. Xu, Y. Cheng, J. R. Keast, P. B. Osborne, 17β-Estradiol Activates Estrogen Receptor β-Signalling and Inhibits Transient Receptor Potential Vanilloid Receptor 1 Activation by Capsaicin in Adult Rat Nociceptor Neurons. *Endocrinology* **149**, 5540–5548 (2008).

208. B. M. Girard, L. Merrill, S. Malley, M. A. Vizzard, Increased TRPV4 expression in urinary bladder and lumbosacral dorsal root ganglia in mice with chronic overexpression of NGF in urothelium. *J Mol Neurosci* **51**, 602–614 (2013).

209. T. Gevaert, *et al.*, Deletion of the transient receptor potential cation channel TRPV4 impairs murine bladder voiding. *J Clin Invest* **117**, 3453–3462 (2007).

210. M. Artero-Morales, S. González-Rodríguez, A. Ferrer-Montiel, TRP Channels as Potential Targets for Sex-Related Differences in Migraine Pain. *Front Mol Biosci* **5** (2018).

211. C. Jung, *et al.*, The progesterone receptor regulates the expression of TRPV4 channel. *Pflugers Arch* **459**, 105–113 (2009).

212. K. Pohóczky, *et al.*, Estrogen-dependent up-regulation of TRPA1 and TRPV1 receptor proteins in the rat endometrium. *Journal of Molecular Endocrinology* **56**, 135–149 (2016).

213. K. P. Keil, *et al.*, Impact of a folic acid-enriched diet on urinary tract function in mice treated with testosterone and estradiol. *American Journal of Physiology-Renal Physiology* **308**, F1431–F1443 (2015).

214. A. Valeri, *et al.*, The soy phytoestrogens genistein and daidzein as neuroprotective agents against anoxia-glucopenia and reperfusion damage in rat urinary bladder. *Pharmacol. Res.* **66**, 309–316 (2012).

215. S. K. Kim, *et al.*, Effects of Panax ginseng on the nerve growth factor expression in testosterone induced benign prostatic hyperplasia. *Saudi J Biol Sci* **25**, 66–70 (2018).

216. C. H. Nauman, J. L. Schaum, Human exposure estimation for 2,3,7,8-TCDD. *Chemosphere* **16**, 1851–1856 (1987).

217. M. Kakeyama, H. Sone, Y. Miyabara, C. Tohyama, Perinatal exposure to 2,3,7,8-tetrachlorodibenzo-p-dioxin alters activity-dependent expression of BDNF mRNA in the neocortex and male rat sexual behavior in adulthood. *Neurotoxicology* **24**, 207–217 (2003).

218. A. E. Turco, *et al.*, In utero and lactational 2,3,7,8-tetrachlorodibenzo-p-dioxin (TCDD) exposure exacerbates urinary dysfunction in hormone-treated C57BL/6J mice through a

non-malignant mechanism involving proteomic changes in the prostate that differ from those elicited by testosterone and estradiol. *Am J Clin Exp Urol* **8**, 59–72 (2020).

219. E. Dodds, W. Lawson, Synthetic strogenic Agents without the Phenanthrene Nucleus | Nature. *1936* (1936) (September 25, 2020).

220. T. M. Nicholson, *et al.*, Endocrine disruptor bisphenol A is implicated in urinary voiding dysfunction in male mice. *Am J Physiol Renal Physiol* **315**, F1208–F1216 (2018).

221. J. A. Taylor, *et al.*, Interactive Effects of Perinatal BPA or DES and Adult Testosterone and Estradiol Exposure on Adult Urethral Obstruction and Bladder, Kidney, and Prostate Pathology in Male Mice. *Int J Mol Sci* **21** (2020).

222. S. T. McMurry, R. L. Lochmiller, S. A. Chandra, C. W. Qualls, Sensitivity of selected immunological, hematological, and reproductive parameters in the cotton rat (Sigmodon hispidus) to subchronic lead exposure. *J. Wildl. Dis.* **31**, 193–204 (1995).

223. X. Wu, *et al.*, A brief exposure to cadmium impairs Leydig cell regeneration in the adult rat testis. *Sci Rep* **7**, 6337 (2017).

224. M. Bornman, *et al.*, Alterations in male reproductive hormones in relation to environmental DDT exposure. *Environ Int* **113**, 281–289 (2018).

225. A. Ben Slima, *et al.*, Endocrine disrupting potential and reproductive dysfunction in male mice exposed to deltamethrin. *Hum Exp Toxicol* **36**, 218–226 (2017).

226. N. R. Janjua, *et al.*, Systemic absorption of the sunscreens benzophenone-3, octyl-methoxycinnamate, and 3-(4-methyl-benzylidene) camphor after whole-body topical application and reproductive hormone levels in humans. *J. Invest. Dermatol.* **123**, 57–61 (2004).

227. J. Gu, *et al.*, Urinary concentration of personal care products and polycystic ovary syndrome: A case-control study. *Environ. Res.* **168**, 48–53 (2019).

228. S. Durrer, K. Maerkel, M. Schlumpf, W. Lichtensteiger, Estrogen target gene regulation and coactivator expression in rat uterus after developmental exposure to the ultraviolet filter 4-methylbenzylidene camphor. *Endocrinology* **146**, 2130–2139 (2005).

229. N. Nakamura, *et al.*, Transcript profiling in the testes and prostates of postnatal day 30 Sprague-Dawley rats exposed prenatally and lactationally to 2-hydroxy-4-methoxybenzophenone. *Reprod. Toxicol.* **82**, 111–123 (2018).

230. M. Krause, *et al.*, Sunscreens: are they beneficial for health? An overview of endocrine disrupting properties of UV-filters. *Int. J. Androl.* **35**, 424–436 (2012).

231. X. Zhang, *et al.*, Testosterone regulates smooth muscle contractile pathways in the rat prostate: emphasis on PDE5 signaling. *American Journal of Physiology-Endocrinology and Metabolism* **302**, E243–E253 (2011).

232. M. Hennenberg, *et al.*, Inhibition of Prostate Smooth Muscle Contraction by Inhibitors of Polo-Like Kinases. *Front Physiol* **9** (2018).

233. R. Kügler, *et al.*, Novel imaging of the prostate reveals spontaneous gland contraction and excretory duct quiescence together with different drug effects. *The FASEB Journal* **32**, 1130–1138 (2018).

234. M. Lam, Y. Shigemasa, B. Exintaris, R. J. Lang, H. Hashitani, Spontaneous Ca2+ signaling of interstitial cells in the guinea pig prostate. *J. Urol.* **186**, 2478–2486 (2011).

235. J. Nakai, M. Ohkura, K. Imoto, A high signal-to-noise Ca(2+) probe composed of a single green fluorescent protein. *Nat. Biotechnol.* **19**, 137–141 (2001).

236. J. W. Wang, A. M. Wong, J. Flores, L. B. Vosshall, R. Axel, Two-photon calcium imaging reveals an odor-evoked map of activity in the fly brain. *Cell* **112**, 271–282 (2003).

237. G. Ji, *et al.*, Ca2+-sensing transgenic mice: postsynaptic signaling in smooth muscle. *J. Biol. Chem.* **279**, 21461–21468 (2004).

238. N. C. Chi, *et al.*, Genetic and physiologic dissection of the vertebrate cardiac conduction system. *PLoS Biol.* **6**, e109 (2008).

239. W. Boesmans, *et al.*, Imaging neuron-glia interactions in the enteric nervous system. *Front Cell Neurosci* **7**, 183 (2013).

240. K. M. Smith-Edwards, J. J. DeBerry, J. L. Saloman, B. M. Davis, C. J. Woodbury, Profound alteration in cutaneous primary afferent activity produced by inflammatory mediators. *Elife* **5** (2016).

241. C. Zhong, J. Schleifenbaum, Genetically Encoded Calcium Indicators: A New Tool in Renal Hypertension Research. *Front Med (Lausanne)* **6** (2019).

242. A. E. Turco, *et al.*, Testosterone and estradiol mediate male voiding dysfunction by reducing prostatic smooth muscle Ppp112b abundance and impairing muscle relaxation. *PNAS* **Under review** (2021).

243. S. Wang, J. A. Hossack, A. L. Klibanov, Targeting of microbubbles - contrast agents for ultrasound molecular imaging. *J Drug Target* **26**, 420–434 (2018).

244. M. A. Ritter, E. B. Ringelstein, The Venturi effect and cerebrovascular ultrasound. *Cerebrovasc. Dis.* **14**, 98–104 (2002).

245. T. M. Nicholson, *et al.*, Estrogen receptor-alpha is a key mediator and therapeutic target for bladder complications of benign prostatic hyperplasia. *J Urol* **193**, 722–729 (2015).

246. C. G. Roehrborn, Pathology of benign prostatic hyperplasia. *Int. J. Impot. Res.* **20 Suppl 3**, S11-18 (2008).

247. N. Hayashi, *et al.*, Effect of extended-term estrogen on voiding in a postpartum ovariectomized rat model. *Can Urol Assoc J* **1**, 256–263 (2007).

248. K. P. Keil, *et al.*, Impact of a folic acid-enriched diet on urinary tract function in mice treated with testosterone and estradiol. *Am J Physiol Renal Physiol* **308**, F1431–F1443 (2015).

249. T. M. Nicholson, *et al.*, Endocrine disruptor bisphenol A is implicated in urinary voiding dysfunction in male mice. *Am J Physiol Renal Physiol* **315**, F1208–F1216 (2018).

Figures and tables

Table 1. Impact of estradiol and testosterone modulation on bladder cells

Bladder Cell type	**Sex Hormone Modulation**	**Characteristic**	**Reference**
Detrusor smooth muscle	Supraphysiological testosterone	1. Thicker in men Increases bladder capacity 2. Increases smooth muscle thickness 3. Reduces or increases collagen depending on concentration	(98, 107)
Detrusor smooth muscle	Subphysiological estrogens	1. Decrease detrusor thickness 2.Gaps in muscle cells 3. Bladder weight decreases 4. Increased collagen accumulation	(100, 101)
Detrusor smooth muscle	Subphysiological testosterone	Bladder atrophy, smooth muscle thickness Increases collagen	(107)
Detrusor function	Supraphysiological estrogens	Increases bladder capacity and compliance	(110)
Urothelium	Supraphysiological testosterone	Male Upk3 null mice have urinary retention, increased bladder pressure	(114)

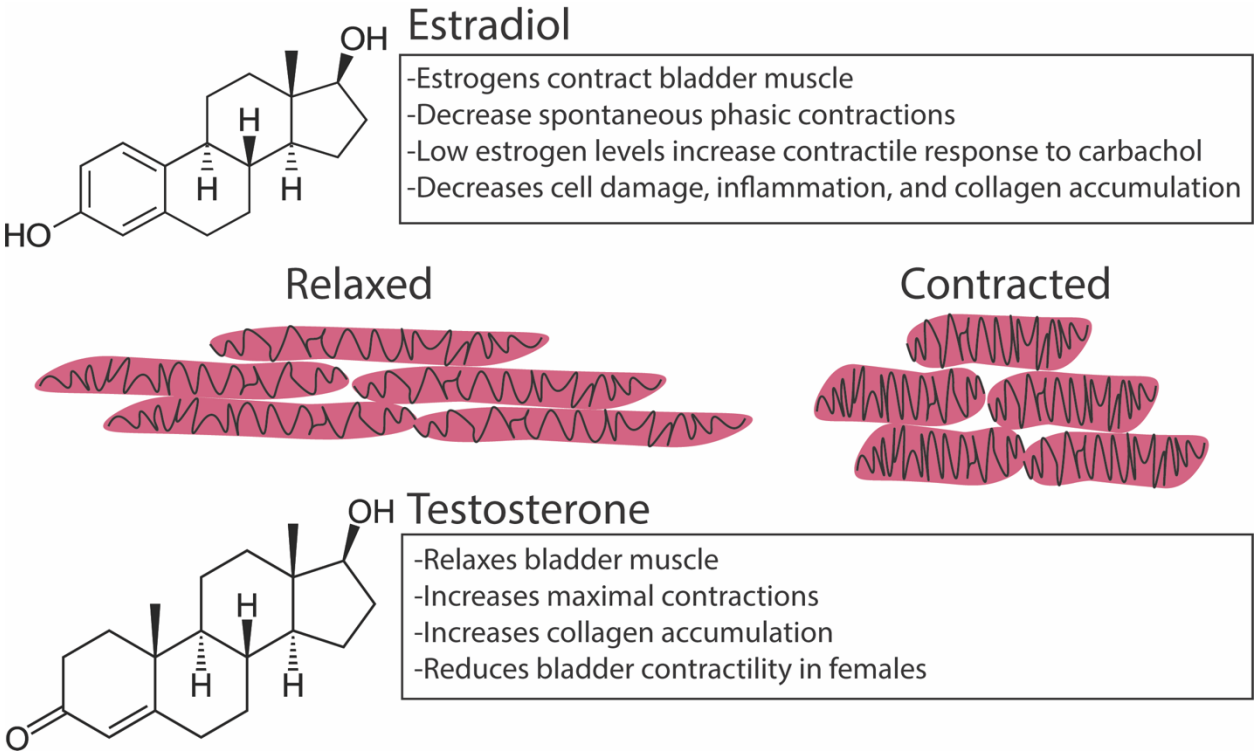

Figure 1. The impact of estradiol and testosterone on bladder muscle contraction and relaxation

Table 2. Impact of testosterone and estradiol modulation on bladder innervation

Sex hormone modulation	**Impact on LUTD**	**Reference**
Subphysiological testosterone	1. Decreased with age and correlated with LUTD severity 2. Decrease volume threshold 3. Decreased mean flow rate 4. Does not impact LUTD severity	(159)
Supraphysiological testosterone	1. Decreased LUTD and post void residual urine 2. Decreases smooth muscle excitability via BK channels 3. Increases bladder capacity and compliance 4. Reduces IPSS scores long term	(161, 178, 185, 186)
Subphysiological estrogen	Improved IPSS after pharmacological treatment	(163)
Estrogen supplementation	1. Ineffective for human LUTD 2. Clomiphene decreased LUTD phenotype in mice	(245–247)
Testosterone + estradiol supplementation	Causes progressive bladder outlet obstruction, fibrosis, and decompensation in mice, rats, and dogs	(3, 166–168)

Table 3. Environmental estrogens can impact bladder structure and function

Chemical	**Modulate Testosterone or estradiol?**	**Impact on bladder**	**Reference**
Folic acid	No	Protects against LUTD in mice	(248)
Soy phytoestrogens	Estrogen	Decrease rat detrusor contractions	(214)
Panax Ginseng	No	Protects against LUTD in mice	(215)
2,3,7,8-tetrachlorodibenzo-p-dioxin (TCDD)	Estrogen	Worsens testosterone and estradiol mediated LUTD after developmental exposure in mice	(2, 218)
BPA	Estrogen	Increases spontaneous voiding and urinary retention in mice	(249)
UV filters	Estrogen	Decrease prostate and testis weight, impact on bladder unknown	(229)

Chapter 2: A Temporal and Spatial Map of Axons in Developing Mouse Prostate

Turco AE, Cadena MT, Zhang HL, Sandhu JK, Oakes SR, Chathurvedula T, Peterson RE, Keast JR, Vezina CM. (2019). Journal of Histochemistry and Cell Biology. PMID: 30976911

Abstract

Prostate autonomic and sensory axons control glandular growth, fluid secretion, and smooth muscle contraction and are remodeled during cancer and inflammation. Morphogenetic signaling pathways reawakened during disease progression may drive this axon remodeling. These pathways are linked to proliferative activities in prostate cancer and benign prostate hyperplasia. However, little is known about which developmental signaling pathways guide axon investment into prostate. The first step in defining these pathways is pinpointing when axon subtypes first appear in prostate. We accomplished this by immunohistochemically mapping three axon subtypes (noradrenergic, cholinergic, and peptidergic) during fetal, neonatal, and adult stages of mouse prostate development. We devised a method for periprostatic axon density quantification and tested whether innervation is uniform across the proximo-distal axis of dorsal and ventral adult mouse prostate. Many axons directly interact with or innervate neuroendocrine cells in other organs, so we examined whether sensory or autonomic axons innervate neuroendocrine cells in prostate. We first detected noradrenergic, cholinergic, and peptidergic axons in prostate at embryonic day (E)14.5. Noradrenergic and cholinergic axon densities are uniform across the proximal-distal axis of adult mouse prostate while peptidergic axons are denser in the periurethral and proximal regions. Peptidergic and cholinergic axons are closely associated with prostate neuroendocrine cells whereas noradrenergic axons are not. These results provide a foundation for understanding mouse prostatic axon development and organization and provides strategies for quantifying axons during progression of prostate disease.

Introduction

Peripheral neurons regulate cellular functions of breast (1), skin (2), lung (3), intestine (4), bladder (5) and kidney (6). Although modulatory actions of peripheral neurons in prostate cancer, benign hyperplasia, and inflammation are increasingly supported by peer-reviewed publications, the function of peripheral neurons in the prostate is not fully understood (7). The structure and function of prostate is maintained by axons, as indicated by denervation studies, but the mechanisms are unclear (7, 8). Noradrenergic axons in healthy mouse prostate contract vascular and non-vascular smooth muscle (9). Cholinergic axons change ion fluxes across the epithelium, promoting secretion in healthy prostate tissue (10). In prostate cancer, prostatic noradrenergic and cholinergic axon outgrowth promotes cancer development, cancer dissemination and tumor invasion, and positively correlates with tumor severity in patients with prostate adenocarcinoma (11–13). The role of sensory axons in the prostate are relatively uncharacterized. In other organs such as the bladder, heart, and stomach, sensory axons sense stretch as the organ fills (15). Prostatic sensory axon density and nerve growth factor (NGF) abundance in prostatic fluid are elevated in men with prostatitis (16, 17). How noradrenergic, cholinergic, and peptidergic axons contribute to prostatic disease is poorly understood, in part because axon development and innervation patterns in healthy developing and mature prostate are incompletely characterized.

Previous studies have examined autonomic and sensory prostate axon innervation. Early studies focused almost exclusively on sympathetic innervation, reporting noradrenergic innervation of the prostate stroma and capsule using immunohistochemistry and pharmacological stimulation studies (18–22). Further, prostate glandular tissue was reported to be innervated by an unidentified type of sympathetic axon (23). A rat study examined location, properties, distribution and spinal connections of autonomic postganglionic pathways innervating prostate using retrograde labeling, nerve lesions, and immunofluorescence (24). This study identified two different cholinergic axons innervating the prostate, parasympathetic and sympathetic (24). These neurons were classified as cholinergic because they lacked detectable tyrosine hydroxylase (TH)

and all TH-negative neurons in the rat pelvic ganglion express the synthetic enzyme for acetylcholine, choline acetyltransferase. Another study examined, over a limited time period, the development of peripheral axons in the prostate and concluded there were very few autonomic axons in mouse reproductive tissue prior to birth, with the density and depth of penetration increasing throughout the postnatal period (25). However, this study did not examine embryonic periods or quantify axon densities in different prostate regions. The current study uniquely builds on previous work by studying the innervation and development patterns of noradrenergic, cholinergic, and peptidergic axons from before birth to sexual maturity in mice. Further, this is the first study, to our knowledge to describe the location and density of sensory axons in mouse prostate. We have also directly identified cholinergic axons using antibodies raised against vesicular acetylcholine transporter (VAChT), whereas many previous studies used the indirect makers, VIP or nNOS that potentially label only a subclass of cholinergic axons.

Here, we immunohistochemically mapped noradrenergic (tyrosine hydroxylase, TH), cholinergic (VAChT) and peptidergic (calcitonin gene-related peptide; CGRP) axon subtypes in fetal, neonatal, and adult mouse prostate to determine when axons first appear. We created a method to quantify axon density within periductal stroma of the periurethral, proximal, and distal regions of dorsal and ventral adult mouse prostate ducts and tested the hypothesis that axon density differs across the proximal-distal duct axis. This will form the foundation for investigating the impact of prostate disease, drug exposure, or environmental contaminants on axon density. We also used multiplex immunostaining to determine which axon subtypes innervate neuroendocrine cells. We found that both autonomic and sensory axons develop at the same time.

Results

TH+, VAChT+, and CGRP+ axons innervate the prostate prior to prostatic bud formation

The first objective was to determine when TH+, VAChT+, and CGRP+ axons appear in the developing prostate. Mouse prostate is specified at E14.5 from a urethral expansion known

as the urogenital sinus (UGS) and prostatic buds are first detected at E16.5 (27, 28). We therefore evaluated axon patterns in the UGS at 24-h intervals beginning at E13.5 and continuing until E16.5. UGS tissue sections were immunostained with antibodies against TH+, VAChT+, and CGRP+ and against KRT5 to visualize epithelial cells. Axons were quantified in 10 μm peri-prostatic stromal bands radiating from the basilar epithelial boundary of the UGS (**Figure 1**). None of the examined axon subtypes are detected in this region at E13.5 (**Figure 2**). TH+, VAChT+, and CGRP+ axons are first observed in the peri-prostatic stroma at E14.5 (**Figure 2**). Taken together, TH+, VAChT+, and CGRP+ axons innervate prior to prostatic bud formation and during prostate specification.

TH+, VAChT+, and CGRP+ axon densities increase during fetal stages, peak during neonatal development, and are maintained in the adult mouse prostate

We examined the density of immunolabeled axons in a 10 μm stromal band around prostatic ducts (periductal stroma, **Figure 1**) to determine whether periductal densities of TH+, CGRP+, and VAChT+ axons change as prostate development progresses from the budding to branching stages and into sexual maturity. We found that periductal TH+, VAChT+, and CGRP+ axons are sparse during fetal periods, progressively increase in density through P9 (during branching morphogenesis) and are maintained at a similar level until at least P50 in dorsal prostate (**Figure 3**). This same pattern was present in ventral prostate (**Supplementary Figure 1**). **Figure 3, 4, and Supplementary Figure 1 and 2** detail some axons containing varicose, small swellings that are more highly immunolabeled. These varicose axons are more directly relevant to understanding function because these swellings typically indicate sites of neurotransmission to communicate with neighboring cell types. We observed varicose TH+ and VAChT+ axons within the 10 μm region of interest at P9 and P50, indicating that direct regulation of smooth muscle is feasible at these times.

TH+ and VAChT+ axon density is uniform along the proximal-distal axis of dorsal and ventral prostate while CGRP+ axons are denser in the periurethral and proximal regions

We used our quantification method to evaluate axon density within the periurethral, proximal, and distal regions (**Figure 4**) of adult mouse dorsal and ventral prostate (P50) to determine whether axon density is uniform. If shown to be non-uniform, in future studies of prostate innervation it will be important to control for proximal-distal location. In dorsal prostate, we found that VAChT+ and TH+ axon densities do not differ across proximal-distal regions, while CGRP+ axon rank order densities were: periurethral > proximal > distal (**Figure 4**). In ventral prostate, we found similarly that VAChT+, and TH+ axon densities did not differ across the proximal-distal regions, while CGRP+ axons rank order densities were: periurethral = proximal > distal (**Supplementary Figure 2**). Graphs quantifying dorsal and ventral TH+, VAChT+, and CGRP+ axon densities across the periurethral, proximal, and distal axis can be found in **Supplementary figures 3 and 4**.

CGRP+ and VAChT+ axons, but not TH+ axons, innervate prostatic neuroendocrine cells

During analysis of axon development and density, we observed that after E17.5, a small population of CGRP+ and VAChT+ axons cross the epithelium to reach the lumen, while TH+ axons are never observed within prostatic epithelium. This sensory and cholinergic epithelial innervation was periodically observed crossing the epithelium at E17.5 and consistently observed in the periurethral and proximal region at P50. Because prostatic neuroendocrine cells are thought to migrate into UGS epithelium from the neural crest or differentiate from endodermal progenitors at this stage (29–31), we tested whether CGRP+ and VAChT+ axons innervate neuroendocrine cells. We identified neuroendocrine cells at E17.5 and P50 by immunolabeling for synaptophysin and found that they are innervated by CGRP+ and VAChT+ axons but not TH+ axons (**Figure 5**). TH+ axons were observed encircling blood vessels and VAChT+ axons were observed in the rhabdosphincter, as previously described (32)(data not shown).

Discussion

Here we identified the timing of noradrenergic, cholinergic, and peptidergic axon investment in prostate, how noradrenergic, cholinergic, and peptidergic axon density changes during development, and whether axon density is uniform along the proximo-distal axis within dorsal and ventral prostate lobes. As the role of axons in prostate disease becomes more apparent, it is important to understand peripheral axon development and density in normal, healthy animals. Results of this study could provide a valuable baseline reference for determining the impact of prostatic diseases and exposure to various drugs and environmental contaminants on prostatic axon patterns.

Pathways responsible for axon pathfinding and patterning have been identified in endoderm-derived lung, gut and bladder but not in prostate (33–35). The principal reason for this study was to pinpoint the critical window in which axons first appear in the developing prostate, thereby supporting future efforts to identify neurotrophins and other relevant neuronal survival or guidance factors. It is possible such factors are expressed later in life to recruit axons to inflamed, benign hyperplastic or neoplastic prostatic tissues. Our observation that critical windows for investment into the prostate are the same for noradrenergic, cholinergic, and sensory axons (E13.5-E14.5) raises the possibility that each axon type is recruited by similar mechanisms. Signaling mechanisms may begin to differ sometime after development, a notion supported by the fact that axon subtype densities differ among prostate diseases which arise from distinct mechanisms. For example, prostate cancer increases autonomic axon density while prostatitis increases sensory axon density (12, 14, 16, 17). Further, nerve growth factor (NGF) abundance decreases during prostate cancer progression (36) while it increases during prostatitis (16). Identities and concentrations of factors recruiting sensory axons into the mouse prostate may differ from those recruiting autonomic axons.

The next question we addressed is how noradrenergic, cholinergic, and peptidergic axon density changes during prostate development. Axon investment into the developing mouse

prostate generally follows the time course of smooth muscle development, which is first detected in the mouse UGS at E14.5 (37) and increases in abundance during the prostatic budding and postnatal branching stages (38). This study reported axons followed a similar time course to smooth muscle development, TH+, VAChT+, and CGRP+ axon densities increase during fetal stages, peak during neonatal development, and are maintained in the adult mouse prostate. Whether prostatic smooth muscle maturation drives axon development or vice versa is an interesting subject for future research, as sympathetic axons are known to contract prostate smooth muscle.

We were interested in mapping the density of noradrenergic, cholinergic, and peptidergic axons along the proximo-distal axis at sexual maturity. Axon density quantification is challenged by histological heterogeneity among and within prostatic lobes. Ductal diameter, smooth muscle content, stromal: epithelial ratios, and abundance of glandular folding differ as a function of age and distance from the urethra (39, 40). As a result, we developed an objective quantification method that enables comparison of axon density between regions of differing histomorphology. While previous research has predominantly focused on proximal and distal regions of mouse prostate, recent studies identify the periurethral region, spanning from the basal surface of urethral epithelium to the internal boundary of the rhabdosphincter, as a region where aging- and inflammation-mediated changes may drive prostate related urinary dysfunction (41). This study found TH+ and VAChT+ axon density is uniform along the proximal-distal axis of dorsal and ventral prostate while CGRP+ axons are denser in the periurethral and proximal regions. CGRP+ axons contain many receptors and channels that influence excitability and growth, including transient receptor potential channels, neurotrophins, and estrogen receptors (42, 43). Therefore, regional differences in axon density across organs have the potential to influence function in many different ways . For example, in bladder, sensory axons are most dense in the neck region where they facilitate the guarding reflex, a stimulation of external urethral sphincter contraction in response to low bladder pressures to prevent bladder leaking (44). Overactive bladder syndrome,

characterized by frequent urination, has been linked to abnormal elevations of peptidergic axon density (45). Sensory axons in lung are most dense in bronchioles where their release of neuropeptides onto underlying target vessels and glands potentiate asthma (46–48). CGRP+ axons in prostate are particularly dense in the periurethral and proximal region where their function is not completely known, but could be linked to detection of local pH changes, infection, or inflammatory responses (49).

Lastly, this study identified CGRP+ and VAChT+ axons penetrating the epithelium. As a result, we were interested in determining whether noradrenergic, cholinergic, and peptidergic axons innervate neuroendocrine cells, a specialized cell type that resides in the epithelium. This study found that both CGRP+ and VAChT+ axons innervate neuroendocrine cells while TH+ axons do not. Because CGRP+ and VAChT+ axons innervate neuroendocrine cells almost immediately after neuroendocrine cells are first detected in the developing prostate (E17), it is possible that nerve-neuroendocrine cell interactions facilitate prostate growth and development. This notion is supported by previous observations that prostatic neuroendocrine cell or nerve depletion reduces prostate size (50)).

In summary, we found that autonomic (TH+ and VAChT+) and sensory (CGRP+) axons innervate the mouse prostate during the same phase of prostate development. The density of each axon population continues to increase until it peaks during the period of branching morphogenesis and sexual maturity. CGRP+ axon density is greatest in the periurethral compared to distal region, while TH+ and VAChT+ axon density is uniform across regions. CGRP+ and VAChT+ axons also penetrate epithelium to potentially regulate neuroendocrine and epithelial cells. Futures studies will focus on factors controlling axon patterning and development and determining the impact of environmental chemical exposure on prostate peripheral axons.

Materials and Methods

Mice

All procedures were approved by the University of Wisconsin Animal Care and Use Committee and conducted in accordance with the National Institutes of Health Guide for the Care and Use of Laboratory Animals. All mice were C57BL/6J and purchased from Jackson Laboratories (stock number 000664, Bar Harbor, ME). Mice were housed in Innovive® HDPE plastic microisolator cages in a room maintained on a 12-h light and dark cycle, ambient temperature of 20.5 ± 1°C and relative humidity of 30-70%. Mice were fed a 5015 Diet (PMI Nutrition International, Brentwood, MO) from conception through weaning (P21) and a 8604 Teklad Rodent Diet thereafter (Harlan Laboratories, Madison, WI). Feed and water were available ad libitum and cages contained corncob bedding. All mice were euthanized by CO_2 asphyxiation. Mice were time-mated by pairing males and females overnight. The morning of definitive copulatory plug identification was considered E0.5. Urogenital sinus and prostate tissues were collected at E13.5, E14.5, E15.5, E16.5, E17.5, P9, and P50, fixed overnight at 4°C in 4% paraformaldehyde dissolved in neutral buffered saline (Thermo Scientific) and dehydrated through a series of graded ethanols. Tissues were cleared in xylenes, embedded in paraffin wax and sectioned at 10 μm thickness on a microtome (Surgipath Medical Industries).

Immunohistochemistry

Tissue sections were deparaffinized with xylene and rehydrated in a series of graded ethanols. Immunofluorescence staining was conducted as described previously (Abler et al. 2011) with the following modifications: microwave decloaking was performed in 10 mM sodium citrate (pH 6.0) and non-specific sites were blocked for 1 h in TBSTw containing 1% Blocking Reagent (Roche Diagnostics, Indianapolis, IN), 5% normal donkey sera, and 1% bovine serum albumin fraction 5 (RDBTw). Immunofluorescence was detected using the recommended settings for each secondary antibody fluorophore. Antibodies are listed in Supplementary Table 1. Tissue sections were imaged using an SP8 confocal microscope (Leica, Wetzlar, Germany) fitted with a 20X oil immersion objective (HC PL Apo CS2 NA = 0.75; Leica, Wetzlar, Germany). Ten z-images were

captured at 1024x1024 resolution and a Z-interval of 1 µm using LASX 8 software at a speed of 700 fps (Leica, Wetzlar, Germany). The detector gain ranged between 10-30 using Hy-D lasers. All fluorescent images were stained using Alexa 488, Rhodamine red, and Alexa 647 nm fluorophores. These fluorophores were detected using the 488, 546, and 633 lasers. Signals from the fluorophores were separated using a sequential imaging protocol. All images were captured at 300 ppl resolution and were manipulated to adjust whole image RGB color intensity using Adobe Photoshop (version 20.0).

Morphometric analysis

For E13.5- E16.5 specimens, presence or absence of axons was determined in the 10 µm stromal band extending from the basal surface of KRT5 or CDH1-stained urogenital sinus (UGS). For P9 and P50 specimens, axon density was determined in a 10 µm stromal band extending from the basal surface of CDH1-stained prostatic ductal epithelium (this region encompasses the majority of periductal smooth muscle). Axon density was quantified in the periurethral (Box 1), proximal (Box 2), and distal (Box 3) regions of dorsal and ventral prostate (**Figure 1**). The periurethral region spanned from the basal surface of urethral epithelium to the rhabdosphincter internal boundary and axon densities were calculated exclusively for ducts with patent openings to the urethra and not for other ducts in this region. The proximal region extended 650 µm from the external rhabdosphincter boundary. The distal region began 650 µm from the external rhabdosphincter and extended to the distal-most portion of prostatic ducts. Immunostained axon pixels were quantified using the thresholding feature (MaxEntropy thresholding) of ImageJ (Version 1.52e11)(26). Image pixel density was scaled to 2.23 pixels/micron. For each age and sampled region, three non-adjacent, near-mid sagittal, technical replicate tissue sections (10 µm) were averaged per mouse and 4-10 biological replicate mice were evaluated per axon subtype.

Three of these biological replicates were evaluated in the transverse orientation and the remaining in sagittal. Mice were derived from at least three separate litters per time point.

Statistical Analysis

Results are reported as mean ± SE, where n= number of mice. Statistical analysis was done using GraphPad Prism 7 and a difference between means was considered significant at $p \leq 0.05$. Bartlett's test was used to determine homogeneity of variance with $p \leq 0.05$ indicating inequality of variance. The Shapiro-Wilk test was used to assess normality of the residuals with $p \leq 0.05$ indicating non-normal data. Data that did not meet the criteria for homogeneity of variance or normality was transformed using either a base-10 log transformation (VAChT regional density in dorsal and ventral prostate) or data was taken to the (1/3) power (TH+ regional density in dorsal and ventral prostate, TH+ temporal comparison in dorsal prostate, VAChT+ temporal comparison in dorsal and ventral prostate, CGRP+ regional density in ventral prostate). All axon density comparisons were assessed using one-way ANOVA followed by Tukey's honestly significant difference post hoc test to identify which groups differed significantly $p \leq 0.05$.

Conflict of Interest

The authors report no conflict of interest.

References

1. G. C. Harburg, L. Hinck, Navigating breast cancer: axon guidance molecules as breast cancer tumor suppressors and oncogenes. *J Mammary Gland Biol Neoplasia* **16**, 257–270 (2011).

2. M. Belle, *et al.*, Tridimensional Visualization and Analysis of Early Human Development. *Cell* **169**, 161-173.e12 (2017).

3. C. Nassenstein, *et al.*, Expression and function of the ion channel TRPA1 in vagal afferent nerves innervating mouse lungs. *J Physiol* **586**, 1595–1604 (2008).

4. J. Hatch, Y.-S. Mukouyama, Spatiotemporal mapping of vascularization and innervation in the fetal murine intestine. *Dev. Dyn.* **244**, 56–68 (2015).

5. J. R. Keast, C. J. A. Smith-Anttila, P. B. Osborne, Developing a functional urinary bladder: a neuronal context. *Front Cell Dev Biol* **3** (2015).

6. U. C. Kopp, Role of renal sensory nerves in physiological and pathophysiological conditions. *Am J Physiol Regul Integr Comp Physiol* **308**, R79–R95 (2015).

7. K. T. McVary, *et al.*, Growth of the rat prostate gland is facilitated by the autonomic nervous system. *Biol. Reprod.* **51**, 99–107 (1994).

8. J. M. Wang, K. E. McKenna, K. T. McVary, C. Lee, Requirement of innervation for maintenance of structural and functional integrity in the rat prostate. *Biol. Reprod.* **44**, 1171–1176 (1991).

9. J. N. Pennefather, W. A. Lau, F. Mitchelson, S. Ventura, The autonomic and sensory innervation of the smooth muscle of the prostate gland: a review of pharmacological and histological studies. *J Auton Pharmacol* **20**, 193–206 (2000).

10. S. Ventura, J. Pennefather, F. Mitchelson, Cholinergic innervation and function in the prostate gland. *Pharmacol. Ther.* **94**, 93–112 (2002).

11. S. Batra, P. I. Christensson, B. Hartley-Asp, Characterization of muscarinic cholinergic receptors in membrane preparations from rat prostatic adenocarcinoma. *Prostate* **17**, 261–268 (1990).

12. C. Magnon, *et al.*, Autonomic nerve development contributes to prostate cancer progression. *Science* **341**, 1236361 (2013).

13. A. H. Zahalka, *et al.*, Adrenergic nerves activate an angio-metabolic switch in prostate cancer. *Science* **358**, 321–326 (2017).

14. S. Batra, P.-I. Christensson, B. Hartley-Asp, Characterization of muscarinic cholinergic receptors in membrane preparations from rat prostatic adenocarcinoma. *The Prostate* **17**, 261–268 (1990).

15. B. D. Umans, S. D. Liberles, Neural Sensing of Organ Volume. *Trends Neurosci.* (2018) https:/doi.org/10.1016/j.tins.2018.07.008.

16. M. A. Pontari, M. R. Ruggieri, Mechanisms In Prostatitis/Chronic Pelvic Pain Syndrome. *J Urol* **172**, 839–845 (2004).

17. T. Watanabe, *et al.*, Nerve growth factor level in the prostatic fluid of patients with chronic prostatitis/chronic pelvic pain syndrome is correlated with symptom severity and response to treatment. *BJU International* **108**, 248–251 (2011).

18. C. Owman, N. O. Sjöstrand, Short adrenergic neurons and catecholamine-containing cells in vas deferens and accessory male genital glands of different mammals. *Zeitschrift für Zellforschung* **66**, 300–320 (1965).

19. N. O. Sjöstrand, The adrenergic innervation of the vas deferens and the accessory male genital glands. *Acta physiol. scand.* **257** (1965).

20. H. G. Baumgarten, B. Falck, A. F. Holstein, C. Owman, T. Owman, Adrenergic innervation of the human testis, epididymis, ductus deferens and prostate: a fluorescence microscopic and fluorimetric study. *Z Zellforsch Mikrosk Anat* **90**, 81–95 (1968).

21. S. Raz, M. Zeigler, M. Caine, The Effect of Progesterone on the Adrenergic Receptors of the Urethra1. *British Journal of Urology* **45**, 131–135 (1973).

22. M. Caine, S. Raz, M. Zeigler, Adrenergic and cholinergic receptors in the human prostate, prostatic capsule and bladder neck. *Br J Urol* **47**, 193–202 (1975).

23. J. Farrell, Y. Lyman, A study of the secretory nerves of, and the action of certain drugs on the prostate gland. *Am J Physiol* **118**, 64–70 (1937).

24. M., J. Keast, Immunohistochemical properties and spinal connections of pelvic autonomic neurons that innervate the rat prostate gland. *Cell Tissue Res.* **281**, 533–542 (1995).

25. H. Yan, J. R. Keast, Neurturin regulates postnatal differentiation of parasympathetic pelvic ganglion neurons, initial axonal projections, and maintenance of terminal fields in male urogenital organs. *J. Comp. Neurol.* **507**, 1169–1183 (2008).

26. J. Kapur, P. Sahoo, A. Wong, A New Method for Gray-Level Picture Thresholding Using the Entropy of the Histogram". *Graphical Models and Image Processing* **29**, 273–285 (1985).

27. T.-M. Lin, N. T. Rasmussen, R. W. Moore, R. M. Albrecht, R. E. Peterson, Region-specific inhibition of prostatic epithelial bud formation in the urogenital sinus of C57BL/6 mice exposed in utero to 2,3,7,8-tetrachlorodibenzo-p-dioxin. *Toxicol. Sci.* **76**, 171–181 (2003).

28. K. P. Keil, *et al.*, Visualization and quantification of mouse prostate development by in situ hybridization. *Differentiation* **84**, 232–239 (2012).

29. P. C. Marker, A. A. Donjacour, R. Dahiya, G. R. Cunha, Hormonal, cellular, and molecular control of prostatic development. *Dev. Biol.* **253**, 165–174 (2003).

30. J. Szczyrba, *et al.*, Neuroendocrine Cells of the Prostate Derive from the Neural Crest. *J. Biol. Chem.* **292**, 2021–2031 (2017).

31. R. Toivanen, M. M. Shen, Prostate organogenesis: tissue induction, hormonal regulation and cell type specification. *Development* **144**, 1382–1398 (2017).

32. K. M. Georgas, *et al.*, An illustrated anatomical ontology of the developing mouse lower urogenital tract. *Development* **142**, 1893–1908 (2015).

33. J. Tollet, A. W. Everett, M. P. Sparrow, Spatial and temporal distribution of nerves, ganglia, and smooth muscle during the early pseudoglandular stage of fetal mouse lung development. *Dev. Dyn.* **221**, 48–60 (2001).

34. S. D. Harding, *et al.*, The GUDMAP database – an online resource for genitourinary research. *Development* **138**, 2845–2853 (2011).

35. L. Aven, X. Ai, Mechanisms of respiratory innervation during embryonic development. *Organogenesis* **9**, 194–198 (2013).

36. B. R. Pflug, M. Onoda, J. H. Lynch, D. Djakiew, Reduced Expression of the Low Affinity Nerve Growth Factor Receptor in Benign and Malignant Human Prostate Tissue and Loss of Expression in Four Human Metastatic Prostate Tumor Cell Lines. *Cancer Res* **52**, 5403–5406 (1992).

37. C. M. Vezina, *et al.*, Dioxin Causes Ventral Prostate Agenesis by Disrupting Dorsoventral Patterning in Developing Mouse Prostate. *Toxicol Sci* **106**, 488–496 (2008).

38. A. A. Thomson, B. G. Timms, L. Barton, G. R. Cunha, O. C. Grace, The role of smooth muscle in regulating prostatic induction. *Development* **129**, 1905–1912 (2002).

39. D. Bianchi-Frias, *et al.*, The Effects of Aging on the Molecular and Cellular Composition of the Prostate Microenvironment. *PLOS ONE* **5**, e12501 (2010).

40. D. S. M. Oliveira, *et al.*, The mouse prostate: a basic anatomical and histological guideline. *Bosn J Basic Med Sci* **16**, 8–13 (2016).

41. T. M. Nicholson, W. A. Ricke, Androgens and estrogens in benign prostatic hyperplasia: past, present and future. *Differentiation* **82**, 184–199 (2011).

42. P. Lanlua, *et al.*, Female steroid hormones modulate receptors for nerve growth factor in rat dorsal root ganglia. *Biol. Reprod.* **64**, 331–338 (2001).

43. L. S. Premkumar, Transient Receptor Potential Channels as Targets for Phytochemicals. *ACS Chem Neurosci* **5**, 1117–1130 (2014).

44. Z. C. Danziger, W. M. Grill, Sensory feedback from the urethra evokes state-dependent lower urinary tract reflexes in rat. *J. Physiol. (Lond.)* **595**, 5687–5698 (2017).

45. W. C. de Groat, N. Yoshimura, Afferent Nerve Regulation of Bladder Function in Health and Disease. *Handb Exp Pharmacol*, 91–138 (2009).

46. J. P. Lamb, M. P. Sparrow, Three-Dimensional Mapping of Sensory Innervation with Substance P in Porcine Bronchial Mucosa. *Am J Respir Crit Care Med* **166**, 1269–1281 (2002).

47. W. Kummer, K. S. Lips, U. Pfeil, The epithelial cholinergic system of the airways. *Histochem Cell Biol* **130**, 219–234 (2008).

48. K. Branchfield, *et al.*, Pulmonary neuroendocrine cells function as airway sensors to control lung immune response. *Science* **351**, 707–710 (2016).

49. C. W. White, J. H. Xie, S. Ventura, Age-related changes in the innervation of the prostate gland. *Organogenesis* **9**, 206–215 (2013).

50. C.-Y. Cheng, Z. Zhou, A. Y. Nikitin, Detection and organ-specific ablation of neuroendocrine cells by synaptophysin locus-based BAC cassette in transgenic mice. *PLoS ONE* **8**, e60905 (2013).

51. J. M. Jimenez-Andrade, *et al.*, Pathological sprouting of adult nociceptors in chronic prostate cancer-induced bone pain. *J. Neurosci.* **30**, 14649–14656 (2010).

52. K. Ishida, T. Kawamata, S. Tanaka, T. Shindo, M. Kawamata, Calcitonin gene-related peptide is involved in inflammatory pain but not in postoperative pain. *Anesthesiology* **121**, 1068–1079 (2014).

53. I. De Proost, *et al.*, Purinergic signaling in the pulmonary neuroepithelial body microenvironment unraveled by live cell imaging. *FASEB J.* **23**, 1153–1160 (2009).

54. J. M. Van Kampen, D. C. Baranowski, H. A. Robertson, C. A. Shaw, D. G. Kay, The Progressive BSSG Rat Model of Parkinson's: Recapitulating Multiple Key Features of the Human Disease. *PLoS ONE* **10**, e0139694 (2015).

55. V. Johnson, M. Xiang, Z. Chen, H. J. Junge, Neurite Mistargeting and Inverse Order of Intraretinal Vascular Plexus Formation Precede Subretinal Vascularization in Vldlr Mutant Mice. *PLoS ONE* **10**, e0132013 (2015).

56. E. Bentea, *et al.*, Nigral proteasome inhibition in mice leads to motor and non-motor deficits and increased expression of Ser129 phosphorylated α-synuclein. *Front Behav Neurosci* **9**, 68 (2015).

57. S. S. Pappas, *et al.*, Forebrain deletion of the dystonia protein torsinA causes dystonic-like movements and loss of striatal cholinergic neurons. *Elife* **4**, e08352 (2015).

58. D. Bajic, M. Soiza-Reilly, A. L. Spalding, C. B. Berde, K. G. Commons, Endogenous Cholinergic Neurotransmission Contributes to Behavioral Sensitization to Morphine. *PLoS One* **10** (2015).

59. D. Atasoy, *et al.*, A genetically specified connectomics approach applied to long-range feeding regulatory circuits. *Nat. Neurosci.* **17**, 1830–1839 (2014).

60. K. C. Kemp, *et al.*, Bone marrow transplantation stimulates neural repair in Friedreich's ataxia mice. *Ann Neurol* **83**, 779–793 (2018).

61. T. Schomann, *et al.*, Neuronal differentiation of hair-follicle-bulge-derived stem cells co-cultured with mouse cochlear modiolus explants. *PLoS ONE* **12**, e0187183 (2017).

62. E. Vasilaki, Z. Kanaki, D. J. Stravopodis, A. Klinakis, Dll1 Marks Cells of Origin of Ras-Induced Cancer in Mouse Squamous Epithelia. *Translational Oncology* **11**, 1213–1219 (2018).

63. V. Drubay, *et al.*, TGF-βRII Knock-down in Pancreatic Cancer Cells Promotes Tumor Growth and Gemcitabine Resistance. Importance of STAT3 Phosphorylation on S727. *Cancers* **10**, 254 (2018).

64. B. Lloyd-Lewis, F. M. Davis, O. B. Harris, J. R. Hitchcock, C. J. Watson, Neutral lineage tracing of proliferative embryonic and adult mammary stem/progenitor cells. *Development* **145**, dev164079 (2018).

65. K. A. Wegner, *et al.*, An immunohistochemical identification key for cell types in adult mouse prostatic and urethral tissue sections. *PLoS ONE* **12**, e0188413 (2017).

66. B. D. Almquist, S. A. Castleberry, J. B. Sun, A. Y. Lu, P. T. Hammond, Combination Growth Factor Therapy via Electrostatically Assembled Wound Dressings Improves Diabetic Ulcer Healing In Vivo. *Adv Healthc Mater* **4**, 2090–2099 (2015).

67. C. Thiele, M. J. Hannah, F. Fahrenholz, W. B. Huttner, Cholesterol binds to synaptophysin and is required for biogenesis of synaptic vesicles. *Nat. Cell Biol.* **2**, 42–49 (2000).

Figures and Tables

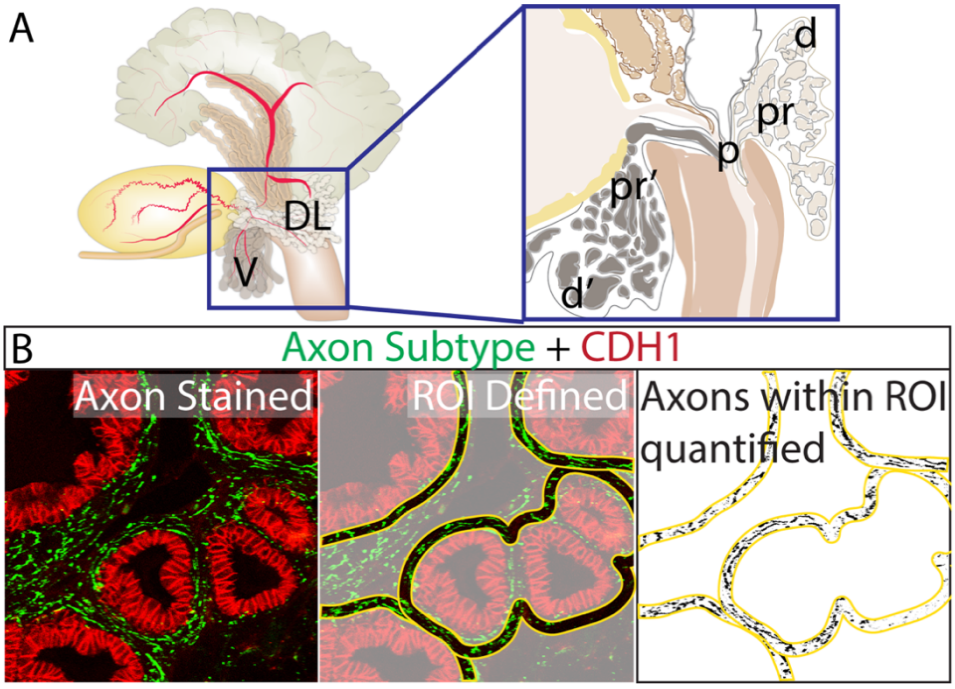

Figure 1. Prostate TH+, VAChT+ and CGRP+ axon density can be quantified and normalized in a 10 μm periductal band (A) Axons were quantified in sagittal sections of ventral and dorsal mouse prostate. Areas of interest included: p = periurethral in dorsal and ventral prostate, pr = proximal, d=distal in dorsal prostate, pr'= proximal ventral, d'= distal in ventral prostate. The periurethral region spanned from the basal surface of the urethral epithelium to the rhabdosphincter internal boundary. Axon densities were calculated exclusively for ducts with patent openings to the urethra and not for other ducts in this region. The proximal region extended 650 μm from the external rhabdosphincter boundary. The distal region began 650 μm from the external rhabdosphincter and extended to the distal-most portion of prostatic ducts. (B) Sections were immunohistochemically stained for markers of several axon subtypes (green) and e-cadherin to visualize prostatic and urethral epithelium (red). (b') Stained sections were imaged using confocal microscopy, imported into ImageJ, and (b'') 10 μm bands (yellow) were traced around all prostate ducts and relative axon pixel densities were quantified using MaxEntropy thresholding. Scale bar is 100 μm.

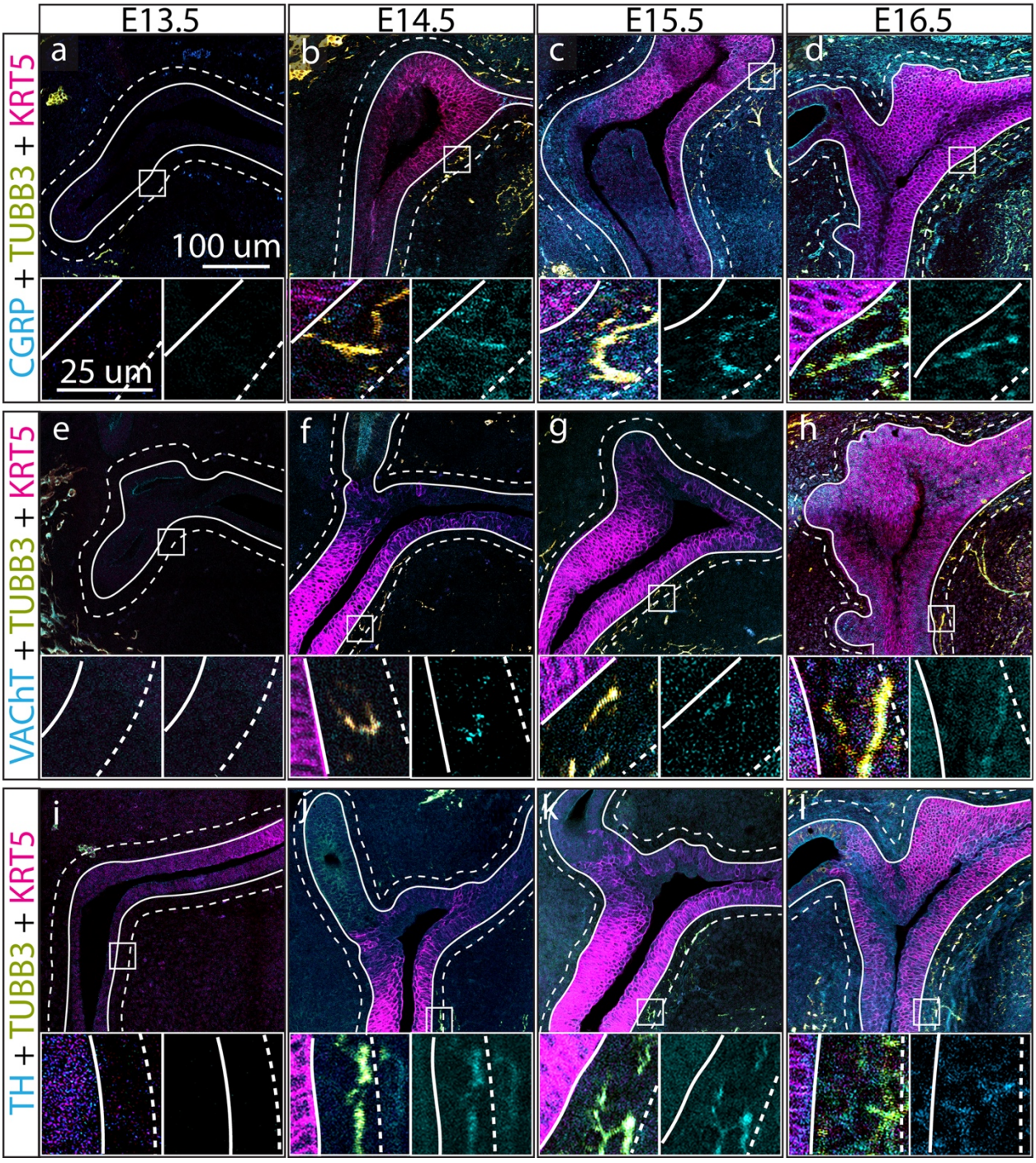

Figure 2. TH+, VAChT+, and CGRP+ axons innervate the prostate before prostate bud formation. (a-l) E13.5, E14.5, E15.5 and E16.5 mouse prostate tissue sections were immunostained with antibodies against TH, VAChT+, or CGRP+ (cyan), the pan neuronal marker beta 3-tubulin (TUBB3)(yellow), and keratin 5 (KRT5) and to visualize prostatic and urethral

epithelium (magenta). Inset images on the left under images a-l show magnified axon subtypes overlaying with TUBB3+ and inset images on the right show the axon subtype alone. Axon density was quantified in 10 μm periductal spaces radiating outward from the basal surface of prostatic/urethral epithelium. Overlap between TUBB3+ and neuronal subtype, shown as white stain from the overlap of yellow and cyan within the 10 um band was considered innervating the developing prostate. A grouping of TH+ axons are visible in the top right corner of panel j. These are likely associated with a microganglion. Three litter independent mice and three non-adjacent sections from each UGS were analyzed for each developmental stage. Large image scale bar is 100 μm. Inset image scale bar is 25 μm.

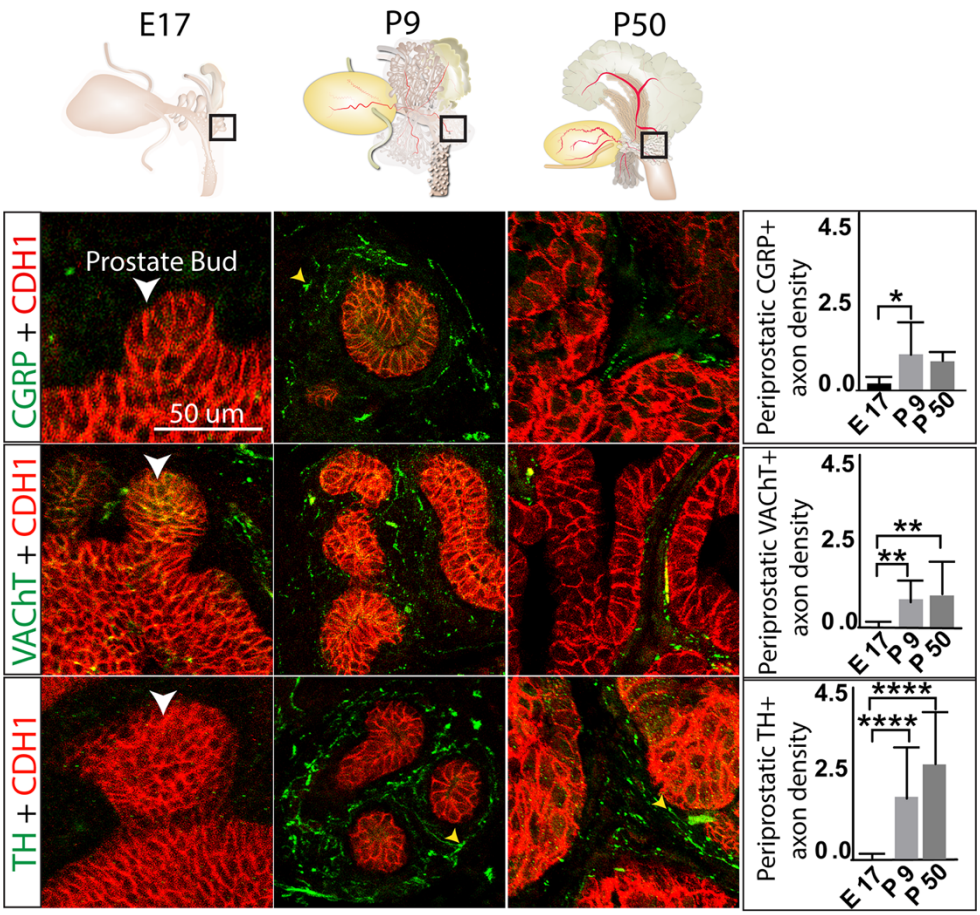

Figure 3. TH+, VAChT+, and CGRP+ axon densities increase during fetal stages of dorsal prostate development, peak during neonatal development, and are maintained in adulthood. E17.5, P9, and P50 mouse dorsal prostate tissue sections were immunostained with antibodies against TH+, VAChT+, or CGRP (green) and e-cadherin (CDH1, to visualize prostatic and urethral epithelium, red). Regions selected for analysis are schematized at the top of the figure and representative images are shown at the bottom left. Axon pixel densities were quantified in 10 μm periductal spaces radiating outward from the basal surface of prostatic epithelium and results graphed at the right. Varicose axons are identified with a yellow arrowhead. Results are mean ± SE of seven mice per group and three non-adjacent tissue sections per mouse. Asterisks indicate significant differences (ANOVA = $p < 0.05$, Tukey Post-Hoc = *$p<0.05$, **$p<0.01$ and ****$p<0.0001$) between groups. White arrowheads indicate prostatic buds. Scale bar is 50 μm

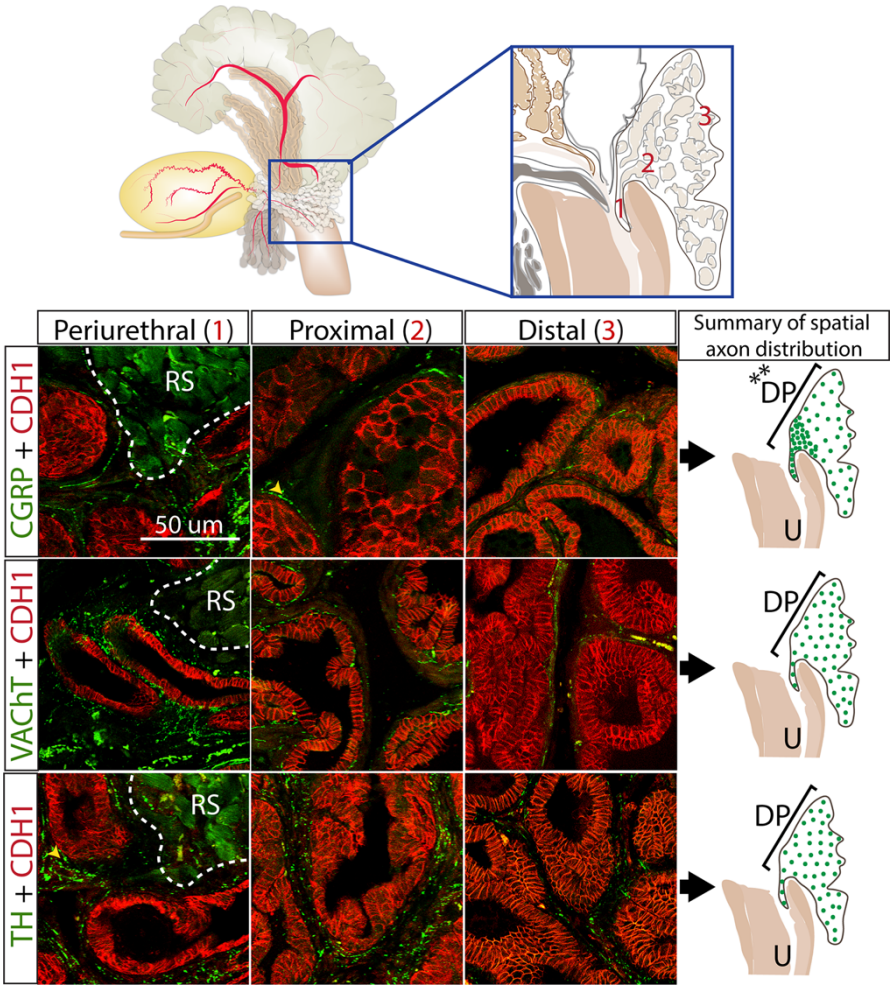

Figure 4. TH+ and VAChT+ axon densities are uniform along the proximal-distal axis of dorsal prostate while CGRP+ axons are denser in the periurethral and proximal versus distal region. P50 mouse dorsal prostate tissue sections were immunostained with antibodies against TH+, VAChT+, or CGRP+ (green) and e-cadherin (CDH1, to visualize prostatic and urethral epithelium (red)). Axon pixel densities were quantified in the 10 μm periductal spaces radiating outward from the basal surface of prostatic epithelium and results are shown pictorially on the right. Varicose axons are identified with a yellow arrowhead. Results are mean ± SE of ten mice per group and three non-adjacent tissue sections per mouse. An asterisk indicates a significant difference (**p<0.01) between regions. RS identifies the rhabdosphincter. Scale bar is 50 μm.

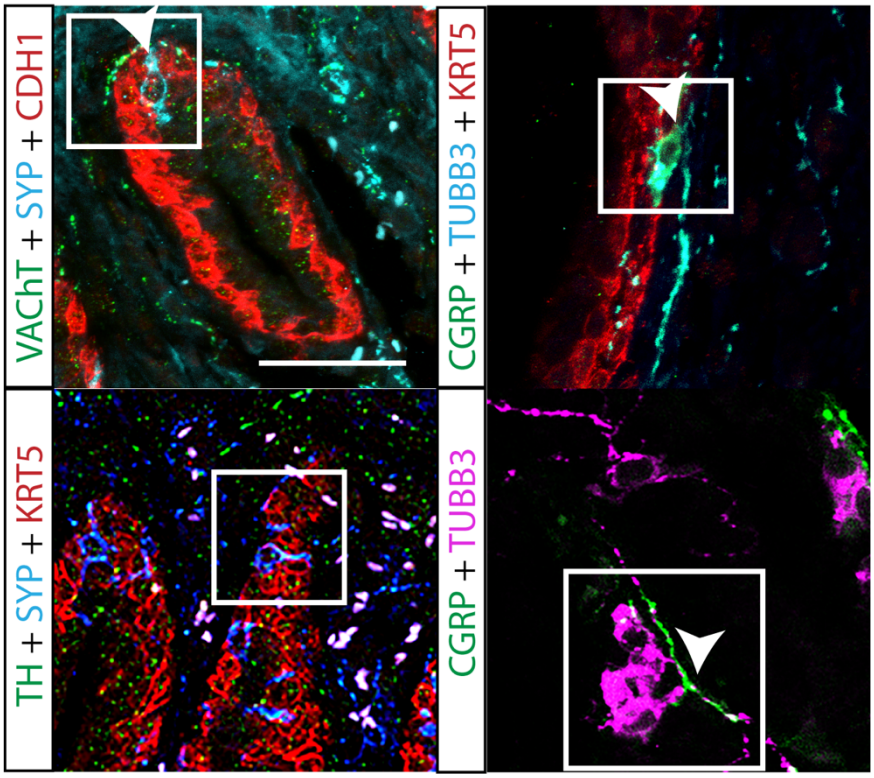

Figure 5. CGRP+ and VAChT+ axons innervate neuroendocrine cells in the periurethral region whereas TH+ axons do not. P50 mouse prostate tissue sections were immunostained with antibodies against TH+, VAChT+, or CGRP+ (green), e-cadherin (CDH1, to visualize prostatic and urethral epithelium, red) and synaptophysin (SYP), to stain neuroendocrine cells (cyan). Neuroendocrine cells were most commonly found in the periurethral region and cells with axons touching the neuroendocrine cell were considered to innervate that cell. Box indicates neuroendocrine cells and arrow heads mark axons. CGRP+ axons are also in other epithelial regions with no neuroendocrine cells, indicated by the green arrowhead. Arrowheads inside boxes indicate innervated neuroendocrine cells. Yellow arrowheads indicate axons that do not innervate neuroendocrine cells. Neuroendocrine cell innervation results were consistent across three litter independent mice. Scale bar is 25 μm.

Table 1. List of primary antibodies used in this study. The antibody target, vendor and catalog number, RRID number, host species, dilution, and proof of specificity is listed.

Antibody	Vendor/ Catalog Number	RRID	Host Species	Dilution	Proof of Specificity
Calcitonin-gene-related peptide (CGRP)	Sigma Aldrich/ C8198	AB_259091	Rabbit Polyclonal	1:200	(51)(52)(53)
Tyrosine hydroxylase (TH)	EMD Millipore/ AB152	AB_390204	Rabbit Polyclonal	1:300	(54)(55)(56)
Vesicular Acetylcholine Transporter (VAChT, SLC18A3)	EMD Millipore/ABN100	AB_2630394	Goat Polyclonal	1:300	(57)(58)(59)
Class III B-tubulin (TUBB3)	Abcam/ ab78078	AB_2256751	Mouse Monoclonal	1:250	(60)(61)
E-Cadherin (CDH1)	Cell Signaling Technology/3195S	AB_2291471	Rabbit Monoclonal	1:200	(62)(63)(64)
E-Cadherin (CDH1)	BD Transduction Labs/610181	AB_39580	Mouse Monoclonal	1:100	(65)
Actin alpha 2 (SMA)	Invitrogen/ PA5-18292	AB_10980764	Goat Polyclonal	1:100	(66)
Actin alpha 2 (SMA)	Leica/ ncl-l-sma	AB_442134	Mouse Monoclonal	1:200	(65)
Keratin 5 (KRT5)	Biolegend/905901	AB_2565054	Chicken Polyclonal	1:500	(65)
Synaptophysin (SYP)	BD transduction laboratories/ 611880	AB_399360	Mouse Monoclonal	1:200	(67)

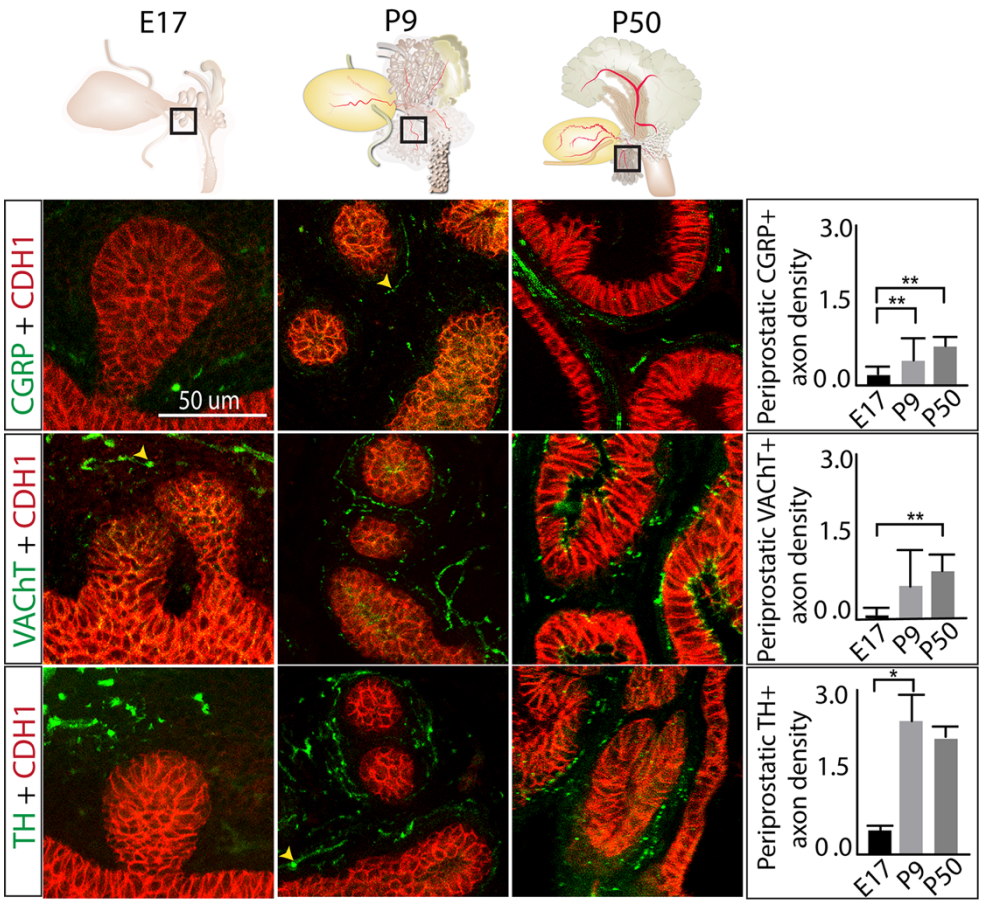

Supplementary Figure 1. CGRP+, VAChT+, and TH+ axons are denser during prostate branching morphogenesis and sexual maturity than during prostatic bud formation. E17.5, P9, and P50 mouse prostate tissue sections were immunostained with antibodies against TH+, VAChT+, and CGRP+ (green) and e-cadherin (CDH1, to visualize prostatic and urethral epithelium, red). Axon pixel densities were quantified in the 10 μM periductal spaces radiating outward from the basilar surface of prostatic epithelium and results are shown pictorially on the right. Varicose axons are identified with a green arrowhead. Results are mean ± SE of seven mice per group and three non-adjacent tissue sections per mouse. Asterisks indicate significant differences (*$p<0.05$, and **$p<0.01$) between regions. Scale bar is 50 μm

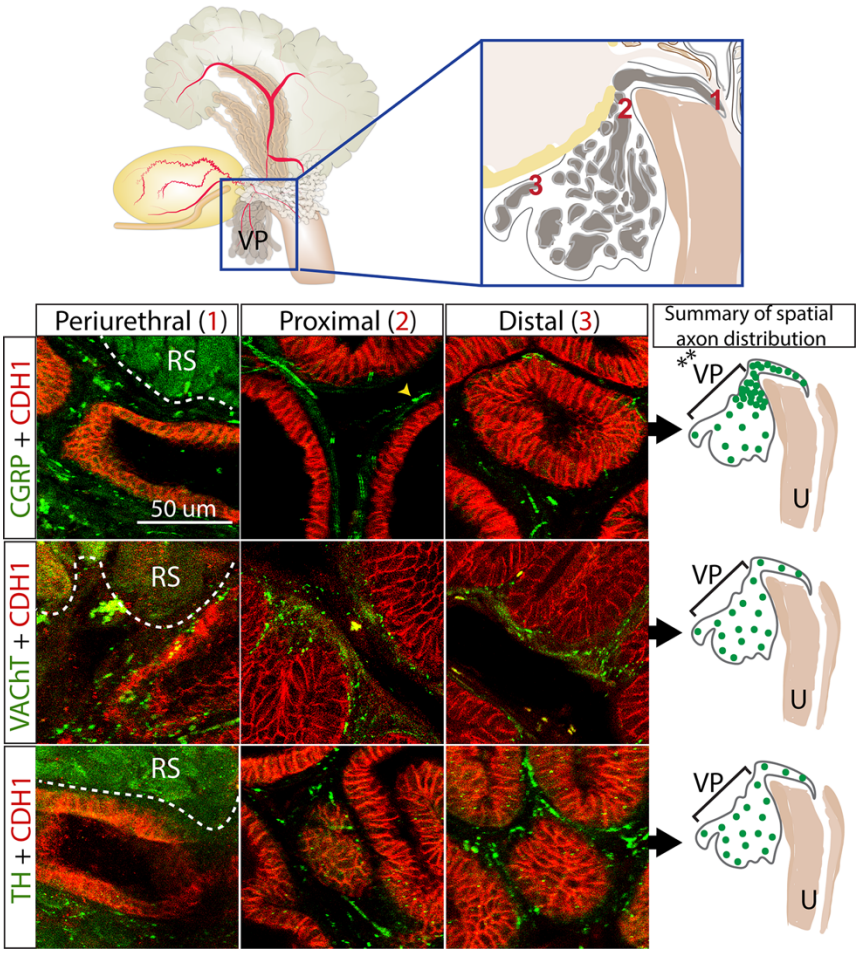

Supplementary Figure 2. CGRP+ axon density in P50 mouse ventral prostate is greater in the periurethral and proximal region than the distal region while VAChT+ and TH+ axon density does not significantly differ between proximal-distal regions. P50 mouse prostate tissue sections were immunostained with antibodies against TH+, VAChT+, or CGRP+ (green) and e-cadherin (CDH1, to visualize prostatic and urethral epithelium, red). Regions selected for analysis are schematized at the top of the figure and representative images are shown at the bottom left. Axon pixel densities were quantified in the 10 μM periductal spaces radiating outward from the basal surface of prostatic epithelium and results are shown pictorially at the right. Results are mean ± SE of ten mice per group and three non-adjacent tissue sections per mouse. Asterisks indicate significant differences (**p<0.01) between regions. Scale bar is 50 μm.

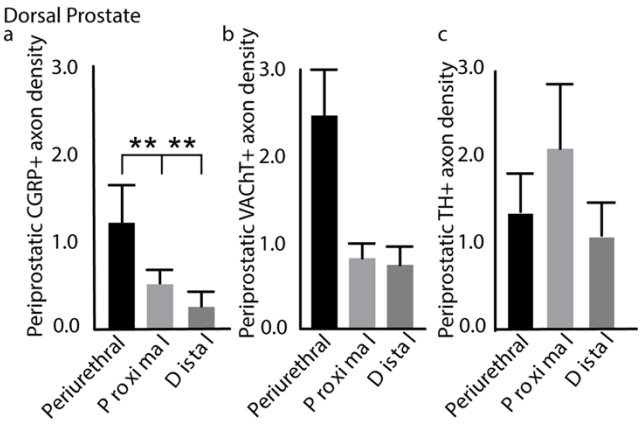

Supplementary Figure 3. Graphs showing CGRP+ axon density in P50 mouse dorsal prostate is greater in the periurethral and proximal region than the distal region while VAChT+ and TH+ axon density does not significantly differ between proximal-distal regions. Axon densities in P50 mouse prostate tissue sections were determined using the procedure described in Methods and Fig. 1 legend. Axon pixel densities were quantified in the 10 μm periductal spaces radiating outward from the basal surface of prostatic epithelium and results graphed. (a) CGRP+ axon density in the periurethral and proximal region is significantly greater than in the distal region. (b) VAChT+ axon density is uniform across the periurethral, proximal, and distal regions. (c) TH+ axon density is uniform across the periurethral, proximal, and distal regions. Results are mean ± SE of ten mice per group and three non-adjacent tissue sections per mouse. Asterisks indicate significant differences (**$p<0.01$) between regions.

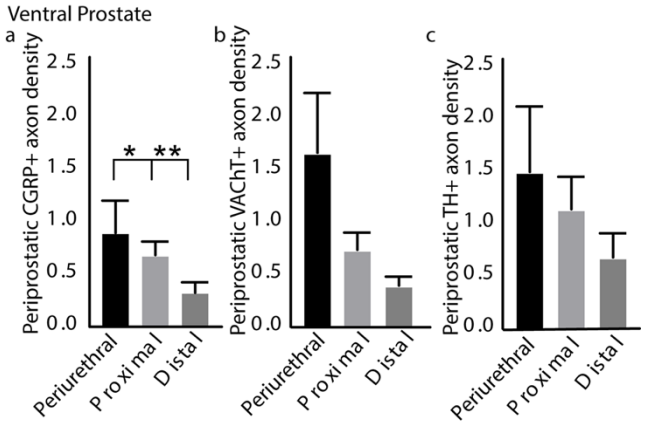

Supplementary Figure 4. Graphs showing CGRP+ axon density in P50 mouse ventral prostate is greater in the periurethral and proximal region than the distal region while VAChT+ and TH+ axon density does not significantly differ between proximal-distal regions. Axon densities in P50 mouse prostate tissue sections were determined using the procedure described in Methods and Fig. 1 legend. Axon pixel densities were quantified in the 10 μm periductal spaces radiating outward from the basal surface of prostatic epithelium and results graphed. (a) The CGRP+ axon density in the periurethral and proximal region is significantly greater than in the distal region. (b) VAChT+ axon density is uniform across the periurethral, proximal and distal regions. (c) TH+ axon density is uniform across the periurethral, proximal and distal regions. Results are mean ± SE of ten mice per group and three non-adjacent tissue sections per mouse. Asterisks indicate significant differences (*$p<0.05$, and **$p<0.01$) between regions

Chapter 3: A developmental origin of lower urinary tract dysfunction

Turco AE, Oakes SR, Keil-Stietz KP, Dunham CL, Joseph DB, Chathurvedula TS, Girardhi NM, Schneider AJ, Gawdzik J, Sheftel CM, Wang P, Wang Z, Bjorling DE, Ricke WA, Tang W, Hernandez LL, Keast JR, Bonev AB, Grimes MD, Tykocki NR, Tanguay RL, Peterson RE, Vezina, (2021). Prepared for Submission

Abstract

Many age-related diseases are linked to risk events incurred in the intrauterine environment, including hypertension and type II diabetes. One exception is lower urinary tract dysfunction (LUTD), a urinary voiding disease of aging men. Lower urinary tract dysfunction researchers have historically focused on benign prostatic hyperplasia and other age-related processes to explain bladder outlet obstruction, with little attention towards early life events. Here, we identify the intrauterine environment as a modifier of adult voiding function and a risk factor for LUTD. To model environmental chemical exposures, we exposed pregnant mice to the environmental contaminant 2,3,7,8 tetrachlorodibenzo-*p*-dioxin (TCDD, 1 μg/kg) at embryonic day 13.5, coinciding with initiation of lower urinary tract development in male fetuses. *In utero* and lactational (IUL) TCDD exposure incites abnormal urodynamics in adult male mice, including increased urinary voiding frequency. It also enhances adult prostate smooth muscle contraction in response to electrical stimuli, indicating a change in autonomic transmission. *In utero* and lactational TCDD induces the neurotrophin artemin (*Artn*) in the developing prostate when noradrenergic axons initially project and stably increases noradrenergic axon density in the prostate beginning in the fetal period and persisting into adulthood. This is the first evidence that intrauterine chemical exposure can reprogram prostate neuroanatomical development and drive prostate smooth muscle hyperactivity in adulthood to contribute to male lower urinary tract dysfunction.

Introduction

Lower urinary tract dysfunction (LUTD) is a clinical syndrome resulting from bladder outlet obstruction and is nearly universal in aging men. If untreated, LUTD can lead to permanent bladder dysfunction, renal injury, and even death (1). Increased prostate/bladder neck smooth muscle tones are proposed to cause outlet resistance and are the target of alpha-adrenergic receptor blockers, a first-line therapy for male LUTD. Aging-related processes such as prostatic enlargement have been the sole focus of male LUTD research for decades. Almost no attention has been directed to the intrauterine environment, even though it serves as a risk modifier for a growing spectrum of aging-related diseases, including hypertension, diabetes, and cancer (2–4).

We recently generated evidence supporting a new paradigm that the male fetal and neonatal environments contribute to the risk of developing LUTD in advancing age (5). To model environmental chemical exposures during the perinatal period, we delivered a single 1 μg/kg maternal dose of the persistent environmental contaminant 2,3,7,8 tetrachlorodibenzo-*p*-dioxin (TCDD) to male mouse fetuses on embryonic day (E)13.5, coinciding with the onset of testicular testosterone synthesis (6) and lower urinary tract development. TCDD has a whole-body elimination half-life of 11 days in C57BL/6J mice, and our exposure paradigm results in continuous TCDD exposure through weaning, which we term as *in utero* and lactational (IUL) TCDD exposure (7). We challenged control- and TCDD-exposed male mice with sustained release implants of testosterone and estradiol in adulthood to mimic aging-related changes to the endocrine environment (8). IUL TCDD exposure increases bladder and kidney weight, elevates the incidence of hydronephrosis, and increases voiding frequency (evidence of severe bladder outlet obstruction) in testosterone- and estradiol-treated mice (5, 9). These phenotypes in the mouse model recapitulate clinical features of human LUTD.

TCDD is a widespread contaminant produced as a byproduct of manufacturing and is ubiquitous in the serum of American men (10). *In utero* and lactational TCDD exposure thickens prostatic smooth muscle in mice (5) and non-human primates (11), suggesting activity-induced

hypertrophy and leading us to propose that enhanced prostate neuromuscular activity underlies TCDD-induced LUTD. The prostate is innervated by noradrenergic axons (12), and prostatic smooth muscle expresses a-1 and -2 adrenoreceptors (13, 14). In fact, noradrenaline-mediated smooth muscle contraction in isolated preparations of rat (15) and human (16) prostate led to the hypothesis that some males are susceptible to bladder outlet obstruction because of elevated prostatic smooth muscle tone. Although α-adrenoreceptor antagonists were developed for treatment of LUTD (17), mechanisms for interindividual variability in prostatic smooth muscle tone have not been identified.

Here, we provide evidence that the intrauterine environment contributes to sympathetic axon patterns and smooth muscle activity in the adult prostate. We show IUL TCDD exposure causes male mice to exhibit abnormal urinary function in adulthood; this is correlated with increased sensitivity of prostate smooth muscle to electrically evoked contraction and a persistent increase in prostate noradrenergic axon density in adults. Neurotrophins contribute to the development of sympathetic pathways by influencing axon guidance, neuronal survival, and axon branching (18, 19). We showed IUL TCDD exposure mediates, in the fetal prostate, an increase in mRNA abundance of artemin (*Artn*), a neurotrophin/survival factor for noradrenergic axons (19, 20). Collectively, our results support the hypothesis that IUL TCDD exposure changes prostatic neuroanatomical development by driving a persistent increase in noradrenergic axon density, which in turn contributes to prostate smooth muscle hyperactivity – a purported mechanism of urinary voiding dysfunction in men of advancing age. These results draw new attention to the perinatal environment as a factor that shapes adult male voiding function and serves as a risk modifier for urinary dysfunction in advancing age.

Results

IUL TCDD exposure is sufficient to change urodynamics in adult male mice

We previously demonstrated in two strains of mice (a genetically modified strain prone to prostate cancer and a C57BL/6J inbred strain) that IUL TCDD exposure exacerbates urinary voiding dysfunction in males treated in adulthood with sustained release testosterone + estradiol (T + E2) implants, which simulate endocrine changes associated with aging (5, 9). Additionally, IUL TCDD exposure was by itself was sufficient to decrease relative ventral prostate weight in genetically modified mice prone to prostate cancer (5). Here, we test the hypothesis that perinatal TCDD exposure is sufficient, in the absence of adulthood T + E2 implants, to change urodynamic function in adult C57BL/6J purebred male mice. A single dose of TCDD (1 μg/kg, oral maternal dose) was given at E13.5. Voiding urodynamics were evaluated by cystometry in anesthetized male mice on postnatal day (P)90-98. *In utero* and lactational TCDD exposure significantly reduces intervoid interval (**Figure 1**). Peak voiding pressure is not significantly changed (**Supplementary Figure S1A**). Previous studies demonstrated IUL TCDD exposure interacts with exogenous testosterone and estradiol to cause severe bladder outlet obstruction; however, this is the first demonstration that IUL TCDD can independently change voiding function in adult male mice.

IUL TCDD exposure increases sensitivity of adult prostatic smooth muscle to electrically evoked contraction.

In utero and lactational TCDD exposure is associated with prostatic smooth muscle hypertrophy in adult mice and rhesus macaques (5, 9, 11). Smooth muscle hyperactivity can drive hypertrophy; therefore, we tested whether IUL TCDD exposure increases nerve-evoked prostate muscle contraction. We introduced a genetically-encoded calcium sensor into prostate smooth muscle to quantify calcium transients as proxies for muscle contraction. *Myh11*^{cre}/+;*GCaMP5g/*+ male mouse fetuses were exposed to TCDD or vehicle (control) on E13.5, as previously described, and euthanized between P90-98. Excised lower urinary tracts (anterior lobes removed and dorsal prostate lobes attached to urethra) were transferred to a heated perfusion bath, and

prostate preparations were stimulated with trains of 0.5 ms pulses at 60 V with 0.1 Hz (below the frequency leading to half maximum response) (21) while continuously recording tissue fluorescence.. Stimulated tissues increase in fluorescence and eventually return to baseline fluorescence. *In utero* and lactational TCDD significantly decreases the rise time in field stimulation-induced calcium fluorescence, with TCDD-treated tissues reaching peak fluorescence (maximal contraction) more quickly than controls. Rise time is an index of muscle sensitivity; peak fluorescence does not change with treatment but the time to reach the maximal contraction is significantly less in IUL TCDD-treated animals. *In utero* and lactational TCDD exposure also increases the percentage of prostate ducts with detectable changes in ductal diameter in response to field stimulation (**Figure 2**).

We complemented imaging experiments with isometric contractility assays to measure prostate smooth muscle tension in response to graded field stimuli. *In utero* and lactational TCDD exposure significantly increases dorsal prostate tension in response to 0.1, 3, 10 and 60 Hz stimuli. We tested whether noradrenaline specifically mediates the TCDD-induced response in the dorsal prostate by blocking the release of catecholamines (including norepinephrine) from autonomic axons with the addition of sympatholytic guanethidine to the tissue bath (1.983 µg/mL) (21). Guanethidine pretreatment significantly attenuates TCDD-mediated enhancement of prostate field stimulation (**Figure 2**). The residual response is potentially due to a cholinergic-mediated contraction (22). The actions of TCDD also exhibit regional specificity for prostate and prostatic urethra, which are under noradrenergic control. The contractile response of the bladder, which is primarily mediated by cholinergic rather than noradrenergic mechanisms, is unchanged by IUL TCDD exposure (**Supplementary Figure S1B**).

From these results, we surmised TCDD could act through two mechanisms: it could directly enhance noradrenergic transmission, or it could increase sensitivity of prostate smooth muscle adrenoreceptors to agonists. Dorsal prostate tension response to increasing concentrations of phenylephrine (0.0001- 200 µM) is unchanged after IUL TCDD exposure, ruling

out a change in smooth muscle adrenergic sensitivity (**Supplementary Figure S1C**). Thus, we conclude that IUL TCDD exposure enhances magnitude and duration of adrenergic outflow within the prostate.

A single dose of TCDD at E13.5 increases prostate noradrenergic axon density beginning in the fetal period and persisting into adulthood

Men with LUTD experience imbalance in their autonomic nervous system activity characterized by decreased high frequency heart rate variability (23). Recent studies demonstrate prostate axon density is modifiable. For example, the prostate tumor microenvironment increases the density of parasympathetic cholinergic axons (24). We next tested whether IUL TCDD exposure influences prostate noradrenergic axon density. Mice were treated with TCDD or vehicle, as previously described, and adult (P90) prostate tissue sections were evaluated by immunostaining. Noradrenergic axons were labeled with antibodies against tyrosine hydroxylase (TH) and quantified in the 10 μm periductal region of prostate stromal tissue extending outward from cadherin 1 (CDH1)-stained prostate epithelium (**Figure 3A**). We focused specifically on the periductal region, as it contains most of the prostate periductal smooth muscle (25). *In utero* and lactational TCDD significantly increases noradrenergic axon density in dorsal prostate, suggesting TCDD modifies axon patterning during organ development (**Figure 3A**).

Noradrenergic axons are first evident in the mouse prostate at E13.5 (25), coinciding with the initiation of IUL TCDD exposure. We next tested whether TCDD acts through a developmental mechanism to increase prostate noradrenergic axon density. To pinpoint the stage of life when TCDD first increases noradrenergic axon density, mice were treated at E13.5 with IUL TCDD or IUL vehicle, and axons were quantified at two time points: 1) P9, coinciding with active prostate ductal branching morphogenesis and when noradrenergic axons are most dense (25); and 2) embryonic day 17.5, during prostate bud initiation (26). *In utero* and lactational TCDD exposure significantly increases noradrenergic axon density at both P9 (**Figure 3B**) and E17.5 (**Figure 3C**).

Thus, TCDD exposure beginning on E13.5 increases prostate noradrenergic axon density during the fetal and perinatal periods, and this change persists at least to adulthood.

TCDD actions on prostate axon density are not caused by changes in prostate size, as TCDD did not significantly change ventral, anterior, or dorsal prostate weights or body weights (**Supplementary Figure S1D and S1E**). Furthermore, TCDD actions on prostate innervation appear to be selective for noradrenergic axons. *In utero* and lactational TCDD exposure does not change immunopositive axon pixel densities at P90, P9, or E17.5 for markers of sensory axons (calcitonin gene-related peptide; CGRP), a pan-axonal marker (βIII tubulin; TUJ1) or cholinergic axons (vesicular acetylcholine transporter; VACHT), (**Supplementary Figure S2, S3, and S4**).

IUL TCDD exposure increases prostate mRNA abundance of ARTN, a neurotrophin linked to axon recruitment

Since IUL TCDD exposure increases prostate axon density during the period when axons project to the prostate, we used RNA sequencing (RNA-seq) to survey the genomic response to TCDD and test whether TCDD induces neurotrophins. We focused on the epithelium, because it is a considerable source of neurotrophins in other developing organs (27) and shifted the timing of TCDD exposure to coincide with prostate specification, the period when axons are actively recruited (28). We also increased the TCDD dose to increase the dynamic range of the transcriptional response. A single maternal dose of 5 μg/kg TCDD was delivered on E15.5, and fetal prostate epithelium was collected for RNA-seq analysis (**Figure 4A-B**). TCDD exposure initially led to the differential expression of 3,276 genes in fetal prostate epithelium (**Figure 4A**). To focus on the most biologically relevant changes while reducing the number of false positives, differential expression was determined using a threshold $\log_2(1.5)$ fold change cutoff, which resulted in 573 significantly differentially expressed genes (n =3-4, Benjamini-Hochberg false discovery rate (FDR)-adjusted p-value <= 0.05). Artemin (*Artn*), a member of the glial cell-derived neurotrophic factor family that recruits noradrenergic axons, was among top 20 most differentially

expressed genes by TCDD ordered by FDR-adjusted *p*--value (log_2(fold change) = 2.51, *n* = 3--4, FDR-adjusted *p* = 1.55 × $^{-}10^{6}$, **Figure 4B**). To validate the RNA-seq results and enhance rigor, we copied the TCDD dose and timing used in **Figures 1-3** (1 µg/kg maternal dose at E13.5) to evaluate TCDD-mediated changes in *Artn*. We used RNAScope to localize *Artn* mRNA in E17.5 urogenital sinus (UGS) epithelium of IUL TCDD and IUL vehicle samples and periepithelial mesenchyme (**Figure 4C**), the same regions where fetal TCDD exposure activates. We used RT-PCR to confirm that TCDD increases *Artn* mRNA abundance in the E17.5 male UGS (**Figure 4D**). We also show the TCDD-mediated increase in *Artn* mRNA abundance is transient; it is limited to the fetal period and is no longer differentially regulated in the P9 prostate (**Supplementary Figure S5**).

Our results collectively support a model by which TCDD exposure during urogenital development in the fetus induces *Artn* to enhance noradrenergic axon recruitment to the developing prostate, thereby increasing the basis for a larger response to sympathetic nerve activity and driving a change in urinary function that persists into adulthood (**Figure 5**). We propose this mechanism as a means by which the intrauterine environment can influence baseline urinary physiology and serve as a risk factor for LUTD in aging men.

Discussion

Chemical exposures during the fetal and neonatal periods influence risk of adult obesity, neurodevelopmental disorders, and some forms of cancer (29–31), but their impact on male urinary function during advancing age has largely been unexamined. Using perinatal exposure to a persistent environmental contaminant (TCDD) as a model, we find the intrauterine and early postnatal environment shapes prostate noradrenergic axon density, leading to lasting changes in prostate smooth muscle response and voiding function that persist into adulthood. It is unclear why prostate baseline tension, smooth muscle activity, and responsiveness to alpha blockers varies so considerably among human males with LUTD (32). We posit that maternal chemical

exposures during fetal urogenital development may underlie this variability, creating a susceptible phenotype that sensitizes males to voiding dysfunction with advancing age. In support of this concept, IUL TCDD exposure worsens urinary voiding dysfunction in mice challenged in adulthood with exogenous testosterone and estradiol implants (5). Here, we show IUL TCDD exposure is, by itself, sufficient to change urinary voiding dynamics in the absence of exogenous hormone challenge. We describe increased noradrenergic axon density and prostate smooth muscle hyperactivity as a mechanism for abnormal voiding in adulthood and for hypersensitivity of IUL TCDD-exposed mice.

The exposure of the fetus to TCDD during the period when noradrenergic axons are recruited into the prostate (25) increases abundance of *Artn,* a neurotrophin driving noradrenergic axon guidance and growth. ARTN mediates sympathetic axon growth along vasculature at the time of initial axon extension, induces sympathetic axon outgrowth *in vitro*, and attracts sympathetic axons *in vitro* and *in vivo* (18, 33). Mice deficient in *Artn* exhibit abnormally short or misdirected proximal axons from sympathetic chain ganglia (19). More than 50% of sympathetic neurons generated in the embryo are killed by apoptosis during normal development (34). One hypothesis for this excessive innervation is that neurons are initially overproduced and once they innervate their target, they compete for limited target-derived neurotrophic factors (35). Our data point to IUL TCDD exposure increasing *Artn* expression, in turn leading to persistent hyperinnervation. We localized *Artn* within fetal mouse prostate and used independent methods and two separate mouse cohorts to show TCDD increases *Artn* mRNA abundance in the fetal prostate. TCDD is a potent ligand of the AHR, a ligand-dependent transcription factor that mediates most, if not all, of TCDD's biological actions (36). Promoting the idea that *Artn* induction is a more generalizable mechanism of AHR action, a recent study found that the activated AHR docks at the *Artn* gene locus, increases *Artn* expression, and drives hyperinnervation of adult mouse skin (37).

A surprising observation in this study is the persistence of the prostate hyperinnervation phenotype induced by fetal TCDD exposure, beginning in the fetal period and continuing into adulthood. *Artn* is transiently upregulated at E17.5 and not observed at other timepoints. Perhaps other neurotrophic pathways are upregulated at later timepoints to cause the persistent increase in axon density. Other neurotrophins such as neuropilin 1, neuropilin 2, and semaphorin 3a (SEMA3A) also control rat and mouse sympathetic axon growth, guidance, and remodeling (38–40). TCDD acts through SEMA3A to disrupt the peripheral nervous system of the red seabream (41). To further define the mechanism underpinning sympathetic hyperinnervation of the prostate, it would be of interest to investigate potentially persistent effects of TCCD exposure on pelvic ganglia, as these are the primary source of sympathetic axons innervating the prostate and other pelvic organs. This approach could determine if TCCD drives hyperinnervation by stimulating the postnatal maturation of pelvic ganglia (where the number of neurons normally continues to increase in the first couple of weeks after birth). Alternatively, TCCD may also stimulate the growth of axon collaterals within the prostate. We previously observed that axon density in the mouse prostate continuously increases from the fetal period to adulthood (25). If chemical exposure causes excessive noradrenergic axons to grow within the developing prostate and this aberrant growth persists postnatally and into adulthood, this may be a fundamental generalizable mechanism of urinary voiding dysfunction in aging men and influence the symptomatic response to inflammation and therapeutic response to alpha blockers. It is important to note that several chemicals have been implicated in abnormal prostate development, including environmental, pharmaceutical, and dietary estrogens (42, 43), plasticizers (44), and bacterial toxins (45), among others. Whether these other chemicals influence innervation of the prostate has not been determined. Investigation of the impact of other AHR agonists on prostate innervation would be of significant interest and relevance to LUTD.

Materials and Methods

Mice

All mice were purchased from Jackson Laboratories (Bar Harbor, ME) and maintained on a C57BL/6J genetic background (Jackson stock #000664), *Polr2a*$^{Tn(pb\text{-}CAG\text{-}GCaMP5g,\text{-}tdTomato)Tvrd}$ (also known as GCaMP5g, Jackson mouse stock #024477), and Tg(*Myh11cre*,-EGFP)2Mik (also known as *Myh11*^{cre}, Jackson mouse stock #007742). Mice were housed in Innovive® HDPE plastic microisolator cages in a room maintained on a 12-h light and dark cycle, ambient temperature of 20.5 ± 1 °C, and relative humidity of 30-70%. Mice were fed a 5015 Diet (PMI Nutrition International, Brentwood, MO) from conception through weaning (postnatal day 21; P21) and an 8604 Teklad Rodent Diet thereafter (Harlan Laboratories, Madison, WI). Food and water were available *ad libitum,* and cages contained corncob bedding. Mice were time-mated by pairing males and females overnight. The morning of definitive copulatory plug identification was considered embryonic day (E)0. For all studies other than RNA-seq, mated females with a body weight increase of 4 g at 13 d post-breeding (indicating pregnancy) (46) were given a single dose of TCDD (1 μg/kg, orally (po), 98% purity, Cambridge Isotope Laboratories, Andover, MA) or corn oil (5 mL/kg, po), vehicle control) on E13.5. The TCDD dose used in this study matches that of a previous reference study (47). Based on the eleven-day whole-body elimination half-life of TCDD in C57BL/6J mice, the TCDD dosing paradigm used in this study results in continuous TCDD exposure from the fetal period through weaning (7). All mice were euthanized by CO_2 asphyxiation. Urogenital sinus and prostate tissues were collected at E17.5, postnatal day (P)9, and P90-98, either snap frozen in liquid nitrogen or fixed overnight at 4 °C in 4% paraformaldehyde dissolved in neutral buffered saline (Thermo Scientific) and dehydrated through a series of graded ethanol concentrations. Tissues were cleared in xylenes, embedded in paraffin wax, and sectioned at 10 μm thickness on a microtome (Surgipath Medical Industries).

Cystometry in anesthetized adult male mice

Cystometry was performed as previously described (48–50). Mice were anesthetized with urethane (1.43 g/kg, subcutaneous (sc)), because isoflurane interferes with normal micturition, and rested for 30 min. An incision was made in the ventral abdomen to expose the bladder. A purse string suture was placed in the bladder dome, and polyethylene cystometry tubing (PE-50; outer diameter: 0.58 mm, inner diameter: 0.28 mm) was inserted into the bladder through the center of the suture and secured. The abdominal wall and skin were closed, and the exterior tubing was sutured to the abdominal skin to prevent movement. Mice were allowed to recover on a heating pad for one hour (hr) post procedure. The exposed tubing was attached to a three-way stopcock and connected to an infusion pump (Harvard Apparatus, Holliston, MA) and pressure transducer (Memscap). Bladder pressure was simultaneously recorded using a PowerLab data collection system (ABInstruments, Colorado Springs, CO). Saline (0.9%) was infused into the bladder at a rate of 1.5 mL/hr. At least one hour of voiding activity was recorded. Three to five consecutive voids, occurring after stabilization of micturition cycles, were used for analysis.

Smooth muscle calcium transient imaging

Myh11cre/+;*GCaMP5g/*+ harbor a genetically-encoded calcium sensor that fluoresces in response to increases in intracellular calcium concentration. *Myh11*^{cre}/+; *GCaMP5g*/+ mice were euthanized at 14 weeks of age, and a tissue complex containing urethra and anterior, dorsal, and ventral prostate was dissected and stored in ice cold HEPES buffer (134 mM NaCl, 10 mM HEPES, 6 mM KCl, 7 mM glucose, 1 mM $MgCl_2$, pH 7). The anterior prostate was dissected and analyzed separately while dorsal prostate was analyzed attached to the urethra due to its small size. The tissue was positioned in a heated (37 °C) chamber for imaging (Warner Instruments #RC-49MFSH). A pressurized perfusion system (Warner Instruments # 641721) fitted with mini-valve controllers (Warner Instruments #VCS–8–MINI–LT) was used to continuously perfuse tissues with HEPES solution (134 mM NaCl, 10 mM HEPES, 6 mM KCl, 7 mM glucose, 1 mM $MgCl_2$, 2 mM $CaCl_2$, pH 7; 1 mL/min), and maintained at 37 °C with an inline heater (Warner

Instruments #SF-28). The tissue was illuminated with an LED light (SOLA-SM2 365 LED Light Engine) and visualized with a Leica MZ16 stereo fluorescent dissecting microscope fitted with a GFP dichroic filter set (Chroma, Bellows Falls, VT). Images were recorded with a Zyla 4.2 Plus sCMOS camera using Nikon Elements Software. A Grass stimulator (model S88, pulse stimulator) was used to deliver electrical impulses for 10 sec at 60 V and 0.1 Hz (21). After a 5 min recovery period, tissues were stimulated again for 10 sec at 60 V and 30 Hz (21). Videos were recorded at 10 frames/sec and analyzed using SparkAn (in-house software designed by Dr. Adrian Bonev, University of Vermont). Investigators were blinded to treatment group by labeling videos with exclusively mouse number and date.

Isometric prostate muscle tension analysis

In vitro organ bath studies were conducted as previously described (51, 52). Excised dorsal prostates and bladder were weighed, and 5-0 sutures were applied to secure the dorsal prostate and subdissected bladder strips at the base to the specimen arm and at the tip of the tissue to the force displacement transducer (Grass FT-03). Tension was recorded using the PowerLab data collection system (ABInstruments, Colorado Springs, CO). The prostate and bladder were suspended in a 37 °C water-jacketed tissue chamber filled with Krebs solution (133 mM NaCl, 16 mM $NaHCO_3$, 5 mM KCl, 1 mM $MgCl_2$, 1.4 mM NaH_2PO_4, 2.5 mM $CaCl_2$ $2H_2O$, 7.8 mM D-glucose, pH 7.2) and aerated with 95% O_2-5% CO_2. Tissues were maintained at 0.7 g of tension for 60 min before experimentation, with Krebs solution changed every 15 min. Tension was recorded using the AxoScope Application of PCLAMP software (Molecular Devices, Sunnyvale, CA). Tissues were stimulated for 5 sec at 0.1, 1, 3, 10, 30, and 60 Hz at 30V, with three minutes between each stimulation. Tissue baths were flushed with Krebs solution, and tissues were allowed to return to baseline (0.7 g) tension for 30 mins, after which a concentration response curve to the α-adrenergic agonist phenylephrine (0.0001, 0.01, 1, 100, and 200 μM) was performed. After washout and return to baseline (0.7 g) tension for 30 mins, tissues were

incubated with guanethidine for 15 minutes (22) before being stimulated as described above at 0.1, 1, 3, 10, and 30 Hz. After a final washout and return to baseline for 30 mins, tissues were maximally contracted with 60 mM KCl. Tissue responses were normalized to maximum response to KCl and expressed as a percentage thereof. Investigators were blinded to treatment group by labeling videos with exclusively mouse number and date.

Immunohistochemistry

Paraffin-embedded tissue sections (10 μm) were deparaffinized with xylene and rehydrated in a series of graded concentrations of ethanol. Immunofluorescence staining was conducted as described previously (25, 53) using antibodies listed in **Supplementary Table S1**. Tissue sections were imaged using an SP8 confocal microscope (Leica, Wetzlar, Germany) fitted with a 20X oil immersion objective (HC PL Apo CS2 NA = 0.75; Leica, Wetzlar, Germany). Ten *z*-stack images were captured at 1024x1024 resolution and a *Z*-interval of 1 μm using LASX 8 software (Leica, Wetzlar, Germany). The detector gain ranged between 10-30 using a Hy-D detector. All fluorescent images were stained using Alexa 488, Rhodamine red, and Alexa 647 secondary antibodies (**Supplementary Table S1**). These fluorophores were excited using the 488 nm, 561 nm, and 633 nm lasers respectively, and images were collected sequentially. Whole-image RGB color intensity was adjusted using Adobe Photoshop only after quantification (version 20.0).

In situ *hybridization*

RNA *in situ* hybridization was performed on 5 μm paraffin sections of mouse tissue using the RNAscope 2.5 HD Assay kit (Catalog number # 322360) from Advanced Cell Diagnostics following manufacturer instructions. Optimized conditions for target retrieval were determined as a 15 min incubation in the target retrieval buffer and a 30 min treatment with proteinase K reagent. The probe against mouse aretmin (Catalog number # 800811) was obtained from the Advanced

Cell Diagnostics probe catalog. Images were obtained at 20x on a Zeiss Axio Scan Z1 microscope and processed using Zen Blue software.

Morphometric analysis

Tyrosine hydroxylase- (TH), βIII tubulin- (TUBB), vesicular acetylcholine transporter- (VAChT), and calcitonin gene-related peptide- (CGRP) positive prostatic axons were quantified in E17.5, P9, and P90 prostate tissue sections, as previously described (25). For the embryonic stage, axons were quantified in the 10 μm stromal band extending from the basal surface of CDH1-stained urogenital sinus (UGS) using ImageJ. For postnatal stages, axons were quantified in the 10 μm stromal band extending from the basal surface of CDH1-stained prostatic ductal epithelium (this region encompasses the majority of periductal smooth muscle). Immunostained axon pixels were quantified using the thresholding feature (MaxEntropy thresholding) of ImageJ (Version 1.52e11) (54). Image pixel density was scaled to 2.23 pixels/μm. For each age and sampled region, three non-adjacent, near-midsagittal, technical replicate tissue sections (10 μm) were averaged per mouse, and 4-10 biological replicate mice were evaluated per axon subtype. Mice of each age were derived from at least three separate litters. Investigators were blinded to treatment group by labeling videos with exclusively mouse number and date.

RNA sequencing of fetal prostate epithelium

Pregnant C57BL/6J mice were treated po with either 5 mL/kg corn oil (control) or 5 μg/kg TCDD on E13.5 following previously established protocols (55). Dams were euthanized at E16.75 via CO_2 asphyxiation, and urogenital sinuses were dissected from fetuses, as previously described (47). Each UGS was immediately placed into 300 μL of 1% trypsin (Difco, 215240) in PBS and incubated on ice for 30 min. Collagenase (Sigma, C9891) was added to a final concentration of 1 mg/mL, followed by an additional 30-45 min incubation on ice. A dissecting microscope was used to mechanically separate UGS mesenchyme from UGS epithelium (UGE) and excise bladder and distal urethra leaving only the portion of UGE from which the prostate

derives. Each treatment group consisted of 4 biological replicates, and each replicate contained 5 or 6 individual UGEs that were pooled for RNA isolation. Total RNA was purified from each UGE using the RNeasy® system (Qiagen) and analyzed using the Agilent Bioanalyzer 2100 and an Agilent RNA 6000 PicoKit (Agilent Technologies). The samples were sequenced at the University of Wisconsin-Madison, Biotechnology Center, using an Illumina HiSeq® 2500.

RNA sequencing analysis

Processing of RNA-seq data followed an updated pipeline for gene-level analysis (55, 56). Briefly, reads were evaluated by FastQC v0.11.9 (57) to detect major sequencing problems, and then trimmed for quality control with two rounds of Skewer v0.2.2 (58) to remove ends of reads with low mean Phred quality score (Skewer round 1 options: x -AAAAAAAAAAAAAAAAAAAAAAAAAAAAAAAAAAAAAAAAAAAAAAAAAAAAAAAAAAAAAAA AA --mode pe --max 100 --cut3 --format auto --compress --threads 9; Skewer round 2 options: x Mouse_adapters.fa- --mode pe --end-quality 30 --mean-quality 30 --min 30 --format auto --compress --threads 9, **Supplementary Table S2**). RNA sequencing alignment and quantification proceeded with Bowtie2 v2.4.1 (59, 60) being used to build HISAT2 v2.1.0 (61, 62) genome index files from the Genome Reference Consortium Mouse Build 38 patch release 6 (GRCm38.p6) genome downloaded from Ensembl (release 100; ftp://ftp.ensembl.org/pub/release-100/fasta/mus_musculus/dna/Mus_musculus.GRCm38.dna.toplevel.fa.gz). To enhance the genome index files, the HISAT2 scripts hisat2_extract_splice_sites.py and hisat2_extract_exons.py were used to extract splice site and exon information, respectively, from the Ensembl 100 gene transfer format (GTF) file (ftp://ftp.ensembl.org/pub/release-100/gtf/mus_musculus/Mus_musculus.GRCm38.100.gtf.gz). The extracted genomic information was incorporated into HISAT2 index files, using the hisat2-build command. After building enhanced genome index files, trimmed reads were aligned with HISAT2 v2.1.0 and then piped

through SAMtools v1.10 (63) to convert aligned reads to binary alignment style (BAM) and then to sort BAM reads by position, using the following command: hisat2 -q --phred33 -rna-strandness- RF --no-mixed --no-discordant --new-summary --threads 9 -x *GENOME_INDEX* -1 *PAIR1_FILE.fastq.gz* -2 *PAIR2_FILE.fastq.gz* | samtools view -u @9 | samtools- sort -n -O bam -o *OUTPUT_FILE_sorted_byName.bam* -@9. Gene counts were estimated using the htseq-count command from HTSeq v0.12.4 (64) with the GRCm38.p6 Ensembl 100 GTF annotation (options: --format=bam --order=name --stranded=reverse --type=exon -idattr=gene_id- --additionalattr=gene_name- --mode=intersection-nonempty).

Analysis of gene counts was conducted using R v4.0.2 (65) and Bioconductor v3.11 (66, 67) packages in the RStudio v1.3.959 (68) integrated development environment with a customized script (**Datafile S1**) based on a maintained Bioconductor workflow package from the Gordon Smyth lab, https://www.bioconductor.org/packages/release/workflows/vignettes/RnaSeqGeneEdgeRQL/inst/doc/edgeRQL.html, last updated 13 June 2020 (69). Counts from technical replicates split across sequencing lanes were averaged, and initial exploratory data analysis (i.e. gene variance heatmaps and PCA plots) revealed an outlier TCDD sample, which was removed. The Bioconductor package, edgeR v3.30.3, was used to normalize gene counts and determine differential expression (70–75). Briefly, genes were filtered using their filterByExpr function to exclude those with low counts in a minimum number of samples across libraries (69, 75). Filtered genes were then normalized across samples using the trimmed mean of M values (TMM) method to minimize composition bias between libraries (73). Differential expression of genes was determined using functions from edgeR, which uses the negative binominal generalized linear model extended by quasi-likelihood methods to fit the count data, the Cox-Reid profile-adjusted likelihood method to calculate dispersions, and empirical Bayes quasi-likelihood F-tests, while differential expression above a logarithmic fold change threshold of $\log_2(1.5)$ between experimental and control samples was subsequently determined using a version of the TREAT

(*t*-tests relative to a threshold) method (74, 76, 77). The 'robust=TRUE' option was used to protect the empirical Bayes estimates against the possibility of outlier genes with wide ranging individual dispersions. Genes with a Benjamini-Hochberg (BH) false discovery rate (FDR)-adjusted $p \leq 0.05$ were considered significantly differentially expressed. The biomaRt v2.44.1 package was used to connect Ensembl gene identifier information to Ensembl BioMart annotation information (e.g. gene symbols, biotypes), and the volcano plot was made using ggplot2 and ggrepel (78–81). Heatmaps were made using the R packages dendextend v1.13.4 and ComplexHeatmap v2.4.2 (78, 79, 82, 83). Heatmap clustering was derived from TMM-normalized, variance-stabilized transformed gene values scaled by *z*-score (84). Sequencing data and processing details have been deposited in the National Center for Biotechnology Information Gene Expression Omnibus (GEO accession number: GSE166395).

RNA Isolation and RT-PCR

Neonatal and fetal prostates were homogenized, as described previously (Tengowski et al., 1997). RNA was purified with Illustra RNAspin minikit (GE Healthcare, Pittsburgh, PA) and reverse transcribed with the SuperScript III First Strand Synthesis System (Invitrogen, Carlsbad, CA). Real time reverse transcriptase polymerase chain reaction (RT-PCR) was performed in 10.5 µL reactions containing 1x SsoFast EvaGreen Supermix (Bi-Rad Laboratories, Hercules, CA), 0.48 uM PCR primers, and 3.75 µL cDNA and amplified using a CFX96 PCR machine (Bio-Rad Laboratories). PCR primers are listed in **Supplementary Table 3** with *Ppia* used as an internal loading control. Relative mRNA abundance was determined by the deltaCt method, as described previously (86).

Statistics

The number of mice per group ranged from 4-11, and groups represented at least three independent litters. Statistical analysis was performed using GraphPad Prism 8 (version 8.2.1)

and a difference between means was considered significant at $p \leq 0.05$. Differences among or between groups were identified using one-sided Student's *t*-test (intervoid interval, TH+, VaCHT+, TUBB3+ axon density quantification, GCaMP analysis, tissue bath analysis, RT-PCR), one-way ANOVA (CGRP axon density quantification), two-way ANOVA (guanethidine quantification), and non-linear regression model (least squares, phenylephrine dose response). Bartlett's test was used to determine homogeneity of variance before using ANOVA to determine if a parametric or nonparametric test could be used. Data that did not meet the criteria for homogeneity of variance or normality were transformed (log or square root). The Grubb's test identified extreme studentized deviates, and significant outliers were excluded from analysis. We concluded these tissues sections were adjacent to an intramural ganglion, and they were removed from statistical analysis.

Study Approval

All procedures were approved by the University of Wisconsin Animal Care and Use Committee and conducted in accordance with the National Institutes of Health Guide for the Care and Use of Laboratory Animals.

Acknowledgments

This work was supported by National Institutes of Health Grants R01 ES001332, R01 DK119615, U01 HD094759, U54 DK104310, R01 DK115477, R00 ES029537, T32 ES007015, F31 ES030968, K12 DK100022. The content is solely the responsibility of the authors and does not necessarily represent the official views of the National Institutes of Health. We would like to thank Dr. Robert Lipinski for careful review and spirited discussion in the formulation of this manuscript.

References

1. H. Lepor, Pathophysiology of Lower Urinary Tract Symptoms in the Aging Male Population. *Rev Urol* **7**, S3–S11 (2005).

2. S. C. Langley-Evans, Fetal programming of cardiovascular function through exposure to maternal undernutrition. *Proc Nutr Soc* **60**, 505–513 (2001).

3. N. Potischman, R. Troisi, In-utero and early life exposures in relation to risk of breast cancer. *Cancer Causes Control* **10**, 561–573 (1999).

4. R. A. Simmons, L. J. Templeton, S. J. Gertz, Intrauterine growth retardation leads to the development of type 2 diabetes in the rat. *Diabetes* **50**, 2279–2286 (2001).

5. W. A. Ricke, *et al.*, In Utero and Lactational TCDD Exposure Increases Susceptibility to Lower Urinary Tract Dysfunction in Adulthood. *Toxicol Sci* **150**, 429–440 (2016).

6. H. M. Scott, J. I. Mason, R. M. Sharpe, Steroidogenesis in the Fetal Testis and Its Susceptibility to Disruption by Exogenous Compounds. *Endocrine Reviews* **30**, 883–925 (2009).

7. T. A. Gasiewicz, L. E. Geiger, G. Rucci, R. A. Neal, Distribution, excretion, and metabolism of 2,3,7,8-tetrachlorodibenzo-p-dioxin in C57BL/6J, DBA/2J, and B6D2F1/J mice. *Drug Metab. Dispos.* **11**, 397–403 (1983).

8. A. Bélanger, *et al.*, Changes in serum concentrations of conjugated and unconjugated steroids in 40- to 80-year-old men. *J. Clin. Endocrinol. Metab.* **79**, 1086–1090 (1994).

9. A. E. Turco, *et al.*, In utero and lactational 2,3,7,8-tetrachlorodibenzo-p-dioxin (TCDD) exposure exacerbates urinary dysfunction in hormone-treated C57BL/6J mice through a non-malignant mechanism involving proteomic changes in the prostate that differ from those elicited by testosterone and estradiol. *Am J Clin Exp Urol* **8**, 59–72 (2020).

10. A. Gupta, *et al.*, Serum Dioxin, Testosterone, and Subsequent Risk of Benign Prostatic Hyperplasia: A Prospective Cohort Study of Air Force Veterans. *Environ Health Perspect* **114**, 1649–1654 (2006).

11. A. Arima, *et al.*, In utero and lactational exposure to 2,3,7,8-tetrachlorodibenzo-p-dioxin (TCDD) induces disruption of glands of the prostate and fibrosis in rhesus monkeys. *Reprod. Toxicol.* **29**, 317–322 (2010).

12. H. G. Baumgarten, B. Falck, A. F. Holstein, C. Owman, T. Owman, Adrenergic innervation of the human testis, epididymis, ductus deferens and prostate: a fluorescence microscopic and fluorimetric study. *Z Zellforsch Mikrosk Anat* **90**, 81–95 (1968).

13. E. Shapiro, H. Lepor, R. D. Jeffs, The inheritance of the exstrophy-epispadias complex. *J. Urol.* **132**, 308–310 (1984).

14. E. Shapiro, H. Lepor, Alpha 2 adrenergic receptors in hyperplastic human prostate: identification and characterization using [3H] rauwolscine. *J. Urol.* **135**, 1038–1042 (1986).

15. S. Raz, M. Zeigler, M. Caine, Pharmacological receptors in the prostate. *Br J Urol* **45**, 663–667 (1973).

16. M. Caine, S. Raz, M. Zeigler, Adrenergic and cholinergic receptors in the human prostate, prostatic capsule and bladder neck. *Br J Urol* **47**, 193–202 (1975).

17. M. Caine, A. Pfau, S. Perlberg, The use of alpha-adrenergic blockers in benign prostatic obstruction. *Br J Urol* **48**, 255–263 (1976).

18. H. Enomoto, *et al.*, RET signaling is essential for migration, axonal growth and axon guidance of developing sympathetic neurons. *Development* **128**, 3963–3974 (2001).

19. Y. Honma, *et al.*, Artemin Is a Vascular-Derived Neurotropic Factor for Developing Sympathetic Neurons. *Neuron* **35**, 267–282 (2002).

20. R. H. Baloh, *et al.*, Artemin, a novel member of the GDNF ligand family, supports peripheral and central neurons and signals through the GFRalpha3-RET receptor complex. *Neuron* **21**, 1291–1302 (1998).

21. W. A. Lau, S. Ventura, J. N. Pennefather, Pharmacology of neurotransmission to the smooth muscle of the rat and the guinea-pig prostate glands. *J Auton Pharmacol* **18**, 349–356 (1998).

22. C. W. White, J. L. Short, J. M. Haynes, R. J. Evans, S. Ventura, The Residual Nonadrenergic Contractile Response to Nerve Stimulation of the Mouse Prostate Is Mediated by Acetylcholine but Not ATP in a Comparison with the Mouse Vas Deferens. *J Pharmacol Exp Ther* **335**, 489–496 (2010).

23. J. B. Choi, J. G. Lee, Y. S. Kim, Characteristics of autonomic nervous system activity in men with lower urinary tract symptoms (LUTD): analysis of heart rate variability in men with LUTD. *Urology* **75**, 138–142 (2010).

24. C. Magnon, *et al.*, Autonomic nerve development contributes to prostate cancer progression. *Science* **341**, 1236361 (2013).

25. A. E. Turco, *et al.*, A temporal and spatial map of axons in developing mouse prostate. *Histochem. Cell Biol.* (2019) https:/doi.org/10.1007/s00418-019-01784-6.

26. T.-M. Lin, N. T. Rasmussen, R. W. Moore, R. M. Albrecht, R. E. Peterson, 2,3,7,8-tetrachlorodibenzo-p-dioxin inhibits prostatic epithelial bud formation by acting directly on the urogenital sinus. *J. Urol.* **172**, 365–368 (2004).

27. W. C. de Groat, Highlights in basic autonomic neuroscience: contribution of the urothelium to sensory mechanisms in the urinary bladder. *Auton Neurosci* **177**, 67–71 (2013).

28. C. M. Vezina, *et al.*, Dioxin causes ventral prostate agenesis by disrupting dorsoventral patterning in developing mouse prostate. *Toxicol. Sci.* **106**, 488–496 (2008).

29. D. O. Carpenter, S. Bushkin-Bedient, Exposure to Chemicals and Radiation During Childhood and Risk for Cancer Later in Life. *Journal of Adolescent Health* **52**, S21–S29 (2013).

30. P. Grandjean, P. Landrigan, Developmental neurotoxicity of industrial chemicals. **368**, 13 (2006).

31. E. D. Levin, S. L. Schantz, R. E. Bowman, Delayed spatial alternation deficits resulting from perinatal PCB exposure in monkeys. *Arch Toxicol* **62**, 267–273 (1988).

32. S. N. Lee, *et al.*, Age Related Differences in Responsiveness to Sildenafil and Tamsulosin are due to Myogenic Smooth Muscle Tone in the Human Prostate. *Sci Rep* **7**, 10150 (2017).

33. N. O. Glebova, D. D. Ginty, Growth and Survival Signals Controlling Sympathetic Nervous System Development. *Annual Review of Neuroscience* **28**, 191–222 (2005).

34. R. W. Oppenheim, Cell death during development of the nervous system. *Annu Rev Neurosci* **14**, 453–501 (1991).

35. R. Levi-Montalcini, H. Meyer, V. Hamburger, In vitro experiments on the effects of mouse sarcomas 180 and 37 on the spinal and sympathetic ganglia of the chick embryo. *Cancer Res* **14**, 49–57 (1954).

36. T. Edamitsu, K. Taguchi, E. H. Kobayashi, R. Okuyama, M. Yamamoto, Aryl Hydrocarbon Receptor Directly Regulates Artemin Gene Expression. *Mol. Cell. Biol.* **39** (2019).

37. T. Hidaka, *et al.*, The aryl hydrocarbon receptor AhR links atopic dermatitis and air pollution via induction of the neurotrophic factor artemin. *Nature Immunology* **18**, 64–73 (2017).

38. M. R. Nangle, J. R. Keast, Semaphorin 3A inhibits growth of adult sympathetic and parasympathetic neurones via distinct cyclic nucleotide signalling pathways. *Br J Pharmacol* **162**, 1083–1095 (2011).

39. C. H. Maden, *et al.*, NRP1 and NRP2 cooperate to regulate gangliogenesis, axon guidance and target innervation in the sympathetic nervous system. *Dev Biol* **369**, 277–285 (2012).

40. A. Richeri, *et al.*, Neuropilin-1 receptor in the rapid and selective estrogen-induced neurovascular remodeling of rat uterus. *Cell Tissue Res* **381**, 299–308 (2020).

41. M. Iida, E.-Y. Kim, Y. Murakami, Y. Shima, H. Iwata, Toxic effects of 2,3,7,8-tetrachlorodibenzo-p-dioxin on the peripheral nervous system of developing red seabream (Pagrus major). *Aquat. Toxicol.* **128–129**, 193–202 (2013).

42. M. Saito, T. Mitsui, T. Mizuno, [Genistein represses the induction of prostatic buds by testosterone]. *J Soc Biol* **194**, 95–97 (2000).

43. B. G. Timms, *et al.*, Estrogenic chemicals in plastic and oral contraceptives disrupt development of the fetal mouse prostate and urethra. *Proc Natl Acad Sci U S A* **102**, 7014–7019 (2005).

44. R. W. Moore, T. A. Rudy, T. M. Lin, K. Ko, R. E. Peterson, Abnormalities of sexual development in male rats with in utero and lactational exposure to the antiandrogenic plasticizer Di(2-ethylhexyl) phthalate. *Environ Health Perspect* **109**, 229–237 (2001).

45. H. Zhang, *et al.*, Toxic effects of microcystin-LR on the development of prostate in mice. *Toxicology* **380**, 50–61 (2017).

46. G. W. Heyne, *et al.*, A Simple and Reliable Method for Early Pregnancy Detection in Inbred Mice. *J. Am. Assoc. Lab. Anim. Sci.* **54**, 368–371 (2015).

47. R. W. Moore, *et al.*, 2,3,7,8-Tetrachlorodibenzo-p-dioxin Has Both Pro-Carcinogenic and Anti-Carcinogenic Effects on Neuroendocrine Prostate Carcinoma Formation in TRAMP Mice. *Toxicol Appl Pharmacol* **305**, 242–249 (2016).

48. H. Ruetten, *et al.*, Impact of sex, androgens, and prostate size on C57BL/6J mouse urinary physiology: functional assessment. *Am J of Physio-Ren- Physio* **317**, F996–F1009 (2019).

49. K. E. Ritter, Z. Wang, C. M. Vezina, D. E. Bjorling, E. M. Southard-Smith, Serotonin Receptor 5-HT3A Affects Development of Bladder Innervation and Urinary Bladder Function. *Front. Neurosci.* **11** (2017).

50. D. E. Bjorling, *et al.*, Evaluation of voiding assays in mice: impact of genetic strains and sex. *American Journal of Physiology-Renal Physiology* **308**, F1369–F1378 (2015).

51. K. P. Keil, *et al.*, Impact of a folic acid-enriched diet on urinary tract function in mice treated with testosterone and estradiol. *American Journal of Physiology-Renal Physiology* **308**, F1431–F1443 (2015).

52. M. W. Tengowski, D. E. Bjorling, R. M. Albrecht, R. Saban, Use of gold-labeled ovalbumin to correlate antigen deposition and localization with tissue response. *J Pharmacol Toxicol Methods* **37**, 15–21 (1997).

53. L. L. Abler, *et al.*, A high throughput in situ hybridization method to characterize mRNA expression patterns in the fetal mouse lower urogenital tract. *J Vis Exp* (2011) https:/doi.org/10.3791/2912.

54. J. Kapur, P. Sahoo, A. Wong, A New Method for Gray-Level Picture Thresholding Using the Entropy of the Histogram". *Graphical Models and Image Processing* **29**, 273–285 (1985).

55. G. R. Garcia, *et al.*, Signaling Events Downstream of AHR Activation That Contribute to Toxic Responses: The Functional Role of an AHR-Dependent Long Noncoding RNA (slincR) Using the Zebrafish Model. *Environ Health Perspect* **126**, 117002 (2018).

56. S. Anders, *et al.*, Count-based differential expression analysis of RNA sequencing data using R and Bioconductor. *Nat Protoc* **8**, 1765–1786 (2013).

57. S. Andrews, FastQC A Quality Control tool for High Throughput Sequence Data. Version 0.11.9. Babraham Bioinformatics (2015).

58. H. Jiang, R. Lei, S.-W. Ding, S. Zhu, Skewer: a fast and accurate adapter trimmer for next-generation sequencing paired-end reads. *BMC Bioinformatics* **15**, 182 (2014).

59. B. Langmead, C. Trapnell, M. Pop, S. L. Salzberg, Ultrafast and memory-efficient alignment of short DNA sequences to the human genome. *Genome Biology* **10**, R25 (2009).

60. B. Langmead, S. L. Salzberg, Fast gapped-read alignment with Bowtie 2. *Nature Methods* **9**, 357–359 (2012).

61. D. Kim, B. Langmead, S. L. Salzberg, HISAT: a fast spliced aligner with low memory requirements. *Nature Methods* **12**, 357–360 (2015).

62. D. Kim, J. M. Paggi, C. Park, C. Bennett, S. L. Salzberg, Graph-based genome alignment and genotyping with HISAT2 and HISAT-genotype. *Nat Biotechnol* **37**, 907–915 (2019).

63. H. Li, *et al.*, The Sequence Alignment/Map format and SAMtools. *Bioinformatics* **25**, 2078–2079 (2009).

64. S. Anders, P. T. Pyl, W. Huber, HTSeq--a Python framework to work with high-throughput sequencing data. *Bioinformatics* **31**, 166–169 (2015).

65. R Core Team, R: The R Project for Statistical Computing. Version 4.0.2. R Foundation for Statistical Computing. *https://www.R-project.org/.* (2020) (February 12, 2021).

66. R. C. Gentleman, *et al.*, Bioconductor: open software development for computational biology and bioinformatics. *Genome Biology* **5**, R80 (2004).

67. W. Huber, *et al.*, Orchestrating high-throughput genomic analysis with Bioconductor. *Nature Methods* **12**, 115–121 (2015).

68. RStudio Team, RStudio: Integrated Development for R. Version 1.3.959. RStudio, Inc, PBC, Boston, MA (2020).

69. Y. Chen, A. T. L. Lun, G. K. Smyth, From reads to genes to pathways: differential expression analysis of RNA-Seq experiments using Rsubread and the edgeR quasi-likelihood pipeline. *F1000Res* **5**, 1438 (2016).

70. M. D. Robinson, G. K. Smyth, Moderated statistical tests for assessing differences in tag abundance. *Bioinformatics* **23**, 2881–2887 (2007).

71. M. D. Robinson, G. K. Smyth, Small-sample estimation of negative binomial dispersion, with applications to SAGE data. *Biostatistics* **9**, 321–332 (2008).

72. M. D. Robinson, D. J. McCarthy, G. K. Smyth, edgeR: a Bioconductor package for differential expression analysis of digital gene expression data. *Bioinformatics* **26**, 139–140 (2010).

73. M. D. Robinson, A. Oshlack, A scaling normalization method for differential expression analysis of RNA-seq data. *Genome Biology* **11**, R25 (2010).

74. D. J. McCarthy, Y. Chen, G. K. Smyth, Differential expression analysis of multifactor RNA-Seq experiments with respect to biological variation. *Nucleic Acids Res* **40**, 4288–4297 (2012).

75. A. T. L. Lun, Y. Chen, G. K. Smyth, It's DE-licious: A Recipe for Differential Expression Analyses of RNA-seq Experiments Using Quasi-Likelihood Methods in edgeR. *Methods Mol Biol* **1418**, 391–416 (2016).

76. Y. Chen, A. T. L. Lun, G. K. Smyth, "Differential Expression Analysis of Complex RNA-seq Experiments Using edgeR" in *Statistical Analysis of Next Generation Sequencing Data*, Frontiers in Probability and the Statistical Sciences., S. Datta, D. Nettleton, Eds. (Springer International Publishing, 2014), pp. 51–74.

77. D. J. McCarthy, G. K. Smyth, Testing significance relative to a fold-change threshold is a TREAT. *Bioinformatics* **25**, 765–771 (2009).

78. S. Durinck, *et al.*, BioMart and Bioconductor: a powerful link between biological databases and microarray data analysis. *Bioinformatics* **21**, 3439–3440 (2005).

79. S. Durinck, P. T. Spellman, E. Birney, W. Huber, Mapping Identifiers for the Integration of Genomic Datasets with the R/Bioconductor package biomaRt. *Nat Protoc* **4**, 1184–1191 (2009).

80. H. Wickham, *ggplot2: Elegant Graphics for Data Analysis* (Springer-Verlag, 2009) https:/doi.org/10.1007/978-0-387-98141-3.

81. K. Slowikowski, ggrepel: Automatically Position Non-Overlapping Text Labels with "ggplot2". R Package version 0.8.2/. *https://CRAN.R-project.org/package=ggrepel.* (February 12, 2021).

82. Z. Gu, R. Eils, M. Schlesner, Complex heatmaps reveal patterns and correlations in multidimensional genomic data. *Bioinformatics* **32**, 2847–2849 (2016).

83. T. Galili, dendextend: an R package for visualizing, adjusting and comparing trees of hierarchical clustering. *Bioinformatics* **31**, 3718–3720 (2015).

84. M. I. Love, S. Anders, V. Kim, W. Huber, RNA-Seq workflow: gene-level exploratory analysis and differential expression. *F1000Res* **4** (2015).

85. C. M. Vezina, *et al.*, Retinoic Acid Induces Prostatic Bud Formation. *Dev Dyn* **237**, 1321–1333 (2008).

86. K. J. Livak, T. D. Schmittgen, Analysis of relative gene expression data using real-time quantitative PCR and the 2(-Delta Delta C(T)) Method. *Methods* **25**, 402–408 (2001).

Figures and Tables

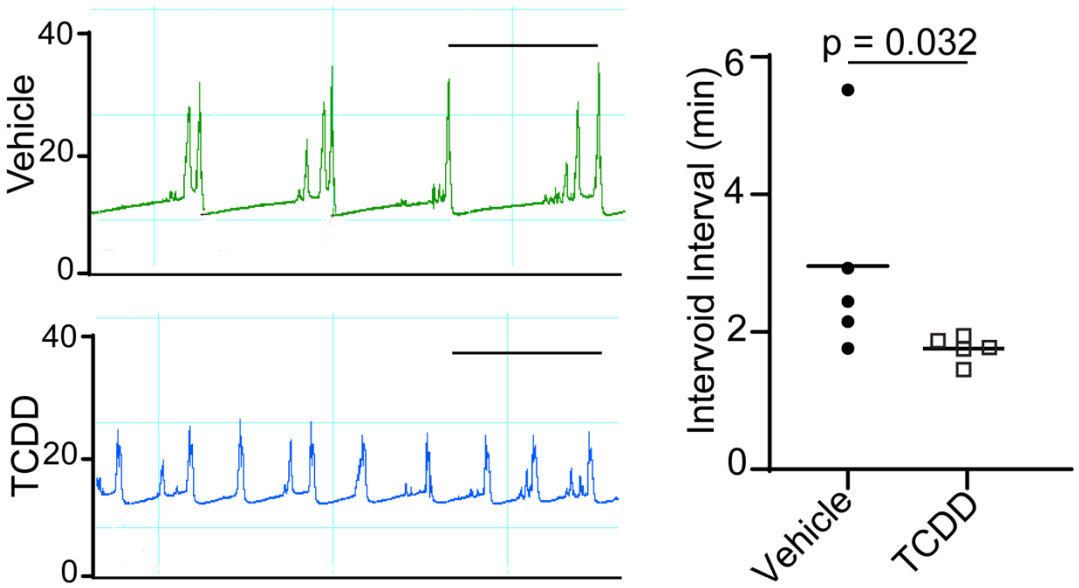

Figure 1. A single dose of TCDD, delivered to male mice during the perinatal period, changes urodynamic voiding behavior in adulthood. C57BL/6J mouse fetuses were exposed to a single dose of TCDD (1 µg/kg maternal dose, orally (po)) or vehicle (5 mL/kg corn oil, po, control) on embryonic day 13 and were evaluated by cystometry between postnatal days 90-98. Mice were anesthetized, a cystostomy catheter was passed through the bladder dome, and saline was infused at a rate of 1.5 mL/hr while continuously measuring bladder pressure in response to filling and emptying. The left panel shows representative pressure vs time traces, with each peak indicating bladder contraction during a voiding event. The Y axis indicates changes in intravesical pressure (mmHg). Three to five consecutive voids were used to quantify mean responses. *In utero* and lactational TCDD exposure decreases the intervoid interval. Results are from five mice per group, representing at least three independent litters. Scale bar is 2.5 minutes. Student's *t*-test was used to identify differences between groups after a log transformation to normalize distribution. Results are from 5 mice per group, representing at least 3 independent litters

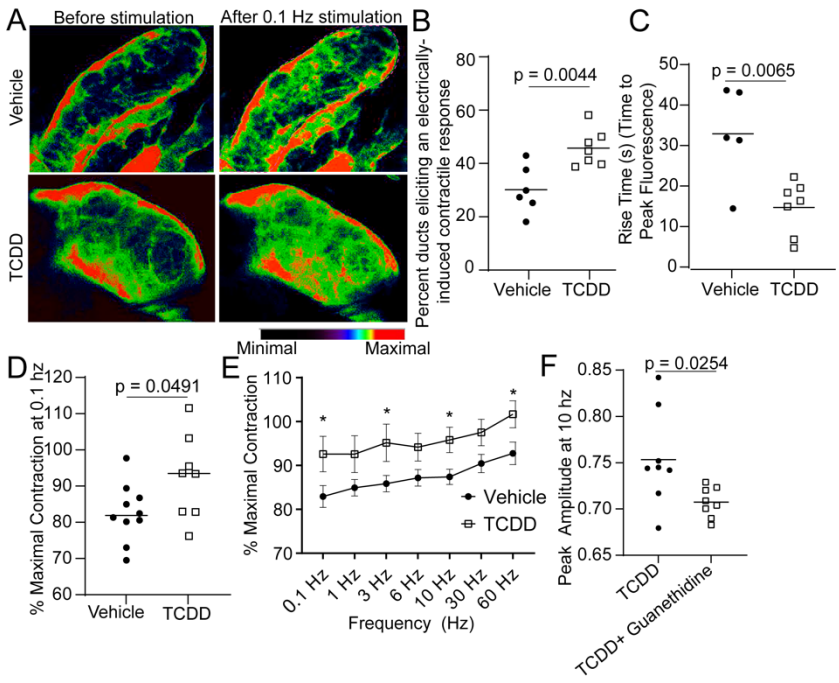

Figure 2. A single dose of TCDD, delivered to male mice during the perinatal period, increases adult prostatic smooth muscle responsiveness to field stimulation. Embryonic day 13 *GCaMP5g/+*;*Mych11*^{cre}/+ male mice were exposed to TCDD (1 µg/kg maternal dose, po) or vehicle (5 mL/kg, po, control). For A-D, prostates were collected between postnatal days 91-98 and placed in a perfusion chamber with 37 °C HEPES buffer. (A) Representative fluorescent images were captured at baseline and (contracted) 40 sec after a 0.1 Hz stimulus. *In utero* and lactational TCDD exposure of *Mych11*^{cre}/+; GCaMP5g/+ mice (B) increases the percentage of prostatic ducts that elicit a change in diameter (contraction) in response to a 0.1 Hz stimulus, (C) reduces the time needed to reach peak fluorescence, and (D) increases the maximum response to 0.1 Hz stimulation compared to vehicle-exposed dorsal prostate tissue. (E-F) In separate experiments, field stimulation was applied to tensioned adult dorsal prostate tissue incubated in 37 °C Krebs buffer. (E) *In utero* and lactational exposure increases the contractile response to 0.1 3, 6, 30 Hz stimuli compared to control with repeated *t*-tests (*$p \leq 0.05$). (F) Pretreatment with 10 µM guanethidine decreased the maximal response of TCDD-exposed tissues to field stimulation. The peak amplitude at 10 Hz is shown as an example indicating axons are

responsible for IUL TCDD-induced sensitization. Results are from 7-10 mice per group, representing at least 3 independent litters. Student's *t*-test was used to identify differences between groups.

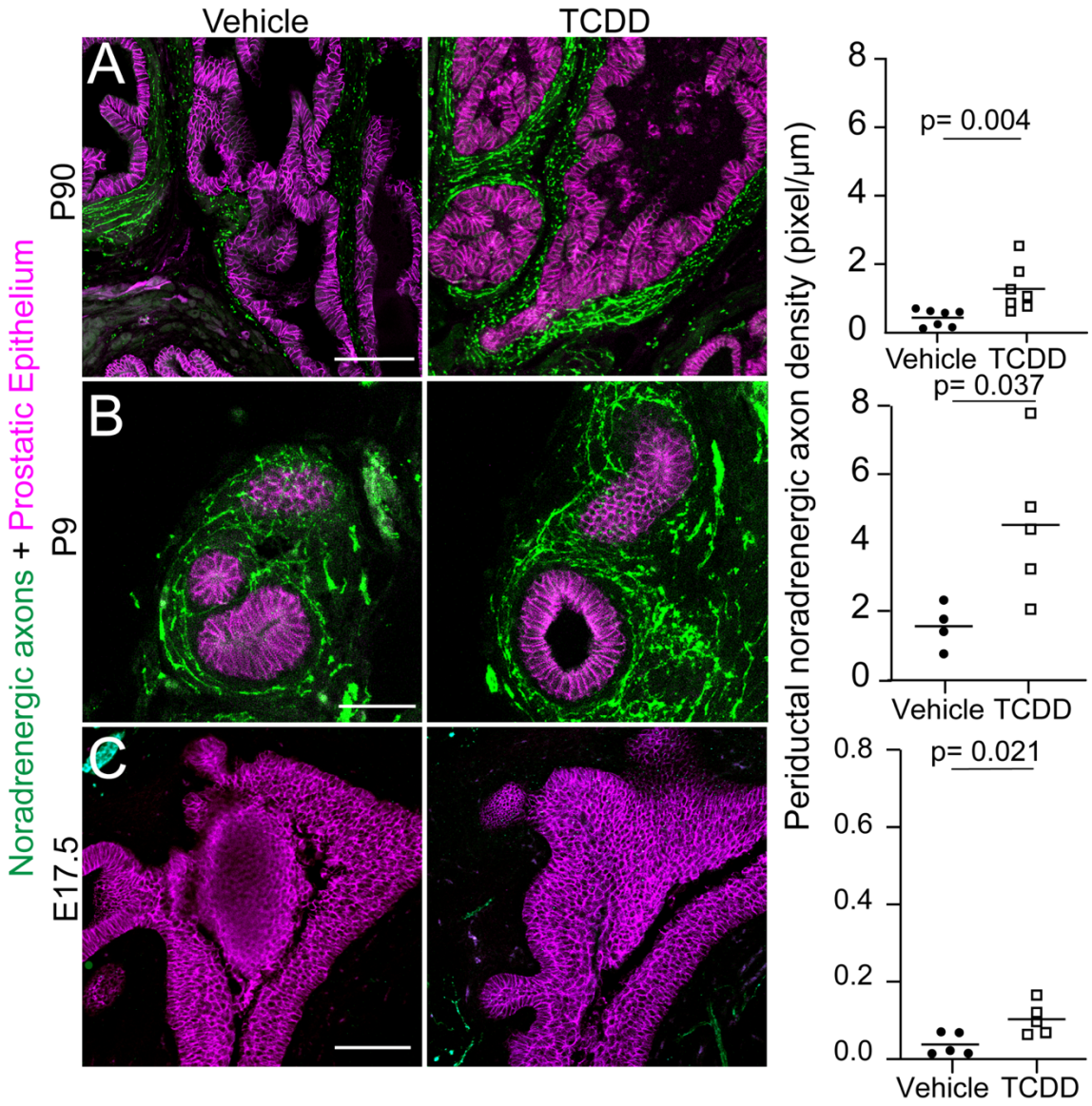

Figure 3. A single perinatal dose of TCDD increases noradrenergic axon density in the prostatic periductal region beginning in the fetal period and persisting into adulthood. Male mice were exposed to TCDD (1 µg/kg, po) or vehicle (5 mL/kg, po, control) at E13.5, and noradrenergic axon density was assessed immunohistochemically in a dorsal prostate tissue sections (3 non-serial sections per animal) at (A) postnatal day 90 (7 mice per group), (B) postnatal day 9 (4-5 mice per group), and (C) embryonic day 17.5 (5 mice per group). Results are from at least three independent litters per group. An antibody against tyrosine hydroxylase (TH+, green) was used to identify noradrenergic axons and an antibody against cadherin 1 (CDH1+,

magenta) was used to localize prostatic epithelium. TH+ axons were quantified in the area extending 10 μm from prostatic epithelium. Vehicle groups at P9 to P90 differ in density due to different tissue structures in neonatal versus adult prostate. Scale bar is 50 μm for P50 and P9 and 100 μm for E17.5. Student's *t*-test was used to identify differences between groups, and $p \leq 0.05$ was considered significant. Results are from 4-7 mice per group, representing at least 3 independent litters.

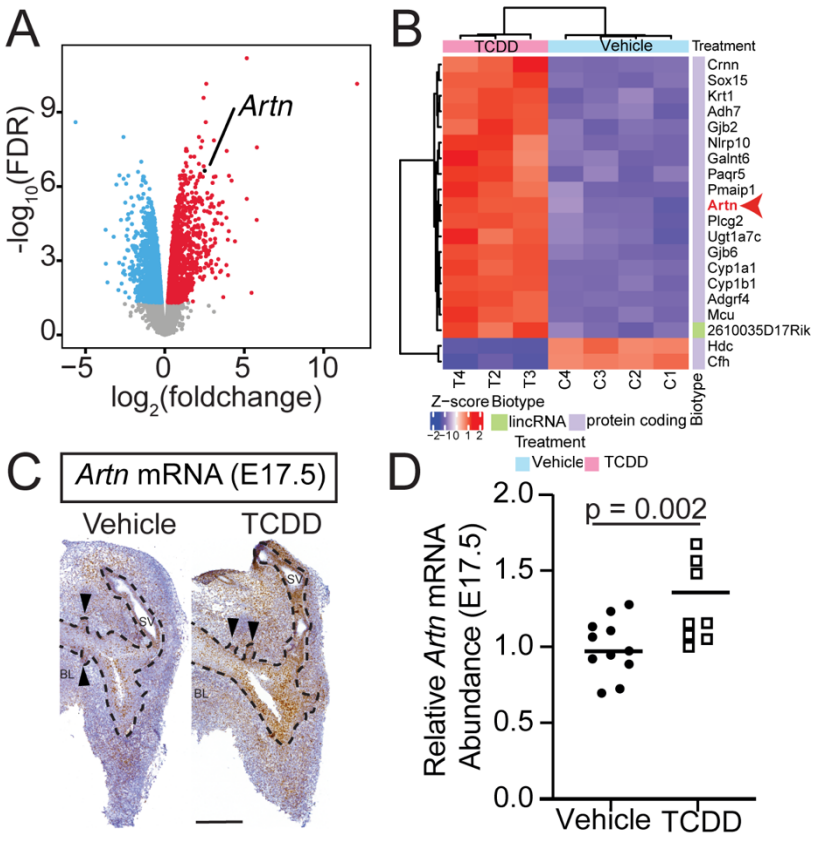

Figure 4. *In utero* TCDD exposure, coinciding with the beginning of prostatic neuroanatomical development, increases mRNA abundance of the GDNF member *Artn* in the fetal prostate. Male mice were exposed to TCDD (5 µg/kg, po maternal dose) or vehicle (5 mL/kg, po maternal dose, control) on E13.5, and urogenital sinus epithelium was collected for RNA-seq on E16.75. (A) Volcano plot showing significantly up- and downregulated genes from TCDD exposure. Red indicates upregulated genes, blue indicates downregulated genes, and *Artn* is identified in black (n = 3-4, FDR-adjusted p-value ≤ 0.05). (B) The top 20 differentially expressed genes, ordered by FDR adjusted p-value, included *Artn*. (C) *In situ* hybridization localized *Artn* mRNA (brown staining) to UGS epithelium, and periprostatic bud mesenchyme of E17.5 (control) C57BL/6J male fetuses. BL= bladder, SV= seminal vesicle, arrowhead = prostatic bud, and the dotted line indicates the boundary between urogenital sinus epithelium and mesenchyme. (D) Real-time RT-PCR indicated a single maternal dose of TCDD (1 ug/kg, po) on E13.5 significantly increased *Artn* mRNA abundance in the E17.5 male UGS compared to vehicle-

exposed mice. Scale bar is 250 μm. Student's t test was used to assess differences in RT PCR data and differential expression of genes was determined using functions from edgeR, the Cox-Reid profile-adjusted likelihood method to calculate dispersions, and empirical Bayes quasi-likelihood F-tests, and a version of the TREAT (*t*-tests relative to a threshold). Results are from 8-11 male fetuses per group, representing 3 independent litters, and $p \leq 0.05$ was considered significant.

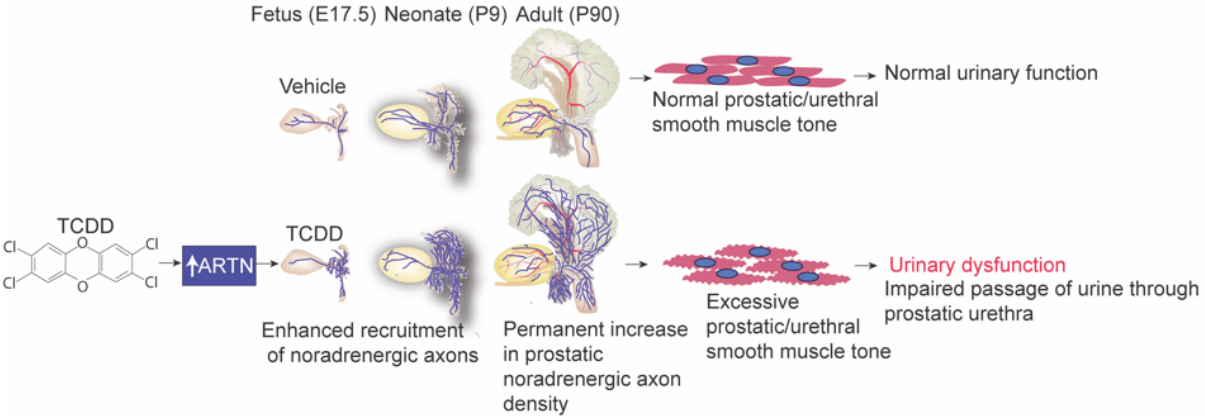

Figure 5. Proposed mechanism underlying IUL TCDD-induced urinary dysfunction in mice. *In utero* and lactational TCDD increases abundance of the neurotrophin *Artn* in the developing prostate and enhances noradrenergic axon growth. These TCDD actions increase prostatic noradrenergic density in the fetus, neonate, and adult and lead to prostatic smooth muscle hyperactivity and urinary dysfunction in adulthood.

Table S1. Antibodies

Antibody	Vendor/Catalog Number	Antibody registry number (RRID)	Host Species	Dilution	Antibody Characterization
Tyrosine hydroxylase (TH)	EMD Millipore/ AB152	AB_390204	Rabbit Polyclonal	1:300	(300)(301)(302)
Vesicular acetylcholine transporter (VAChT)	EMD Millipore/ ABN100	AB_2630394	Goat Polyclonal	1:250	(30)
Calcitonin gene-related peptide (CGRP)	Sigma Aldrich/ C8198	AB_259091	Rabbit Polyclonal	1:100	(30)
βIII tubulin (TUBB3)	Abcam/ab78078	AB_2256751	Rabbit Polyclonal	1:100	(30)
E-Cadherin (CDH1)	Cell Signaling Technology/3195S	AB_2291471	Rabbit Monoclonal	1:200	(308)(309)(310)
E-Cadherin (CDH1)	BD Transduction Labs/610181	AB_39580	Mouse Monoclonal	1:100	(311)
Alexa Fluor 488- AffiniPure Anti-mouse IgG	Jackson ImmunoResearch 715-545-150	AB_2340846	Donkey	1:250	
Rhodamine-red-X AffiniPure Anti-Rabbit IgG	Jackson ImmunoResearch 711-295-152	AB_2340613	Donkey	1:250	
Alexa Fluor 647- AffiniPure Anti-Rabbit IgG	Jackson ImmunoResearch 711-605-152	AB_2492288	Donkey	1:250	
Alexa Fluor 488- AffiniPure Anti- Goat IgG	Jackson ImmunoResearch 705-545-003	AB_2340428	Donkey	1:250	

Table S2. FASTA sequences used in Mouse_Adapters.fa for Skewer adapter trimming

>Illumina Multiplexing Adapter 1
GATCGGAAGAGCACACGTCT
>Illumina_TruSeq_Adapter_Index_1
GATCGGAAGAGCACACGTCTGAACTCCAGTCACATCACG
>Illumina_TruSeq_Adapter_Index_2
GATCGGAAGAGCACACGTCTGAACTCCAGTCACCGATGT
>Illumina_TruSeq_Adapter_Index_3
GATCGGAAGAGCACACGTCTGAACTCCAGTCACTTAGGC
>Illumina_TruSeq_Adapter_Index_3a
ATCGGAAGAGCACACGTCTGAACTCCAGTCACTTAGGC
>Illumina_TruSeq_Adapter_Index_4
GATCGGAAGAGCACACGTCTGAACTCCAGTCACTGACCA
>Illumina_TruSeq_Adapter_Index_5
GATCGGAAGAGCACACGTCTGAACTCCAGTCACACAGTG
>Illumina_TruSeq_Adapter_Index_6
GATCGGAAGAGCACACGTCTGAACTCCAGTCACGCCAAT
>Illumina_TruSeq_Adapter_Index_7
GATCGGAAGAGCACACGTCTGAACTCCAGTCACCAGATC
>Illumina_TruSeq_Adapter_Index_8
GATCGGAAGAGCACACGTCTGAACTCCAGTCACACTTGA
>Illumina_read2_adapter_segment
AGATCGGAAGAGCGTCGTGTAGGGAAAGAGTGTAGATCTCGGTGGTCGCCG
>Illumina_read2_adapter_segment01
GATCGGAAGAGCGTCGTGTAGGGAAAGAGTGTAGATCTCGGTGGTCGCCG
>Illumina Multiplexing Index Read Sequencing Primer
GATCGGAAGAGCACACGTCTGAACTCCAGTCAC
>Illumina_read_adapter_segment_1
AGATCGGAAGAGCACACGTCTGAACTCCAGTCAC
>Illumina_read_adapter_segment_2
AGATCGGAAGAGCGTCGTGTAGGGAAAGAGTGTA

Table S3. RT-PCR primers

Target	NM Number	Left Primer	Right Primer
Artn	NM_011037.4	CTGGACCCAATGTCCCGCAG	AGTGTGTCCCCCTACCAGGC
Ppia	NM_008907.2	TCTCTCCGTAGATGGACCTG	ATCACGGCCGATGACGAGCC

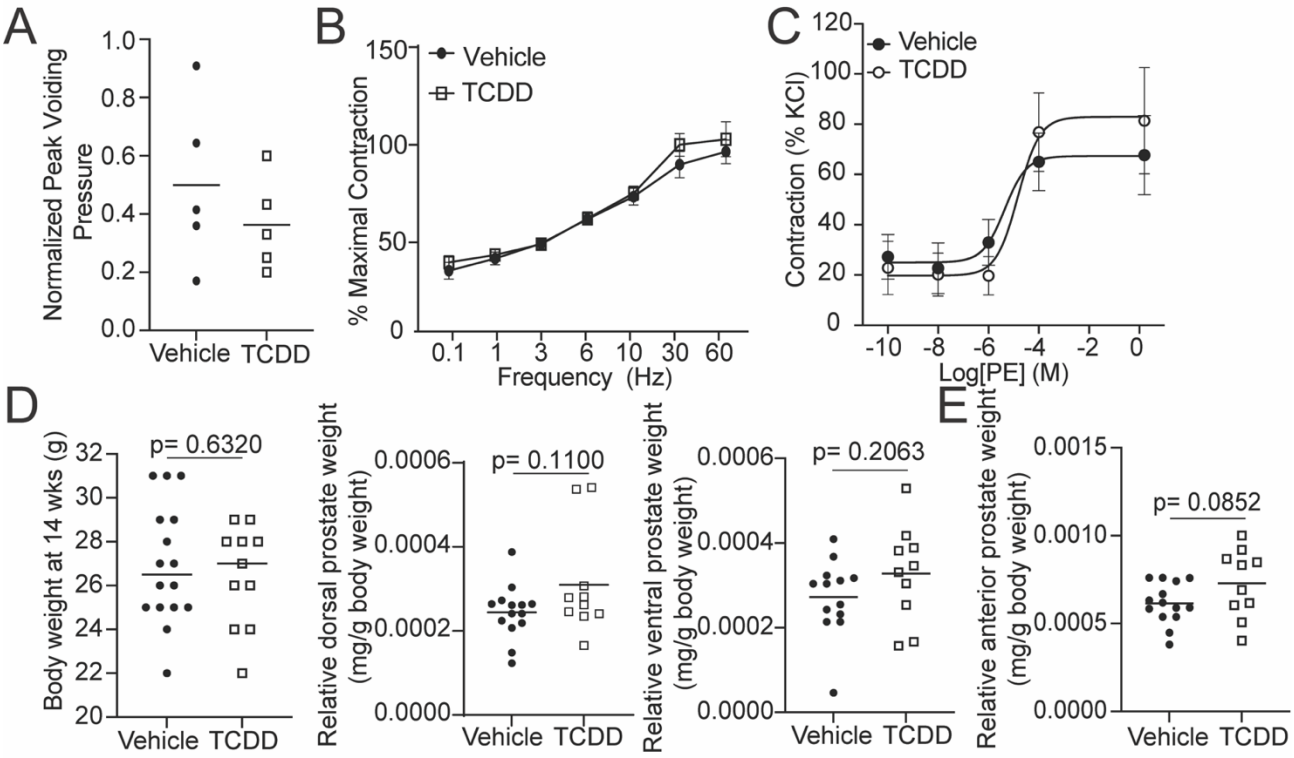

Figure S1. *In utero* and lactational TCDD exposure does not change body weight, prostate weight, response to alpha adrenergic agonist, or frequency dose response in bladder. (A) *In utero* and lactational TCDD exposure does not change the peak voiding pressure during anesthetized cystometry. (B) *In utero* and lactational TCDD exposure in the bladder does not significantly change the response to electrical field stimulation at any frequency (0.1-60 Hz) compared to vehicle. (C) *In utero* and lactational TCDD does not significantly shift the dose response to α-adrenergic agonist (phenylephrine), and the EC_{50} is the same for both groups (p = 0.8031, EC_{50} = 1.932). The baseline was set to 0.7g so tissues are considered baseline at 70%, shown by the dotted line. (D) *In utero* and lactational TCDD exposure does not change body weight (grams) at 14 weeks. (E) *In utero* and lactational TCDD exposure does not change the dorsal, ventral, or anterior prostate weight normalized to body weight. Students t-test was used to assess differences between groups in panel A, D, and E. Panel B an two-way ANOVA was used to analyze differences between groups at various frequencies. Non-linear regression analysis was used to analyze the phenylephrine dose response in panel C.

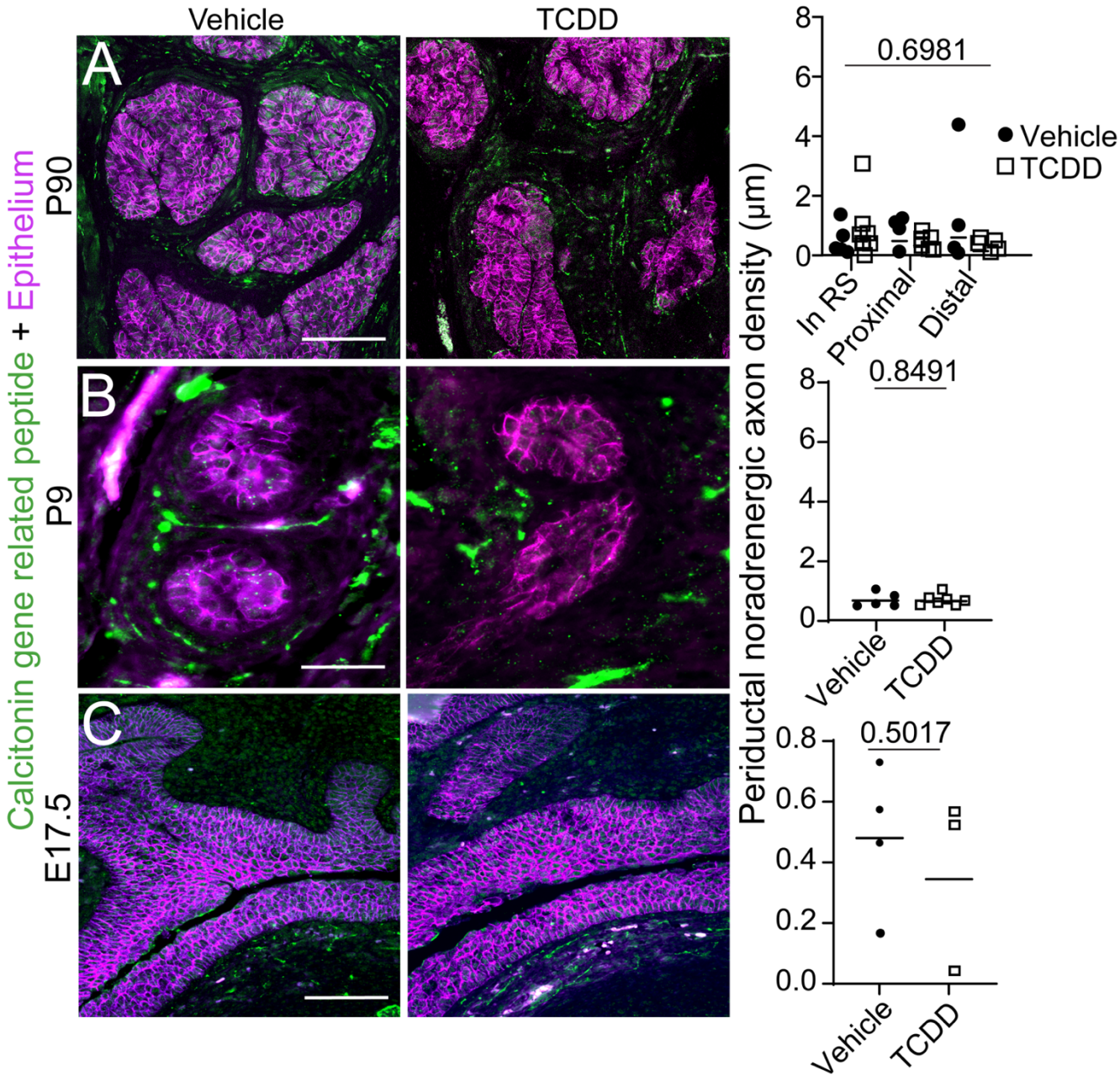

Figure S2. *In utero* and lactational TCDD does not change the density of CGRP densities in dorsal prostate. IUL TCDD does not change the axon densities of calcitonin gene-related peptide (CGRP+) axon in dorsal prostate. Pregnant C57BL/6J mice were dosed with TCDD (1 µg/kg, po) or vehicle (5 mL/kg, po), and prostates were collected on E17.5, P9, and P90 (Panel A-C). P90 axon density was quantified in three distinct regions: inside the rhabdosphincter (In RS), proximal to the rhabdosphincter, and distal to the rhabdosphincter because sensory axon

density changes along the proximo-distal ductal axis. Prostate tissue sections were stained via immunohistochemistry to identify axons (green) and epithelium (magenta). The density of CGRP+ axons was quantified within a 10 μm band around the prostate ducts. CGRP+ density was not significantly changed in P90 mice exposed *in utero* and via lactation to TCDD compared to vehicle. Results are from 4-7 mice per group belonging to at least three independent litters per group, and differences of $p \leq 0.05$ were considered significant. Students t-test was used to assess differences between groups. Scale bars represent 50 μm for P90 and P9 and 100 μm for E17.5.

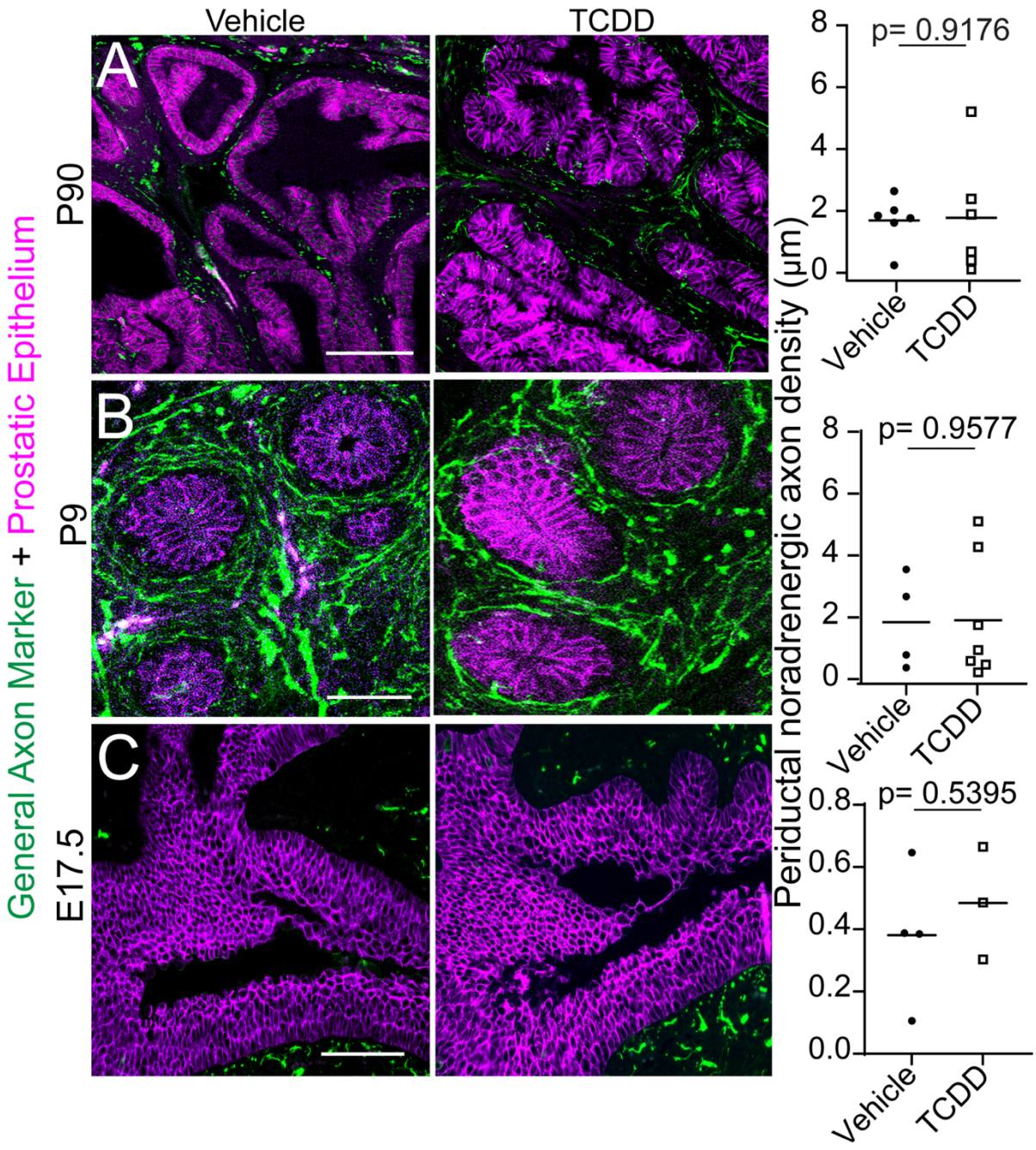

Figure S3. *In utero* and lactational TCDD does not change TUBB3+ axon densities in dorsal prostate. IUL TCDD does not change the axon densities of TUBB3+ axon subtypes in dorsal prostate. Pregnant C57BL/6J mice were dosed with TCDD (1 µg/kg, po) or vehicle (5 mL/kg, po), and prostates were collected on postnatal day E17.5, P9, and P90. Prostate tissue sections were stained via immunohistochemistry to identify TUBB3+ axons (green) and epithelium (magenta). The density of TUBB3+ axons was quantified within a 10 µm band around the prostate ducts. The

density of TUBB3+ axons did not differ between vehicle and IUL TCDD dosed groups. Results are from 4-5 mice per group belonging to at least three independent litters per group, and differences of $p \leq 0.05$ were considered significant. Student's t-test was used to assess differences between groups. Scale bars represent 50 μm for P90 and P9 and 100 μm for E17.5.

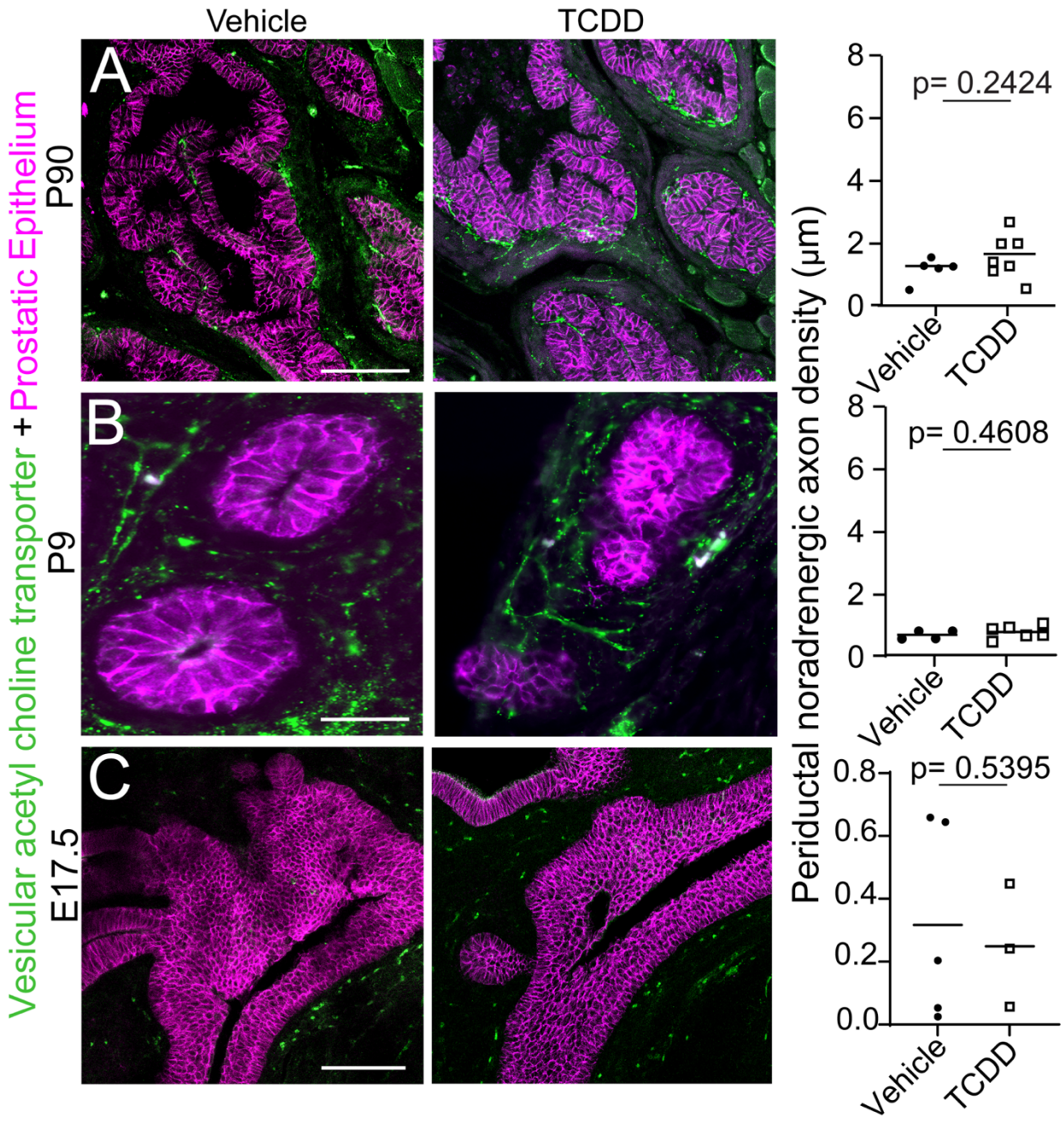

Figure S4. *In utero* and lactational TCDD does not change the density of VAChT+ densities in dorsal prostate. *In utero* and lactational TCDD does not change the axon densities of vesicular acetylcholine transporter (VAChT+) axon subtypes in dorsal prostate. Pregnant C57BL/6J mice were dosed with TCDD (1 µg/kg, po) or vehicle (5 mL/kg, po), and prostates were collected on E17.5, P9, and P90. Prostate tissue sections were stained via immunohistochemistry to identify axons (green) and epithelium (magenta). VAChT was not significantly changed in E17.5, P9, and

P90 mice exposed *in utero* and via lactation to TCDD compared to vehicle. Results are from 4-5 mice per group belonging to at least three independent litters per group, and differences of $p \leq 0.05$ were considered significant. Students t-test was used to assess differences between groups. Scale bars represent 50 μm for P90 and P9 and 100 μm for E17.5.

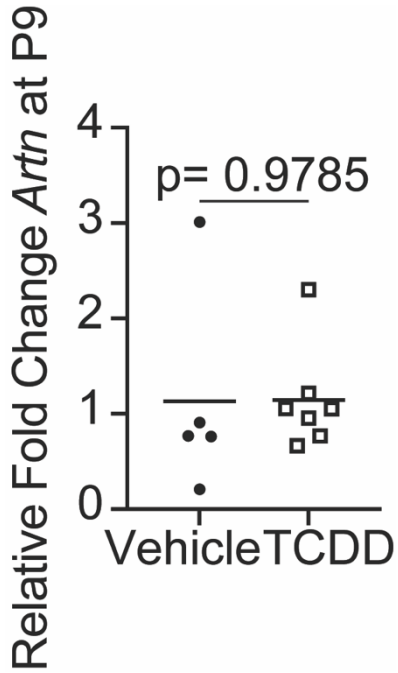

Figure S5. Postnatal day 9 mouse prostatic *Arnt* mRNA abundance no longer differs between mice that were exposed to TCDD (1 µg/kg, po) or vehicle (5 mL/kg, po) on E13.5. RT-PCR was performed on isolated P9 urogenital sinuses and normalized to *Ppia* abundance as an internal control. Results are from 6-7 mice deriving from at least three independent litters, and differences of $p \leq 0.05$ were considered significant. Students t-test was used to assess differences between groups.

Chapter 4: In utero and lactational 2,3,7,8-tetrachlorodibenzo-p-dioxin (TCDD) exposure exacerbates urinary dysfunction in hormone-treated C57BL/6J mice through a non-malignant mechanism involving proteomic changes in the prostate that differ from those elicited by testosterone and estradiol

Turco AE, Thomas S, Crawford LK, Tang W, Peterson RE, Li L, Ricke WA, Vezina CM. (2020) *American Journal of Clinical and Experimental Urology*. PMID: 32211455

Abstract

A recent study directed new focus on the fetal and neonatal environment as a risk factor for urinary dysfunction in aging males. Male mice were exposed *in utero* and via lactation (IUL) to the persistent environmental contaminant 2,3,7,8-tetrachlorodibenzo-*p*-dioxin (TCDD) and then administered slow-release, subcutaneous implants of testosterone and estradiol (T+E2) as adults to mimic the hormonal environment of aging men. IUL TCDD exposure worsened T+E2-induced voiding dysfunction. Mice in the previous study were genetically prone to prostatic neoplasia and it was therefore unclear whether TCDD exacerbates voiding dysfunction through a malignant or non-malignant mechanism. We demonstrate here that IUL TCDD exposure acts via a non-malignant mechanism to exacerbate T+E2-mediated male mouse voiding dysfunction characterized by a progressive increase in spontaneous void spotting. We deployed a proteomic approach to narrow the possible mechanisms. We specifically tested whether IUL TCDD exacerbates urinary dysfunction by acting through the same prostatic signaling pathways as T+E2. The prostatic protein signature of TCDD/T+E2-exposed mice differed from that of mice exposed to T+E2 alone, indicating that the mechanism of action of TCDD differs from that of T+E2. We identified 3641 prostatic proteins in total and determined that IUL TCDD exposure significantly changed the abundance of 102 proteins linked to diverse molecular and physiological processes. We shed new light on the mechanism of IUL TCDD-mediated voiding dysfunction by demonstrating that the mechanism is independent of tumorigenesis and involves molecular pathways distinct from those affected by T+E2.

Introduction

Urinary voiding dysfunction can lead to a constellation of lower urinary tract dysfunction (LUTD) such as increased urgency and frequency (especially at night) and pain (1). LUTD occur at a high rate in aging men (2), are expensive (3), and diminish quality of life (4). The pathogenesis of voiding dysfunction in aging men is now considered complex and can include nodular benign prostatic hyperplasia (BPH), prostatic and/or bladder fibrosis, enhanced prostatic smooth muscle contractility and neural dysfunction, among other mechanisms (5, 6). Many of these pathologies cause voiding dysfunction and symptoms by obstructing urine passage through the prostatic urethra.

We developed a mouse model of spontaneous urinary voiding dysfunction characterized by an obstructive voiding pattern to identify new mechanisms and disease confounders. Adult male mice are treated with slow-release, subcutaneous implants of testosterone and estradiol (T+E2) to mimic hormonal changes occurring in aging men (7). T+E2 treatment drives mouse prostatic proliferation and enlargement, prostatic smooth muscle thickening, and urinary dysfunction characterized by more frequent small volume urine deposits, retention of urine in the bladder, increased bladder wet weight (hypertrophy), and progression towards hydronephrosis and renal impairment (8–10). T+E2-induced mouse pathologies parallel those observed in men with prostate related voiding dysfunction (11).

We used T+E2-treated mice to screen for risk modifiers of male urinary voiding dysfunction (10, 12). A paradigm-shifting outcome was the recognition that adult male voiding function is not only shaped by the adult environment, but also by the fetal and neonatal environments. For example, *in utero* and lactational exposure to the persistent environmental contaminant 2,3,7,8-tetrochlorodibenzo-*p*-dioxin (TCDD) worsened T+E2-induced urinary dysfunction in male Tg(CMV-*cre*);*Nkx3-1*(+/-);*Pten*(fl/+) mice that are genetically prone to prostatic neoplasia (12). Therefore, it was unclear whether TCDD exacerbates voiding dysfunction through a malignant or non-malignant mechanism. Resolving the mechanism is important because there is precedence

that TCDD can accelerate and increase aggressiveness of prostate cancer in susceptible mice (13, 14) and because prostate cancer in mice and men can cause urinary voiding dysfunction (15).

The present study involved wild type mice (C57BL/6J) that are not genetically prone to prostate cancer and that were divided into four experimental groups: 1) unexposed control mice (control), 2) mice exposed *in utero* and via lactation to TCDD only and not to T+E2 (TCDD alone), 3) mice exposed to T+E2 beginning at six weeks of age but not TCDD (T+E2 alone), and 4) mice exposed to TCDD and T+E2 (TCDD/T+E2). We used the void spot assay to test the hypothesis that voiding dysfunction is worse in TCDD/T+E2 than T+E2 alone mice. While deposited urine spots did not differ between TCDD alone and control mice, TCDD/T+E2 mice deposited more urine spots than T+E2 alone mice. This outcome is important because it suggests that early life TCDD exposure exacerbates T+E2-mediated voiding dysfunction through a mechanism independent of tumorigenesis.

Early-life TCDD exposure could exacerbate urinary voiding dysfunction by further changing T+E2-affected genes and signaling pathways or by acting through distinct, but physiologically complementary pathways. We leveraged results from a previous study in which we identified a T+E2 prostatic protein signature (33 proteins significantly altered in abundance by T+E2 alone compared to control). We tested whether TCDD/T+E2 exposure changes the abundance of these 33 proteins beyond the changes elicited by T+E2 alone (16). TCDD/T+E2 surprisingly had little additional impact, significantly changing the abundance of just one of the 33 proteins. Instead, TCDD/T+E2 changed the abundance of a distinct group of proteins *vs* T+E2 alone, including proteins linked to smooth muscle and neural function and development, fibrosis, and inflammation. We shed new light on the mechanism of IUL TCDD-mediated voiding dysfunction by demonstrating that TCDD/T+E2 acts independent of a tumorigenic mechanism and through molecular pathways distinct from those affected by T+E2 alone.

Results

In utero *and lactational TCDD exposure acts by a non-malignant mechanism to exacerbate voiding dysfunction in T+E2-treated mice*

We previously demonstrated that TCDD worsens T+E2-induced voiding dysfunction in mice (12), but that study was conducted with a mouse strain genetically prone to prostate cancer. It was therefore unclear whether TCDD acts through a malignant or non-malignant mechanism to impair urinary voiding. IUL TCDD exposure has the capacity to accelerate prostate cancer in genetically prone mice (14), but IUL TCDD exposure is not sufficient to drive neoplasia in non-susceptible C57BL/6J control mice (13). Pregnant dams were exposed to TCDD (1 μg/kg oral maternal dose at E13.5) or corn oil vehicle (5 mL/kg) and male offspring were then given T+E2 implants or sham surgeries at six weeks of age. We evaluated prostate histology two weeks after implantation surgery to test for the presence of neoplasia. Coalescing regions of epithelial hyperplasia and metaplasia were noted with infrequent areas of nuclear atypia. However, there was no evidence of high grade or invasive prostate neoplasia noted in the examined sections (**Figure 2**). TCDD/T+E2-treated mice therefore appear to be free of prostate malignancy when histological and physiological assessments were conducted in this study.

Frequent urination and dribbling are hallmarks of urinary dysfunction in aging men (32) and arise in T+E2-treated male mice (8). We therefore evaluated spontaneous voiding behavior to test whether TCDD/T+E2 exacerbates voiding dysfunction. Evaluations included control mice (not exposed to either TCDD or T+E2), mice exposed to TCDD alone, T+E2 alone and TCDD/T+E2. Voiding behavior was evaluated two weeks after implantation surgery. There are no significant differences in urine spot count between TCDD alone and unexposed control mice (**Figure 3**). T+E2 alone significantly increased urine spot counts two weeks post-implantation surgery and there was no further increase by TCDD/T+E2 at this time (**Figure 3**). Voiding behaviors were evaluated again at eight weeks post-implantation surgery because obstructive voiding dysfunction is often progressive in mice and men. There were more urine spots at eight

weeks post T+E2 in both groups compared to than two weeks, indicating urinary dysfunction had progressed. TCDD/T+E2 treatment resulted in a greater number of urine spots compared to mice treated with T+E2 alone at eight weeks post-implantation surgery (**Figure 3**). We conclude that voiding function in the T+E2 alone group progressively worsens between two and eight weeks post-implantation surgery and that TCDD/T+E2 exacerbates this response through a non-malignant mechanism.

TCDD/T+E2 mice have thicker prostatic periductal smooth muscle than T+E2 alone mice

Prostatic smooth muscle dysfunction is one potential cause of urinary voiding dysfunction (6). We previously demonstrated in a prostate cancer-prone mouse strain that prostatic smooth muscle was thicker in TCDD/T+E2 than T+E2 alone mice (12). Others have reported increased peri-prostatic stroma thickness in rhesus macaques exposed *in utero* and via lactation to TCDD (33). We conducted alpha smooth muscle actin immunostaining on prostate sections of wild type C57BL/6J mice (not genetically susceptible to prostate cancer) and found that prostatic periductal smooth muscle is thicker in TCDD/T+E2 mice (average of 15 microns) than T+E2 alone mice (average of seven microns) (**Figure 4**). We conclude that TCDD/T+E2 drives prostatic smooth muscle hypertrophy in mice that are not genetically prone to prostate cancer.

In utero *and lactational TCDD exposure changes the abundance of a different set of proteins compared to those changed by T+E2 alone*

We used a proteomic approach to refine the possible mechanisms by which TCDD/T+E2 exposure exacerbates voiding dysfunction. One possibility is that TCDD/T+E2 exposure acts by the same mechanism as T+E2 alone to impair voiding function. In such a scenario, we would expect that TCDD/T+E2 would act upon the same proteins and further increase the magnitude of abundance changes elicited by T+E2 alone. We previously identified a T+E2 prostatic protein signature (33 C57Bl/6J prostatic proteins significantly altered in abundance by T+E2 exposure,

(**Table S-1**; (16)). We tested whether TCDD/T+E2 significantly changed the abundance of these 33 proteins compared to T+E2 alone. All proteins from the signature except Glutathione *S*-transferase A2 (GSTA2) were successfully identified and quantified (**Table S-2**). TCDD/T+E2 significantly altered the abundance of only one of the 33 signature proteins (Retinal dehydrogenase 2, ALDH1A2) compared to T+E2 alone, suggesting TCDD/T+E2 exacerbates voiding function through a different mode of action than T+E2 alone (**Table S-2**).

In our global proteomics analysis, we identified 3641 mouse prostatic proteins by nanoLC-MS^2 **(Table S-3).** Here we determined that TCDD/T+E2 significantly altered the abundance of 102 proteins compared to T+E2 alone (volcano plot: Student's *t*-test α = 0.05, ≥50% fold-change) (**Figure 5**). Biological processes significantly enriched among these 102 proteins included neural dysfunction, regulation of muscle and apoptosis, and metabolism of antioxidants (**Figure 6**). Specifically, among the proteins most increased by TCDD/T+E2 compared to T+E2 alone are four with roles in muscle function: Ryanodine receptor 1 (RYR1), Obscurin (OBSCN), Tripartate motif-containing protein 72 (TRIM72), and Myc box-dependent-interacting protein 1 (BIN1). Others that increased have roles in neural function: Myelin basic protein (MBP), Catenin alpha-2 (CTNNA2), and Major prion protein (PRNP); fibrosis: Collagen alpha-1(I) chain (COL1A1); metabolism: Glutathione *S*-transferase omega-1 (GSTO1), Glutathione *S*-transferase A3 (GSTA3); and drug metabolism: Cytochrome P450 2F2 (CYP2F2) (**Table 1**). Proteins that decreased in TCDD/T+E2 compared to T+E2 alone also have potential roles in urinary dysfunction, including the collagen crosslinker Procollagen-lysine, 2-oxoglutarate 5-dioxygenase 2 (PLOD2), the extracellular matrix component Laminin subunit beta-3 (LAMB3), the DNA repair protein BRISC and BRCA1-A complex member 2 (BABAM2*)*, the nerve regulator Huntingtin-interacting protein 1 (HIP1), and the inflammation-related proteins Neutral cholesterol ester hydrolase 1 (NCEH1) and Ig gamma-2A chain C region secreted form (N/A) (**Table 2**). For a complete diagram of significantly enriched protein families see **Figure S1**.

Immunohistochemistry was conducted to visualize the distribution of ryanodine receptor 1 protein, which was the protein that was most increased in abundance (among all proteins significantly increased) by TCDD/T+E2 compared to T+E2 alone. Ryanodine receptor 1 was distributed in the mouse prostatic stroma, where it encircled ducts and stained the area between ducts. Ryanodine receptor 1 immunostained pixel density was more abundant in TCDD/T+E2 dorsal prostate stroma compared to T+E2 alone, thereby validating an outcome of proteomics with an independent method (**Figure 7**).

Discussion

We found evidence that IUL TCDD exposure exacerbates urinary voiding dysfunction in T+E2-treated wild type C57Bl6/J male mice. We show that T+E2 increases spontaneous urine spotting as early as two weeks and that the number of spots increase through at least eight weeks post-implantation surgery. Though TCDD/T+E2 and T+E2 alone groups did not significantly differ in urine spotting at two weeks, TCDD/T+E2 drove significantly more urine spotting at eight weeks compared to T+E2 alone (**Figure 3**). The pattern of urinary dysfunction (increased urine spots) is consistent with a progressive increase in voiding frequency, a bothersome symptom in men. The mechanism by which TCDD deteriorates voiding function in T+E2-treated mice has not been resolved. Prostate cancer in men and mice has been linked to urinary dysfunction phenotypes (15). As a result, our previous findings that TCDD/T+E2 exacerbated urinary dysfunction compared to T+E2 alone could not discriminate between a TCDD-driven progression of prostate malignancy and a separate action on benign urinary function. Here, we refine the potential mechanisms by demonstrating TCDD acts independent of tumorigenesis (**Figure 2**).

We show that TCDD/T+E2 thickens dorsal prostate smooth muscle compared to T+E2 alone, validating our previous finding in mice predisposed to neoplasia (**Figure 4**) (12). This TCDD action on prostate anatomy has been observed in other tissues, specifically that TCDD hypertrophies penile smooth muscle (34). Thickened prostate smooth muscle may indicate the muscle is contracting more frequently or with a greater intensity. Prostate smooth muscle

thickening could be relevant because many men with urinary dysfunction are treated with alpha-1 adrenergic antagonists, which relax prostate smooth. It is unknown why some men may experience hyperactive prostatic smooth muscle. In addition, proteomic analysis revealed dysregulated muscle and calcium flux proteins, indicating smooth muscle may be an important target to investigate as a mechanism for TCDD-mediated exacerbation of T+E2-induced urinary voiding dysfunction **(Figure 6).** Additional studies into the impact of TCDD/T+E2 on prostate smooth muscle contractility would be beneficial in determining whether environmental chemical exposure can contribute to hypercontracted prostate smooth muscle.

To identify whether TCDD/T+E2 has a mode of action that differs from T+E2 alone, the trajectory of prostatic protein abundance changes was captured by sampling at two weeks post-implantation surgery, while urinary dysfunction was developing. Our prior analysis of prostatic proteomic changes in mice treated with T+E2 alone led us to hypothesize that TCDD/T+E2 exacerbated urinary dysfunction by further changing the abundance of proteins affected by T+E2. However, just one of 33 proteins known to be altered by T+E2 was further altered by TCDD/T+E2, suggesting the mode of action of TCDD/T+E2 differs from that of T+E2 treatment alone. T+E2 modulated proteins related to the acute phase response and oxidative stress defense whereas TCDD/T+E2 significantly modulated other proteins representing processes that are important in urinary dysfunction, including muscle and calcium flux, neurologic function, fibrosis, response to oxidative stress, and inflammation (**Figure 5, Figure 6**). TCDD/T+E2 dysregulated prostatic proteins linked to neurologic function (**Table 1**). TCDD and other AHR agonists can be toxic to the peripheral nervous system (35). TCDD disrupts neural control of golden hamster thermoregulation (36) and increases activity of axons controlling rat aortic smooth muscle tone (37). Dysregulation of axon function within the prostate is a potential mechanism of TCDD-mediated exacerbation of urinary voiding dysfunction, as men with urinary dysfunction often have increased autonomic activity (38).

We discovered that TCDD/T+E2 increases fibrillar collagen (COL1A1) protein abundance and decreases collagen crosslinker (PLOD2) abundance in C57BL/6J mouse prostate. Collagen deposition and prostate rigidity have been linked to lower urinary tract symptom severity and treatment resistance (39, 40). TCDD/T+E2 exposure has been shown to disrupt collagen distribution (12). Additionally, a maternal TCDD dose given to rhesus macaques during pregnancy caused increased prostatic fibrosis in male offspring (33). Disrupted collagen distribution could stiffen the prostate, impairing passage of urine through the prostatic urethra. Further studies linking environmental chemical exposure to prostatic fibrosis would be beneficial for deciphering whether TCDD/T+E2 is acting via this mechanism.

We show that antioxidant proteins and inflammation-related proteins were dysregulated in the TCDD/T+E2 group compared to T+E2 alone. TCDD is a known immunomodulator (41) and promotes inflammation in the mouse testes (42), and modulates superoxide in mice (37). It has been shown that men with prostate inflammation have significantly exacerbated urinary dysfunction (43). Further research investigating prostate inflammation after TCDD/T+E2 exposure would determine whether inflammation is involved in the mechanism by which TCCD exacerbates of urinary dysfunction.

Materials and Methods

Mouse Treatment

All mouse protocols and procedures were approved by the University of Wisconsin Animal Care and Use Committee and performed following the National Institutes of Health Guide for the Care and Use of Laboratory Animals. All mice were C57Bl6/J and purchased from Jackson Laboratories (stock number 0.000664, Bar Harbor, ME). Mice were housed in Innovive® HDPE plastic microisolator cages in a room maintained on a 12-h light and dark cycle with ambient temperature of 20.5 ± 1 °C and relative humidity of 30-70%. Mice were fed a 5015 Diet (PMI Nutrition International, Brentwood, MO) from conception through weaning (P21) and a 8604

Teklad Rodent Diet after weaning (Harlan Laboratories, Madison, WI). Feed and water were available *ad libitum* and cages contained corncob bedding. All mice were euthanized by isoflurane overdose and cervical dislocation. Male mice were generated by time-mating males and females overnight. The morning of definitive copulatory plug identification was considered E0.5. Females with a body weight increase of 4 g (indicating pregnancy) were given either a single dose of TCDD (1 μg/kg, *per os*) or corn oil (vehicle) (5 mL/kg) at E13.5. TCDD (98% purity) was purchased from Cambridge Isotope Laboratories (Andover, MA). The TCDD dose matches that of a previous reference study [12]. Based on the established whole body elimination half-life of TCDD in C57Bl/6J mice, the TCDD dosing paradigm used in this study results in continuous TCDD exposure from the fetal period through weaning (17). Male offspring were aged to six weeks, anesthetized and an implantation surgery was performed either as a sham surgery or to subcutaneously deliver a slow-release 25 mg testosterone implant (Steraloids, Newport Rhode Island) and a 2.5 mg 17β-estradiol + 22.5 mg cholesterol implant (Sigma Aldrich, St. Louis, MO) as previously described (8). Experimental mice underwent contrast-enhanced ultrasound (following NIH reduce and reuse policy) before euthanasia. As a result, each mouse had Tamsulosin (10 μg/kg) in their system for 15 minutes prior to euthanasia. Graphical abstract illustrates the sequential methods.

Void Spot Assay (VSA)

Void spot assays (VSA) were conducted as described (18) two weeks post implantation surgery on 23 control, 17 TCDD alone, 19 T+E2 alone, and 16 TCDD/T+E2 mice. VSAs were also conducted eight weeks post implantation surgery on 11 control, six TCDD alone, 14 T+E2 alone, and seven TCDD/T+E2 mice. Briefly, male experimental mice were housed for four h in clean cages lined with three mm Whatman filter paper (Fisher Scientific No. 057163W). Assays were conducted in a lighted room in the same quiet location and time of day. Food was provided during the assay but not water. Filter papers were imaged using ultraviolet light on a transilluminator and analyzed using Void Whizzard Software (18).

Mass Spectrometry

Prostates (half of the anterior, ventral, and dorsolateral prostate lobes) were collected two weeks after implantation surgery from seven male TCDD/T+E2 mice and six T+E2 alone mice, frozen on dry ice, and stored at -80 °C until further processing (**Figure 1).** Each mouse was analyzed as a single biological unit. Prostates were digested and further processed into peptides using a modified surfactant-aided technique as previously described (19). Briefly, frozen prostates were thawed and homogenized in a solution containing sodium dodecyl sulfate, deoxycholic acid, and a reducing agent in an ammonium bicarbonate buffer (Sigma, St. Louis, MO). Aliquots of homogenate were added to pre-passivated 30 kDa centrifugal filter units (Millipore, Burlington, MA) for urea buffer exchange and alkylation, followed by 18 h digestion with sequencing-grade trypsin (Promega, Madison, WI), and final collection of peptides. Peptides were desalted via C18 OMIX pipette tips (Agilent, Santa Clara, CA) before BCA assay (Thermo, Waltham, MA). Lyophilized peptides were stored at -80 °C until analysis.

Mass spectrometry-based, label-free proteomics with relative quantification was used to assess prostatic protein abundance differences between TCDD/T+E2 and T+E2 mice. Prostatic peptides were analyzed on a Thermo Dionex nanoLC system coupled to a Thermo Q Exactive HF mass spectrometer. A C18 column was fabricated in-house with an integrated electrospray ionization emitter (75.1 µm × 150 mm, BEH 1.7 µm, 130 Å). Samples were kept at 4 °C in the autosampler. Mobile phase A was 0.1% formic acid in H_2O and mobile phase B was 0.1% formic acid in acetonitrile (Fisher, Hampton, NH). The flow rate was 0.3 µL/min. The nanoLC gradient was as follows: 0-16 min 3% B, 16-106 min 3-30% B (linear), 106-106.5 min 30-75% B (linear), 106.5-116 min 75% B, 116-116.5 min 75-95% B (linear), 116.5-126 min 95% B, 126-126.5 min 95-3% B (linear), 126.5-141 min 3% B. We previously identified 66 peptide ions representing 33 proteins (2 peptides per protein) with abundance differences in urine and prostates of T+E2 alone compared to control mice (**Table S-1**; (16)). We describe these proteins collectively as the T+E2 prostatic protein signature. The T+E2 prostatic protein signature includes proteins involved in

inflammation, oxidative stress defense, and other processes. Global proteomics data were collected, with preference to peptide ions belonging to the T+E2 prostatic protein signature (as an inclusion list). Mass spectra were scanned from *m/z* 300-1,500 at a resolving power of 60K (at *m/z* 200) and an S-lens radio frequency of 30. Parent masses were isolated in the quadrupole with an isolation window of 1.4 *m/z* and fragmented with higher-energy collisional dissociation with a normalized collision energy of 30 eV. MS/MS scans were detected in the Orbitrap using the rapid scan rate, a dynamic exclusion time of 45 s, and a resolution of 15K (at *m/z* 200). Automatic gain control targets were 1×10^6 for MS and 1×10^5 for MS/MS acquisitions. Maximum injection times were 100 ms for MS and 110 ms for MS/MS.

Immunostaining

Whole lower urinary tracts from three male TCDD/T+E2 mice and three T+E2 alone mice were collected two weeks after T+E2 implantation for Harris hematoxylin and eosin Y staining and evaluated by a board-certified veterinary pathologist for the presence of neoplasia (**Figure 2**). The dorsal prostate was imaged in representative regions.

Whole lower urinary tracts from three TCDD/T+E2 mice and three T+E2 alone mice were collected two weeks after implantation surgery and tissue sections were immunostained for ryanodine receptor 1 according to a previously described protocol (20, 21) (**Figure 1**). The dorsal prostate was imaged in representative regions. Briefly, lower urinary tracts were fixed in a sagittal orientation in 10% formalin overnight, dehydrated in graded alcohols, embedded in paraffin wax, and cut into five-micron sections. Tissue sections were dewaxed, rehydrated, and stained with antibodies against ryanodine receptor 1 (RYR1) (Abcam: ab2827, RRID: AB_2183052, 1:100, (22)). RYR1 was identified by proteomic analysis as the protein with the largest increase in abundance between TCDD/T+E2 and T+E2 alone groups. Tissues were co-stained with antibodies against E-Cadherin (CDH1) to visualize prostatic and urethral epithelium as histological landmarks (Cell signaling: 3195S, RRID: AB_2291471, 1:200, (23–25)). All

fluorescent images used the following secondary antibodies: rhodamine red (Jackson ImmunoResearch: 711-295-152, RRID: AB_2340613, 1:250) and Alexa 647 (Jackson ImmunoResearch: 715-605-150, RRID: AB_2340862, 1:250). Fluorophores were detected using 546 nm and 633 nm lasers and imaged using a SP8 confocal microscope (Leica, Wetzlar, Germany) fitted with a 20x oil-immersion objective (HC PL Apo CS2 NA = 0.75; Leica, Wetzlar, Germany). Intensity levels across the entire image were adjusted using Adobe Photoshop (version 20.0). Immunofluorescent pixels were quantified using the Max Entropy thresholding feature of ImageJ (Version 1.52e11) to determine the percent of immunostained stained pixels within the optical field (**Figure 7**).

Whole lower urinary tracts from five male TCDD/T+E2 mice and six T+E2 alone mice were collected eight weeks after T+E2 implantation for prostatic smooth muscle immunostaining. The dorsal prostate was imaged in representative regions. Tissues were stained with antibodies against actin alpha 2 (ACTA2) (Invitrogen: PA5-18292, RRID: AB_10980764, 1:100, (26) and (ACTA2) (Leica: ncl-l-sma, RRID: AB_442134, 1:200, (27)). Primaries were recognized with the following secondary antibodies: Rhodamine red (Jackson ImmunoResearch: 705-295-147, RRID: AB_2340423, 1:250), Rhodamine red (Jackson ImmunoResearch: 715-295-151, RRID: AB_2340832, 1:250). Smooth muscle thickness was determined as described previously (12), from two nonadjacent tissue sections per mouse using an optical micrometer in ImageJ (Version 1.52e11). Twenty measurements were made in a 20x field and averaged for each mouse and treatment group (**Figure 4**).

Data Processing and Statistical Analysis

Differences in void spot assay outcomes, prostatic smooth muscle thickness, and immunofluorescent pixel density were evaluated using Student's *t*-test to identify significant differences ($p < 0.05$) between groups. Protein identification and relative quantification for prostate samples were achieved using MaxQuant software (v1.6.2.10; Max Planck Institute, Martinsried, Germany) (28), with protein- and peptide-level false discovery rate at 0.01, match

between runs, intensity-based absolute quantification, and the Swiss-Prot *Mus musculus* database (v2019_05). Significant changes in prostate tissue proteomics were determined via volcano plot using Student's *t*-test and a permutation-based FDR (α = 0.05; Perseus v1.6.2.3; Max Planck Institute, Martinsried, Germany) (29). Significantly overrepresented biological processes in the prostate proteomics dataset were determined using the Hypergeometric test with Benjamini & Hochberg FDR correction (α = 0.05; BiNGO tool, Cytoscape v3.6.1) (30, 31).

Conclusion

Human exposure to TCDD continues despite widespread regulatory action. Human urological outcomes of TCDD exposure, particularly exposure occurring during fetal and neonatal periods, are unknown. We showed that *in utero* and lactational TCDD exposure predisposes C57Bl6/J mice to T+E2-induced urinary dysfunction and increases prostatic periductal smooth muscle thickness. Future efforts will test the capacity of antifibrotics and muscle relaxers to alleviate voiding dysfunction and examine the specific contributions of proteins affected by TCDD exposure on prostate and urinary function.

Data deposition

The mass spectrometry proteomics data have been deposited to the ProteomeXchange Consortium via the PRIDE partner repository (44) with the dataset identifier PXD014752.

References

1. M. Oelke, *et al.*, EAU guidelines on the treatment and follow-up of non-neurogenic male lower urinary tract symptoms including benign prostatic obstruction. *Eur Urol* **64**, 118–140 (2013).

2. R. Rosen, *et al.*, Lower urinary tract symptoms and male sexual dysfunction: the multinational survey of the aging male (MSAM-7). *Eur Urol* **44**, 637–649 (2003).

3. C. S. Saigal, G. Joyce, Economic costs of benign prostatic hyperplasia in the private sector. *J Urol* **173**, 1309–1313 (2005).

4. D. Mitropoulos, *et al.*, Symptomatic benign prostate hyperplasia: impact on partners' quality of life. *Eur Urol* **41**, 240–244; discussion 244-245 (2002).

5. K. T. McVary, A. Rademaker, G. L. Lloyd, P. Gann, Autonomic nervous system overactivity in men with lower urinary tract symptoms secondary to benign prostatic hyperplasia. *J. Urol.* **174**, 1327–1433 (2005).

6. M. Caine, S. Raz, M. Zeigler, Adrenergic and cholinergic receptors in the human prostate, prostatic capsule and bladder neck. *Br J Urol* **47**, 193–202 (1975).

7. A. Bjørnerem, *et al.*, Endogenous sex hormones in relation to age, sex, lifestyle factors, and chronic diseases in a general population: the Tromsø Study. *J Clin Endocrinol Metab* **89**, 6039–6047 (2004).

8. T. M. Nicholson, *et al.*, Testosterone and 17β-estradiol induce glandular prostatic growth, bladder outlet obstruction, and voiding dysfunction in male mice. *Endocrinology* **153**, 5556–5565 (2012).

9. T. M. Nicholson, *et al.*, Estrogen receptor-alpha is a key mediator and therapeutic target for bladder complications of benign prostatic hyperplasia. *J Urol* **193**, 722–729 (2015).

10. K. P. Keil, *et al.*, Impact of a folic acid-enriched diet on urinary tract function in mice treated with testosterone and estradiol. *American Journal of Physiology-Renal Physiology* **308**, F1431–F1443 (2015).

11. H. Lepor, Pathophysiology of Lower Urinary Tract Symptoms in the Aging Male Population. *Rev Urol* **7**, S3–S11 (2005).

12. W. A. Ricke, *et al.*, In Utero and Lactational TCDD Exposure Increases Susceptibility to Lower Urinary Tract Dysfunction in Adulthood. *Toxicol Sci* **150**, 429–440 (2016).

13. W. A. Fritz, T.-M. Lin, R. W. Moore, P. S. Cooke, R. E. Peterson, In utero and lactational 2,3,7,8-tetrachlorodibenzo-p-dioxin exposure: effects on the prostate and its response to castration in senescent C57BL/6J mice. *Toxicol. Sci.* **86**, 387–395 (2005).

14. R. W. Moore, *et al.*, 2,3,7,8-Tetrachlorodibenzo-p-dioxin Has Both Pro-Carcinogenic and Anti-Carcinogenic Effects on Neuroendocrine Prostate Carcinoma Formation in TRAMP Mice. *Toxicol Appl Pharmacol* **305**, 242–249 (2016).

15. J. A. Clark, *et al.*, Patients' Perceptions of Quality of Life After Treatment for Early Prostate Cancer. *JCO* **21**, 3777–3784 (2003).

16. S. Thomas, *et al.*, Spatiotemporal proteomics reveals the molecular consequences of hormone treatment in a mouse model of lower urinary tract dysfunction. *J Proteome Res* **19**, 1375–1382 (2020).

17. T. A. Gasiewicz, L. E. Geiger, G. Rucci, R. A. Neal, Distribution, excretion, and metabolism of 2,3,7,8-tetrachlorodibenzo-p-dioxin in C57BL/6J, DBA/2J, and B6D2F1/J mice. *Drug Metab. Dispos.* **11**, 397–403 (1983).

18. K. A. Wegner, *et al.*, Void spot assay procedural optimization and software for rapid and objective quantification of rodent voiding function, including overlapping urine spots. *Am. J. Physiol. Renal Physiol.* **315**, F1067–F1080 (2018).

19. D. Bajic, M. Soiza-Reilly, A. L. Spalding, C. B. Berde, K. G. Commons, Endogenous cholinergic neurotransmission contributes to behavioral sensitization to morphine. *PLoS ONE* **10**, e0117601 (2015).

20. L. L. Abler, *et al.*, A high-resolution molecular atlas of the fetal mouse lower urogenital tract. *Dev. Dyn.* **240**, 2364–2377 (2011).

21. A. E. Turco, *et al.*, A temporal and spatial map of axons in developing mouse prostate. *Histochem. Cell Biol.* (2019) https:/doi.org/10.1007/s00418-019-01784-6.

22. K. Basnayake, *et al.*, Fast calcium transients in dendritic spines driven by extreme statistics. *PLOS Biology* **17**, e2006202 (2019).

23. E. Vasilaki, Z. Kanaki, D. J. Stravopodis, A. Klinakis, Dll1 Marks Cells of Origin of Ras-Induced Cancer in Mouse Squamous Epithelia. *Transl Oncol* **11**, 1213–1219 (2018).

24. V. Drubay, *et al.*, TGF-βRII Knock-down in Pancreatic Cancer Cells Promotes Tumor Growth and Gemcitabine Resistance. Importance of STAT3 Phosphorylation on S727. *Cancers (Basel)* **10** (2018).

25. B. Lloyd-Lewis, F. M. Davis, O. B. Harris, J. R. Hitchcock, C. J. Watson, Neutral lineage tracing of proliferative embryonic and adult mammary stem/progenitor cells. *Development* **145** (2018).

26. B. D. Almquist, S. A. Castleberry, J. B. Sun, A. Y. Lu, P. T. Hammond, Combination Growth Factor Therapy via Electrostatically Assembled Wound Dressings Improves Diabetic Ulcer Healing In Vivo. *Adv Healthc Mater* **4**, 2090–2099 (2015).

27. K. A. Wegner, *et al.*, An immunohistochemical identification key for cell types in adult mouse prostatic and urethral tissue sections. *PLoS ONE* **12**, e0188413 (2017).

28. J. Cox, M. Mann, MaxQuant enables high peptide identification rates, individualized p.p.b.-range mass accuracies and proteome-wide protein quantification. *Nature Biotechnology* **26**, 1367–1372 (2008).

29. S. Tyanova, *et al.*, The Perseus computational platform for comprehensive analysis of (prote)omics data. *Nat Methods* **13**, 731–740 (2016).

30. P. Shannon, *et al.*, Cytoscape: a software environment for integrated models of biomolecular interaction networks. *Genome Res* **13**, 2498–2504 (2003).

31. S. Maere, K. Heymans, M. Kuiper, BiNGO: a Cytoscape plugin to assess overrepresentation of Gene Ontology categories in Biological Networks. *Bioinformatics* **21**, 3448–3449 (2005).

32. J. M. Reynard, C. Lim, T. J. Peters, P. Abrams, The significance of terminal dribbling in men with lower urinary tract symptoms. *Br J Urol* **77**, 705–710 (1996).

33. A. Arima, *et al.*, In utero and lactational exposure to 2,3,7,8-tetrachlorodibenzo-p-dioxin (TCDD) induces disruption of glands of the prostate and fibrosis in rhesus monkeys. *Reprod. Toxicol.* **29**, 317–322 (2010).

34. D. G. Moon, *et al.*, Effect of TCDD on corpus cavernosum histology and smooth muscle physiology. *International Journal of Impotence Research* **16**, 224–230 (2004).

35. M. Iida, E.-Y. Kim, Y. Murakami, Y. Shima, H. Iwata, Toxic effects of 2,3,7,8-tetrachlorodibenzo-p-dioxin on the peripheral nervous system of developing red seabream (Pagrus major). *Aquat. Toxicol.* **128–129**, 193–202 (2013).

36. C. J. Gordon, Y. Yang, L. E. Gray, Autonomic and behavioral thermoregulation in golden hamsters exposed perinatally to dioxin. *Toxicol. Appl. Pharmacol.* **137**, 120–125 (1996).

37. P. G. Kopf, J. K. Huwe, M. K. Walker, Hypertension, cardiac hypertrophy, and impaired vascular relaxation induced by 2,3,7,8-tetrachlorodibenzo-p-dioxin are associated with increased superoxide. *Cardiovasc. Toxicol.* **8**, 181–193 (2008).

38. C. W. White, J. H. Xie, S. Ventura, Age-related changes in the innervation of the prostate gland: implications for prostate cancer initiation and progression. *Organogenesis* **9**, 206–215 (2013).

39. T. M. Bauman, *et al.*, Characterization of Fibrillar Collagens and Extracellular Matrix of Glandular Benign Prostatic Hyperplasia Nodules. *PLOS ONE* **9**, e109102 (2014).

40. J. Ma, *et al.*, Prostatic Fibrosis is Associated with Lower Urinary Tract Symptoms. *J Urol* **188**, 1375–1381 (2012).

41. E. A. Stevens, J. D. Mezrich, C. A. Bradfield, The aryl hydrocarbon receptor: a perspective on potential roles in the immune system. *Immunology* **127**, 299–311 (2009).

42. M. Jin, *et al.*, Exposure to 2,3,7,8-tetrachlorodibenzo-p-dioxin promotes inflammation in mouse testes: The critical role of Klotho in Sertoli cells. *Toxicol. Lett.* **295**, 134–143 (2018).

43. S. S. Cakir, *et al.*, The effect of prostatic inflammation on clinical outcomes in patients with benign prostate hyperplasia. *Prostate Int* **6**, 71–74 (2018).

44. J. A. Vizcaíno, *et al.*, The PRoteomics IDEntifications (PRIDE) database and associated tools: status in 2013. *Nucleic Acids Res* **41**, D1063-1069 (2013).

Figures and Tables

Table 1. Top 30 increased prostatic proteins in TCDD/T+E2 *vs* T+E2 alone (*n* = 7 *vs n* = 6, respectively).

Accession	Protein name	Protein Symbol	$-\log_{10}$ (*p*-value)	$\log_2$ (fold-change) TCDD/T+E2 to T+E2 alone
E9PZQ0	Ryanodine receptor 1	RYR1	1.35	3.04
Q921M4	Golgin subfamily A member 2	GOLGA2	1.65	2.74
O08539	Myc box-dependent-interacting protein 1	BIN1	2.18	2.49
Q8CHG3	GRIP and coiled-coil domain-containing protein 2	GCC2	1.56	2.46
P07744	Keratin, type II cytoskeletal 4	KRT4	1.58	2.45
P97443	Histone-lysine N-methyltransferase Smyd1	SMYD1	1.44	2.25
A2AAJ9	Obscurin	OBSCN	2.51	2.19
Q9R062	Glycogenin-1	GYG1	2.00	1.97
P33267	Cytochrome P450 2F2	CYP2F2	1.37	1.95
Q3V1D3	AMP deaminase 1	AMPD1	2.62	1.89
Q9CQ80	Vacuolar protein-sorting-associated protein 25	VPS25	1.62	1.79
Q8R3B1	1-phosphatidylinositol 4,5-bisphosphate phosphodiesterase delta-1	PLCD1	2.10	1.75
Q1XH17	Tripartite motif-containing protein 72	TRIM72	1.34	1.69
P04370	Myelin basic protein	MBP	1.38	1.57
P62322	U6 snRNA-associated Sm-like protein LSm5	LSM5	3.66	1.32
O09131	Glutathione S-transferase omega-1	GSTO1	2.23	1.31
O89001	Carboxypeptidase D	CPD	1.51	1.26
P04925	Major prion protein	PRNP	1.63	1.22
Q61206	Platelet-activating factor acetylhydrolase IB subunit beta	PAFAH1B2	2.46	1.20
Q9QZD8	Mitochondrial dicarboxylate carrier	SLC25A10	1.40	1.19
Q61301	Catenin alpha-2	CTNNA2	2.98	1.18
Q7TNV0	Protein DEK	DEK	1.86	1.18
P30115	Glutathione S-transferase A3	GSTA3	3.28	1.15
O55126	Protein NipSnap homolog 2	NIPSNAP2	1.31	1.13
Q9JKY5	Huntingtin-interacting protein 1-related protein	HIP1R	1.82	1.12
Q9D1H7	Golgi to ER traffic protein 4 homolog	GET4	1.73	1.11
Q62165	Dystroglycan	DAG1	1.59	1.05
Q8BHL8	Proteasome inhibitor PI31 subunit	PSMF1	2.09	1.04
P11087	Collagen alpha-1(I) chain	COLI1A1	1.54	1.02
P36993	Protein phosphatase 1B	PPM1B	4.27	1.01

Table 2. Top 30 decreased prostatic proteins in TCDD/T+E2 *vs* T+E2 alone (*n* = 7 *vs* *n* = 6, respectively).

Accession	Protein name	Protein Symbol	-$\log_{10}$ (*p*-value)	$\log_2$ (fold-change) TCDD/T+E2 to T+E2
Q8CI04	Conserved oligomeric Golgi complex subunit 3	COG3	2.06	-2.26
A2RSQ1	Beta-galactosidase-1-like protein 3	GLB1L3	2.35	-2.14
Q9QXZ0	Microtubule-actin cross-linking factor 1	MACF1	1.40	-2.03
Q9R0B9	Procollagen-lysine,2-oxoglutarate 5-	PLOD2	2.88	-1.98
Q8BTY8	Sec1 family domain-containing protein 2	SCFD2	1.31	-1.87
Q91VA1	Choline transporter-like protein 4	SLC4Aa4	1.36	-1.85
P97494	Glutamate--cysteine ligase catalytic subunit	GCLC	2.25	-1.73
Q61087	Laminin subunit beta-3	LAMB3	1.94	-1.58
Q8K3W0	BRISC and BRCA1-A complex member 2	BABAM2	1.51	-1.51
Q9Z2Q6	Septin-5	SEPTIN5	3.70	-1.46
P01864	Ig gamma-2A chain C region secreted form	N/A	2.19	-1.40
Q61194	Phosphatidylinositol 4-phosphate 3-kinase	PIK3C2A	2.06	-1.37
Q8VD75	Huntingtin-interacting protein 1	HIP1	2.22	-1.34
Q62264	Thyroid hormone-inducible hepatic protein	THRSP	1.93	-1.32
P06281	Renin-1	REN1	1.34	-1.29
P35282	Ras-related protein Rab-21	RAB21	1.63	-1.24
P33622	Apolipoprotein C-III	APOCc3	1.37	-1.21
Q9Z1G3	V-type proton ATPase subunit C 1	ATP6V1C1	1.64	-1.17
P01837	Immunoglobulin kappa constant	IGKC	2.72	-1.15
Q99K30	Epidermal growth factor receptor kinase	EPS8L2	1.70	-1.11
Q8VE62	Polyadenylate-binding protein-interacting	PAIP1	1.89	-1.11
Q00493	Carboxypeptidase E	CPE	1.52	-1.06
Q9CX30	Protein YIF1B	YIF1B	1.89	-1.05
Q02357	Ankyrin-1	ANK1	1.36	-1.03
Q8R0G9	Nuclear pore complex protein Nup133	NUP133	1.49	-1.01
Q69ZS7	HBS1-like protein	HBS1I	1.78	-0.96
Q8BLF1	Neutral cholesterol ester hydrolase 1	NCEH1	2.12	-0.89
Q8BK64	Activator of 90 kDa heat shock protein ATPase	AHSA1	1.71	-0.89
P0DOV1	Interferon-activable protein 205-B	MNDA	1.49	-0.88
P24547	Inosine-5'-monophosphate dehydrogenase 2	IMPDH2	1.74	-0.87

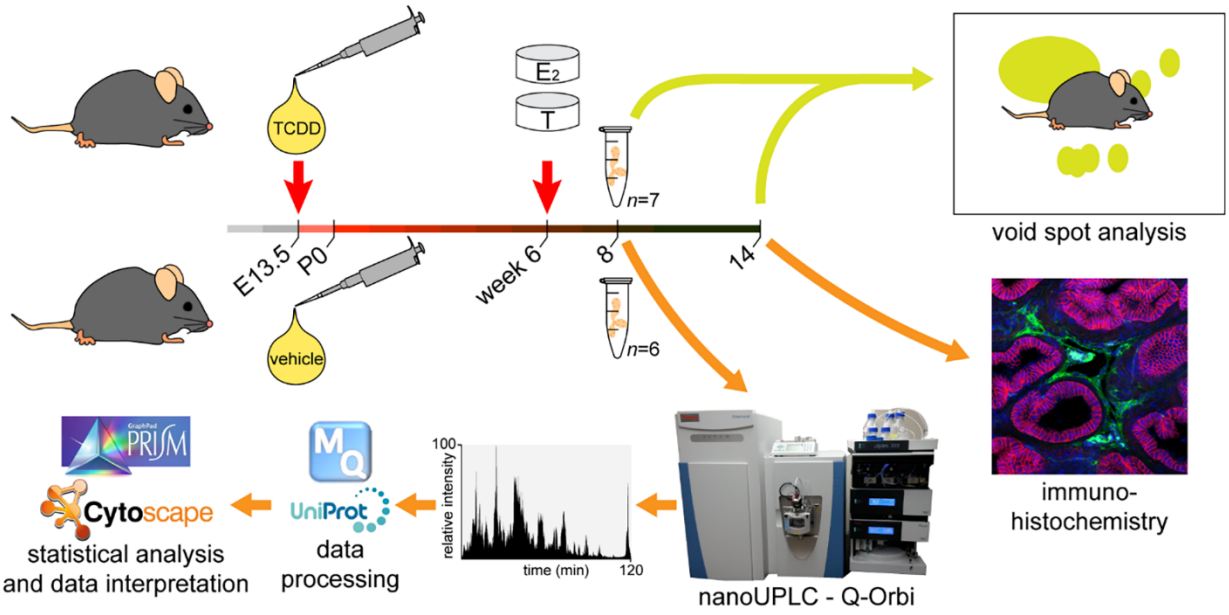

Figure 1. Experimental design. Male mice were exposed *in utero* and via lactation to TCDD (1 µg/kg oral maternal dose) or vehicle (5 mL/kg corn oil). Mice were aged to six weeks and given a sham surgery or implanted with hormone pellets consisting of 25 mg testosterone, 2.5 mg estradiol, and 22.5 mg cholesterol. Void spot assays were conducted two and eight weeks after implantation surgery to test for progressive urinary dysfunction. Prostate tissue was collected two and eight weeks post-implantation surgery for proteomic analysis or for staining.

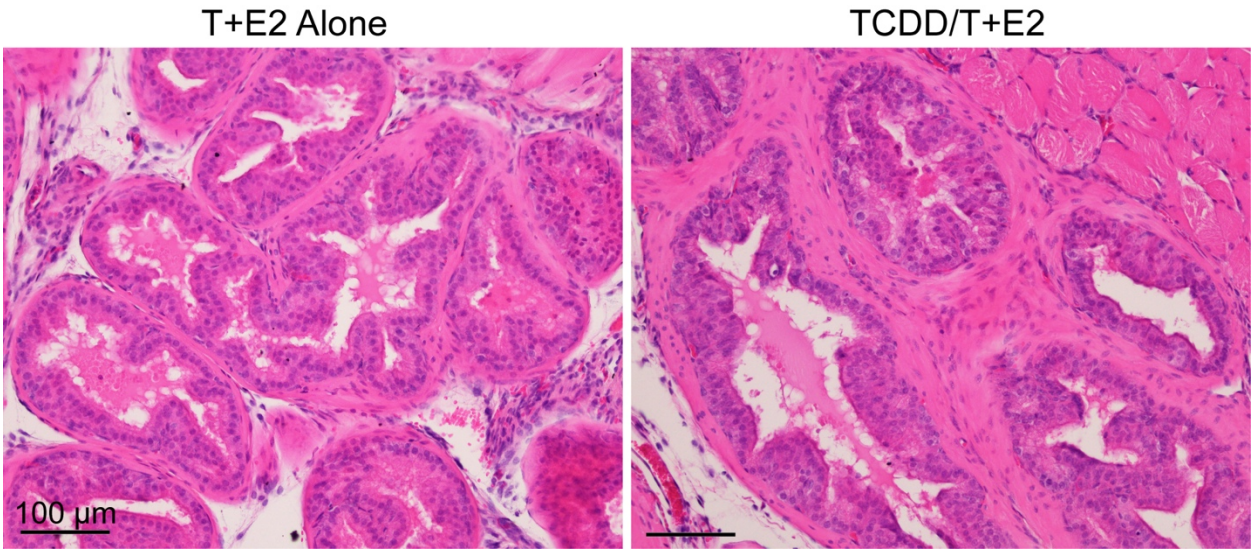

Figure 2. The effect of TCDD/T+E2 exposure compared to T+E2 alone in C57Bl6/J mice. Mouse prostate tissue sections (10 µm) from TCDD/T+E2 and T+E2 alone were stained using hematoxylin and eosin and examined by a board-certified veterinary pathologist. There was no evidence of high grade neoplasia or invasive carcinoma in either group. Images depict proximal dorsal prostate after two weeks of T+E2. Scale bar represents 100 µm. (*n* = 3)

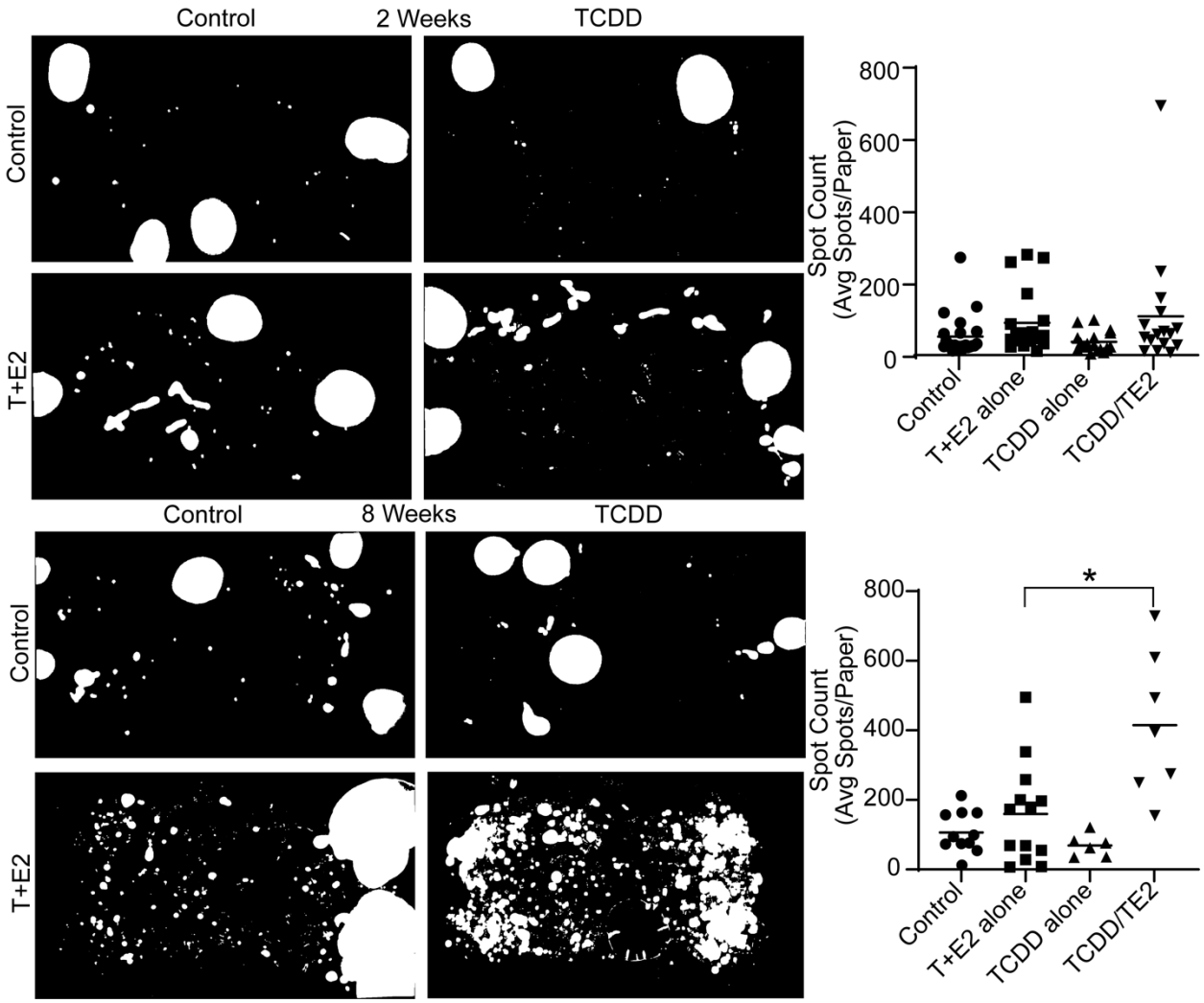

Figure 3. *In utero* and lactational TCDD exposure exacerbates voiding dysfunction in T+E2-treated wild type mice. Mice were treated as described in Fig. 1 and voiding function was measured by the void spot assay two and eight weeks post-implantation surgery. A representative void spot assay image is inset above each group (urine spots in white). Control mice and mice exposed to TCDD alone did not differ significantly in urinary spot count at two or eight weeks. TCDD/T+E2 mice did not differ in spot count at two weeks but had significantly more urine spots compared to T+E2 alone at eight weeks. Results are mean ± SE, n = 7 to 19. Differences between groups were evaluated by Student's t-test. An asterisk identifies a difference between the TCDD/T+E2 group and T+E2 alone group, p = 0.0343).

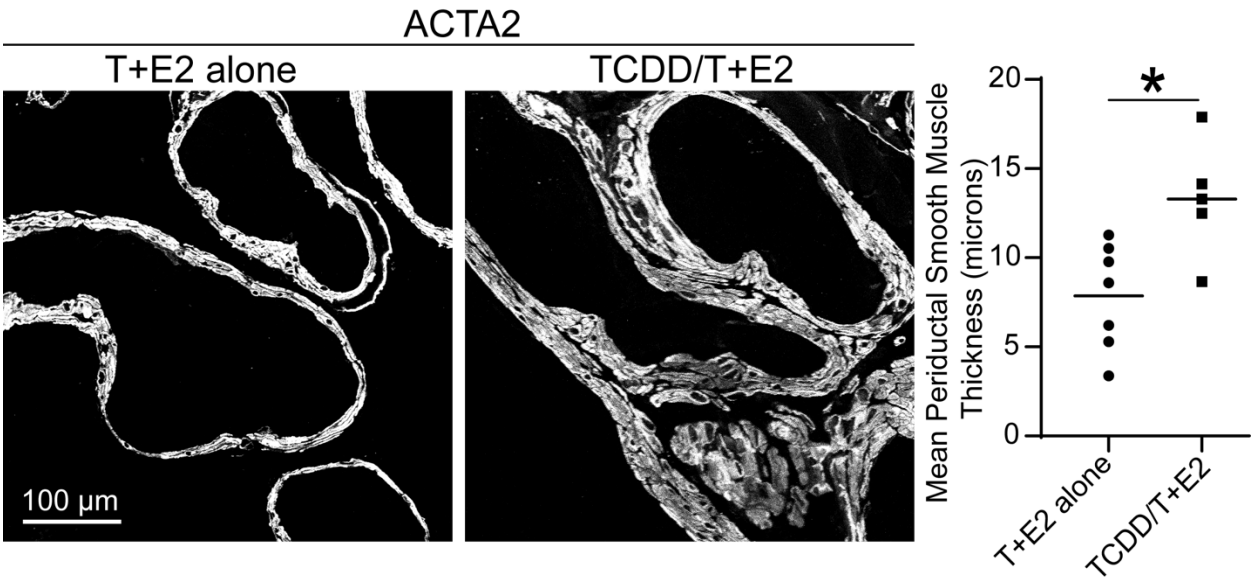

Figure 4. TCDD/T+E2 thickens dorsal prostate smooth muscle compared to T+E2 alone in C57Bl6/J mice. Dorsal prostate sections from mice treated with T+E2 alone or TCDD/T+E2 for eight weeks were stained with an antibody recognizing smooth muscle. Representative images of smooth muscle staining (white) are on the left. TCDD/T+E2 mice had significantly thicker smooth muscle in the proximal dorsal prostate of TCDD exposed mice (Student's *t*-test, mean ± SEM, $\alpha = 0.05$, $p = 0.0137$, $n = 5$ to 7). Scale bar represents 100 µm.

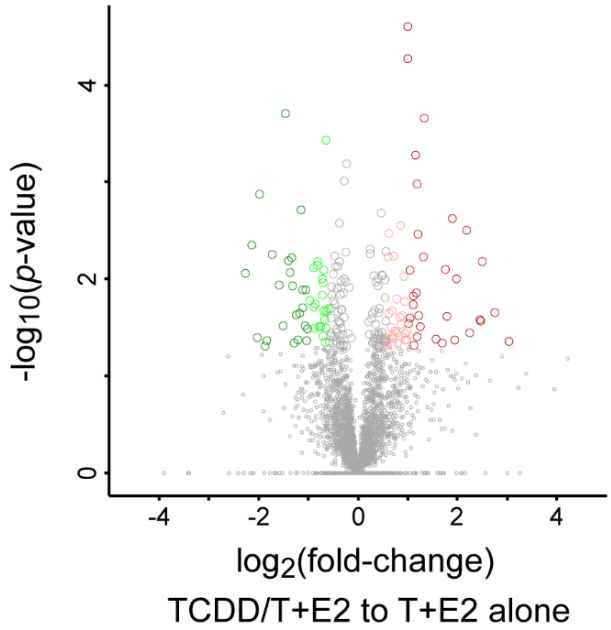

Figure 5. Prostate proteomic differences between TCDD/T+E2 and T+E2 alone mice. Volcano plot shows that 102 of 3641 identified proteins differ significantly in abundance ($p < 0.05$, Student's *t*-test; fold-change ≥ 50%) between TCDD/T+E2 and T+E2 alone groups. Results are representative of seven TCDD/T+E2 mice and six T+E2 mice. Light colored shapes indicate proteins with abundance differences of 50-100% between groups and dark colored shapes indicate peptides with abundance differences of >100%.

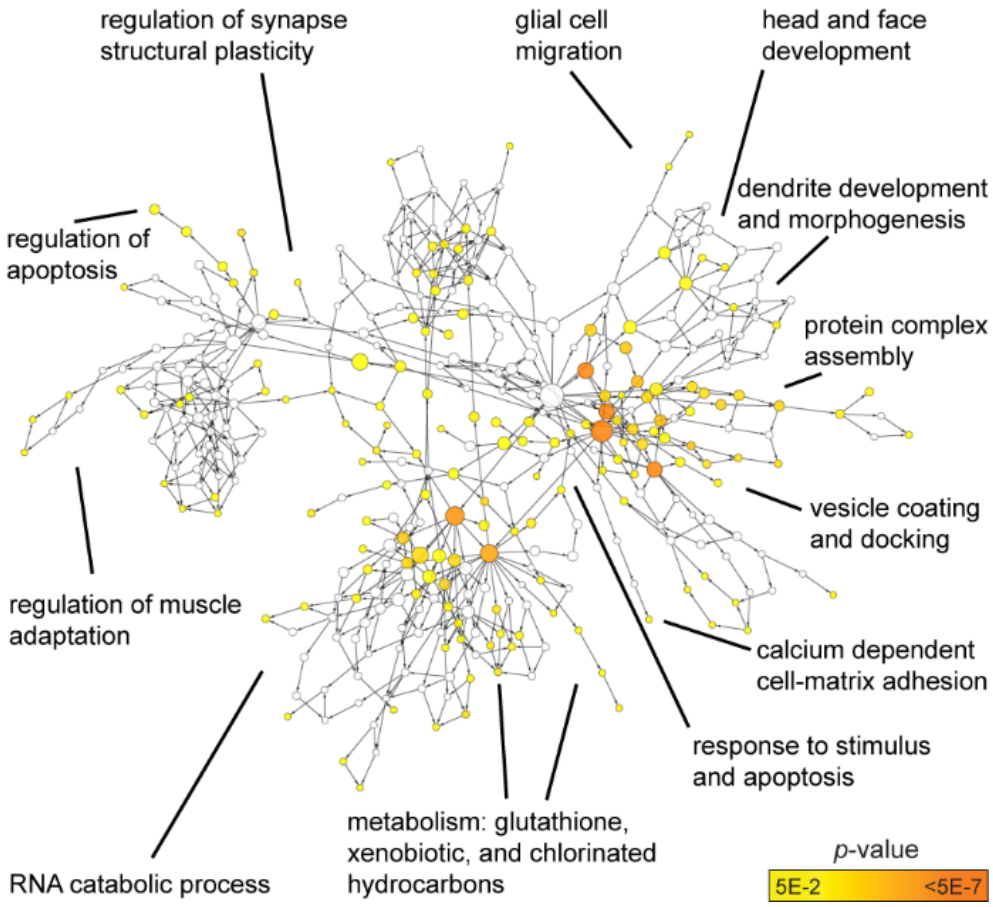

Figure 6. Significantly overrepresented biological processes among prostatic proteins that were more abundant in TCDD/T+E2 than T+E2 alone mice, as determined by gene ontology software (Cytoscape BiNGO tool, Hypergeometric test with B&H FDR correction; *n* = 6 to 7). Node size increases with increasing connectivity and color darkens with decreasing *p*-value.

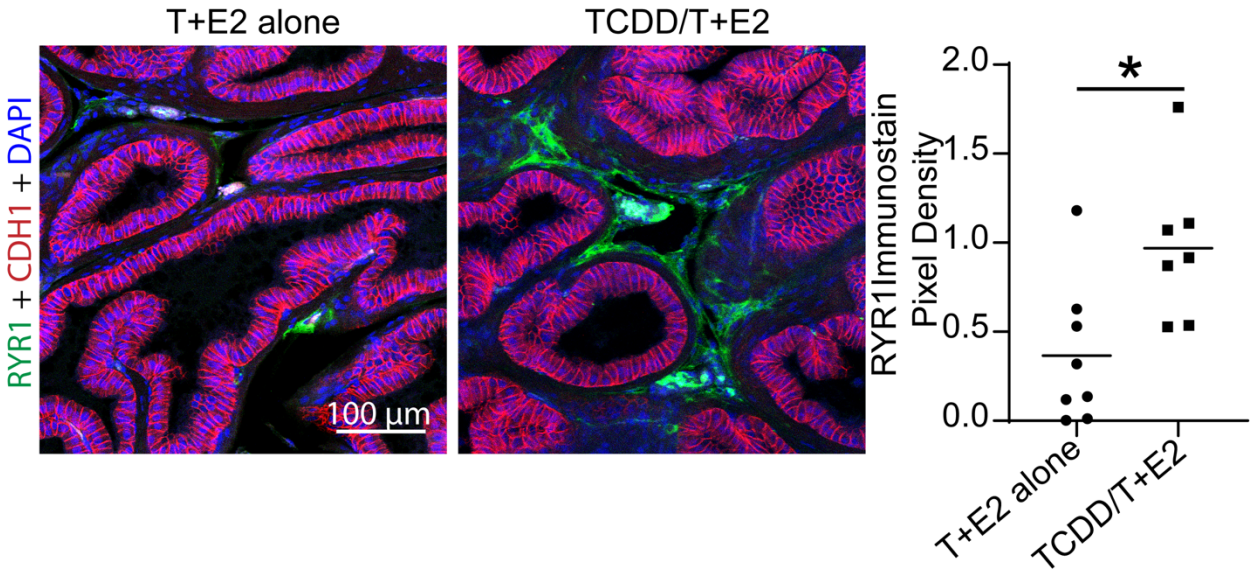

Figure 7. Ryanodine receptor (RYR1) immunostaining is more abundant in TCDD/T+E2 than T+E2 alone mice. Prostate tissue sections (10 µm) treated with TCDD/T+E2 or T+E2 alone were stained for ryanodine receptor 1 (RYR1) (green), CDH1 for epithelial cells (red), and DAPI for nuclei (blue). Quantification was performed on all prostate lobes and representative images in the dorsal prostate are shown above. The staining for RYR1 was significantly increased in TCDD/T+E2-treated prostate lobes compared to T+E2 alone (Student's *t*-test, $\alpha = 0.05$, $p = 0.014$; $n = 3$; mean ± SEM; line represents mean of data). Scale bar is 100 µm.

Chapter 5: Testosterone and estradiol mediate male voiding dysfunction by reducing prostatic smooth muscle *Ppp112b* abundance and impairing muscle relaxation

Turco AE, Popovics P, Oakes SR, Rogers A, Sheftel C, Peterson RE, Hernandez L, Grimes MD, Kumar S, Bjorling DE, Bonev A, Watters J, Strand DW, Hacker T, Ricke WA, Tykocki NR, Vezina CM. (2021). Prepped for submission

Abstract

Bladder outflow obstruction and voiding dysfunction affect nearly all aging men and are linked to excessive prostatic smooth muscle tone. The prevailing theory is that prostatic smooth muscle recovers spontaneously after stimulation, and that agents that block muscle stimulation will also reduce muscle tone. This theory led to the development of alpha blockers, which are effective in some but not all men. Here, we show that prostatic smooth muscle recovery is not always spontaneous and that testosterone (T) and estradiol (E2), which change in concentration with age, mediate bladder outflow obstruction by interfering with prostatic smooth muscle relaxation. We delivered sustained-release T and E2 implants to male mice and evaluated prostatic urethral flow dynamics by contrast enhanced ultrasound. A single bolus of the smooth muscle contractile agonist phenylephrine sustainably increases urine velocity in T+E2 treated, but not in control mice. Using phenylephrine to increase smooth muscle tension and drive intracellular calcium release in mouse prostate preparations, we find that T+E2 delays recovery after pharmacological stimulation. T+E2 treatment is mechanistically linked to a reduction of protein phosphatase 1 regulatory subunit 12B (PPP1R12B) abundance in prostate but not bladder. A genetic approach to deplete *Ppp1r12b* in mice delays prostatic tissue recovery after phenylephrine stimulation. Collectively, these results support the hypothesis that aging-related changes in circulating T and E2 concentrations drive bladder outflow obstruction by reducing PPP1R12B abundance and impairing prostatic smooth muscle relaxation.

Introduction

Lower Urinary Tract Dysfunction (LUTD) is prevalent in most aging men and is associated with symptoms such as straining to urinate, weak stream, incomplete bladder emptying, and increased urinary frequency, especially at night (1). Male LUTD significantly decreases quality of life, associates with depression and sleep deprivation and, if untreated, can cause permanent bladder and renal impairment (2). An aging-related reduction in the ratio of circulating testosterone (T) to estradiol (E2) is associated with LUTD (3–6). Experimental manipulations of T and E2 concentrations in mice, dogs, and non-human primates, to mimic those that occur during aging, yield diverse anatomic and physiologic changes including prostatic hypertrophy and inflammation (6–10) and abnormal urethral muscle tone (11, 12).

Smooth muscle contraction is regulated by receptor activation and mechanical stretch. Myosin light chain kinase phosphorylates the 20-kDa myosin light chain, causing myosin to crossbridge with actin and driving muscle contraction (13). Smooth muscle relaxation is mediated by myosin phosphatase, which hydrolyzes phosphorylated myosin light chain (13). Myosin phosphatase is a trimer consisting of a catalytic type 1 protein phosphatase (Pp1c) subunit, a targeting subunit that controls the catalytic subunit, and a non-catalytic subunit (M20). The targeting subunit is encoded by one of five different genes, which differ in relative abundance across tissues: protein phosphatase 1 regulatory subunit (PPP1R)12A, PPP1R12B, PPP1R12C, PPP1R16A, and PPP1R16B (14). Smooth muscle activity is known to be regulated at the level of myosin phosphatase and most of the current understanding derives from studies involving PPPR12A. Mechanisms of PPP1R12A regulation include phosphorylation, subunit aggregation and disaggregation, isoform switching, and transcriptional regulation (15–17). PPP1R12A is essential for smooth muscle relaxation (18) and even subtle variations in its activity can convey differences in smooth muscle contractile kinetics across organ systems (19). Much less is known about the requirement and regulation of other PPP1R isoforms, including PPP1R12B.

Here, we offer new support for the new paradigm that changes in circulating T and E2 concentrations, like those that occur naturally in the aging male, cause bladder outflow obstruction by reducing PPP1R12B abundance and sustaining prostatic smooth muscle contraction over time. We delivered slow-release T and E2 implants to drive voiding dysfunction in male mice and deployed contrast enhanced ultrasound to measure changes in urine velocity in the prostatic urethra, signifying urethral obstruction (20). A single bolus dose of phenylephrine (10 μg/kg *iv*) causes a sustained increase in urine velocity through the urethra of T+E2 treated mice. We used a pulse of phenylephrine to increase muscle tension and intracellular calcium release of *ex vivo* prostate tissue. Prostates from T+E2 treated mice return more slowly to baseline than control mice, indicating impaired muscle relaxation. We discovered that protein phosphatase 1 regulatory subunit 12B (PPP1R12B), a myosin phosphatase subunit, is functionally and genetically repressed by T and E2. Genetic ablation of *Ppp1r12b* also reduces the kinetics of prostate smooth muscle relaxation. Though adrenoreceptors that regulate smooth muscle contraction are already a medical target for urinary voiding symptoms (21–23), our results are significant because they direct new attention to smooth muscle relaxation as a clinically significant and hormone-sensitive mechanism of bladder outflow obstruction.

Results

T+E2 treatment increases the magnitude and duration of the prostatic urethral response to alpha-adrenoreceptor-evoked stimulation

An aging-related decline in the ratio of circulating T to E2 has been identified as a potential contributor to male LUTD in multiple studies (24, 25). T+E2-mediated changes in mouse urinary physiology (urethral narrowing, increased bladder capacity, wet weight, urinary retention, and hydronephrosis) suggest a mechanism involving bladder outflow obstruction at the level of the urethra (6, 26, 27)(28–30), but technical limitations in urethral physiology testing made this difficult to confirm. We pioneered a contrast-enhanced ultrasound method to visualize urethral fluid

dynamics *in vivo*. Mice were implanted with slow-release T+E2 implants, or given a sham surgery, and two weeks later were anesthetized. Contrast agent was infused directly into the bladder while urethra fluid dynamics were measured with an ultrasound probe (**Figure 1A**). Though velocity of an incompressible fluid is expected to increase when passing through a constriction (**Figure 1B**), T+E2 does not change basal velocity of the contrast agent as it passes through the prostatic urethra ($p = 0.7977$, **Figure 1C**) even though T+E2 changes spontaneous voiding behavior (**Supplementary Figure S1**). These results suggest no appreciable T+E2 induced changes in basal urethral tone. Many factors evoke increases in urethral tone including basal phosphorylation (13), inflammation (31) and autonomic dysfunction (32) and we considered that evoked smooth muscle contraction may be necessary to reveal the T+E2 phenotype. A single dose of phenylephrine (10 μg/kg, *iv*) was delivered to control and T+E2 treated mice and urine velocity was measured one, five, 15, and 30 min later (**Figure 1D**). Phenylephrine increased the velocity of contrast agent through the urethras of T+E2 treated but not control mice, and the velocity remained elevated for at least 15 minutes. The duration of phenylephrine action in T+E2 treated mice is surprising, considering the half-life in mice of approximately 5 minutes (33). We conclude that T+E2 treatment increases the magnitude and duration of the prostatic urethral response to alpha-adrenoreceptor-evoked stimulation.

T+E2 impairs prostate smooth muscle relaxation after adrenoreceptor-mediated contraction

It was previously speculated that T and E2 obstructs bladder outflow by increasing the sensitivity of prostatic and urethral smooth muscle α1 adrenoreceptors to ligand-mediated activation (34, 35) and this is a logical mechanism for the changes we observed in urethral fluid dynamics in **Figure 1**. We measured prostatic smooth muscle isometric contractility in response to a range of phenylephrine concentrations (0.0001- 200 μM) but to our surprise, T+E2 did not enhance the phenylephrine-mediated response ($n = 6$, $p= 0.6923$) (**Figure 2A**). It was also previously suggested that T and E2 may enhance urethral tone by driving transcription of alpha-

1-adrenergic receptor 1A (*Adra1a*) (36–38), but we found no evidence to support this mechanism. In fact, *Adra1a* mRNA abundance is unaffected by T+E2 treatment (**Figure 2B**).

Nearly all studies of prostatic muscle activity have focused on mechanisms of muscle stimulation, with little attention towards muscle relaxation. However, the kinetics of muscle recovery differ across organ systems (39), suggesting a modifiable endpoint that should also be considered. We evaluated the influence of T+E2 on prostatic smooth muscle relaxation kinetics by inducing isometric contraction with a bolus of phenylephrine (100 μM) and monitoring tension over time until a return to baseline. T+E2 prolonged the interval between maximal and minimal (basal) tension ($n = 6$, $p = 0.0442$), suggesting interference with muscle relaxation (**Figure 2C**).

We used a complementary approach to confirm our results by introducing a genetically encoded calcium sensor into smooth muscle and measuring calcium transients as proxies of muscle contraction. Mice were given sustained release T+E2 implants or sham surgery and two weeks later, prostates were dissected and placed in a heated perfusion chamber for fluorescent imaging. Fluorescence was recorded during a 1-min perfusion with phenylephrine (10 μg/mL) and for 10 min after washout with drug-free media. Representative still images are shown in **Figure 2D**, and representative traces of fluorescence intensity over time are shown in **Figure 2D**. T+E2 treatment significantly ($n = 6$-10, $p= 0.014$) prolongs the interval between peak fluorescence and the return to baseline (**Figure 2E**); additional evidence that T+E2 interferes with prostatic muscle relaxation.

T+E2 reduces prostatic abundance of myosin phosphatase subunit PPP1R12B

We surmised that T+E2 may act by driving down the abundance of factors that mediate smooth muscle relaxation. Using RT-PCR to measure mRNA abundance in anterior prostate, we discovered that T+E2 uniquely decreases ($p = 0.0392$, $n= 4$) *Ppp1r12b* mRNA in anterior prostate (**Figure 3A**) without significantly changing abundance of other *Ppp1r* subunits (**Supplementary Figure S2**). We identified that T+E2 exposure also decreases Ppp1r12b expression in ventral and dorsal prostate (**Supplementary Figure S3**). Furthermore, T+E2 uniquely decreases

Ppp1r12b in prostate but not bladder (p= 0.7922, n= 5)(**Figure 3B**). We localized PPP1R12B protein to prostatic smooth muscle using immunohistochemistry (**Figure 3C**). We followed with western blotting to reveal that T+E2 also decreases PPP1R12B protein abundance in prostate (p= 0.0296, n= 4) (**Figure 3D**).

PPP1R12B null mice impaired prostatic smooth muscle relaxation after adrenoreceptor-mediated contraction

If T+E2 interferes with prostatic muscle recovery by reducing PPP1R12B, we predicted that prostatic tissues from untreated *Ppp1r12b* null mice would phenocopy the T+E2 treated mouse prostate response to phenylephrine. Using isometric contraction assays, we found evidence to support this paradigm: *Ppp1r12b* null mouse prostatic tissue recovers more slowly than that of wild type mice from phenylephrine-evoked stimulation (p= 0.0117, n= 4-9) (**Figure 4A),** even though both genotypes are equally responsive to phenylephrine (p=0.3101, n=4-9) (**Figure 4B**). Collectively, our results support the hypothesis that T+E2 drives bladder outflow obstruction by reducing PPP1R12B abundance and interfering with prostatic smooth muscle recovery after stimulation (**Figure 5**).

Discussion

Smooth muscle dysfunction is a key driver of male LUTD. Evidence that phenylephrine increases prostatic smooth muscle tone and α1-adrenergic receptor blockers reduce tone and relieve LUTD led to the theory that prostatic noradrenaline abundance or activity increases with age to mediate an increase in prostatic smooth muscle tone (40). Yet, there is little evidence to support this theory. Prostatic norepinephrine content does not significantly correlate with lower urinary tract symptom score (41) and prostate contractile response to phenylephrine does not differ between men with symptomatic and asymptomatic BPH (42). Alpha-1 adrenergic antagonists reduces the clinical risk of progression of BPH in only 39% of men (43). The inefficiency of alpha blocker therapies for treating LUTD is in part due to a lack of knowledge on

how prostatic smooth muscle changes with age. In particular, almost no attention has been directed towards the possibility that LUTD derives from a defect in prostatic smooth muscle relaxation. We provide evidence that T+E2 implants delivered subcutaneously to mice, to mimic changes in circulating hormone concentrations that occur in men of advancing age, slow prostatic smooth muscle recovery after stimulation and cause a sustained impairment of bladder outflow (24, 25).

Using ultrasound to measure urethral obstruction, we demonstrated that basal velocity is similar in control and T+E2 mice under anesthesia, but, more importantly, is uniquely enhanced by phenylephrine in T+E2 treated mice. The *in vivo* urinary voiding response to T+E2 is supported by *in vitro* evidence that prostate preparations from T+E2 treated mice are slower to recover after stimulation than tissues from sham operated mice. It is unknown why LUTS patients have a variable response to alpha-1 adrenoceptor drugs. It is common for men who initially respond to alpha blockers to develop tolerance, necessitating higher doses or a change to a different drug to achieve therapeutic benefit (44). An aging-related decline in the ratio of circulating T to E2, coupled with a decline in prostatic smooth muscle recovery, offers one explanation for why urinary voiding symptoms change with age and alpha blocker responsiveness differs among patients.

Several previous studies examined the influence of testosterone and estradiol on prostatic smooth muscle activity by few focused on the influence of these hormones on muscle relaxation. Nguyen et al (45) reported that testosterone and certain testosterone:estradiol ratios significantly enhance noradrenaline-mediated calcium signals in immortalized prostatic smooth muscle cells, supporting the concept that the age-related change in the steroid hormone milieu may affect smooth muscle contractility. Others found that aromatase depletion, which impairs metabolism of testosterone into estradiol, does not significantly affect electrically- or pharmacologically evoked prostatic smooth muscle contraction (46). As evidenced from the present study, the ratio of testosterone to estradiol is critical for prostate smooth muscle contractility and adds support to the idea that patient variability in circulating T and E2 concentrations may underlie patient

variation in response to alpha-blockers. Another study found testosterone and estradiol may act by enhancing the action of noradrenaline on increasing the expression of contractile filaments, prostate smooth muscle actin and myosin (47) and Zhang et al. showed increased abundance of smooth muscle markers in response to both steroid hormones on prostatic cells in culture (48). Increased abundance of smooth muscle markers could be explained by thickening prostate smooth muscle due to chronic impairment of relaxation. Overall, studies that attempted to establish a direct connection between aging-associated steroid levels and the change in smooth contractility have not provided significant progress or consistant results leading to the mechanism by which T+E2 drives bladder outflow obstruction.

By screening for T+E2-mediated expression changes in myosin phosphatase subunits, our study directs new focus on prostate smooth relaxation as a modifiable endpoint and contributor to LUTD, uniquely through changes in PPP1R12B abundance. Previous studies of PPP1R12B describe functional connections to breast and colorectal cancer, asthma, pregnancy and labor, atherosclerosis, cardiac muscle, and skeletal muscle degeneration (49–55). This is the first study to link PPP1R12B to prostatic smooth muscle activity and to provide evidence that T+E2 reduce PPP1R12B abundance. Interestingly, T+E2 uniquely reduces *Pp1r12b* in prostate but not bladder, and the selective response to hormones raises the possibility that prostatic PPP1R12B could be targeted selectively for therapeutic benefit.

Collectively, we offer evidence to support the hypothesis that changes in circulating T and E2 concentrations, like those that occur as men age, drive urinary dysfunction by decreasing PPP1R12B abundance in prostate and urethral smooth muscle and interfering with muscle relaxation after adrenoreceptor-mediated contraction. Future studies will examine the impact of *Ppp1r12b* depletion on female mouse urination to determine if this mechanism of urinary dysfunction is sex specific and investigate other potential mechanisms of T+E2 exposure. Screening of human prostate biopsy specimens could determine whether prostatic *Ppp1r12b*

abundance is reduced with aging, inversely correlates with the ratio of circulating T to E2 and predicts patient responsiveness to therapy.

Materials and Methods

Mice

All procedures were approved by the University of Wisconsin Animal Care and Use Committee and conducted in accordance with the National Institutes of Health Guide for the Care and Use of Laboratory Animals. All mice were from Jackson laboratories (Bar Harbor, ME) and maintained on a C57Bl/6J genetic background (Jackson stock #000664). Strains included: C57Bl6/J (#000664), *Polr2a*$^{Tn(pb\text{-}CAG\text{-}GCaMP5g,\text{-}tdTomato)Tvrd}$ (also known as GCaMP5g, Jackson mouse stock #024477), Tg(*Myh11cre*,-EGFP)2Mik (also known as *Myh11*^{cre}, Jackson mouse stock #007742), and C57Bl/6NJ-*Ppp1r12b*$^{em1(MPC)J}$ /Mmjax (also known as *Ppp1r12b* null, Jackson mouse stock #46179-JAX). *Mych11*^{cre}/+; GCaMP5g/+, pups were used in experimentation. All mice were aged to six weeks and used in experimentation. Mice were housed in Innovive® HDPE plastic microisolator cages in a room maintained on a 12 h light and dark cycle, ambient temperature of 20.5 ± 1°C and relative humidity of 30-70%. Mice were fed a 5015 Diet (PMI Nutrition International, Brentwood, MO) from conception through weaning (P21) and a 8604 Teklad Rodent Diet thereafter (Harlan Laboratories, Madison, WI). Feed and water were available *ad libitum* and cages contained corncob bedding. Six-week-old C57Bl6/J male mice were given subcutaneous hormone implants (25 mg testosterone and 2.5 mg 17-β estradiol) or a sham surgery as described previously (6, 56) and then individually housed to prevent fighting. All mice were euthanized by CO_2 asphyxiation. Prostate tissues were collected at 8 weeks and either snap frozen in liquid nitrogen or fixed overnight at 4°C in 4% paraformaldehyde dissolved in neutral buffered saline (Thermo Scientific) and dehydrated through a series of graded ethanol concentrations. Tissues were cleared in xylenes, embedded in paraffin wax, and sectioned at 5 μm thickness on a microtome (Surgipath Medical Industries).

Contrast-Enhanced Ultrasound

Contrast-enhanced ultrasound was performed as a terminal procedure as described previously (20) using a Vevo 300 ultrasound at the University of Wisconsin-Madison Cardiovascular Core. Mice were anesthetized with 2.5% isoflurane and placed in dorsal recumbency. An incision was made in the ventral abdomen to expose the bladder. A cystostomy catheter was passed across the bladder wall and secured with a purse-string suture. Acoustic gel was applied to the abdomen and contrast (DEFINITY, Lantheus Medical Imaging #DE4) was delivered at 1.5 mL/min into the bladder. Contrast velocity was recorded at baseline, and 1, 5, 15 and 30 min after a single bolus dose of phenylephrine (10 µg/kg *iv*). Mice were euthanized via cervical dislocation.

Smooth Muscle Calcium Transient Imaging

Myh11^{cre}/+;GCaMP5g/+ harbor a genetically-encoded intensiometric calcium sensor that fluoresces in response to increases in intracellular calcium concentration. *Myh11*^{cre}/+;GCaMP5g/+ mice were euthanized two weeks after T+E2 implantation or sham surgery and a tissue complex containing urethra, dorsal and ventral prostate was dissected and stored in ice cold HEPES buffer (134 mM NaCl, 10 mM HEPES, 6 mM KCl, 7 mM glucose, 1 mM $MgCl_2$, pH 7). The anterior prostate was dissected out and analyzed separately. The tissue was positioned in a heated (37°C) chamber for imaging (Warner Instruments #RC-49MFSH). A pressurized perfusion system (Warner Instruments # 641721) fitted with mini-valve controllers (Warner Instruments #VCS–8–MINI–LT) was used to continuously superfuse tissues with HEPES solution (134 mM NaCl, 10 mM HEPES, 6 mM KCl, 7 mM glucose, 1 mM $MgCl_2$, 2 mM $CaCl_2$, pH 7) (1 mL/min), and maintained at 37°C with an inline heater (Warner Instruments #SF-28). The tissue was illuminated with a LED light (SOLA-SM2 365 LED Light Engine), visualized with a Leica MZ16 stereo fluorescent dissecting microscope fitted with a GFP Dichroic filter set (Chroma, Bellows Falls, VT), and images were recorded with a Zyla 4.2 Plus sCMOS camera using Nikon Elements Software. Phenylephrine (Sigma P6126-5G, 10 µM in HEPES solution) was introduced

into the chamber at 0.5 ml/min for one minute using a pressurized perfusion system (Warner Instruments # 641721) fitted with mini-valve controllers (Warner Instruments #VCS–8–MINI–LT). Response was recorded at 10 frames/second and analyzed using SparkAn software (designed by Dr. Adrian Bonev, University of Vermont).

Isolated Prostate Muscle Isometric Contractility

In vitro organ bath studies were conducted as previously described (56, 57). Excised anterior prostates were weighed and sutures (5-0) were used to secure the prostate and bladder at the base to the specimen arm and the tip of the prostate to the force displacement transducer. Prostates were suspended in 37°C water-jacketed tissue chamber filled with Krebs solution (133 mM NaCl, 16 mM $HaHCO_3$, 5 mM KCl, 1 mM $mgCl_2$, 1.4 mM NaH_2PO_4, 2.5 mM $CaCl_2$, 7.8 mM D-Glucose, pH 7.2) aerated with 95% O_2 / 5% CO_2. Tissues were maintained at a tension of 0.7 g for 60 min before experimentation, with Krebs solution changed every 15 min. Tension was recorded using the AxoScope Application of PCLAMP software (Molecular Devices, Sunnyvale, CA). Tissue baths stimulated with a concentration response curve to the alpha-adrenergic agonist phenylephrine (0.0001 μM, 0.01 μM, 1 μM, 100 μM, and 200 μM) was performed. Next, 100 μM phenylephrine was added and tension was recorded until baseline was reached to measure relaxation response. After a final washout and return to baseline for 30 mins, tissues were maximally contracted with 60 mM KCl. Tissue responses were normalized to maximum response to KCl and expressed as a percentage thereof.

Assessment of myosin light chain phosphorylation

Six-week-old C57Bl6/J male mice were given subcutaneous hormone implants (25 mg testosterone and 2.5 mg 17-β estradiol) or a sham surgery as described previously (6, 56) and aged to eight weeks. Mice were euthanized via CO_2 asphyxiation and anterior prostates were removed and stored in ice cold 1X phosphate buffered saline (pH=7). At the time of experimentation, prostates were suspended in 37°C water-jacketed tissue chamber filled with Krebs solution (133 mM NaCl, 16 mM $HaHCO_3$, 5 mM KCl, 1 mM $mgCl_2$, 1.4 mM NaH_2PO_4, 2.5

mM $CaCl_2$, 7.8 mM D-Glucose, pH 7.2) aerated with 95% O_2 / 5% CO_2. Tissues were pre-incubated for 10 minutes to normalize to temperature and buffer. Phenylephrine (100 μM) was added to the media and tissues were snap frozen .5, 3, 6, and 12 minutes later. *RNA Isolation and RT-PCR*

Prostate lobes were homogenized as described previously (Tengowski et al., 1997). RNA was purified with Illustra RNAspin Minikit (GE Healthcare, Pittsburgh, PA) and reverse transcribed with the SuperScript III First Strand Synthesis System (Invitrogen, Carlsbad, CA). Real time PCR was performed in 10.5 μl reactions containing 1x SsoFast EvaGreen Supermix (Bi-Rad Laboratories, Hercules, CA), 0.48 μM PCR primers, and 3.75 μL cDNA and amplified using CFX96 PCR machine (Bio-Rad Laboratories). Relative abundance of *Ppp1r12b, Ppp1r12a*, *Ppp1r16b*, *Ppp1r12c*, and *Ppp1r16a* mRNAs was determined by RT-PCR. PCR primers are listed in **Supplementary Table 1**. Relative mRNA abundance was determined by the deltaC_T method as described previously (Livak KJ, Schmittgen TD. 2001) and results were normalized to the abundance of *Ppia*.

SDS- PAGE and Western Immunoblotting

Prostates from mice exposed to T+E2 for two weeks or from mice receiving a sham surgery were homogenized using the TissueLyser LT system (Qiagen) in RIPA buffer containing protease and phosphatase inhibitors (Santa Cruz Biotechnology, Dallas, TX). Equal amounts of proteins (15 μg) were separated by SDS-PAGE and transferred to a PVDF membrane. Membranes were blocked in TBS-T (50 mM Tris [pH 7.5], 300 mM NaCl, 0.5% Tween 20) containing 5% non-fat milk for 1 hour and incubated with primary antibody (anti-PPP1R12B, Atlas Antibodies, Sweden, HPA024171, 1:5000 dilution or anti-GAPDH, Cell Signaling Technology, Danvers, MA, 5174, 1:2000 dilution) in blocking buffer overnight at 4°C. Membranes were then washed in TBS-T and incubated with anti-rabbit HRP-conjugated secondary antibody (1:1000 dilution, Bethyl Laboratories, Motngomery, TX) in blocking buffer for 1 hour at room temperature.

Proteins were visualized using a chemiluminescent substrate and the BioRad ChemiDocMP Imaging system. Densitometry was performed using ImageJ software.

Immunohistochemistry

Paraffin embedded tissue sections (10 μm) were deparaffinized with xylene and rehydrated in a series of graded concentrations of ethanol. Immunofluorescence staining was conducted as described previously (59, 60). Anti-smooth muscle actin (Leica, ncl-l-sma, RRID: AB_442134, 1:250) and anti-PPP1R12B (abcam, ab32519, RRID: AB_2168426, 1:100), primary antibodies were used to identify smooth muscle and PPP1R12B, respectively. Tissue sections were imaged using an SP8 confocal microscope (Leica Wetzlar, Germany) fitted with a 20X oil immersion objective (HC PL Apo CS2 NA = 0.75; Leica, Wetzlar, Germany). Ten z-stack images were captured at 1024x1024 resolution and a Z-interval of 1 μm using LASX 8 software (Leica, Wetzlar, Germany). The detector gain ranged between 10-30 using Hy-D detector. All fluorescent images were stained using Alexa 488, Rhodamine red, and Alexa 647 secondary antibodies fluorophore signals were separated using the sequential imaging protocol. All images were manipulated to adjust whole image RGB color intensity using Adobe Photoshop for figures (version 20.0).

Void Spot Assay

Urinary function in C57Bl6/J sham and T+E2 treated, Ppp1r12b wildtype, heterozygous, and null mice was assessed in six-, seven-, and eight-week-old male mice via the void spot assay as previously described (61). Briefly, mice were placed on chromatography paper for 4 hours. Papers were imaged using an Autochemi AC1 Darkroom ultraviolet imaging cabinet (UVP, Upland, CA) equipped with an Auto Chemi Zoom lens 2UV and an epi-illuminator. Image capture settings were adjusted using UVP VisonWorksLS image-acquisition software and settings remained the same throughout imaging. Images were captured using an ethidium bromide filter set (570-640 nm) and 365-nm epi-illumination. Void Whizzard, an in-house software, was downloaded at http://imagej.net/Void_Whizzard and used to analyze the void spot papers (61).

Analyzed parameters included: total spot count, total void area (cm^2), percent area in corners, percent area in center, and mass distribution of spots.

Statistical Analysis

The number of mice per group ranged from 4-22 and each experimental group represented at least three independent litters. GraphPad Prism was used for statistical analysis (version 8.2.1) and differences at $p \leq 0.05$ were considered significant. Bartlett's test was used to determine homogeneity of variance and when necessary, data were transformed to achieve homogeneity of variance The Shapiro-Wilk test was used to assess normality of residuals ($p \leq 0.05$ indicating non-normal data). Differences ($P \leq 0.05$) between or among groups were identified using Student's t-test (analysis of absolute urine velocity, RT-PCR expression, tissue bath relaxation analysis, GCaMP relaxation analysis, western blot expression), analysis of variance (ANOVA) (tissue bath relaxation comparing Ppp1r12b genetic depletion genotypes), nonlinear regression (phenylephrine dose response analysis). Two-way ANOVA with Sidak's multiple comparisons test was used to identify significant differences among treatment groups over multiple timepoints post phenylephrine administration. Data that did not meet the criteria for homogeneity of variance or normality were transformed (log or square root transformed).

Acknowledgements

This work was supported by National Institutes of Health Grants R01ES001332, R01DK119615, R01HD094759, U54DK104310, T32ES007015, F31ES030968. The content is solely the responsibility of the authors and does not necessarily represent the official views of the National Institutes of Health.

References

1. H. Lepor, Pathophysiology of Lower Urinary Tract Symptoms in the Aging Male Population. *Rev Urol* **7**, S3–S11 (2005).

2. A. B. Araujo, *et al.*, Sleep-related problems and urologic symptoms: Testing the hypothesis of bi-directionality in a longitudinal, population-based study. *J Urol* **191** (2014).

3. A. Bélanger, *et al.*, Changes in serum concentrations of conjugated and unconjugated steroids in 40- to 80-year-old men. *J. Clin. Endocrinol. Metab.* **79**, 1086–1090 (1994).

4. M. Caine, R. Shlomo, Z. Marcia, *Adrenergic adn Cholinergic Receptors in teh Human Prostate, Prostatic Capsule and Bladder Neck* (British Journal of Urology, 1975).

5. J. Ma, *et al.*, Prostatic Fibrosis is Associated with Lower Urinary Tract Symptoms. *J Urol* **188**, 1375–1381 (2012).

6. T. M. Nicholson, *et al.*, Testosterone and 17β-estradiol induce glandular prostatic growth, bladder outlet obstruction, and voiding dysfunction in male mice. *Endocrinology* **153**, 5556–5565 (2012).

7. J. Bernoulli, *et al.*, Prostatic inflammation and obstructive voiding in the adult noble rat: Impact of the testosterone to estradiol ratio in serum. *The Prostate* **68**, 1296–1306 (2008).

8. T. Streng, *et al.*, Developmental, estrogen induced infravesical obstruction is reversible in adult male rodents. *J. Urol.* **168**, 2263–2268 (2002).

9. T. K. Streng, A. Talo, K.-E. Andersson, R. Santti, A dose-dependent dual effect of oestrogen on voiding in the male mouse? *BJU Int.* **96**, 1126–1130 (2005).

10. P. C. Walsh, J. D. Wilson, The induction of prostatic hypertrophy in the dog with androstanediol. *J. Clin. Invest.* **57**, 1093–1097 (1976).

11. J. K. Byron, K. H. Taylor, G. S. Phillips, M. S. Stahl, Urethral Sphincter Mechanism Incompetence in 163 Neutered Female Dogs: Diagnosis, Treatment, and Relationship of Weight and Age at Neuter to Development of Disease. *J Vet Intern Med* **31**, 442–448 (2017).

12. M. Gopal, *et al.*, Association of Change in Estradiol to Lower Urinary Tract Symptoms During the Menopausal Transition. *Obstet Gynecol* **112**, 1045 (2008).

13. R. C. Webb, Smooth muscle contraction and relaxation. *Advances in Physiology Education* **27**, 201–206 (2003).

14. M. E. Grassie, L. D. Moffat, M. P. Walsh, J. A. MacDonald, The myosin phosphatase targeting protein (MYPT) family: A regulated mechanism for achieving substrate specificity of the catalytic subunit of protein phosphatase type 1δ. *Archives of Biochemistry and Biophysics* **510**, 147–159 (2011).

15. A. Chao, *et al.*, Site-Specific Phosphorylation of Protein Phosphatase 1 Regulatory Subunit 12A Stimulated or Suppressed by Insulin. *J Proteomics* **75**, 3342–3350 (2012).

16. E. Scotto-Lavino, M. Garcia-Diaz, G. Du, M. A. Frohman, Basis for the Isoform-specific Interaction of Myosin Phosphatase Subunits Protein Phosphatase 1c β and Myosin Phosphatase Targeting Subunit 1. *J Biol Chem* **285**, 6419–6424 (2010).

17. R. P. Dippold, S. A. Fisher, A bioinformatic and computational study of myosin phosphatase subunit diversity. *Am J Physiol Regul Integr Comp Physiol* **307**, R256–R270 (2014).

18. W.-Q. He, *et al.*, Altered contractile phenotypes of intestinal smooth muscle in mice deficient in myosin phosphatase target subunit 1. *Gastroenterology* **144**, 1456–1465, 1465.e1–5 (2013).

19. M. C. Payne, *et al.*, Dynamic changes in expression of myosin phosphatase in a model of portal hypertension. *Am J Physiol Heart Circ Physiol* **286**, H1801-1810 (2004).

20. T. T. Liu, *et al.*, Ultrasonography of the Adult Male Urinary Tract for Urinary Functional Testing. *J Vis Exp* (2019) https:/doi.org/10.3791/59802 (October 7, 2019).

21. K. E. Andersson, H. Lepor, M. G. Wyllie, Prostatic alpha 1-adrenoceptors and uroselectivity. *Prostate* **30**, 202–215 (1997).

22. K.-E. Andersson, C. Gratzke, Pharmacology of alpha1-adrenoceptor antagonists in the lower urinary tract and central nervous system. *Nat Clin Pract Urol* **4**, 368–378 (2007).

23. C. G. Roehrborn, D. A. Schwinn, Alpha1-adrenergic receptors and their inhibitors in lower urinary tract symptoms and benign prostatic hyperplasia. *J. Urol.* **171**, 1029–1035 (2004).

24. W. A. Ricke, *et al.*, Prostatic hormonal carcinogenesis is mediated by in situ estrogen production and estrogen receptor alpha signaling. *FASEB J.* **22**, 1512–1520 (2008).

25. W. A. Ricke, *et al.*, Steroid hormones stimulate human prostate cancer progression and metastasis. *Int. J. Cancer* **118**, 2123–2131 (2006).

26. C.-L. Cheng, W. C. de Groat, Effect of orchiectomy and testosterone replacement on lower urinary tract function in anesthetized rats. *American Journal of Physiology-Renal Physiology* **311**, F864–F870 (2016).

27. N. N.-C. Tam, *et al.*, Increased susceptibility of estrogen-induced bladder outlet obstruction in a novel mouse model. *Laboratory Investigation* **95**, 546–560 (2015).

28. T. T. Liu, *et al.*, Prostate enlargement and altered urinary function are part of the aging process. *Aging (Albany NY)* **11**, 2653–2669 (2019).

29. D. T. McLean, *et al.*, MRI-based method for lower urinary tract dysfunction in adult male mice. *Am J Clin Exp Urol* **7**, 153–158 (2019).

30. M. Tojo, *et al.*, Relationship Between Bladder Neck Diameter and Hydraulic Energy at Maximum Flow. *The Journal of Urology* **152**, 144–149 (1994).

31. J. L. St. Sauver, S. J. Jacobsen, Inflammatory Mechanisms Associated with Prostatic Inflammation and Lower Urinary Tract Symptoms. *Curr Prostate Rep* **6**, 67–73 (2008).

32. J. C. Kim, *et al.*, Alteration of Autonomic Function in Female Urinary Incontinence. *Int Neurourol J* **14**, 232–237 (2010).

33. National Toxicology Program, NTP Toxicology and Carcinogenesis Studies of Phenylephrine Hydrochloride (CAS No. 61-76-7) in F344/N Rats and B6C3F1 Mice (Feed Studies). *Natl Toxicol Program Tech Rep Ser* **322**, 1–172 (1987).

34. Freay Ana D., Curtis Sylvia W., Korach Kenneth S., Rubanyi Gabor M., Mechanism of Vascular Smooth Muscle Relaxation by Estrogen in Depolarized Rat and Mouse Aorta. *Circulation Research* **81**, 242–248 (1997).

35. X. Zhang, *et al.*, Testosterone regulates smooth muscle contractile pathways in the rat prostate: emphasis on PDE5 signaling. *American Journal of Physiology-Endocrinology and Metabolism* **302**, E243–E253 (2011).

36. X. Gamé, *et al.*, Estradiol increases urethral tone through the local inhibition of neuronal nitric oxide synthase expression. *Am J Physiol Regul Integr Comp Physiol* **294**, R851-857 (2008).

37. J. Hajagos-Tóth, *et al.*, The effects of estrogen on the α2-adrenergic receptor subtypes in rat uterine function in late pregnancy in vitro. *Croat Med J* **57**, 100–109 (2016).

38. M. Phillippe, T. Saunders, S. Bangalore, A mechanism for testosterone modulation of alpha-1 adrenergic receptor expression in the DDT1 MF-2 smooth muscle myocyte. *Mol Cell Biochem* **100**, 79–90 (1991).

39. W. P. Dirksen, F. Vladic, S. A. Fisher, A myosin phosphatase targeting subunit isoform transition defines a smooth muscle developmental phenotypic switch. *Am J Physiol Cell Physiol* **278**, C589-600 (2000).

40. K. T. McVary, A. Rademaker, G. L. Lloyd, P. Gann, Autonomic nervous system overactivity in men with lower urinary tract symptoms secondary to benign prostatic hyperplasia. *J. Urol.* **174**, 1327–1433 (2005).

41. M. Ishigooka, *et al.*, Correlation between morphometric differences and norepinephrine content in benign prostatic hyperplasia. *Prostate* **28**, 385–391 (1996).

42. D. I. Gup, E. Shapiro, M. Baumann, H. Lepor, Contractile properties of human prostate adenomas and the development of infravesical obstruction. *Prostate* **15**, 105–114 (1989).

43. S. A. Kaplan, Factors in Predicting Failure with Medical Therapy for BPH. *Rev Urol* **7**, S34–S39 (2005).

44. C. G. Roehrborn, BPH progression: concept and key learning from MTOPS, ALTESS, COMBAT, and ALF-ONE. *BJU Int.* **101 Suppl 3**, 17–21 (2008).

45. S. T. Nguyen, R. Prakash, C. J. Anderson, M. Frydenberg, J. M. Haynes, Sex steroids modulate α1-adrenoceptor-stimulated Ca2+ elevation in human cultured prostatic stromal cells. *The Prostate* **67**, 74–82 (2007).

46. K. T. Gray, J. L. Short, E. R. Simpson, S. Ventura, The effects of targeted deletion of the aromatase enzyme on prostatic contractile responses to noradrenaline in mice. *J. Endocrinol.* **195**, 495–502 (2007).

47. P. Smith, N. P. Rhodes, Y. Ke, C. S. Foster, Modulating effect of estrogen and testosterone on prostatic stromal cell phenotype differentiation induced by noradrenaline and doxazosin. *The Prostate* **44**, 111–117 (2000).

48. J. Zhang, *et al.*, Human prostatic smooth muscle cells in culture: estradiol enhances expression of smooth muscle cell-specific markers. *Prostate* **30**, 117–129 (1997).

49. C. Ding, *et al.*, The PEAK1-PPP1R12B axis inhibits tumor growth and metastasis by regulating Grb2/PI3K/Akt signalling in colorectal cancer. *Cancer Lett.* **442**, 383–395 (2019).

50. M. B. Freidin, A. V. Polonikov, Validation of PPP1R12B as a candidate gene for childhood asthma in Russians. *J. Genet.* **92**, 93–96 (2013).

51. S. M. Kas, *et al.*, Insertional mutagenesis identifies drivers of a novel oncogenic pathway in invasive lobular breast carcinoma. *Nat. Genet.* **49**, 1219–1230 (2017).

52. J. Lartey, J. Taggart, S. Robson, M. Taggart, Altered Expression of Human Smooth Muscle Myosin Phosphatase Targeting (MYPT) Isovariants with Pregnancy and Labor. *PLOS ONE* **11**, e0164352 (2016).

53. A. S. Pereyra, *et al.*, BDA-410 Treatment Reduces Body Weight and Fat Content by Enhancing Lipolysis in Sedentary Senescent Mice. *J. Gerontol. A Biol. Sci. Med. Sci.* **72**, 1045–1053 (2017).

54. X. Xing, *et al.*, Adipose-derived mesenchymal stem cells-derived exosome-mediated microRNA-342-5p protects endothelial cells against atherosclerosis. *Aging (Albany NY)* **12**, 3880–3898 (2020).

55. W. Y, *et al.*, Cyclic Stretch-Induced the Cytoskeleton Rearrangement and Gene Expression of Cytoskeletal Regulators in Human Periodontal Ligament Cells. *Acta odontologica Scandinavica* **75** (2017) Available at: https://pubmed.ncbi.nlm.nih.gov/28681629/?from_term=Ppp1r12b&from_page=2&from_pos=1 [Accessed April 9, 2020].

56. K. P. Keil, *et al.*, Impact of a folic acid-enriched diet on urinary tract function in mice treated with testosterone and estradiol. *American Journal of Physiology-Renal Physiology* **308**, F1431–F1443 (2015).

57. M. W. Tengowski, D. E. Bjorling, R. M. Albrecht, R. Saban, Use of gold-labeled ovalbumin to correlate antigen deposition and localization with tissue response. *J Pharmacol Toxicol Methods* **37**, 15–21 (1997).

58. C. M. Vezina, *et al.*, Retinoic Acid Induces Prostatic Bud Formation. *Dev Dyn* **237**, 1321–1333 (2008).

59. A. E. Turco, *et al.*, A temporal and spatial map of axons in developing mouse prostate. *Histochem. Cell Biol.* (2019) https:/doi.org/10.1007/s00418-019-01784-6.

60. L. L. Abler, *et al.*, A high throughput in situ hybridization method to characterize mRNA expression patterns in the fetal mouse lower urogenital tract. *J Vis Exp* (2011) https:/doi.org/10.3791/2912.

61. K. A. Wegner, *et al.*, Void spot assay procedural optimization and software for rapid and objective quantification of rodent voiding function, including overlapping urine spots. *Am. J. Physiol. Renal Physiol.* **315**, F1067–F1080 (2018).

Figures and Tables

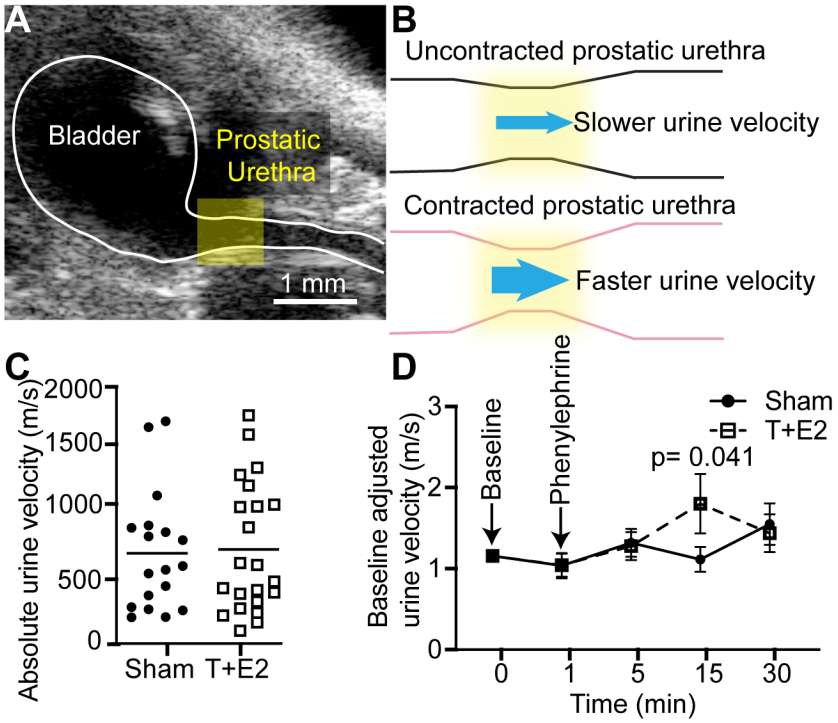

Figure 1. **Subcutaneous testosterone and estradiol (T+E2) implants increase the magnitude and sustain the urodynamic response to the alpha 1 adrenoreceptor agonist phenylephrine**. Six-week-old male C57BL/6J mice were sham operated or treated with subcutaneous implants of testosterone (T, 25 mg) and estradiol (E2, 2.5 mg). Two weeks later, mice were anaesthetized and a cystostomy tube was placed in the bladder to deliver DEFINITY contrast agent. (A) An ultrasound probe measures contrast agent velocity as it passes through the prostatic urethra. (B) Contracted prostatic urethra causes increased urethral urine velocity compared to uncontracted. Contrast agent velocity is related to prostatic urethral cross-sectional diameter. (C) Student's t-test determined the velocity of contrast agent measured at baseline was not impacted by T+E2 exposure alone. (D) Velocity of contrast agent was measured at baseline and 5, 10 and 15 min after phenylephrine exposure 10 µg/kg single bolus injection into the jugular vein. Using two-way ANOVA, T+E2 significantly enhances the urodynamic response to phenylephrine by increasing the velocity of contrast agent as it passes through the prostatic

urethra at 15 min post phenylephrine injection compared to the pre-phenylephrine treatment baseline (time zero). Results are n= 12-22 mice per group, representing 3 independent litters, $p \leq 0.05$ was considered significant.

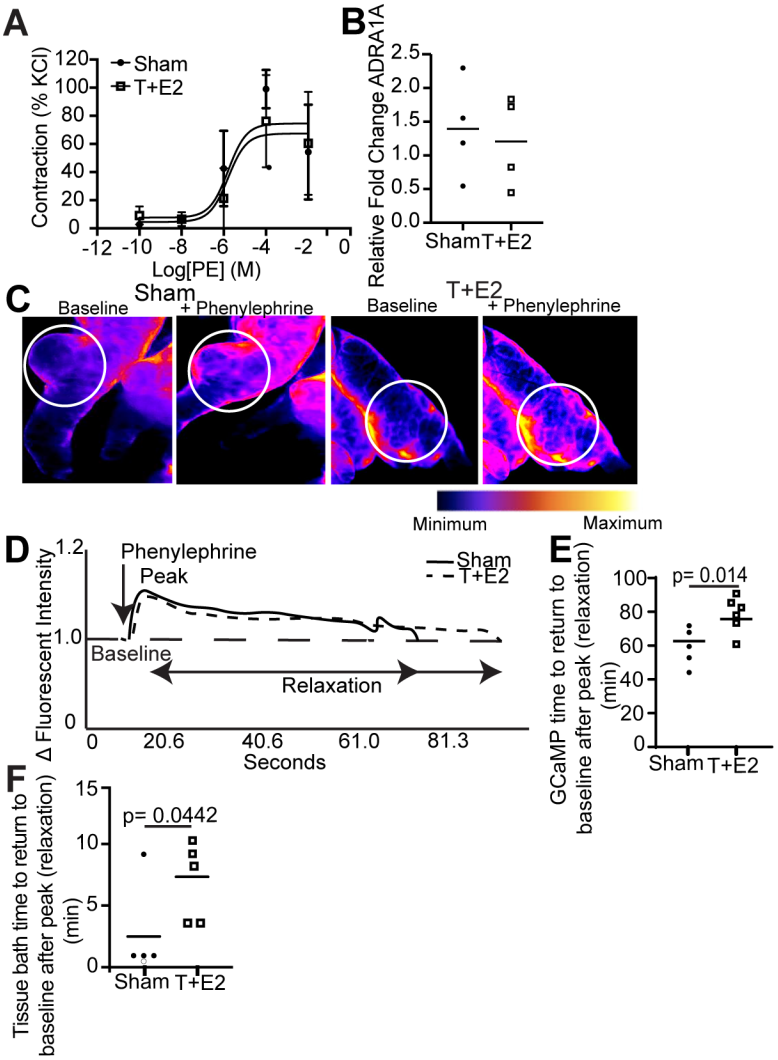

Figure 2. **Subcutaneous testosterone and estradiol (T+E2) implants slow prostatic smooth muscle recovery after alpha 1 adrenoreceptor mediated stimulation.** Six-week-old male *Myh11*$^{cre/+}$;gt(ROSA6f)/+ harboring fluorescent calcium sensors in prostatic smooth muscle, *Mych11*^{cre}/+; GCaMP5g/+)(GCaMP) or C57Bl/6J mice (tissue bath) were sham operated or treated with subcutaneous implants of testosterone (T, 25 mg) and estradiol (E2, 2.5 mg). Two weeks later, prostates were collected to quantify fluorescence or isometric contractility. GCaMP mouse prostates were placed in a perfusion chamber with 37°C HEPES buffer. Baseline fluorescence was recorded for 30 seconds and phenylephrine was administered for one minute. The prostatic response to phenylephrine was recorded for 10 minutes. Wild type mouse prostate

tissue was collected and stretched to 0.7 gram of tension, exposed to phenylephrine, and contraction and relaxation responses were examined. (A) Anterior prostate tension response to increasing concentrations of phenylephrine (0.0001- 200 μM) was unchanged after T+E2 exposure (percent maximum response to KCl) using non-linear regression. (B) Relative expression of *Adra1a* receptor mRNA levels were unchanged by T+E2 exposure in anterior prostate using Student's t-test. (C) A single dose of phenylephrine (100 mM) was added to the bath media to induce muscle contraction, the media was replaced with drug-free media and the time to return to baseline (0.7 g tension, recovery) was determined. T+E2 exposure significantly prolongs the recovery from phenylephrine-mediated prostatic smooth muscle contraction using Student's t-test. (D) Representative images of GCaMP fluorescence are shown 30 sec before (baseline) and 100 sec after phenylephrine administration into the perfusion chamber. Fluorescence intensity peaked after phenylephrine administration (0.2037 ug/ml) and the time from peak fluorescence to return to baseline was considered the recovery period. (E) T+E2 exposure significantly prolongs the recovery from phenylephrine-mediated prostatic smooth muscle contraction using Student's t-test. Results are n= 4-6 mice per group, representing 3 independent litters, $p \leq 0.05$ was considered significant.

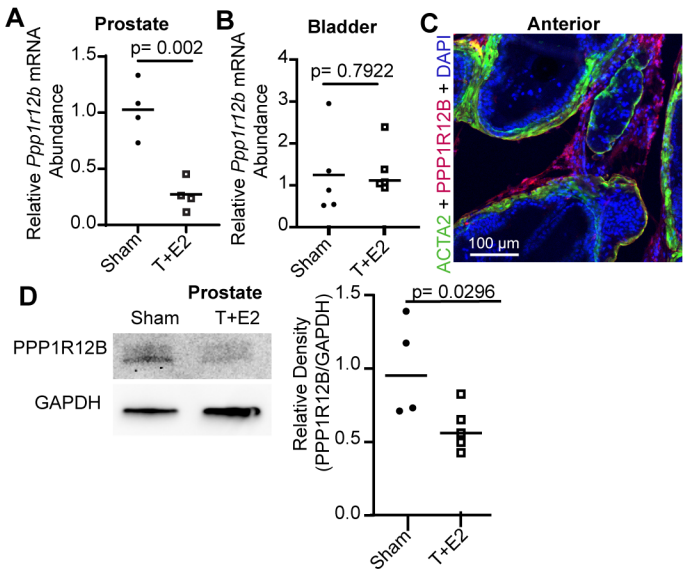

Figure 3. Myosin phosphatase PPP1R12B protein is expressed by prostatic smooth muscle and T+E2 significantly decreases its abundance. (A) Six-week-old male C57BL/6J mice were sham operated or treated with subcutaneous implants of testosterone (T, 25 mg), estradiol (E2, 2.5 mg) or a combination of T+E2 for two weeks. RT-PCR was used to assess anterior prostatic *Ppp1r12b* mRNA abundance two weeks later. *Ppp1r12b* expression is significantly downregulated by T+E2 exposure. *Pppr1r12b* mRNA abundance is normalized to that of *Ppia*. (B) RT-PCR was used to assess bladder *Ppp1r12b* mRNA abundance two weeks later and normalized to that of *Ppia*. (C) Immunostaining was used to localize PPP1R12B to actin alpha 2 (ACTA2) positive prostatic smooth muscle in the ventral prostate of eight-week-old mice. Nuclei are stained with DAPI. (D) Immunoblotting was used to quantify PPP1R12B protein in mice given a sham or subcutaneous implant of T+E2 for two weeks. Relative protein abundance is normalized to GAPDH abundance. T+E2 significantly reduces *Ppp1r12b* mRNA abundance in dorsal and anterior prostate. Student's t-test assessed differences between treatments and groups. Results are n= 4-5 mice per group, representing 3 independent litters, $p \leq 0.05$ was considered significant.

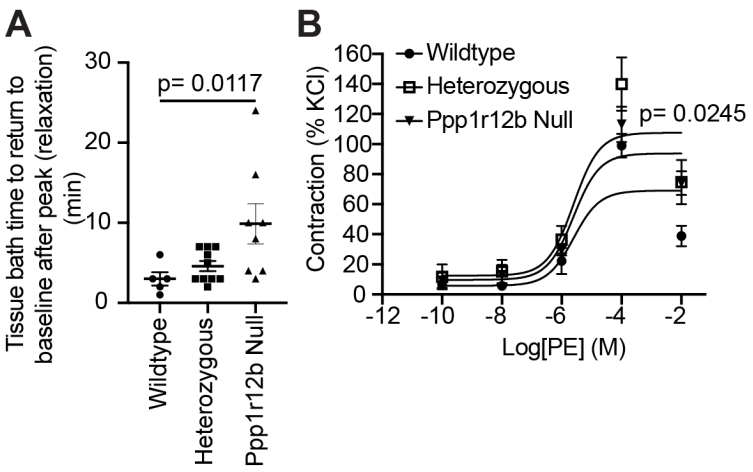

Figure 4. Genetic depletion of *Ppp1r12b* slows recovery of stimulated prostatic smooth muscle. (A) Prostate tissue was collected and stretched to 0.7 gram of tension and contraction and relaxation responses were examined. A single dose of phenylephrine (100 mM) was added to the bath media to induce muscle contraction and the time to return to baseline (0.7 g tension) was determined. (A) *Ppp1r12b* null (mutant) mouse prostate takes significantly longer than wild type mouse prostate to recovery from phenylephrine-mediated contraction. (B) Graded doses of phenylephrine were added to the media and response to each dose was normalized to the maximal contraction from KCL. No significant shift in the dose response curves was observed with genotype but the max response to -2 M phenylephrine was significantly greater in mutant mice than wildtype mice, indicating significantly delayed relaxation in mutant mice. One-way ANOVA, two-way ANOVA, and non-linear regression analysis was used to analyze differences between genotypes. Results are mean ± SE, n= 6-10 mice per group, representing 3 independent litters, $p \leq 0.05$ was considered significant.

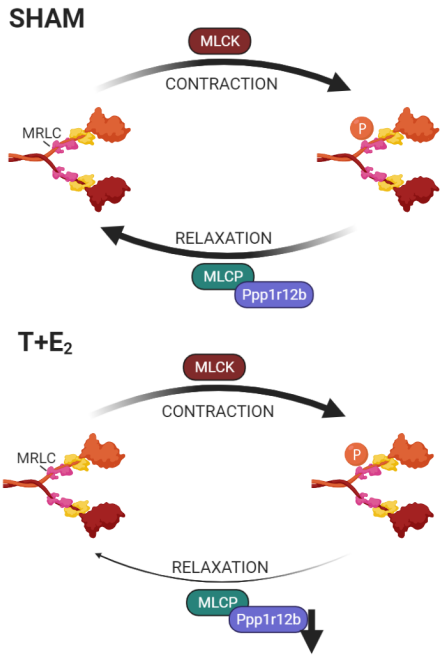

Figure 5. Proposed mechanism underlying T+E2-induced urinary dysfunction in mice. The ratio of testosterone to estradiol that men experience as they age causes bladder outlet obstruction due to delayed prostate smooth muscle relaxation caused by downregulation of PPP1R12B.

Supplementary Table 1. RT-PCR primers

Target	Left Primer	Right Primer
Ppp1r12a	AGGAGAAAGACACTGCAGGCG	AGTCGCCTTGGGATTGTAGG
Ppp1r12b	CAATCCGACCAGCAGCGATTC	CTGTCCTCTTCTACCCGGCTG
Ppp1r16a	TCTGTTGATGCTGGGACCTCC	CTTCTCCACAGACGCCTCCTC
Ppp1r12c	CACAAGGTGCTGGCTGAATGG	TCACCTCGATGTAGCCCTTGG
Ppp1r16b	CTTGCCTCACTCAATGCCTGC	TGCAGAAGTGAGATCCCAGGC
Adra1a	ACTGCTTACTCCGCTGCCTTC	AGCCAAGAGAGAAAGCCGAGG

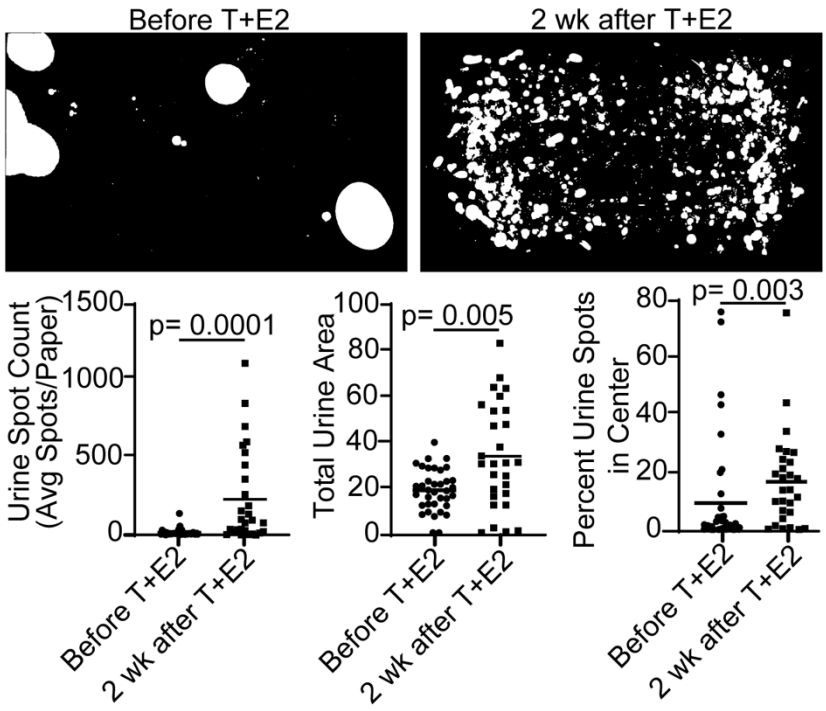

Figure S1. Subcutaneous testosterone and estradiol (T+E2) implants drive voiding dysfunction in male mice. Six-week-old male C57BL/6J mice were sham operated or treated with subcutaneous implants of testosterone (T, 25 mg) and estradiol (E2, 2.5 mg). The void spot assay was used to measure spontaneous voiding behaviors one day before (pre-pellet) and two weeks after T+E2 implants. (Top) Images of void spot filter papers before and two weeks after T+E2 treatment were evaluated using Void Whizzard software to quantify voiding patterns. Results are of 30-35 mice per group. Student's t-test (percent urine spots in center) and Mann-Whitney test (urine spot count, total urine area) were used to identify differences between groups. T+E2 exposure at two weeks significantly increases urine spot count, total urine area, and percent of urine spots in the center of the filter paper.

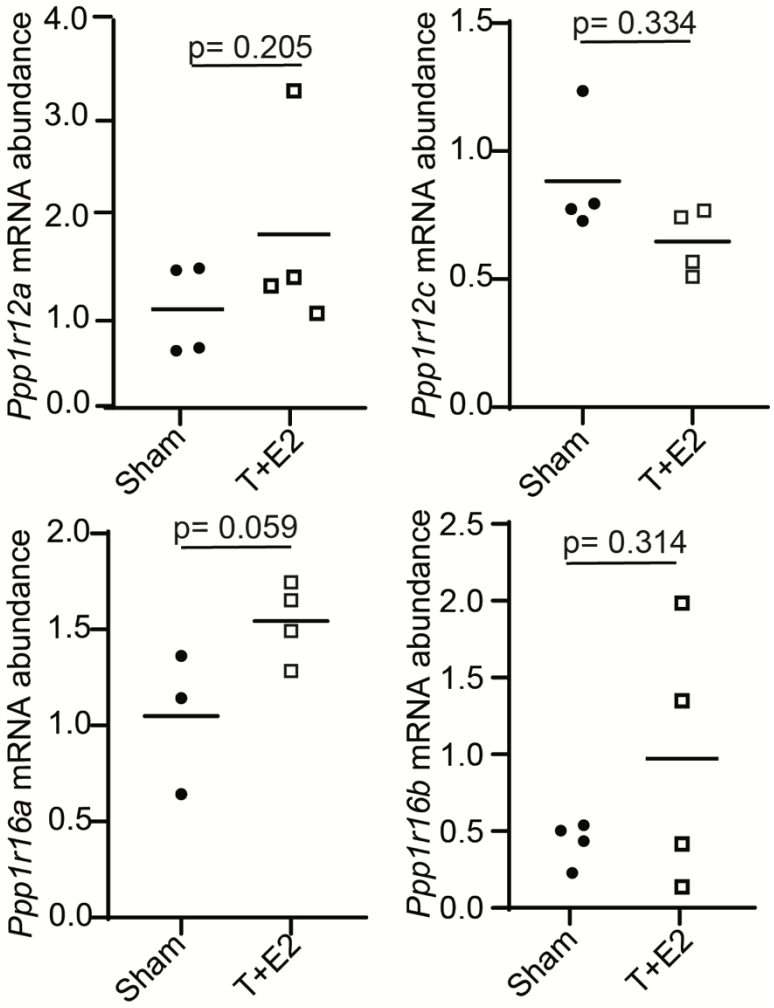

Figure S2. T+E2 implants do not significantly change mRNA abundance of r myosin phosphatase regulatory subunits *Ppp1r12a*, *Ppp1r12c, Ppp1r16a, or Ppp1r16b* in the anterior prostate. Six-week-old male C57BL/6J mice were sham operated or treated with subcutaneous implants of testosterone (T, 25 mg), estradiol (E2, 2.5 mg) or a combination of T+E2 for two weeks. RT-PCR was used to assess anterior prostatic *Ppp1r12a*, *Ppp1r12c, Ppp1r16a, Ppp1r16b,* mRNA abundance two weeks later. *Pppr1r* mRNA abundance is normalized to that of *Ppia*. Groups are compared using Student's t-test. Results are n= 4 mice per group, each group represents 3 independent litters, $p \leq 0.05$ was considered significant.

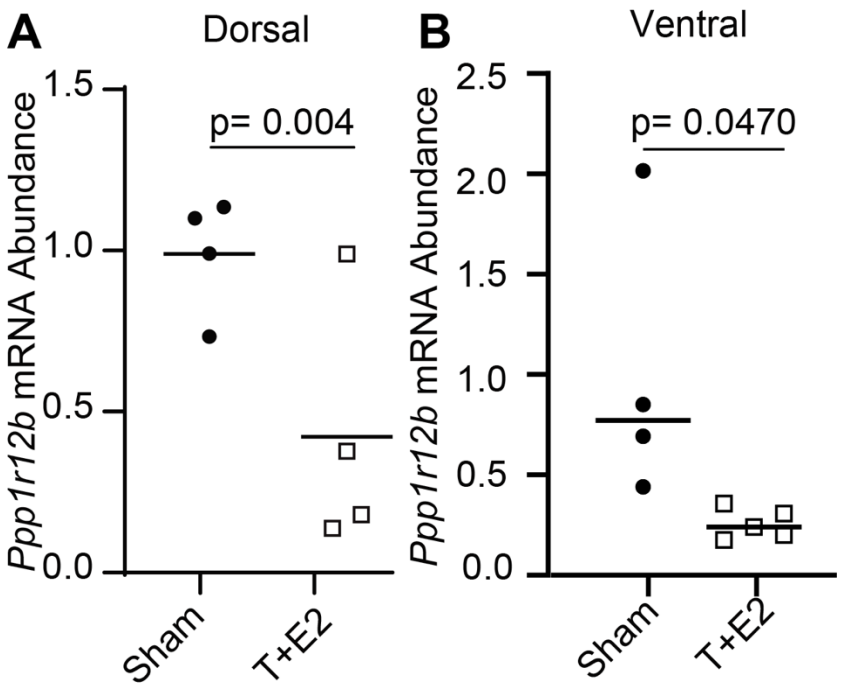

Figure S3. T+E2 significantly reduces *Ppp1r12b* mRNA abundance in ventral and dorsal prostate . Six-week-old male C57BL/6J mice were sham operated or treated with subcutaneous implants of testosterone (T, 25 mg), estradiol (E2, 2.5 mg) or a combination of T+E2 for two weeks. RT-PCR was used to assess anterior prostatic *Ppp1r12b* mRNA abundance two weeks later. *Pppr1r12b* mRNA abundance is normalized to that of *Ppia*. (A) *Ppp1r12b abundance* is significantly downregulated by T+E2 exposure in dorsal prostate lobes. (B) *Ppp1r12b* expression is significantly downregulated by T+E2 exposure in ventral prostate lobes. Groups are compared using Student's t-test. Results are n= 4 mice per group, each group represented 3 independent litters, $p \leq 0.05$ was considered significant.

Chapter 6: Conclusions and Future Directions

Turco AE

Identify the mechanism of prostate smooth muscle dysfunction in mice

The causes of LUTD in aging men are not fully known, but excessive prostate smooth muscle tone is a likely contributor. No studies have conclusively determined if or how prostate smooth muscle tone is increased in men with LUTD, and no study has determined why therapeutic responses to alpha-1 adrenergic receptor antagonists are so variable. I identified two mechanisms by which aggregate prostate smooth muscle tone may be increased: by endocrine-mediated impairment of muscle relaxation and by an environmentally mediated increase in the density of axons that drive prostatic smooth muscle contraction. Further, I created and validated tools to quantify axons in histological sections of the prostate, to measure prostate smooth muscle dynamics, and determine the impact of smooth muscle contraction on urethral urine flow. These methods enable future research to determine why some individuals are predisposed to prostatic smooth muscle dysfunction and why some men are resistant to alpha blockers. I offer my recommendations for future directions of my dissertation work.

Non-biased quantification of axons in developing and adult prostate

The prostate is innervated with various axon subtypes including noradrenergic, cholinergic, and sensory that regulate prostate smooth muscle contraction, secretion, and homeostasis (1, 2). Axons have been mapped and studied using immunohistochemistry and retrograde axon tracing dyes that, when injected into prostate, travel to the spinal cord (3, 4). In chapter 2, I discussed the difficulty of quantifying axons in mouse prostate because the tissue is heterogeneous, and counts can be skewed by differences in the density and size of prostate ducts in randomly sampled sections. We developed a robust method of quantification that is unbiased by the density and size of prostatic ducts in a microscopic field. Axon quantification was performed using FIJI, a free image analysis software developed by researchers at UW Madison. This versatile quantification technique can be modified to quantify fibrosis, immune cells, and smooth muscle density.

Changes in development, subtypes, or density of axons contribute to prostate disease. For example, autonomic axons infiltrate the tumor microenvironment and are denser in men with prostate cancer (5). Identifying the organization, density, composition, and development of axons in healthy prostate is critical to understand deviations caused by disease. To fill this gap, we provide a map of axons in healthy mouse prostate in chapter 2 (6). We determined the timing of noradrenergic, cholinergic, and sensory axon innervation of the prostate, we evaluated how the density of each axon subtype changes as prostate development proceeds, and how noradrenergic, cholinergic, and sensory axon density is distributed across the proximo-distal ductal axis of mouse prostate lobes (6). We determined that noradrenergic, cholinergic, and sensory axons innervate prostate at the same developmental stage, but further studies we conducted identified they likely migrate to the organ through different mechanisms. Future studies could identify which neurotrophic factors are expressed by the developing prostate, which are required for axon subtype development in prostate, which mediate axon spine development in prostate cancer, during benign hyperplastic prostate growth in aging men, or during prostate inflammation.

While my analysis of prostate neuroanatomical development was conducted in mice, I have not yet determined whether the results are generalizable across species. Future studies could use RNAScope and RNA-Sequencing to survey neurotrophin expression patterns in developing prostates of dogs, non-human primates, and humans. These studies could also examine the development of axons to determine whether the stage in which axons migrate to prostate is evolutionarily conserved across species, how axon patterns change during development, how axons are organized in healthy adult prostate, and how axon patterns change during clinically relevant disease processes such as benign hyperplasia and inflammation.

The strength of autonomic activity and density of prostate peripheral axons are susceptible to environmental chemical exposure

Environmental exposures to chemicals including alcohol, ethinylestradiol, heavy metals, pesticides, and di(2-ethylhexyl) phthalate) influence the prostate in many ways, from changing ductal development to driving cell proliferation to sensitizing to prostate cancer or LUTD (7–14). While previous toxicological studies involving the chemicals above focused on glandular development, they did not specifically examine prostate neuroanatomical development, even though peripheral axons are clearly susceptible to environmental chemicals. For example, TCDD disrupts the neural control of temperature regulation in golden hamsters and increases the activity of axons controlling rat aortic smooth muscle tone (15, 16). TCDD is also toxic to peripheral nervous system projections in red sea bream embryos (17). In chapter 3, we show TCDD exposure during the perinatal period increases the density of noradrenergic axons in the fetus, neonate, and adult and these changes are associated with heightened sensitivity of prostate smooth muscle to axon-evoked stimulation and LUTD (18). We provide evidence the key mechanism by which TCDD increases prostatic noradrenergic axon density is through an increase in the expression of artemin (*Artn*), a neurotrophin transcriptionally induced by the activated aryl hydrocarbon receptor (18, 19).

Our findings are paradigm shifting because no previous studies have shown a single exposure to an environmental chemical can permanently affect peripheral axon density and organ function leading to disease. We identify prostate axons as sensitive targets to the environmental contaminant TCDD. There are several interesting future directions that can advance our findings:

1. Study axon guidance factors and their role in healthy and diseased prostate. Our study identified dysregulation of one neurotrophin, Artemin (*Artn*), results in noradrenergic axon hyperinnervation, but does not change the density of other subtypes. It is known that nerve growth factor abundance decreases during prostate cancer progression while it increases during prostatitis, suggesting neurotrophic factors are malleable and activated or repressed in response to prostatic disease processes (20). In chapter 3, we identified *Artn* as a neurotrophic factor expressed in the developing prostate and it appears to

mediate noradrenergic axon recruitment to the developing prostate. Yet, it is not clear whether *Artn* is the only factor that mediates noradrenergic axon recruitment, whether it is required for prostate development, whether androgens control *Artn* abundance and whether *Artn* also recruits noradrenergic axons to the female urethra. Addressing these questions is critically important for understanding the scope of developmental origins of LUTD and determining whether a broader spectrum of endocrine disrupting chemicals, beyond TCDD, can also disrupt prostate neuroanatomical development. TCDD is a prototypical ligand for the AhR, but many ubiquitous environmental contaminants also serve as potent ligands, including members of the polychlorinated dibenzo furan, polychlorinated biphenyl, polycyclic aromatic hydrocarbon, and heterocyclic aromatic amine families. These chemicals are created through organic combustion, industrial byproducts, paper bleaching, and other processes and are present in trace amounts of cigarette smoke, personal care products, and animal food products. A future study could use *Artn* knockout mice to test whether *Artn* is required for TCDD-mediated hyperinnervation of the prostate or whether other AhR agonists lead to the same endpoint.

2. Identify whether environmental chemical exposure during adulthood impacts prostate innervation, smooth muscle function, or diseases susceptibility. In chapter 3, we established that environmental chemical exposure during development increases noradrenergic axon density, smooth muscle sensitivity to electrical field stimuli, and disease susceptibility. Environmental exposures to a range of chemicals during the critical window of prostate development may therefore be a risk factor for LUTD later in life. The fact that fetal exposure to the prototypical AhR ligand TCDD is associated with LUTD in adult mice contrasts with the outcomes from other studies focused on adult exposure, in which exposure to TCDD or other AhR ligands appears to be protective against LUTD (21, 22). It is clear from the results of other studies, and my own, that sensitivity to TCDD changes over the course of life, perhaps coinciding with the beginning and end of critical

developmental milestones (such as completion of prostate innervation), and that TCDD is likely to mediate its effects through diverse mechanisms that are life stage dependent. A study investigating peripheral axon density, muscle function, and neurotrophic factor expression in mice exposed in adulthood to TCDD would be valuable to further understand of the actions of TCDD in LUTD. I predict the window of vulnerability to TCDD-mediated increases in prostatic noradrenergic axon density closes after puberty, when I've previously shown that there is a plateau in the density of noradrenergic axons (18). Further, it would be interesting to examine whether administration of AHR agonist is protective in models of LUTD. Studying whether AHR activation in adulthood can reverse the damages caused by developmental exposure would provide insight into critical windows and potential new treatments for LUTD.

3. Elucidate the process of axon pruning in prostate and bladder by identifying which neurotrophic factors are involved, the developmental stage in which the factors are most highly expressed, and whether those factors are re-expressed during BPH or by injury / repair processes, such as those associated with prostatitis. These studies are important because axon pruning typically occurs during the final stages of organ development or after injury repair (23). Axons begin to invest in prostate at E13.5, the same developmental stage when TCDD was delivered in chapter 3. A study investigating how axon pruning in prostate is regulated, whether it is impacted by environmental chemical exposure, and how damaged prostate axons are repaired is critical to understanding whether prostate axon pruning is unique or whether it could be a new mechanism for disease.
4. Develop and optimize advanced methods for quantifying axons in peripheral tissues. We showed that IUL TCDD exposure increases noradrenergic axon density in the developing prostate through upregulation of *Artn*. ARTN controls noradrenergic axon development across many organ systems, and notably in vascular smooth muscle, which could be the mechanism for TCDD-induced hypertension (24, 25). Therefore, IUL TCDD exposure may

also increase noradrenergic axon density in these organ systems, offering a central mechanism for a host of disease processes that have already been linked to IUL TCDD exposure. The quantification method developed in chapter 2 is effective, but time consuming. Whole mount staining of axons with advanced clearing techniques to increase imaging depth and resolution could be a new method to qualitatively identify axon density changes using minimal prostate tissue and as a supplement for traditional two-dimensional immunostaining. Whole mount images can be quantified using the software Neurolucida. This software can accurately reconstruct neurons from histological samples and is capable of over 500 quantitative morphometric analyses including dendrite number, length width, and volume quantifications, and neural network quantification.

5. Examine whether prostates of men who respond to alpha-1 adrenergic antagonists have a lower density of noradrenergic axons than men who do not respond to the drug. It is unknown why some men have increased smooth muscle tone and respond to alpha blockers while others are resistant or develop resistance over time. We found the TCDD-mediated increase in prostatic noradrenergic axon density is associated with an increase in prostate smooth muscle sensitivity to electrical field stimulation (18). Prostatic noradrenergic axon density should be examined to test whether men with greater density are also at greater risk for LUTD. The results in chapter 3 reveal the importance of peripheral innervation as a driver of disease and we identified a new functionally relevant endpoint that could be examined as part of chemical and pharmaceutical risk assessments. The current battery of developmental and reproductive toxicity assays does not consider or address the potential for a chemical to cause LUTD by acting on the developing prostate, even though LUTD is experienced by nearly all men.

TCDD exposure acts through a non-malignant mechanism, independent if exogenous testosterone and estradiol, to cause LUTD

The foundational study involving TCDD and LUTD used Tg(CMV-*cre*);*Nkx3-1*(+/-);*Pten*(fl/+) mice that are genetically prone to prostatic neoplasia and concluded IUL TCDD exacerbates LUTD in a T+E2 induced mouse model of LUTD (11). The study did not pinpoint a mechanism of TCDD action and, because of the model system, created questions about whether TCDD exacerbated LUTD through a malignant or non-malignant mechanism. Addressing the mechanism of TCDD action was a priority because TCDD can accelerate and increase aggressiveness of prostate cancer in susceptible mice and prostate cancer can cause LUTD (26–28). It was critical to separate the effects of neoplasia from the effects of developmental environmental chemical exposure. In chapter 4, we treated C57Bl6/J mice which are not prone to prostate neoplasia with IUL TCDD and identified that TCDD exacerbated LUTD in mice that are not predisposed to neoplasia.

We showed that TCDD/T+E2 thickened prostate smooth muscle across two different strains of mice (11, 29). Our proteomic analysis also indicated that calcium flux and muscle proteins were dysregulated by TCDD/T+E2 exposure (29). Thickened prostate smooth muscle may indicate the muscle is stimulated more frequently or with greater intensity. Prostate smooth muscle may thicken in men with LUTD, but the causes are unknown. Similarly, heart muscle thickens in response to resistance due to atherosclerosis (30). A future study could investigate whether TCDD/T+E2 exposure causes excessive prostatic smooth muscle stimulation and whether administration of an alpha-1 adrenergic receptor antagonist reverses urinary frequency.

T+E2 interferes with prostatic smooth muscle relaxation to obstruct bladder outflow and LUTD

Increased prostate smooth muscle tone has been proposed as a mechanism for LUTD since the 1970's (31). The idea has persisted because drugs that relax prostate smooth muscle reduce LUTD symptoms in some men (32). Urethral pressure profiles identify the prostatic urethra

as the urethral segment with the greatest pressure, but the mechanism is not clear. Many factors can contribute to intraurethral pressure including benign prostatic hyperplasia, increased urethral stiffness due to prostatic fibrosis, and increased prostatic and urethral muscle tone (33). Mice treated with T+E2 void more frequently, have larger bladders, and are at increased risk of hydronephrosis, all phenotypes of obstructed bladder outflow obstruction (34). We proposed that T+E2 obstructs bladder outflow by increasing prostatic smooth muscle tone. Using a novel ultrasound-based assay to examine urethral fluid dynamics *in vivo*, we found that a single bolus dose of an alpha-adrenoreceptor agonist, given to T+E2 mice, increases urethral fluid velocity for at least 15 minutes (35). Although we did not directly determine whether T+E2 increases urine velocity by driving muscle contraction, prostatic hyperplasia, or fibrosis, because phenylephrine activates alpha-1 adrenoceptors, the influence of T+E2 on urethral tone appears to be mediated by a sustained prostatic muscle contraction. The idea of prostate smooth muscle contraction contributing to LUTD is not novel, but the idea that T+E2 levels contribute to impaired relaxation has not been explored. We draw new attention to the myosin phosphatase subunit, PPP1R12B which, when downregulated by T+E2, obstructs bladder outflow, increases voiding frequency, and slows prostate smooth muscle relaxation.

Our novel findings offer an aging-related decline in serum testosterone levels as a potential mechanism for resistance to alpha-1 adrenoceptor antagonists. Future isometric contractility experiments with human prostate tissue could correlate the ratio of serum testosterone to estradiol and the response to phenylephrine mediated contraction and relaxation and the prostatic abundance of PPP1R12B. Previous studies have suggested men may vary in the degree of prostate smooth muscle hyperactivity from spontaneous myogenic tone or excessive autonomic activity (36–39). Chemical library screens for small molecular inhibitors of PPP1R12B would be extremely valuable if expression in humans is variable. Inhibitors could be tested against individuals with LUTD or urinary stress incontinence, both which may benefit from

modulation of smooth muscle tone. If there is a correlation, the other subunits of the myosin phosphatase should be measured in humans to determine if they impact LUTD.

PPP1R12B is not localized exclusively to prostate. Previous studies linked PPP1R12B to breast and colorectal cancer, asthma, pregnancy and labor, atherosclerosis, cardiac muscle and skeletal muscle degeneration (40–46). We found T+E2 downregulates PPP1R12B in prostate and genetic depletion of *Ppp1r12b* interferes with smooth muscle relaxation (35). An extension of chapter 5 could quantify and compare expression of PPP1R12B in healthy mouse smooth muscle in heart, lung, ovary, urethra, prostate, and determine whether age and T+E2 treatment influences PPP1R12B abundance. It would also be interesting to test whether *Ppp1r12b* knockout mice exhibit abnormal smooth muscle relaxation in organs outside of the prostate. This possibility is supported by previously published evidence that reductions in testosterone increase blood pressure and temper asthma symptoms whereas increases in estrogen increase asthma symptoms (47, 48). Studies in *Ppp1r12b* null mice could elucidate what other effects tonic smooth muscle contraction has an impact on these organs.

Overall conclusions: prostate smooth muscle dysfunction in LUTD

The prostate clearly contributes to male LUTD because if removed, symptoms are eliminated. It is now clear prostate size is not the sole cause of LUTD in men. Multiple factors can make up the constellation of variable symptoms men experience. Some men achieve symptom relief from alpha-1 adrenergic antagonists, which relax prostate smooth muscle. It is unclear why some men have increased smooth muscle tone and respond to alpha-1 adrenergic antagonists. In this dissertation, I have proposed two novel mechanisms through which men may experience smooth muscle dysfunction in LUTD: fetal exposure to the environmental contaminant TCDD and an aging-related decline in testosterone and estradiol concentrations. **Figure 1** outlines how the two mechanisms identified in this thesis interact to exacerbate LUTD in mice. Developmental exposure to TCDD increases noradrenergic axon density and smooth muscle sensitivity to

contraction and adult T+E2 exposure downregulate *Ppp1r12b* to impair prostate smooth muscle relaxation leading to exacerbated LUTD. I have also developed and implemented several novel methodologies that enable new questions to be answered. My dissertation work along with the work of others will help shed light on a complex and multifactorial disease that will afflict most aging men and ultimately help to solidify understanding of the disease to create effective therapies for symptom relief.

References

1. J. N. Pennefather, W. A. Lau, F. Mitchelson, S. Ventura, The autonomic and sensory innervation of the smooth muscle of the prostate gland: a review of pharmacological and histological studies. *J Auton Pharmacol* **20**, 193–206 (2000).

2. S. Ventura, J. Pennefather, F. Mitchelson, Cholinergic innervation and function in the prostate gland. *Pharmacol. Ther.* **94**, 93–112 (2002).

3. M. Kepper, J. Keast, Immunohistochemical properties and spinal connections of pelvic autonomic neurons that innervate the rat prostate gland. *Cell Tissue Res.* **281**, 533–542 (1995).

4. I. Nadelhaft, Cholinergic axons in the rat prostate and neurons in the pelvic ganglion. *Brain Research* **989**, 52–57 (2003).

5. B. March, *et al.*, Tumour innervation and neurosignalling in prostate cancer. *Nat Rev Urol*, 1–12 (2020).

6. A. E. Turco, *et al.*, A temporal and spatial map of axons in developing mouse prostate. *Histochem. Cell Biol.* (2019) https:/doi.org/10.1007/s00418-019-01784-6.

7. L. S. Gomes, *et al.*, Aluminum disrupts the prenatal development of the male and female gerbil prostate (Meriones unguiculatus). *Exp. Mol. Pathol.* **107**, 32–42 (2019).

8. L. M. Lacorte, *et al.*, Early changes induced by short-term low-dose cadmium exposure in rat ventral and dorsolateral prostates. *Microsc. Res. Tech.* **74**, 988–997 (2011).

9. A. P. S. Perez, *et al.*, Prenatal exposure to ethinylestradiol alters the morphologic patterns and increases the predisposition for prostatic lesions in male and female gerbils during ageing. *Int J Exp Pathol* **97**, 5–17 (2016).

10. A. A. Pochettino, *et al.*, Effects of 2,4-dichlorophenoxyacetic acid on the ventral prostate of rats during the peri-pubertal, pubertal and adult stage. *Drug Chem Toxicol* **39**, 392–399 (2016).

11. W. A. Ricke, *et al.*, In Utero and Lactational TCDD Exposure Increases Susceptibility to Lower Urinary Tract Dysfunction in Adulthood. *Toxicol Sci* **150**, 429–440 (2016).

12. S. Roozen, *et al.*, Nocturnal incontinence in children with fetal alcohol spectrum disorders (FASD) in a South African cohort. *J Pediatr Urol* **13**, 496.e1-496.e7 (2017).

13. B. Xia, *et al.*, In utero and lactational exposure of DEHP increases the susceptibility of prostate carcinogenesis in male offspring through PSCA hypomethylation. *Toxicol. Lett.* **292**, 78–84 (2018).

14. L. You, K. A. Brenneman, H. d'A. Heck, In Utero Exposure to Antiandrogens Alters the Responsiveness of the Prostate to p,p′-DDE in Adult Rats and May Induce Prostatic Inflammation. *Toxicology and Applied Pharmacology* **161**, 258–266 (1999).

15. R. M. Bruno, *et al.*, Sympathetic regulation of vascular function in health and disease. *Front Physiol* **3**, 284 (2012).

16. C. J. Gordon, Y. Yang, L. E. Gray, Autonomic and behavioral thermoregulation in golden hamsters exposed perinatally to dioxin. *Toxicol. Appl. Pharmacol.* **137**, 120–125 (1996).

17. M. Iida, E.-Y. Kim, Y. Murakami, Y. Shima, H. Iwata, Toxic effects of 2,3,7,8-tetrachlorodibenzo-p-dioxin on the peripheral nervous system of developing red seabream (Pagrus major). *Aquat. Toxicol.* **128–129**, 193–202 (2013).

18. A. E. Turco, *et al.*, A developmental origin of lower urinary tract dysfunction. *JCI Insight* **Under Review** (2021).

19. T. Hidaka, *et al.*, The aryl hydrocarbon receptor AhR links atopic dermatitis and air pollution via induction of the neurotrophic factor artemin. *Nature Immunology* **18**, 64–73 (2017).

20. M. A. Pontari, M. R. Ruggieri, Mechanisms In Prostatitis/Chronic Pelvic Pain Syndrome. *J Urol* **172**, 839–845 (2004).

21. A. Gupta, *et al.*, Serum Dioxin, Testosterone, and Subsequent Risk of Benign Prostatic Hyperplasia: A Prospective Cohort Study of Air Force Veterans. *Environ Health Perspect* **114**, 1649–1654 (2006).

22. A. Gupta, A. Schecter, C. C. Aragaki, C. G. Roehrborn, Dioxin exposure and benign prostatic hyperplasia. *J Occup Environ Med* **48**, 708–714 (2006).

23. L. K. Low, H.-J. Cheng, Axon pruning: an essential step underlying the developmental plasticity of neuronal connections. *Philos Trans R Soc Lond B Biol Sci* **361**, 1531–1544 (2006).

24. L. N. Agbor, K. M. Elased, M. K. Walker, Endothelial cell-specific aryl hydrocarbon receptor knockout mice exhibit hypotension mediated, in part, by an attenuated angiotensin II responsiveness. *Biochem Pharmacol* **82**, 514–523 (2011).

25. Y. Honma, *et al.*, Artemin Is a Vascular-Derived Neurotropic Factor for Developing Sympathetic Neurons. *Neuron* **35**, 267–282 (2002).

26. J. A. Clark, *et al.*, Patients' Perceptions of Quality of Life After Treatment for Early Prostate Cancer. *JCO* **21**, 3777–3784 (2003).

27. W. A. Fritz, T.-M. Lin, R. W. Moore, P. S. Cooke, R. E. Peterson, In utero and lactational 2,3,7,8-tetrachlorodibenzo-p-dioxin exposure: effects on the prostate and its response to castration in senescent C57BL/6J mice. *Toxicol. Sci.* **86**, 387–395 (2005).

28. R. W. Moore, *et al.*, 2,3,7,8-Tetrachlorodibenzo-p-dioxin Has Both Pro-Carcinogenic and Anti-Carcinogenic Effects on Neuroendocrine Prostate Carcinoma Formation in TRAMP Mice. *Toxicol Appl Pharmacol* **305**, 242–249 (2016).

29. A. E. Turco, *et al.*, In utero and lactational 2,3,7,8-tetrachlorodibenzo-p-dioxin (TCDD) exposure exacerbates urinary dysfunction in hormone-treated C57BL/6J mice through a

non-malignant mechanism involving proteomic changes in the prostate that differ from those elicited by testosterone and estradiol. *Am J Clin Exp Urol* **8**, 59–72 (2020).

30. M. Rafieian-Kopaei, M. Setorki, M. Doudi, A. Baradaran, H. Nasri, Atherosclerosis: Process, Indicators, Risk Factors and New Hopes. *Int J Prev Med* **5**, 927–946 (2014).

31. M. Caine, S. Raz, M. Zeigler, Adrenergic and cholinergic receptors in the human prostate, prostatic capsule and bladder neck. *Br J Urol* **47**, 193–202 (1975).

32. H. Lepor, Alpha Blockers for the Treatment of Benign Prostatic Hyperplasia. *Rev Urol* **9**, 181–190 (2007).

33. T. Ishii, Y. Kambara, T. Yamanishi, Y. Naya, T. Igarashi, Urine Flow Dynamics Through Prostatic Urethra With Tubular Organ Modeling Using Endoscopic Imagery. *IEEE J Transl Eng Health Med* **2**, 1800709 (2014).

34. T. M. Nicholson, *et al.*, Testosterone and 17β-estradiol induce glandular prostatic growth, bladder outlet obstruction, and voiding dysfunction in male mice. *Endocrinology* **153**, 5556–5565 (2012).

35. A. E. Turco, *et al.*, Testosterone and estradiol mediate male voiding dysfunction by reducing prostatic smooth muscle Ppp112b abundance and impairing muscle relaxation. *PNAS* **Under review** (2021).

36. B. Chakrabarty, S. Lee, B. Exintaris, “Generation and Regulation of Spontaneous Contractions in the Prostate” in *Smooth Muscle Spontaneous Activity: Physiological and Pathological Modulation*, Advances in Experimental Medicine and Biology., H. Hashitani, R. J. Lang, Eds. (Springer Singapore, 2019), pp. 195–215.

37. S. N. Lee, *et al.*, Age Related Differences in Responsiveness to Sildenafil and Tamsulosin are due to Myogenic Smooth Muscle Tone in the Human Prostate. *Sci Rep* **7**, 10150 (2017).

38. K. T. McVary, A. Rademaker, G. L. Lloyd, P. Gann, Autonomic nervous system overactivity in men with lower urinary tract symptoms secondary to benign prostatic hyperplasia. *J. Urol.* **174**, 1327–1433 (2005).

39. J. Vincent, W. Dachman, T. F. Blaschke, B. B. Hoffman, Pharmacological tolerance to alpha 1-adrenergic receptor antagonism mediated by terazosin in humans. *J Clin Invest* **90**, 1763–1768 (1992).

40. C. Ding, *et al.*, The PEAK1-PPP1R12B axis inhibits tumor growth and metastasis by regulating Grb2/PI3K/Akt signalling in colorectal cancer. *Cancer Lett.* **442**, 383–395 (2019).

41. M. B. Freidin, A. V. Polonikov, Validation of PPP1R12B as a candidate gene for childhood asthma in Russians. *J. Genet.* **92**, 93–96 (2013).

42. S. M. Kas, *et al.*, Insertional mutagenesis identifies drivers of a novel oncogenic pathway in invasive lobular breast carcinoma. *Nat. Genet.* **49**, 1219–1230 (2017).

43. J. Lartey, J. Taggart, S. Robson, M. Taggart, Altered Expression of Human Smooth Muscle Myosin Phosphatase Targeting (MYPT) Isovariants with Pregnancy and Labor. *PLOS ONE* **11**, e0164352 (2016).

44. A. S. Pereyra, *et al.*, BDA-410 Treatment Reduces Body Weight and Fat Content by Enhancing Lipolysis in Sedentary Senescent Mice. *J. Gerontol. A Biol. Sci. Med. Sci.* **72**, 1045–1053 (2017).

45. X. Xing, *et al.*, Adipose-derived mesenchymal stem cells-derived exosome-mediated microRNA-342-5p protects endothelial cells against atherosclerosis. *Aging (Albany NY)* **12**, 3880–3898 (2020).

46. W. Y, *et al.*, Cyclic Stretch-Induced the Cytoskeleton Rearrangement and Gene Expression of Cytoskeletal Regulators in Human Periodontal Ligament Cells. *Acta odontologica Scandinavica* **75** (2017) Available at: https://pubmed.ncbi.nlm.nih.gov/28681629/?from_term=Ppp1r12b&from_page=2&from_pos=1 [Accessed April 9, 2020].

47. Y.-Y. Han, E. Forno, J. C. Celedón, Sex Steroid Hormones and Asthma in a Nationwide Study of U.S. Adults. *Am J Respir Crit Care Med* **201**, 158–166 (2020).

48. K. T. Khaw, E. Barrett-Connor, Blood pressure and endogenous testosterone in men: an inverse relationship. *J Hypertens* **6**, 329–332 (1988).

Figures

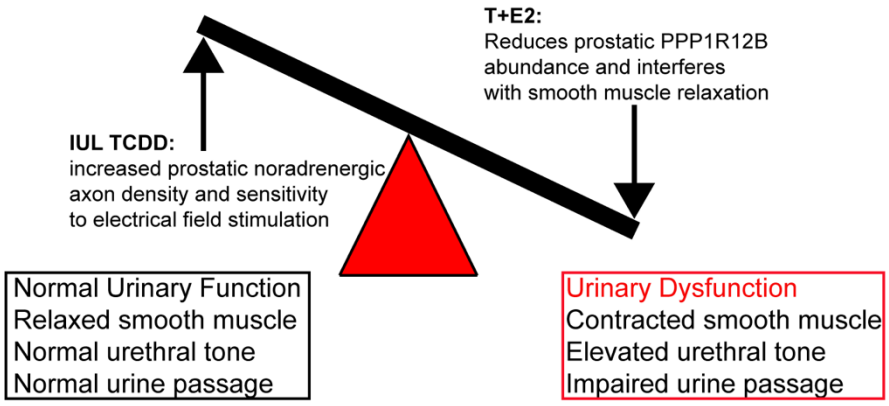

Figure 1. In utero and lactational TCDD exposure exacerbates urinary dysfunction by increasing prostate noradrenergic axon density and smooth muscle sensitivity to contraction. In adulthood, aging-related alterations in the levels of testosterone and estradiol cause urinary dysfunction by downregulating Ppp1r12b expression to impair prostate smooth muscle relaxation. Together, IUL TCDD exposure combined with adult T+E2 causes the “perfect storm”- increased sensitivity to contraction combined with prostate smooth muscle that is unable to relax causes exacerbated urinary dysfunction.